dc_1254_16

Nonsingular delamination modeling in orthotropic composite plates by semi-layerwise analysis

András Szekrényes
Budapest University of Technology and Economics
Department of Applied Mechanics

A thesis submitted for the degree of

Doctor of HAS (DSc)

Budapest, 2016

Acknowledgments

First of all I would like to thank the patient of my family. Many parts and figures of this thesis were created in the course of the weekends, so that my children, Marcell (age 7) and Adrián (age 2) sat on my lap and were around me in the 24 hours of the day. I am also grateful to my wife, Alexandra, who reminded me so many times that family is more important than work and carrier.

This thesis was greatly supported by the Bolyai János Research Scholarship of the Hungarian Academy of Sciences between 2008-2011 and 2012-2015. The Bolyai János Research Scholarship inspired me significantly during six years, and I am very grateful for the support. All of the articles that this thesis was written from, were published in these years. The support of the Hungarian Scientific Research Fund (OTKA) between 2013 and 2016 is also greatly acknowledged.

dc_1254_16

Abstract

This thesis deals with the development of semi-layerwise models for the mechanical analysis of delaminated composite plates. The first-, second- and third-order laminated plate theories were applied to capture the mechanical fields in delaminated composite plates with material orthotropy. The methods of two and four equivalent single layers were proposed and a general third-order displacement field was utilized in each layer. The kinematic continuity between the layers was established by the system of exact kinematic conditions. Apart from the continuity of the in-plane displacements between the interfaces of the layers even the continuity of shear strains, their first and second derivatives was imposed. A so-called shear strain control condition was also introduced, which means that the shear strains at two or more points located along the thickness were imposed to be the same. Using these conditions a modified displacement field was developed by introducing the vector of primary parameters and the displacement multiplicator matrix. Based on the principle of virtual work the invariant form of the equilibrium equations were derived for the delaminated and undelaminated regions of the plate. The system of partial differential equations were reduced to system of ordinary differential equations through the Lévy plate formulation. The state-space model of the delaminated and undelaminated region was developed, the continuity and boundary conditions of the boundary value problem were also derived. The theorem of autocontinuity was introduced, which is essentially related to the continuity conditions between the delaminated and undelaminated parts. Delaminated plates with different geometrical parameters were solved as examples. The stress and displacement fields as well as the J-integral were determined in the examples and compared to results by 3D finite element calculations. The results indicate that the proposed semi-layerwise technique is very useful, moreover, the best solution can be obtained by the second-order plate theory for the problems investigated in this thesis. Moreover, the second-order theory can be the basis for the development of a plate/shell finite element.

Contents

Nomenclature

Acronyms

AC	Autocontinuity
B.C.	Boundary condition
C.C.	Continuity condition
CFRP	Carbon-fibre reinforced plastic
CLPT	Classical laminated plate theory
ERR	Energy release rate
ESL	Equivalent single layer
FE	Finite element
FEM	Finite element method
FSDT	First-order shear deformable plate theory
GFRP	Glass-fibre reinforced plastic
LEFM	Linear elastic fracture mechanics
ODE	Ordinary differential equation
PDE	Partial differential equation
SEKC	System of exact kinematic conditions
SIF	Stress intensity factor
SSCC	Shear strain control condition
SSDT	Second-order shear deformable plate theory
TSDT	Third-order shear deformable plate theory
VCCT	Virtual crack closure technique

Greek Symbols

$\bar{\sigma}_{n(i)}$, $\bar{\tau}_{ns(i)}$, $\bar{\tau}_{nz(i)}$	Stresses imposed on the curved edge of the i^{th} ESL of the plate
$\boldsymbol{\psi}_{(p)}$	Vector of primary parameters

$\delta\boldsymbol{\sigma}$	Virtual stress tensor
$\delta\boldsymbol{\varepsilon}$	Virtual strain tensor
$\Gamma_{\sigma(i)}$	Curved edge domain in the plate boundary
γ_{xz}, γ_{yz}	Transverse shear strains
λ	Third-order displacement term
ν_{xy}, ν_{xz}, ν_{yz}	Poisson's ratios in the $x-y$, $x-z$ and $y-z$ planes
Ω_0	Surface domain of the plate
Ω_D	Plane of delamination
ϕ	Second-order displacement term
$\psi_{(s)j}$, $\psi_{(n)j}$	Vectors of primary parameters in the s, n, z coordinate system
$\psi_{(x)j}$, $\psi_{(y)j}$	Vectors of primary parameters in the x, y, z coordinate system
σ_{ij}	Stress tensor
θ	Angle of rotation
ε_{ij}	Strain tensor

Roman Symbols

$\delta u, \delta v, \delta w$	Virtual displacement field components
$\Delta x, \Delta y, \Delta z$	Size of crack tip elements
$\hat{\mathbf{L}}^{(x,xy)}$, $\hat{\mathbf{P}}^{(x,xy)}$	Vectors of equivalent higher-order stress resultants
$\hat{\mathbf{M}}^{(x,xy)}$	Vector of equivalent bending and twisting moments
$\hat{Q}_x$, $\hat{Q}_y$	Equivalent transverse shear forces
$\mathcal{U}$	Strain energy
$\mathcal{W}$	Strain energy density
$\mathcal{W}_F$	Work of external forces
$\overline{\mathbf{C}}_{(i)}^{(m)}$	Stiffness matrix
a	Delamination length
A_{pq}	Extensional stiffness matrix
b	Plate width
B_{pq}	Coupling stiffness matrix
c	Undelaminated length

NOMENCLATURE

D_{pq}	Bending stiffness matrix
E_x, E_y, E_z	Moduli of elasticity in the x, y and z directions
E_{pq}, F_{pq}, G_{pq}, H_{pq}	Higher-order stiffness matrices
G_{III}	Mode-III energy release rate
G_{II}	Mode-II energy release rate
G_I	Mode-I energy release rate
G_T	Total energy release rate
G_{xy}, G_{xz}, G_{yz}	Shear moduli in the $x-y$, $x-z$ and $y-z$ planes
h	The number of ESLs in the bottom plate
J_m	J-integral, $m = 1, 2, 3$
J_{III}	Mode-III J-integral
J_{II}	Mode-II J-integral
k	The number of ESLs over the whole thickness
K_{ij}	Displacement multiplicator matrix
L_x, L_y, L_{xy}	Higher-order stress resultants
M_x, M_y, M_{xy}	Bending and twisting moments
N_l	The number of layers in the whole plate
N_x, N_y, N_{xy}	In-plane forces
n_x, n_y	Components of outward normal on the plate edge
$N_{l(i)}$	The number of layers in the i^{th} ESL
P_x, P_y, P_{xy}	Higher-order stress resultants
q_b, q_t	Surface loads on the bottom and top boundaries
Q_x, Q_y	Transverse shear forces
R_x, R_y	Higher-order shear forces
S_x, S_y	Higher-order shear forces
t_b	Thickness of the bottom plate
t_i	Thickness of the i^{th} ESL
t_t	Thickness of the top plate
u, v, w	Displacement field components

dc_1254_16

u_0, v_0	Global membrane displacements
u_{0i}, v_{0i}	Local membrane displacements
u_{0n}, u_{0s}	Membrane displacements in the coordinate system of the curved edge of the plate
$z^{(i)}$	Local through the thickness coordinate
$z_R^{(i)}$	Coordinate of the global reference plane in the i^{th} ESL
$z_m^{(i)}$, $z_{m+1}^{(i)}$	Local coordinates of the m^{th} layer in the i^{th} ESL

dc_1254_16

1
Introduction

1.1 Application of laminated composite materials in engineering structures

Composites are heterogeneous materials, wherein the high stiffness is provided by the combination of fibres and the matrix material. In many applications the low weight is very important beside the high stiffness and strength. Typical examples are shown in Figures 1.1 and 1.2 discussed briefly in the sequel. The examples were searched and found by using Google.

The first example in Figure 1.1 is the bicycle: the frame and even the wheel is made mostly from carbon composites for professional cyclers. The construction in Figure 1.1a enables some elastic deformation for the point of the saddle in contrast with constructions made of metals. The second example is the racing car/bodywork construction (Figure 1.1b). Formula one cars are constructed by the racing teams themselves by carbon-fibre and other ultra-weight materials. Example 3 in Figure 1.1c is the airplane. The materials used in the Boeing 747 are 50% composites, fiberglass and carbon sandwich materials. Pressure vessels (Figure 1.1d) are manufactured from carbon and glass fiber composites by different technologies. The most important advantage of composite materials over metals in this field is the chemical resistance (*Phillips (1989)*). Figure 1.1 ends in the helicopters (Figure 1.1e), where lightweight and whisper quiet ride provided by composite materials is very important.

The examples are continued in Figure 1.2 with boats (Figure 1.2a) that are made out of many type of composites. Glass reinforced (polyester and vinylester) plastics have become the most prevalent composites in boatbuilding providing resistance against aggressive marine environment. Helmets (Figure 1.2b) are equally used in sports and military industry. Open and full face helmets are typically manufactured from carbon composites. The excellent shock resistance of composite materials should be highlighted again. Pole vault is one of the most technical of athletic events (Figure 1.2c). The vaulting poles are made out of combination of different materials. The most commonly used are carbon-fibre (CFRP) and glass-fibre reinforced plastics (GFRP). The pole has a diameter of about 50 mm and it is bent to a radius of curvature of about 1 m. The strength of the glass fiber composites is about 2-3 GPa. The key feature in the vaulting pole is the absence of large flaws and the

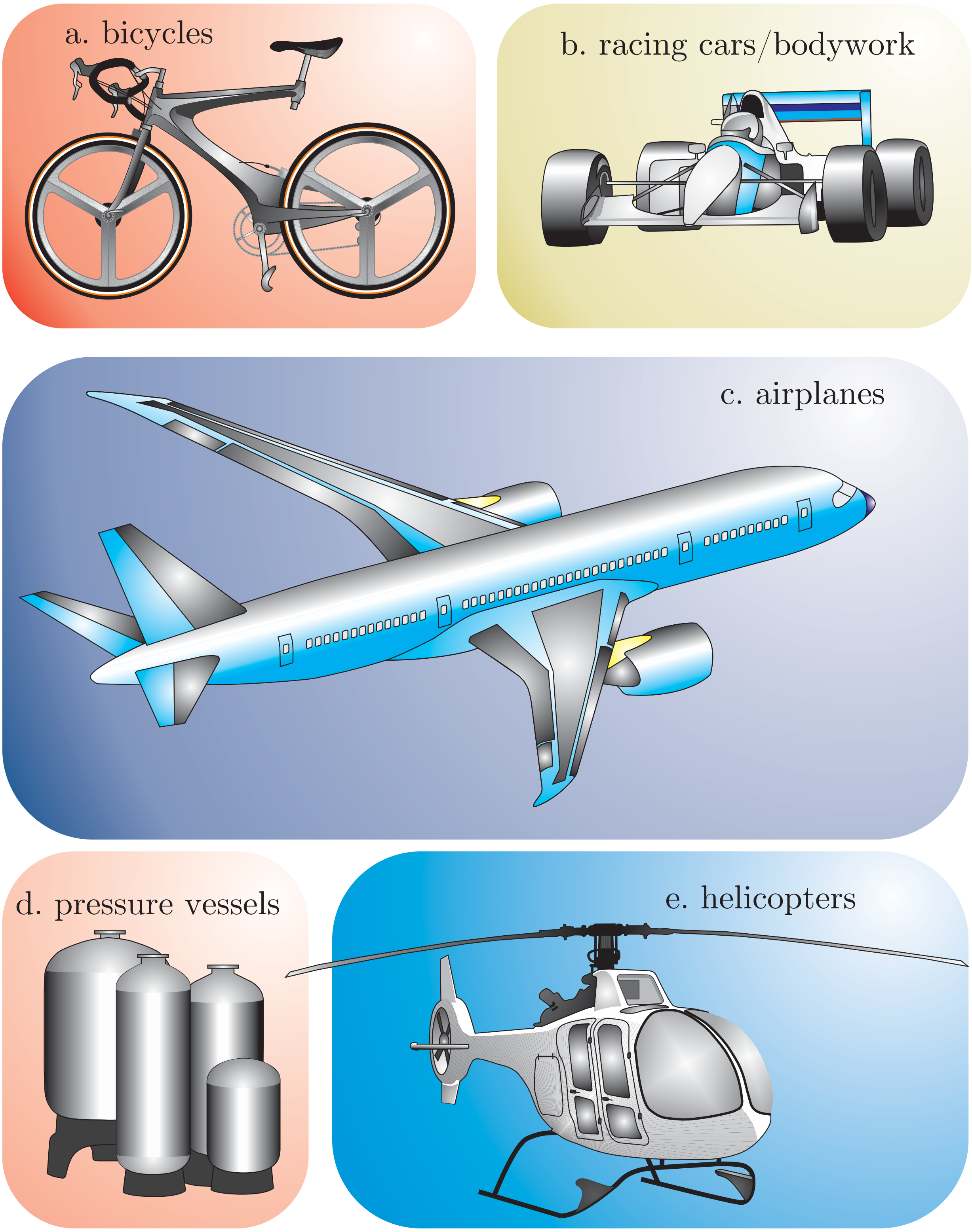

Figure 1.1: Application examples of composite materials in the engineering life - Part 1.

high toughness providing excellent resistance to fracture. In the field of submarines (Figure 1.2d) the benefits of composite materials - beside resistance against marine environment - are weight reduction, acoustic transparency, damping, thermal insulation and the fact that there is no magnetic signature which makes it very difficult to locate the submarine's position. The manufacturing technologies of wind turbine blades (Figure 1.2e) has evolved

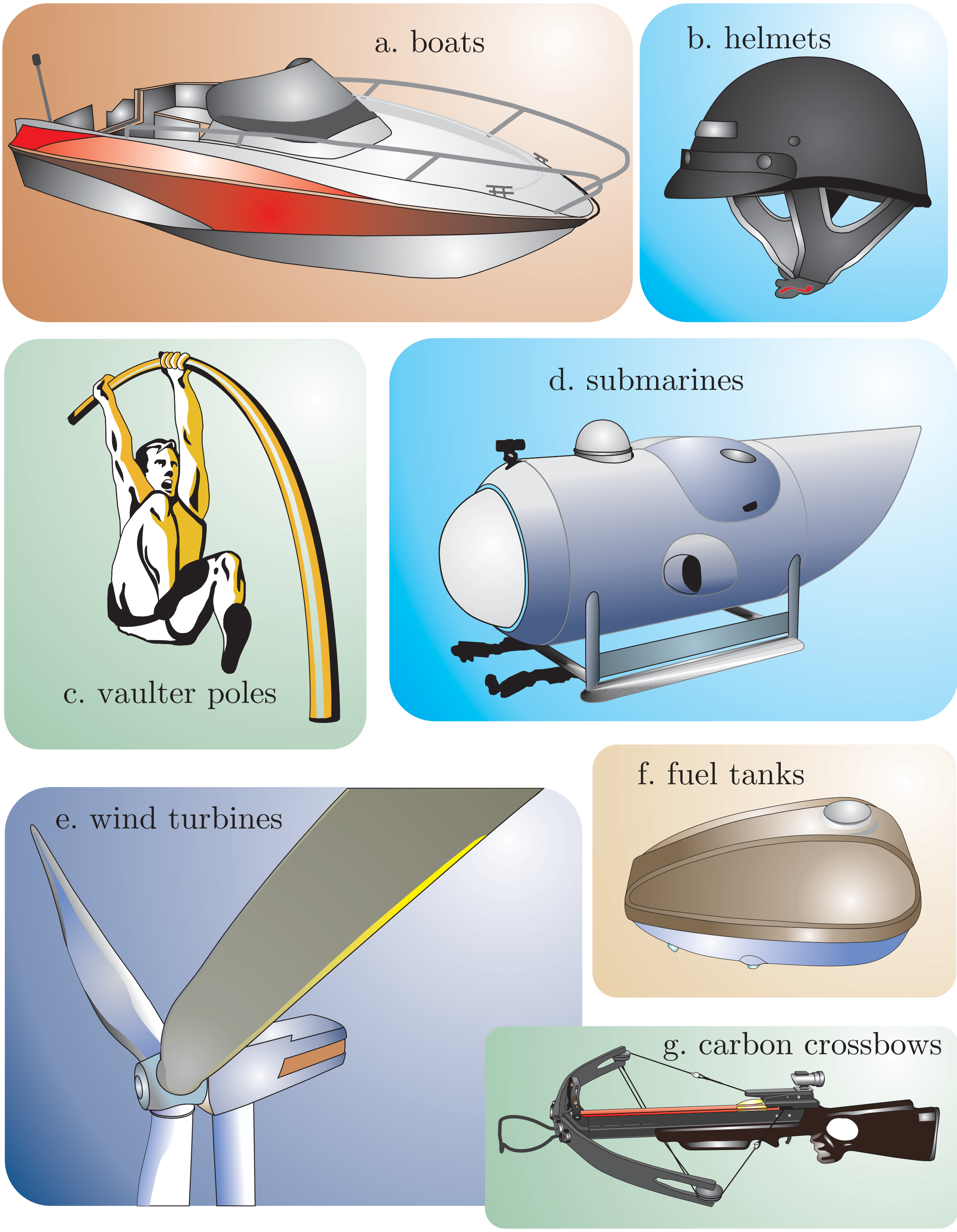

Figure 1.2: Application examples of composite materials in the engineering life - Part 2.

over the past twenty years. Lightweight construction is a keyword again in this field. The last two examples are: fuel tanks (Figure 1.2f) and carbon crossbows (Figure 1.2g), wherein the lightweight construction and accurate manufacturing is important again.

Beside the many advantages, composite materials are susceptible to various damage modes such as fiber breakage, matrix failure, fiber pull-out (*Adams et al. (2000); Phillips*

(1989)) and among others interlaminar fracture or delamination, which is the main object of this thesis.

1.2 Delamination in composite structures

As it can be seen in Figures 1.1 and 1.2 the basic application area of composite materials is thin- and thick-walled structures, like beams, plates and shells. Delamination fracture in this kind of structures (*Kiani et al. (2013); Marat-Mendes and de Freitas (2013); Zhou et al. (2013)*) can take place e.g. as the result of low velocity impact (*Burlayenko and Sadowski (2012); Christoforou et al. (2008); Ganapathy and Rao (1998); Goodmiller and TerMaath (2014); Rizov et al. (2005); Wang et al. (2012); Zammit et al. (2011)*), manufacturing defects (*Zhang and Fox (2007); Zhou et al. (2013)*) and free edge effect (*Ahn et al. (2013); Sarvestani and Sarvestani (2012)*). The resistance to delamination is characterized by experimental tests under different fracture modes. The main parameters of linear elastic fracture mechanics (LEFM) are the stress intensity factor (SIF) (*Anderson (2005); Cherepanov (1997); Hills et al. (1996)*) and energy release rate (ERR) (*Adams et al. (2000); Anderson (2005)*), respectively. The three basic fracture modes are shown in Figure 1.3. The fracture tests are carried out on different type of delamination specimens including mode-I (*Hamed et al. (2006); Islam and Kapania (2011); Jumel et al. (2011a); Kim et al. (2011); Peng et al. (2011); Romhany and Szebenyi (2012); Salem et al. (2013); Sorensen et al. (2007)*), mode-II (*Argüelles et al. (2011); Arrese et al. (2010); Budzik et al. (2013); Jumel et al. (2013); Kutnar et al. (2008); Mladensky and Rizov (2013b); Rizov and Mladensky (2012)*), mixed-mode I/II (*Bennati et al. (2009, 2013a,b); Fernández et al. (2013); Jumel et al. (2011b); Kenane et al. (2010); Nikbakht and Choupani (2008); da Silva et al. (2011); Szekrényes (2007); Yoshihara and Satoh (2009)*), mode-III (*Johnston et al. (2012); Marat-Mendes and Freitas (2009); Mehrabadi and Khosravan (2013); de Morais and Pereira (2009); de Morais et al. (2011); de Moura et al. (2009); Pereira et al. (2011); Rizov et al. (2006); Suemasu and Tanikado (2012); Szekrényes (2009a)*), mixed-mode I/III (*Pereira and de Morais (2009); Szekrényes (2009b)*) mixed-mode II/III (*Ho and Tay (2011); Kondo et al. (2011, 2010); Mehrabadi (2013); Miura et al. (2012); Mladensky and Rizov (2013a); de Morais and Pereira (2008); Nikbakht et al. (2010); Suemasu et al. (2010); Suemasu and Tanikado (2012); Szekrényes (2007); Szekrényes (2012)*) and mixed-mode I/II/III (*Davidson and Sediles (2011); Davidson et al. (2010); Szekrényes (2011)*) tests, respectively. In the former works beam and plate specimens were applied. While for beams the closed-form solutions for the ERRs are available, for plates similar solutions exist only for some relatively simple systems including special or in-plane loads (*Lee and Tu (1993); Saeedi et al. (2012a,b)*).

The plate theories of laminated materials are originated to the classical theories shown in Figure 1.4, which are based on an assumed displacement field. The displacement vector field is: $\mathbf{u} = \begin{pmatrix} u & v & w \end{pmatrix}^T$. In the sequel small displacements and rotations are assumed. The simplest plate theory is the classical laminated plate theory (CLPT) (*Kollár and Springer (2003); Kumar and Lal (2012); Reddy (2004)*), which is based on the Kirchhoff hypothesis:

$$u(x,y,z) = u_0(x,y) - z\frac{\partial w}{\partial x}, \quad v(x,y,z) = v_0(x,y) - z\frac{\partial w}{\partial y}, \quad w(x,y) = w_0(x,y), \quad (1.1)$$

where there are three independent parameters: u_0, v_0 are the membrane displacements and w is the transverse deflection, moreover z is the thickness coordinate. The cross section rotations are approximated by the derivatives of the deflection. The first-order shear

dc_1254_16

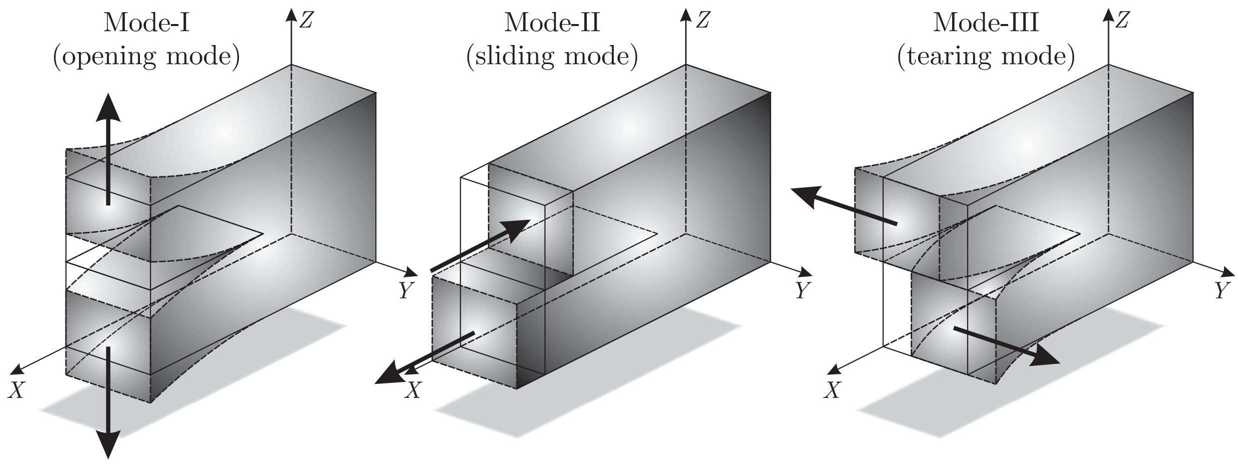

Figure 1.3: Basic fracture modes in linear elastic fracture mechanics.

deformable plate theory (FSDT or Reissner-Mindlin theory) (*Ovesy et al. (2015); Reddy (2004); Thai and Choi (2013)*) assumes independent rotations (θ_y and θ_x) about the x and y axes:

$$u(x,y,z) = u_0(x,y)+\theta_{(x)}(x,y)z, \quad v(x,y,z) = v_0(x,y)+\theta_{(y)}(x,y)z, \quad w(x,y,z) = w_0(x,y).$$

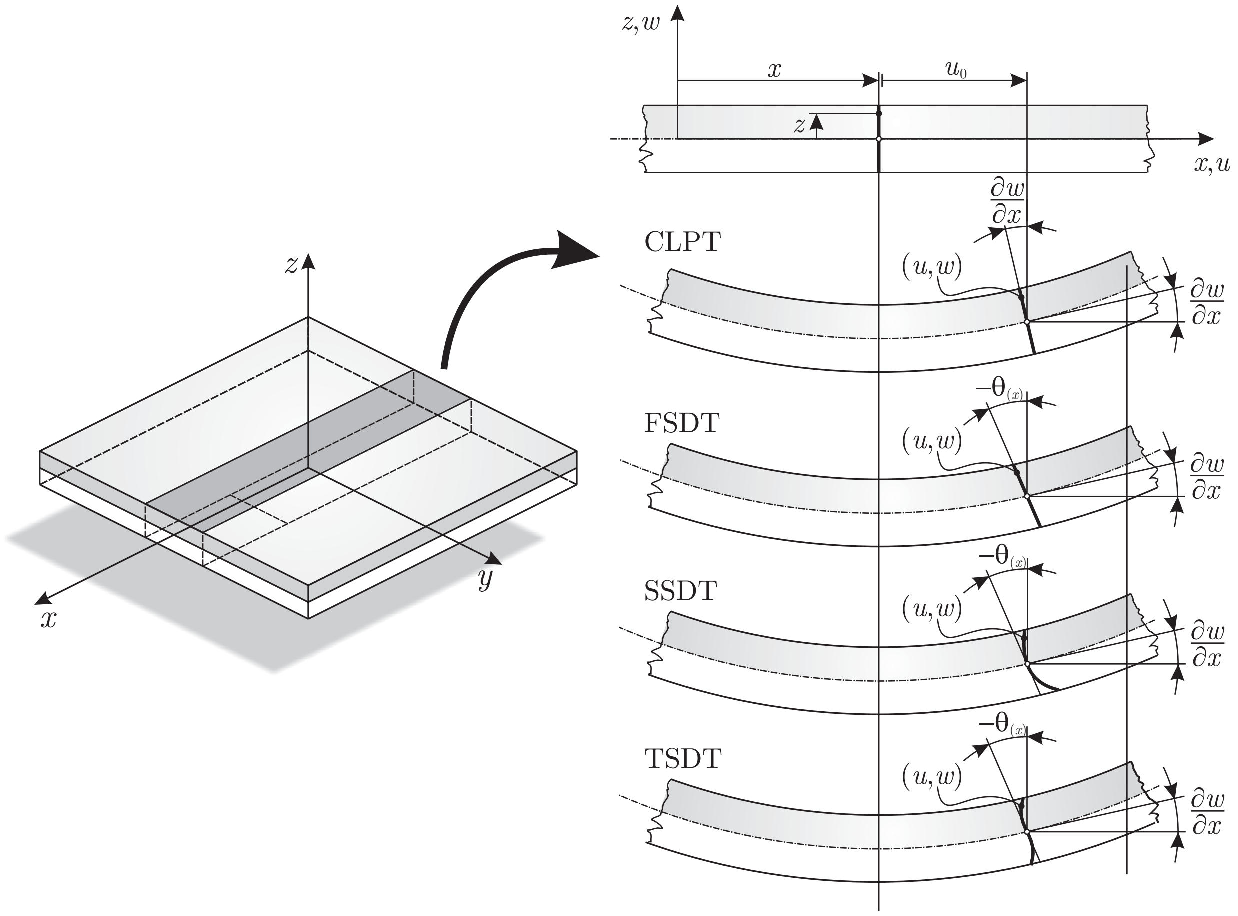

Figure 1.4: The deformation of a material line of a laminated plate on the $x - z$ plane in accordance with the different plate theories.

dc_1254_16

(1.2)

The higher-order plate theories can be obtained by the generalization of the FSDT displacement field even in the thickness direction:

$$\begin{aligned} u(x,y,z) &= u_0(x,y) + \theta_{(x)}(x,y)z + \phi_{(x)}(x,y)z^2 + \lambda_{(x)}(x,y)z^3 + \ldots, \\ v(x,y,z) &= v_0(x,y) + \theta_{(y)}(x,y)z + \phi_{(y)}(x,y)z^2 + \lambda_{(y)}(x,y)z^3 + \ldots, \\ w(x,y,z) &= w_0(x,y) + \theta_{(z)}(x,y)z + \phi_{(z)}(x,y)z^2 + \lambda_{(z)}(x,y)z^3 + \ldots, \end{aligned} \tag{1.3}$$

where $\theta_{(m)}$ means the angle of rotation (or first-order term), $\phi_{(m)}$ is the second-order, $\lambda_{(m)}$ ($m = x, y, z$) is the third-order displacement term. Moreover, the second-order shear deformable plate theory (SSDT) (*Izadi and Tahani (2010);Szekrényes (2013b, 2015)*) is obtained if we consider the terms in the displacement field upto z^2, a general third-order plate theory (TSDT) means that each component is approximated by a cubic function (*Panda and Singh (2011); Singh and Panda (2014);Szekrényes (2014d)*). If even the normal deformation is taken into account then the approach means a shear and normal deformable theory (*Sahoo et al. (2016)*). Among these approaches the Reddy third-order shear deformable theory should be mentioned (*Reddy (2004)*). This theory satisfies the dynamic boundary condition at the top and bottom plate surfaces (traction-free surfaces). The original idea is related to the name of *Levinson (1980)*, who applied the concept to isotropic materials. Later, Reddy extended this theory to laminated composites. The displacement field of Reddy TSDT takes the form of:

$$\begin{aligned} u(x,y,z) &= u_0(x,y) + \theta_{(x)}(x,y)z - \frac{4}{3t^2}\left(\theta_{(x)} + \frac{\partial w_0}{\partial x}\right)z^3, \\ v(x,y,z) &= v_0(x,y) + \theta_{(y)}(x,y)z - \frac{4}{3t^2}\left(\theta_{(y)} + \frac{\partial w_0}{\partial y}\right)z^3, \\ w(x,y) &= w_0(x,y), \end{aligned} \tag{1.4}$$

where t is the plate thickness and it is conspicuous that the second-order terms are missing.

These are the so-called equivalent single-layer theories (ESL), in which a heterogeneous laminated plate is treated as a statically equivalent single layer having a complex constitutive behavior *Reddy (2004)*. Within an ESL the displacement field is approximated by a given set of functions. An important aspect of these approaches is that if the normal deformability is not taken into account, then plane stress condition is assumed, therefore the transverse normal stress σ_z does not appear in the equations. The literature also offers the 3D elasticity solution and the layerwise or multilayer approaches (*Batista (2012); Ferreira et al. (2011); Reddy (2004); Saeedi et al. (2012a,b)*) (3D solutions), which can further improve the accuracy of the solution. In the book of *Reddy (2004)* and *Kollár and Springer (2003)* the application of the ESL theories to perfect plates (no imperfections and material defects) is well-documented and many examples are presented. It is important to note that *Reddy (2004)* concluded that the contribution of the higher-order theories to the solution of the plate bending problems compared to the CLPT and FSDT is not meaningful, however these are computationally significantly more expensive and sometimes it is absolutely sufficient to apply the CLPT or FSDT.

This paper puts emphasis essentially on the application of plate theories in fracture mechanics under mixed-mode II/III condition. In this respect the work by *Davidson et al. (2000)* is noteworthy, wherein the ERRs in delaminated plates were calculated by using

Mindlin-type plate finite elements (FSDT). The results were compared to 3D FE calculations, but the agreement was not satisfactory in all cases. One of the reasons for that could be the lack of higher-order plate finite elements in the commercial FE packages. A similar work was published by (*Sankar and Sonik (1995)*), as well. Some late works investigated the same problem (*Bruno et al. (2003, 2005)*) with the aid of interface and contact elements providing accurate results, however, the formulation was quite complicated and difficult to implement in commercial FE packages. Other formulations are available in the field, however, each is based on the FSDT and the virtual crack closure concept (*Qing et al. (2011); Zou et al. (2001)*).

1.3 Main aims and analysis methods

In delaminated plates and shells the presence of the delamination tips means a perturbation in the mechanical fields and a more accurate description could be necessary for a fracture mechanical analysis than those provided by CLPT and FSDT. The main aim of this thesis is to solve the most essential plate bending problems in that case when the plate contains a through-width delamination using higher-order plate theories. To the best of the author's knowledge these examples are not yet documented in the literature. A successful assessment of plate theories can be the basis for the development of plate and shell finite elements for the modeling of delaminations.

This thesis is organized as follows. In Chapter 2 the basic equations of laminated third-order plates is presented. This chapter is based on the system of exact kinematic conditions. A modified third-order displacement field and the displacement multiplicator matrix is developed and the principle of virtual work is utilized to derive the equilibrium equations of delaminated plates. The formulation is valid for laminated composite plates made out of any materials (e.g. polymer matrix composite) that behave as linear elastic material. Chapter 3 describes the method of 2ESLs and the general equations are derived for FSDT, SSDT and Reddy TSDT. It has to be mentioned that the CLPT was found to be inappropriate to capture the problems discussed in this thesis with an acceptable accuracy (*Szekrényes (2012, 2013a, 2014a)*). An important part of Chapter 3 is the introduction of the equivalent stress resultants. Chapter 4 contains the details of the method of 4ESLs, wherein four subplates are applied over the thickness of the plate. In this chapter the FSDT, SSDT and TSDT equations are given. In Chapter 5 two examples are solved by using the Lévy plate formulation. The state-space model of the plate system is derived separately for the undelaminated and delaminated regions, respectively. At the same time the generalized continuity conditions are given by parameter sets, even the boundary conditions are described for simply supported, built-in and free edges. Chapter 6 presents the results for the displacement and stress fields and a comparison is made to 3D FE results. In Chapter 7 the 3D J-integral is applied using the higher-order plate theories and analytical expressions are developed for the calculation of the mode-II and mode-III energy release rates. In the same chapter the distribution of the J-integrals along the delamination front of delaminated composite plates is presented and compared to the result of the 3D FE analysis. The methods of 2ESLs and 4ESLs are also compared to each other and the ranking of the different theories is made. Chapter 8 summarizes the main results and presents the novel scientific results in the form of theses. Finally, the possible application areas of the results are briefly given.

2

The basic equations of delaminated composite plates

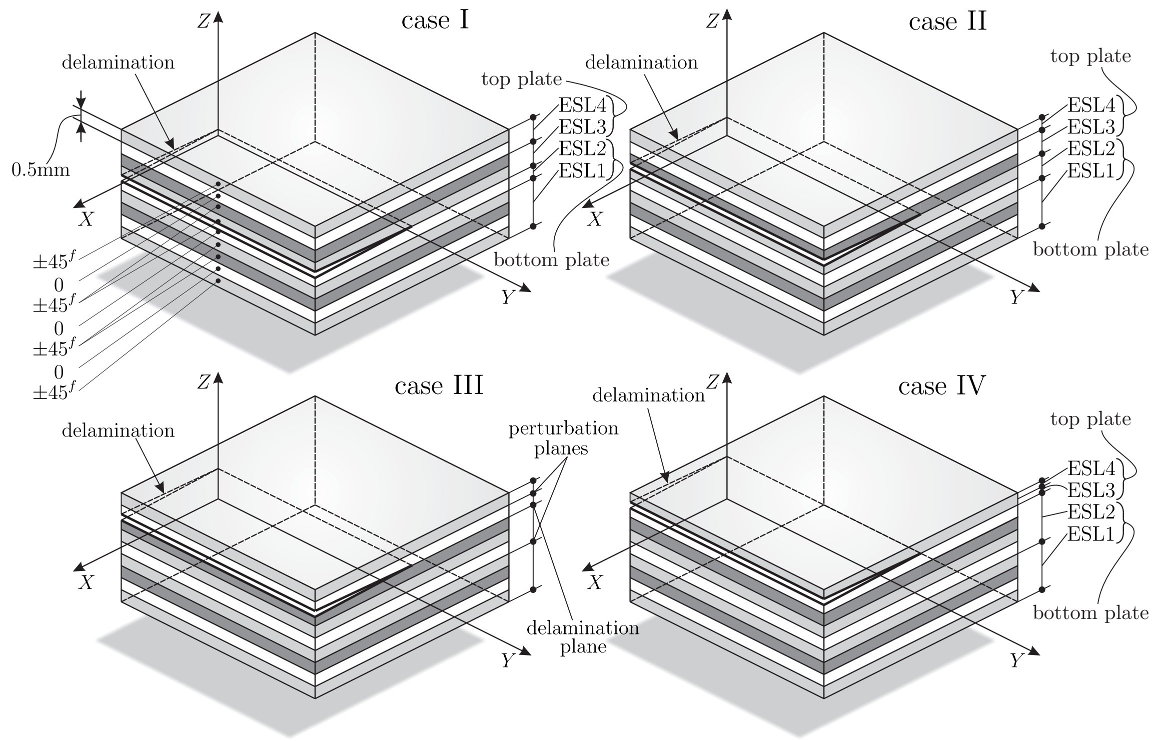

Figure 2.1: Plate elements with orthotropic plies and the position of the delamination over the plate thickness, cases I, II, III and IV.

In this chapter the basic equations of delaminated plates are presented. The formulation is based on the semi-layerwise modeling technique. The concept is shown in Figure 2.1 indicating plate elements with an interfacial delamination. The delamination divides the plate into a top and a bottom subplate. The top and the bottom subplates are further divided into equivalent single layers. In Figure 2.1 the method of 4ESLs is presented, i.e. the top and bottom plates are captured by two ESLs (altogether 4ESLs are applied).

Definition:*semi-layerwise plate model.* If a laminated plate with N_l number of layers is modeled by N_{ESL} number of equivalent single layers and $N_{ESL} < N_l$ then the model is called semi-layerwise plate model. In this case the stiffness parameters and matrices of each ESL has to be determined with respect to the local reference planes of the ESLs. The interface planes between the neighboring ESLs are the perturbation planes. If $N_{ESL} = N_l$ then the model is a standard layerwise model.

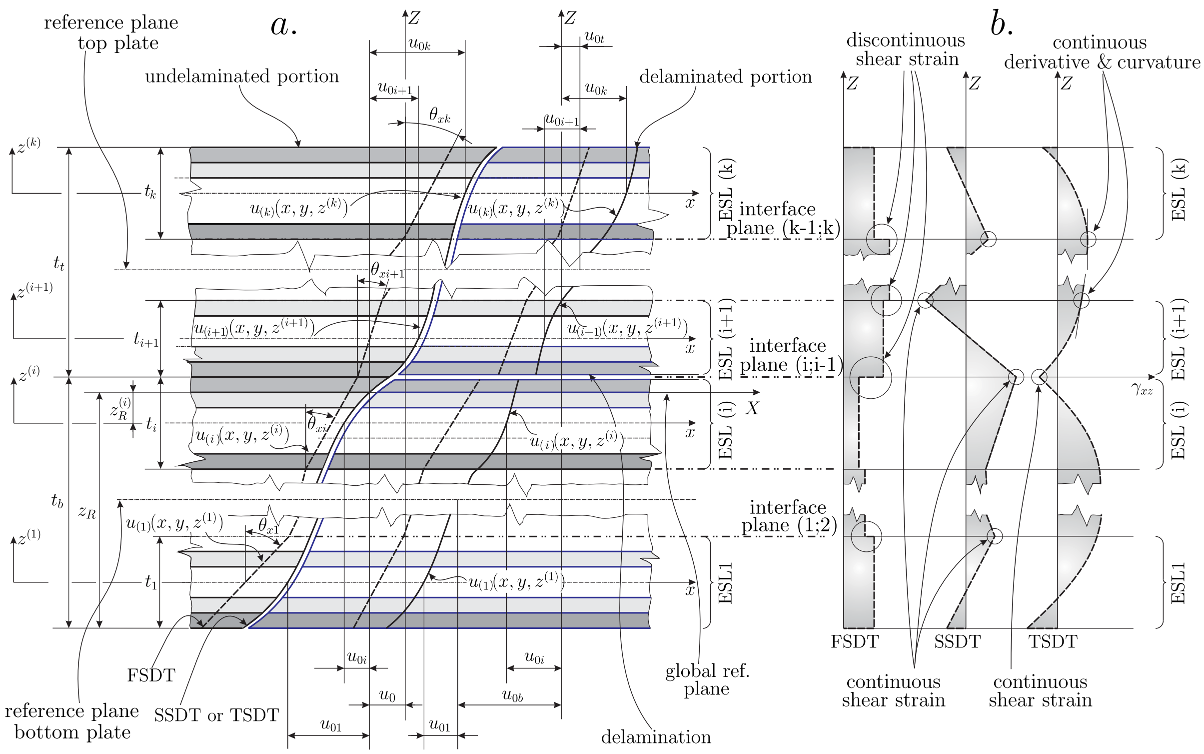

Figure 2.2: Cross sections and deformation of the top and bottom plate elements of a delaminated plate in the X-Z plane (a). Distribution of the transverse shear strains by FSDT, SSDT and TSDT (b).

Figure 2.2 shows the section of the transition between the delaminated and undelaminated regions of the layered plate element in the $X - Z$ plane, while in Figure 2.3 the $Y - Z$ plane is shown. The two coordinate systems are to show the displacement parameters in the undelaminated and delaminated parts. The elements contain an interfacial delamination (delaminated portion) parallel to the Y axis, i.e. it goes across the entire plate width (refer to Figure 2.1). The general case involves k number of ESLs applied through the whole thickness. The transverse splitting means that the undelaminated and delaminated regions are captured by different mathematical models. In accordance with the literature review the ESLs can be captured by different plate theories. In this chapter we apply the FSDT, SSDT and TSDT theories. The general third-order Taylor series expansion of the in-plane displacement functions results in the following displacement field (*Panda and Singh (2009, 2011); Singh and Panda (2014); Talha and Singh (2010)*):

$$\begin{aligned}
u_{(i)}(x,y,z^{(i)}) &= u_0(x,y) + u_{0i}(x,y) + \theta_{(x)i}(x,y)z^{(i)} + \phi_{(x)i}(x,y)[z^{(i)}]^2 + \lambda_{(x)i}(x,y)[z^{(i)}]^3, \\
v_{(i)}(x,y,z^{(i)}) &= v_0(x,y) + v_{0i}(x,y) + \theta_{(y)i}(x,y)z^{(i)} + \phi_{(y)i}(x,y)[z^{(i)}]^2 + \lambda_{(y)i}(x,y)[z^{(i)}]^3, \\
w_{(i)}(x,y) &= w(x,y),
\end{aligned} \tag{2.1}$$

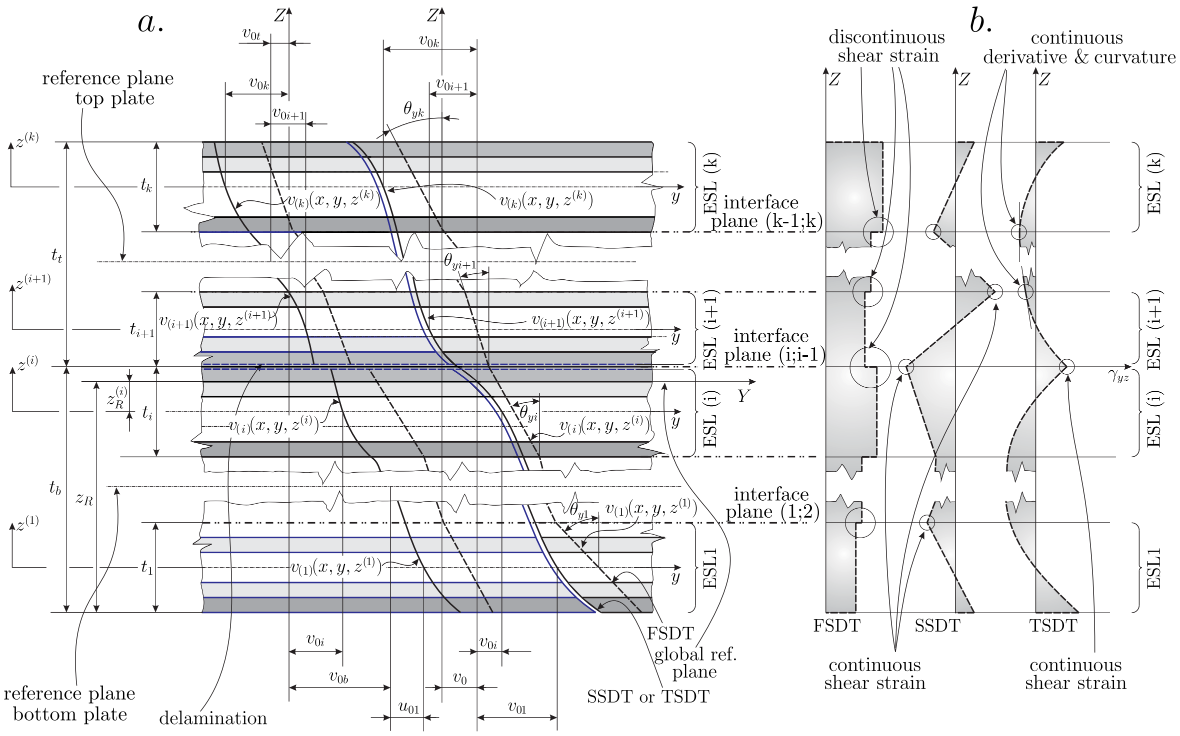

Figure 2.3: Cross sections and deformation of the top and bottom plate elements of a delaminated plate in the Y-Z plane (a). Distribution of the transverse shear strains by FSDT, SSDT and TSDT (b).

where i is the index of the actual ESL, $z^{(i)}$ is the local through thickness coordinate of the i^{th} ESL and always coincides with the local midplane, u_0 and v_0 are the global, u_{0i} and v_{0i} are the local membrane displacements, moreover, θ means the rotations of the cross sections about the X and Y axes (refer to Figure 2.1), ϕ denotes the second-order, λ represents the third-order terms in the displacement functions. Finally $w_{(i)}$ is the transverse deflection function. Eq.(2.1) will be applied equally to the undelaminated and delaminated portions and the continuity between these parts will be established. In this thesis only shear deformable plate models are developed, in other words the deflection is inextensible in the through-thickness direction involving that $w_{(i)}(x,y) = w(x,y)$. The displacement functions of FSDT and SSDT can be obtained by reducing Eq.(2.1) and taking $\phi_{(x)i} = \phi_{(y)i} = 0$ and $\lambda_{(x)i} = \lambda_{(y)i} = 0$, respectively (*Izadi and Tahani (2010); Petrolito (2014)*). The displacement field given by Eq.(2.1) is associated to each ESL.

2.1 The system of exact kinematic conditions

The displacement vector field for the i^{th} ESL is $\mathbf{u}_{(i)} = \begin{pmatrix} u_{(i)} & v_{(i)} & w_{(i)} \end{pmatrix}^T$. The kinematic continuity between the displacement fields of adjacent ESLs is established by the system of exact kinematic conditions (SEKC), which was originally developed by *Szekrényes (2013c, 2014c, 2015, 2016a,b)*. The first set of conditions formulates the continuity of the in-plane and transverse displacements between the neighboring plies as (refer to Figures 2.2 and 2.3):

$$(u_{(i)}, v_{(i)}, w_{(i)})\big|_{z^{(i)}=t_i/2} = (u_{(i+1)}, v_{(i+1)}, w_{(i+1)})\big|_{z^{(i+1)}=-t_{i+1}/2}, \tag{2.2}$$

where t_i is the thickness of the specified layer. It has to be noted that the result of Eq.(2.2) was applied by *Davidson et al. (2000)* and *Zou et al. (2001)*, however their equations are valid only for the FSDT. On the contrary, Eq.(2.2) is more general and applicable to any plate theory. Moreover, there are large number of works referred to in the book of *Reddy (2004)* applying displacement continuity between the layers. Those works apply full layerwise models to perfect plates, in contrast with this thesis, which deals with the semi-layerwise analysis of delaminated plates. The second set of conditions defines the global membrane displacements (u_0, v_0) at the reference plane of the actual region. If the coordinate of the global reference plane is $z_R^{(i)}$ and is located in the i^{th} layer, then the conditions become:

$$u_{(i)}\big|_{z^{(i)}=z_R^{(i)}} - u_0 = 0, \quad v_{(i)}\big|_{z^{(i)}=z_R^{(i)}} - v_0 = 0. \tag{2.3}$$

The two sets of conditions given by Eqs.(2.2)-(2.3) are sufficient to develop semi-layerwise models using the FSDT. If the SSDT or TSDT is applied, then we can impose the shear strain continuity at the interface (or perturbation) planes. In accordance with Figures 2.2b and 2.3b these conditions are formulated as:

$$\left(\gamma_{xz(i)}, \gamma_{yz(i)}\right)\big|_{z^{(i)}=t_i/2} = \left(\gamma_{xz(i+1)}, \gamma_{yz(i+1)}\right)\big|_{z^{(i+1)}=-t_{i+1}/2}. \tag{2.4}$$

It has to be mentioned that in general layerwise models assume continuous shear stresses at the interfaces (*Reddy (2004)*). For the TSDT theory two more sets of conditions are reasonable to introduce. The imposition of continuity of the first and second derivatives of the shear strain (*Szekrényes (2016b)*) prevents the unwanted oscillations (and the too large compliance) in the shear stress distributions (see Figures 2.2b and 2.3b):

$$\left(\frac{\partial\gamma_{xz(i)}}{\partial z^{(i)}}, \frac{\partial\gamma_{yz(i)}}{\partial z^{(i)}}\right)\Bigg|_{z^{(i)}=t_i/2} = \left(\frac{\partial\gamma_{xz(i+1)}}{\partial z^{(i+1)}}, \frac{\partial\gamma_{yz(i+1)}}{\partial z^{(i+1)}}\right)\Bigg|_{z^{(i+1)}=-t_{i+1}/2}, \tag{2.5}$$

and:

$$\left(\frac{\partial^2\gamma_{xz(i)}}{\partial (z^{(i)})^2}, \frac{\partial^2\gamma_{yz(i)}}{\partial (z^{(i)})^2}\right)\Bigg|_{z^{(i)}=t_i/2} = \left(\frac{\partial^2\gamma_{xz(i+1)}}{\partial (z^{(i+1)})^2}, \frac{\partial^2\gamma_{yz(i+1)}}{\partial (z^{(i+1)})^2}\right)\Bigg|_{z^{(i+1)}=-t_{i+1}/2}. \tag{2.6}$$

An important addition to Eqs.(2.2)-(2.6) is the so-called shear strain control condition (SSCC, *Szekrényes (2016a)*). The set of conditions applied is:

$$\left(\gamma_{xz(l)}, \gamma_{yz(l)}\right)\big|_{z^{(l)}=-t_l/2} = \left(\gamma_{xz(m)}, \gamma_{yz(m)}\right)\big|_{z^{(m)}=t_m/2}, \tag{2.7}$$

where l and m denote ESLs at the boundaries, where the shear strains are equal to each other and $m > l$ always. In accordance with Reddy theory (*Reddy (2004)*) the top and bottom surfaces of the plate are traction-free (zero shear stresses). If the system is modeled by 4ESLs the traction-free conditions leads to overconstraining (or stiffening) of the model and wrong results are obtained. Therefore, instead of imposing zero stresses at the free surfaces we impose the identical shear strain values at the boundary planes by Eq.(2.7). Essentially, the SSCC is applicable only if at least 4ELSs and the SDDT or TSDT are applied.

Based on the linear elasticity and assuming transversely inextensible deflection in each ESL, the SEKC formulates conditions using the in-plane displacement functions: $\frac{\partial^n (u_{(i)}, v_{(i)})}{\partial (z^{(i)})^n}$, $n = 0, 1, 2, 3$, where $n = 0$ means condition against in-plane displacement, $n = 1$ means condition for shear strain, if $n = 2$ and $n = 3$ then a condition for the shear strain's first and second derivative is formulated. The SEKC conditions can be applied equally to the undelaminated and delaminated portions of the plate. Moreover these conditions can be implemented into any plate theory.

2.2 Kinematically admissible displacement fields

In Eq.(2.1) the displacement functions are modified in order to satisfy Eqs.(2.2)-(2.7). In the general sense, by applying the FSDT, SSDT and TSDT theories the in-pane displacement functions can be written as:

$$\begin{aligned} u_{(i)} &= u_0 + \left(K_{ij}^{(0)} + K_{ij}^{(1)} z^{(i)} + K_{ij}^{(2)}[z^{(i)}]^2 + K_{ij}^{(3)}[z^{(i)}]^3\right)\psi_{(x)j}, \quad i = 1..k, \\ v_{(i)} &= v_0 + \left(K_{ij}^{(0)} + K_{ij}^{(1)} z^{(i)} + K_{ij}^{(2)}[z^{(i)}]^2 + K_{ij}^{(3)}[z^{(i)}]^3\right)\psi_{(y)j}, \quad i = 1..k, \end{aligned} \tag{2.8}$$

where K_{ij} is the displacement multiplicator matrix and related exclusively to the geometry (ESL thicknesses), i refers to the ESL number, the summation index j defines the component in $\boldsymbol{\psi}$, which is the vector of primary parameters (see later), finally $w_{(i)}(x,y) = w(x,y)$ for each ESLs, i.e. the transverse normal of each ESL is inextensible (*Reddy (2004)*). Eq.(2.8) can be obtained by parameter elimination. It is important to note that the size and the elements of $\boldsymbol{\psi}$ depend on the applied theory, the number of ESLs and the number of conditions applied.

Definition: *Parameter elimination, primary and secondary parameters.* Certain parameters of the in-plane displacement functions can be eliminated using the SEKC requirements. The remaining (or *primary*) parameters are untouched, the parameters to be eliminated are the *secondary* parameters. The local membrane displacements are typically secondary parameters, the global membrane displacements are primary parameters, the rotations, second- and third-order parameters are mixed (either primary or secondary) parameters.

In the subsequent sections the undelaminated and delaminated regions are discussed separately. First, the TSDT is considered and the SSDT and FSDT field equations are obtained by the reduction of TSDT model.

2.3 Virtual work principle and constitutive equations

The strain field in an elastic body in terms of the displacement field is obtained by the following equation (assuming small displacements and strains) (*Chou and Pagano (1967)*):

$$\varepsilon_{pq} = \frac{1}{2}(u_{p,q} + u_{q,p}), \quad p,q = 1,2 \text{ or } 3, \tag{2.9}$$

where ε_{pq} is the strain tensor, u_p is the displacement vector field and the comma means differentiation with respect to the index right after. By assuming plane stress state ($\sigma_{z(i)} = 0$) in the plate and using Eqs.(2.1)-(2.9) the vector of in-plane strains becomes (*Reddy (2004)*):

$$\begin{pmatrix} \varepsilon_x \\ \varepsilon_y \\ \gamma_{xy} \end{pmatrix}_{(i)} = \begin{pmatrix} \varepsilon_x^{(0)} \\ \varepsilon_y^{(0)} \\ \gamma_{xy}^{(0)} \end{pmatrix}_{(i)} + z^{(i)} \cdot \begin{pmatrix} \varepsilon_x^{(1)} \\ \varepsilon_y^{(1)} \\ \gamma_{xy}^{(1)} \end{pmatrix}_{(i)} + \left[z^{(i)}\right]^2 \cdot \begin{pmatrix} \varepsilon_x^{(2)} \\ \varepsilon_y^{(2)} \\ \gamma_{xy}^{(2)} \end{pmatrix}_{(i)} + \left[z^{(i)}\right]^3 \cdot \begin{pmatrix} \varepsilon_x^{(3)} \\ \varepsilon_y^{(3)} \\ \gamma_{xy}^{(3)} \end{pmatrix}_{(i)}, \tag{2.10}$$

or $\{\varepsilon\}_{(i)} = \left\{\varepsilon^{(0)}\right\}_{(i)} + z^{(i)} \cdot \left\{\varepsilon^{(1)}\right\}_{(i)} + \left[z^{(i)}\right]^2 \cdot \left\{\varepsilon^{(2)}\right\}_{(i)} + \left[z^{(i)}\right]^3 \cdot \left\{\varepsilon^{(3)}\right\}_{(i)}$ which is third-order in terms of the through-thickness coordinate, $z^{(i)}$. The vector of transverse shear strains is:

$$\begin{pmatrix} \gamma_{xz} \\ \gamma_{yz} \end{pmatrix}_{(i)} = \begin{pmatrix} \gamma_{xz}^{(0)} \\ \gamma_{yz}^{(0)} \end{pmatrix}_{(i)} + z^{(i)} \cdot \begin{pmatrix} \gamma_{xz}^{(1)} \\ \gamma_{yz}^{(1)} \end{pmatrix}_{(i)} + \left[z^{(i)}\right]^2 \cdot \begin{pmatrix} \gamma_{xz}^{(2)} \\ \gamma_{yz}^{(2)} \end{pmatrix}_{(i)}, \tag{2.11}$$

or in a compact form: $\{\gamma\}_{(i)} = \left\{\gamma^{(0)}\right\}_{(i)} + z^{(i)} \cdot \left\{\gamma^{(1)}\right\}_{(i)} + \left[z^{(i)}\right]^2 \cdot \left\{\gamma^{(2)}\right\}_{(i)}$, which is second-order in terms of $z^{(i)}$. To derive the governing equations of the plate system we apply the virtual work principle (*Reddy (2004)*):

$$\int\limits_{T_0}^{T_1} (\delta\mathcal{U} - \delta\mathcal{W}_F)dt = 0, \quad \delta\mathcal{U} = \sum_i \delta\mathcal{U}_{(i)}, \quad \delta\mathcal{W}_F = \sum_i \delta\mathcal{W}_{F(i)}, \tag{2.12}$$

where $\mathcal{U}$ is the strain energy, $\mathcal{W}_F$ is the work of external forces and t is the time ($\mathcal{L} = \mathcal{U} - \mathcal{W_F}$ is the Lagrange function). The virtual strain energy for the i^{th} ESL of the plate system including the delaminated and undelaminated regions is (*Reddy (2004)*):

$$\begin{aligned}\delta\mathcal{U}_{(i)} &= \int\limits_V \boldsymbol{\sigma}_{(i)} : \delta\boldsymbol{\varepsilon}_{(i)} dV = \\ &\int\limits_{\Omega_0} \left\{ \int\limits_{-t_i/2}^{t_i/2} \left(\sigma_{x(i)}\delta\varepsilon_{x(i)} + \sigma_{y(i)}\delta\varepsilon_{y(i)} + \tau_{xy(i)}\delta\gamma_{xy(i)} + \tau_{xz(i)}\delta\gamma_{xz(i)} + \tau_{yz(i)}\delta\gamma_{yz(i)}\right) dz^{(i)} \right\} dxdy,\end{aligned} \tag{2.13}$$

where $\boldsymbol{\sigma}_{(i)}$ is the stress tensor, $\delta\boldsymbol{\varepsilon}_{(i)}$ is the virtual strain tensor of the i^{th} ESL, Ω_0 denotes the surface domain of the plate in the global $X-Y$ (or $x-y$) plane. The double dot product means: $\boldsymbol{\sigma}_{(i)} : \delta\boldsymbol{\varepsilon}_{(i)} = \sigma_{ij(i)}\delta\varepsilon_{ij(i)}$. The virtual work of the external forces for a single ESL is:

$$\begin{aligned}\delta\mathcal{W}_{F(i)} &= \int\limits_{\Omega_0} \left(q_{b(i)}(x,y)\delta w(x,y,-t_i/2) + q_{t(i)}(x,y)\delta w(x,y,t_i/2)\right) dxdy \\ &+ \int\limits_{\Gamma_{\sigma(i)}} \left\{ \int\limits_{-t_i/2}^{t_i/2} \left(\bar{\sigma}_{n(i)}\delta u_{n(i)} + \bar{\tau}_{ns(i)}\delta u_{s(i)} + \bar{\tau}_{nz(i)}\delta w_{(i)}\right) dz^{(i)} \right\} ds,\end{aligned} \tag{2.14}$$

where q_b and q_t are the surface loads on the top and bottom plane of the i^{th} ESL. The second term in the expression above is related to the virtual work of the imposed stress components ($\bar{\sigma}_{n(i)}$, $\bar{\tau}_{ns(i)}$ and $\bar{\tau}_{nz(i)}$) acting on the curved edge boundary denoted by $\Gamma_{\sigma(i)}$, moreover s and n are the tangential and normal directions (*Reddy (2004)*). Taking back the strain field (Eqs.(2.10)-(2.11)) into Eq.(2.13) we obtain:

$$\begin{aligned}\delta\mathcal{U}_{(i)} = \int\limits_{\Omega_0} \Bigg\{ \int\limits_{-t_i/2}^{t_i/2} &\Big[\sigma_{x(i)} \left(\delta\varepsilon^{(0)}_{x(i)} + z^{(i)}\delta\varepsilon^{(1)}_{x(i)} + (z^{(i)})^2\delta\varepsilon^{(2)}_{x(i)} + (z^{(i)})^3\delta\varepsilon^{(3)}_{x(i)}\right) \\ &+\sigma_{y(i)} \left(\delta\varepsilon^{(0)}_{y(i)} + z^{(i)}\delta\varepsilon^{(1)}_{y(i)} + (z^{(i)})^2\delta\varepsilon^{(2)}_{y(i)} + (z^{(i)})^3\delta\varepsilon^{(3)}_{y(i)}\right) \\ &+\tau_{xy(i)} \left(\delta\gamma^{(0)}_{xy(i)} + z^{(i)}\delta\gamma^{(1)}_{xy(i)} + (z^{(i)})^2\delta\gamma^{(2)}_{xy(i)} + (z^{(i)})^3\delta\gamma^{(3)}_{xy(i)}\right) \\ &+\tau_{xz(i)} \left(\delta\gamma^{(0)}_{xz(i)} + z^{(i)}\delta\gamma^{(1)}_{xz(i)} + (z^{(i)})^2\delta\gamma^{(2)}_{xz(i)}\right) \\ &+\tau_{yz(i)} \left(\delta\gamma^{(0)}_{yz(i)} + z^{(i)}\delta\gamma^{(1)}_{yz(i)} + (z^{(i)})^2\delta\gamma^{(2)}_{yz(i)}\right)\Big] dz^{(i)} \Bigg\} dxdy.\end{aligned} \tag{2.15}$$

The third-order displacement field component in Eq.(2.8) can be written as: $u_{p(i)} = u^{(0)}_{p(i)} + z^{(i)}u^{(1)}_{p(i)} + [z^{(i)}]^2 u^{(2)}_{p(i)} + [z^{(i)}]^3 u^{(3)}_{p(i)}$, where $p = s$ or n. Taking its virtual form, the virtual work of external forces becomes:

$$\begin{aligned}\delta\mathcal{W}_{F(i)} &= \int\limits_{\Omega_0} \left(q_{b(i)}(x,y)\delta w(x,y,-t_i/2) + q_{t(i)}(x,y)\delta w(x,y,t_i/2)\right) dxdy \\ &+ \int\limits_{\Gamma_{\sigma(i)}} \left\{ \int\limits_{-t_i/2}^{t_i/2} \left(\sigma_{n(i)}\left[\delta u^{(0)}_{n(i)} + z^{(i)}\delta u^{(1)}_{n(i)} + (z^{(i)})^2\delta u^{(2)}_{n(i)} + (z^{(i)})^3\delta u^{(3)}_{n(i)}\right]\right.\right. \\ &\left.\left. + \tau_{ns(i)}\left[\delta u^{(0)}_{s(i)} + z^{(i)}\delta u^{(1)}_{s(i)} + (z^{(i)})^2\delta u^{(2)}_{s(i)} + (z^{(i)})^3\delta u^{(3)}_{s(i)}\right] + \tau_{nz(i)}\delta w_{(i)}\right) dz^{(i)} \right\} ds.\end{aligned} \tag{2.16}$$

To derive $\delta\mathcal{U}_{(i)}$ and $\delta\mathcal{W}_{F(i)}$ in terms of the stress resultants and the virtual displacement parameters of the plate system we use the constitutive equation. The constitutive equation for orthotropic materials under plane stress state is $\boldsymbol{\sigma}^{(m)}_{(i)} = \overline{\mathbf{C}}^{(m)}_{(i)}\boldsymbol{\varepsilon}^{(m)}$ (*Kollár and Springer (2003); Reddy (2004)*), which expands to:

$$\begin{pmatrix} \sigma_x \\ \sigma_y \\ \tau_{yz} \\ \tau_{xz} \\ \tau_{xy} \end{pmatrix}^{(m)}_{(i)} = \begin{pmatrix} \overline{C}_{11} & \overline{C}_{12} & 0 & 0 & 0 \\ \overline{C}_{12} & \overline{C}_{22} & 0 & 0 & 0 \\ 0 & 0 & \overline{C}_{44} & 0 & 0 \\ 0 & 0 & 0 & \overline{C}_{55} & 0 \\ 0 & 0 & 0 & 0 & \overline{C}_{66} \end{pmatrix}^{(m)}_{(i)} \begin{pmatrix} \varepsilon_x \\ \varepsilon_y \\ \gamma_{yz} \\ \gamma_{xz} \\ \gamma_{xy} \end{pmatrix}_{(i)}, \tag{2.17}$$

where $\overline{\mathbf{C}}^{(m)}_{(i)}$ is the stiffness matrix of the m^{th} layer within the i^{th} ESL. By using the constitutive equations the stress resultants are calculated by integrating the stresses over the thicknesses of each ESL:

$$\begin{pmatrix} N_{\alpha\beta} \\ M_{\alpha\beta} \\ L_{\alpha\beta} \\ P_{\alpha\beta} \end{pmatrix}_{(i)} = \int\limits_{-t_i/2}^{t_i/2} \sigma_{\alpha\beta} \begin{pmatrix} 1 \\ z \\ z^2 \\ z^3 \end{pmatrix}_{(i)} dz^{(i)}, \quad \begin{pmatrix} Q_\alpha \\ R_\alpha \\ S_\alpha \end{pmatrix}_{(i)} = \int\limits_{-t_i/2}^{t_i/2} \tau_{\alpha z} \begin{pmatrix} 1 \\ z \\ z^2 \end{pmatrix}_{(i)} dz^{(i)}, \tag{2.18}$$

where α and β takes x or y. The relationship between the strain field and the stress resultants can be determined by taking back Eqs.(2.17) and (2.10)-(2.11) resulting in the following: (*Szekrényes (2014c)*):

$$\begin{pmatrix} \{N\} \\ \{M\} \\ \{L\} \\ \{P\} \end{pmatrix}_{(i)} = \begin{bmatrix} [A] & [B] & [D] & [E] \\ [B] & [D] & [E] & [F] \\ [D] & [E] & [F] & [G] \\ [E] & [F] & [G] & [H] \end{bmatrix}_{(i)} \begin{pmatrix} \{\varepsilon^{(0)}\} \\ \{\varepsilon^{(1)}\} \\ \{\varepsilon^{(2)}\} \\ \{\varepsilon^{(3)}\} \end{pmatrix}_{(i)}, \tag{2.19}$$

$$\begin{pmatrix} \{Q\} \\ \{R\} \\ \{S\} \end{pmatrix}_{(i)} = \begin{bmatrix} [A] & [B] & [D] \\ [B] & [D] & [E] \\ [D] & [E] & [F] \end{bmatrix}_{(i)} \begin{pmatrix} \{\gamma^{(0)}\} \\ \{\gamma^{(1)}\} \\ \{\gamma^{(2)}\} \end{pmatrix}_{(i)}, \tag{2.20}$$

where: $\{N\}^{\mathrm{T}}_{(i)} = \{ N_x \ \ N_y \ \ N_{xy} \}_{(i)}$ is the vector of in-plane plate forces, $\{M\}^{\mathrm{T}}_{(i)} = \{ M_x \ \ M_y \ \ M_{xy} \}_{(i)}$ is the vector of bending and twisting moments, $\{Q\}^{\mathrm{T}}_{(i)} = \{ Q_x \ \ Q_y \}_{(i)}$ is the vector of transverse shear forces, and finally $\{L\}^{\mathrm{T}}_{(i)} = \{ L_x \ \ L_y \ \ L_{xy} \}_{(i)}$, $\{P\}^{\mathrm{T}}_{(i)} = \{ P_x \ \ P_y \ \ P_{xy} \}_{(i)}$ and $\{R\}^{\mathrm{T}}_{(i)} = \{ R_x \ \ R_y \}_{(i)}$, $\{S\}^{\mathrm{T}}_{(i)} = \{ S_x \ \ S_y \}_{(i)}$ are the vectors of higher-order stress resultants. In Eqs.(2.19)-(2.20) A_{pq} is the extensional, B_{pq} is coupling, D_{pq} is the bending, E_{pq}, F_{pq}, G_{pq} and H_{pq} are higher-order stiffnesses defined as (*Szekrényes (2014c)*):

$$(A_{pq}, B_{pq}, D_{pq}, E_{pq}, F_{pq}, G_{pq}, H_{pq})_{(i)} = \sum_{m=1}^{N_{l(i)}} \int\limits_{z_m^{(i)}}^{z_{m+1}^{(i)}} \overline{C}_{pq}^{(m)} (1, z, z^2, z^3, z^4, z^5, z^6)^{(i)} dz^{(i)}, \tag{2.21}$$

where $N_{l(i)}$ is the number of layers in the i^{th} ESL. The stiffnesses above have to be calculated with respect to the local reference planes (midplanes) for each ESL. This leads to:

$$\begin{aligned}
A_{pq(i)} &= \sum_{m=1..N_{l(i)}} \bar{C}_{pq}^{(m)} (z_{m+1}^{(i)} - z_m^{(i)}), & B_{pq(i)} &= \tfrac{1}{2} \sum_{m=1..N_{l(i)}} \bar{C}_{pq}^{(m)} ((z_{m+1}^{(i)})^2 - (z_m^{(i)})^2), \\
D_{pq(i)} &= \tfrac{1}{3} \sum_{m=1..N_{l(i)}} \bar{C}_{pq}^{(m)} ((z_{m+1}^{(i)})^3 - (z_m^{(i)})^3), & E_{pq(i)} &= \tfrac{1}{4} \sum_{m=1..N_{l(i)}} \bar{C}_{pq}^{(m)} ((z_{m+1}^{(i)})^4 - (z_m^{(i)})^4), \\
F_{pq(i)} &= \tfrac{1}{5} \sum_{m=1..N_{l(i)}} \bar{C}_{pq}^{(m)} ((z_{m+1}^{(i)})^5 - (z_m^{(i)})^5), & G_{pq(i)} &= \tfrac{1}{6} \sum_{m=1..N_{l(i)}} \bar{C}_{pq}^{(m)} ((z_{m+1}^{(i)})^6 - (z_m^{(i)})^6), \\
H_{pq(i)} &= \tfrac{1}{7} \sum_{m=1..N_{l(i)}} \bar{C}_{pq}^{(m)} ((z_{m+1}^{(i)})^7 - (z_m^{(i)})^7),
\end{aligned} \tag{2.22}$$

where $z_{m+1}^{(i)}$ and $z_m^{(i)}$ are the local top and bottom coordinates of the m^{th} layer in the i^{th} ESL. By using the stress resultants by Eqs.(2.19)-(2.20) and the virtual strains the virtual strain energy of the i^{th} ESL becomes:

$$\begin{aligned}
\delta\mathcal{U}_{(i)} = \int\limits_{\Omega_0} \Big\{ & N_{x(i)} \delta\varepsilon_{x(i)}^{(0)} + M_{x(i)} \delta\varepsilon_{x(i)}^{(1)} + L_{x(i)} \delta\varepsilon_{x(i)}^{(2)} + P_{x(i)} \delta\varepsilon_{x(i)}^{(3)} \\
& + N_{y(i)} \delta\varepsilon_{y(i)}^{(0)} + M_{y(i)} \delta\varepsilon_{y(i)}^{(1)} + L_{y(i)} \delta\varepsilon_{y(i)}^{(2)} + P_{y(i)} \delta\varepsilon_{y(i)}^{(3)} \\
& + N_{xy(i)} \delta\gamma_{xy(i)}^{(0)} + M_{xy(i)} \delta\gamma_{xy(i)}^{(1)} + L_{xy(i)} \delta\gamma_{xy(i)}^{(2)} + L_{xy(i)} \delta\gamma_{xy(i)}^{(3)} \\
& + Q_{x(i)} \delta\gamma_{xz(i)}^{(0)} + R_{x(i)} \delta\gamma_{xz(i)}^{(1)} + S_{x(i)} \delta\gamma_{xz(i)}^{(2)} \\
& + Q_{y(i)} \delta\gamma_{yz(i)}^{(0)} + R_{y(i)} \delta\gamma_{yz(i)}^{(1)} + S_{y(i)} \delta\gamma_{yz(i)}^{(2)} \Big\} dxdy,
\end{aligned} \tag{2.23}$$

moreover, the work done on the i^{th} ESL is:

$$\begin{aligned}
\delta\mathcal{W}_{F(i)} = & \int\limits_{\Omega_0} \big(q_{b(i)}(x,y) \delta w(x,y,-t_i/2) + q_{t(i)}(x,y) \delta w(x,y,t_i/2) \big) dxdy \\
& + \int\limits_{\Gamma_{\sigma(i)}} \Big\{ \bar{N}_{n(i)} \delta u_{n(i)}^{(0)} + \bar{M}_{n(i)} \delta u_{n(i)}^{(1)} + \bar{L}_{n(i)} \delta u_{n(i)}^{(2)} + \bar{P}_{n(i)} \delta u_{n(i)}^{(3)} \\
& + \bar{N}_{ns(i)} \delta u_{s(i)}^{(0)} + \bar{M}_{ns(i)} \delta u_{s(i)}^{(1)} + \bar{L}_{ns(i)} \delta u_{s(i)}^{(2)} + \bar{P}_{ns(i)} \delta u_{s(i)}^{(3)} + \bar{Q}_{n(i)} \delta w_{(i)} \Big\} ds,
\end{aligned} \tag{2.24}$$

where the overline means imposed loads at the curved boundary, viz. $\bar{N}_{n(i)}$ and $\bar{N}_{ns(i)}$ are imposed forces, $\bar{Q}_{n(i)}$ is the imposed shear force, $\bar{M}_{n(i)}$ and $\bar{M}_{ns(i)}$ are imposed moments, $\bar{L}_{n(i)}$, $\bar{L}_{ns(i)}$, $\bar{P}_{n(i)}$ and $\bar{P}_{ns(i)}$ are imposed higher-order forces and moments. By using Eq.(2.8) we arrive the following expression:

$$\begin{aligned}\delta W_{F(i)} = &\int\limits_{\Omega_0} \left(q_{b(i)}(x,y)\delta w(x,y,-t_i/2) + q_{t(i)}(x,y)\delta w(x,y,t_i/2)\right) dxdy \\ &+ \int\limits_{\Gamma_{\sigma(i)}} \Big\{ \bar{N}_{n(i)}\delta u^{(0)}_{n(i)} + (\bar{N}_{n(i)}K^{(0)}_{ij} + \bar{M}_{n(i)}K^{(1)}_{ij} + \bar{L}_{n(i)}K^{(2)}_{ij} + \bar{P}_{n(i)}K^{(3)}_{ij})\delta\psi_{(n)j} \\ &+ (\bar{N}_{ns(i)}K^{(0)}_{ij} + \bar{M}_{ns(i)}K^{(1)}_{ij} + \bar{L}_{ns(i)}K^{(2)}_{ij} + \bar{P}_{ns(i)}K^{(3)}_{ij})\delta\psi_{(s)j} + \bar{Q}_{n(i)}\delta w_{(i)} \Big\} ds,\end{aligned} \tag{2.25}$$

where $\delta\psi_{(n)j}$ and $\delta\psi_{(s)j}$ are the components of the virtual vector of primary parameters in the coordinate system of the curved boundary of the plate. To determine the virtual strain components in Eq.(2.23) in terms of the virtual displacement parameters, we apply the virtual form of Eq.(2.9) resulting in $\delta\varepsilon^{(0)}_{x(i)} = \partial(\delta u_0 + K^{(0)}_{ij}\delta\psi_{(x)j})/\partial x$, ...etc., for each ESL. To transform Eq.(2.23) we apply the chain rule and the divergence theorem (*Reddy (2004)*):

$$N_x\frac{\partial(\delta u_0)}{\partial x} = \frac{\partial(N_x\delta u_0)}{\partial x} - \frac{\partial N_x}{\partial x}\delta u_0..., \quad \int_\Omega \frac{\partial(N_x\delta u_0)}{\partial x}d\Omega = \oint_\Gamma n_x(N_x\delta u_0)ds..., \text{etc.} \tag{2.26}$$

Thus, we have:

$$\begin{aligned}\delta\mathcal{U}_{(i)} = &\int\limits_{\Omega_0} \big\{ -(N_{x(i),x} + N_{xy(i),y})\delta u_0 - (N_{xy(i),x} + N_{y(i),y})\delta v_0 \\ &-(N_{x(i),x} + N_{xy(i),y})K^{(0)}_{ij}\delta\psi_{(x)j} - (N_{xy(i),x} + N_{y(i),y})K^{(0)}_{ij}\delta\psi_{(y)j} \\ &-(M_{x(i),x} + M_{xy(i),y})K^{(1)}_{ij}\delta\psi_{(x)j} - (M_{xy(i),x} + M_{y(i),y})K^{(1)}_{ij}\delta\psi_{(y)j} \\ &-(L_{x(i),x} + L_{xy(i),y})K^{(2)}_{ij}\delta\psi_{(x)j} - (L_{xy(i),x} + L_{y(i),y})K^{(2)}_{ij}\delta\psi_{(y)j} \\ &-(P_{x(i),x} + P_{xy(i),y})K^{(3)}_{ij}\delta\psi_{(x)j} - (P_{xy(i),x} + P_{y(i),y})K^{(3)}_{ij}\delta\psi_{(y)j} \\ &+Q_{x(i)}K^{(1)}_{ij}\delta\psi_{(x)j} - Q_{x(i),x}\delta w + R_{x(i)}K^{(2)}_{ij}\delta\psi_{(x)j} + S_{x(i)}K^{(3)}_{ij}\delta\psi_{(x)j} \\ &+Q_{y(i)}K^{(1)}_{ij}\delta\psi_{(y)j} - Q_{y(i),y}\delta w + R_{y(i)}K^{(2)}_{ij}\delta\psi_{(y)j} + S_{y(i)}K^{(3)}_{ij}\delta\psi_{(y)j} \big\} dxdy \\ &+ \int\limits_{\Gamma_\sigma} \big[(N_{x(i)}n_{x(i)} + N_{xy(i)}n_{y(i)})\delta u_0 + (N_{xy(i)}n_{x(i)} + N_{y(i)}n_{y(i)})\delta v_0 \\ &+(N_{x(i)}n_{x(i)} + N_{xy(i)}n_{y(i)})K^{(0)}_{ij}\delta\psi_{(x)j} + (N_{xy(i)}n_{x(i)} + N_{y(i)}n_{y(i)})K^{(0)}_{ij}\delta\psi_{(y)j} \\ &+(M_{x(i)}n_{x(i)} + M_{xy(i)}n_{y(i)})K^{(1)}_{ij}\delta\psi_{(x)j} + (M_{xy(i)}n_{x(i)} + M_{y(i)}n_{y(i)})K^{(1)}_{ij}\delta\psi_{(y)j} \\ &+(L_{x(i)}n_{x(i)} + L_{xy(i)}n_{y(i)})K^{(2)}_{ij}\delta\psi_{(x)j} + (L_{xy(i)}n_{x(i)} + L_{y(i)}n_{y(i)})K^{(2)}_{ij}\delta\psi_{(y)j} \\ &+(P_{x(i)}n_{x(i)} + P_{xy(i)}n_{y(i)})K^{(3)}_{ij}\delta\psi_{(x)j} + (P_{xy(i)}n_{x(i)} + P_{y(i)}n_{y(i)})K^{(3)}_{ij}\delta\psi_{(y)j} \\ &+(Q_{x(i)}n_{x(i)} + Q_{y(i)}n_{y(i)})\delta w\big] ds,\end{aligned} \tag{2.27}$$

where the comma means differentiation. The first term in Eq.(2.27) is the virtual strain energy related to the volume domain of the ESL, the second term is an expression related to the boundary. By utilizing the simple transformation equations below it is possible to transform the boundary expression in Eq.(2.27) to the same form as that in Eq.(2.24):

$$\begin{aligned}&u_0 = n_x u_{0n} - n_y u_{0s}, \quad v_0 = n_y u_{0n} + n_x u_{0s}, \\ &\psi_{(x)j} = n_x\psi_{(n)j} - n_y\psi_{(s)j}, \quad \psi_{(y)j} = n_y\psi_{(n)j} + n_x\psi_{(s)j},\end{aligned} \tag{2.28}$$

where u_{0n} and u_{0s} are the membrane displacements, $\psi_{(n)j}$ and $\psi_{(s)j}$ are the vectors of primary parameters in the coordinate system of the curved edge of the plate. The equilibrium equations and the natural boundary conditions can be obtained by setting the coefficients of the virtual displacement parameters in the virtual work expression (Eq.(2.12)) using Eqs.(2.27) and (2.24) on the domains Ω_0 and Γ_σ (*Reddy (2004)*). The equilibrium equations are detailed in the next section.

2.4 Equilibrium equations - Invariant form

To derive the equilibrium equations of the plate system in a compact and invariant form we define the following vectors:

$$\begin{aligned} \mathbf{N}_i^{(x,xy)} &= \begin{pmatrix} N_x & N_{xy} \end{pmatrix}^T_{(i)}, \quad \mathbf{N}_i^{(xy,y)} = \begin{pmatrix} N_{xy} & N_y \end{pmatrix}^T_{(i)}, \\ \mathbf{M}_i^{(x,xy)} &= \begin{pmatrix} M_x & M_{xy} \end{pmatrix}^T_{(i)}, \quad \mathbf{M}_i^{(xy,y)} = \begin{pmatrix} M_{xy} & M_y \end{pmatrix}^T_{(i)}. \end{aligned} \tag{2.29}$$

The vectors of higher-order stress resultants become:

$$\begin{aligned} \mathbf{L}_i^{(x,xy)} &= \begin{pmatrix} L_x & L_{xy} \end{pmatrix}^T_{(i)}, \quad \mathbf{L}_i^{(xy,y)} = \begin{pmatrix} L_{xy} & L_y \end{pmatrix}^T_{(i)}, \\ \mathbf{P}_i^{(x,xy)} &= \begin{pmatrix} P_x & P_{xy} \end{pmatrix}^T_{(i)}, \quad \mathbf{P}_i^{(xy,y)} = \begin{pmatrix} P_{xy} & P_y \end{pmatrix}^T_{(i)}. \end{aligned} \tag{2.30}$$

Finally, the vectors of shear and higher-order forces become:

$$\mathbf{Q}_i = \begin{pmatrix} Q_x & Q_y \end{pmatrix}^T_{(i)}, \quad \mathbf{R}_i = \begin{pmatrix} R_x & R_y \end{pmatrix}^T_{(i)}, \quad \mathbf{S}_i = \begin{pmatrix} S_x & S_y \end{pmatrix}^T_{(i)}. \tag{2.31}$$

In the sequel the equilibrium equations are derived separately for the undelaminated and delaminated regions.

2.4.1 Undelaminated region

By setting the sum of coefficients for the virtual membrane displacements (δu_0, δv_0), primary parameters ($\delta\psi_{(x)j}$, $\delta\psi_{(y)j}$) and the deflection (δw) in Eq.(2.12) (using Eqs.(2.27) and (2.25)) to zero leads to three sets of equations. The equilibrium of the in-plane forces involves the equations above independently of the applied theory (FSDT, SSDT or TSDT):

$$\delta u_0: \quad \sum_{i=1}^{k} \nabla \cdot \mathbf{N}_i^{(x,xy)} = 0, \quad \delta v_0: \quad \sum_{i=1}^{k} \nabla \cdot \mathbf{N}_i^{(xy,x)} = 0, \tag{2.32}$$

where $\nabla = \frac{\partial}{\partial x}\mathbf{i} + \frac{\partial}{\partial y}\mathbf{j}$ is the Hamilton differential operator (*Chou and Pagano (1967)*) and k is the total number of ESLs. In the general sense (using FSDT, SSDT or TSDT) the number of primary parameters (ignoring the global membrane displacements) in the displacement field is r, which is equal to the number of elements in $\boldsymbol{\psi}_{(p)}$ and $j = 1..r$. By collecting the coefficients of the virtual primary displacement parameters in Eq.(2.12) and equating the result to zero we have the following equations:

$$\left.\begin{matrix} \delta\psi_{(x)j}: \\ \delta\psi_{(y)j}: \end{matrix}\right\} \quad \sum_{i=1}^{k} K_{ij}^{(0)} \begin{pmatrix} \nabla \cdot \mathbf{N}_i^{(x,xy)} \\ \nabla \cdot \mathbf{N}_i^{(xy,y)} \end{pmatrix} + K_{ij}^{(1)} \begin{pmatrix} \nabla \cdot \mathbf{M}_i^{(x,xy)} \\ \nabla \cdot \mathbf{M}_i^{(xy,y)} \end{pmatrix} + K_{ij}^{(2)} \begin{pmatrix} \nabla \cdot \mathbf{L}_i^{(x,xy)} \\ \nabla \cdot \mathbf{L}_i^{(xy,y)} \end{pmatrix} +$$
$$K_{ij}^{(3)} \begin{pmatrix} \nabla \cdot \mathbf{P}_i^{(x,xy)} \\ \nabla \cdot \mathbf{P}_i^{(xy,y)} \end{pmatrix} - K_{ij}^{(1)} \begin{pmatrix} Q_{x(i)} \\ Q_{y(i)} \end{pmatrix} - 2K_{ij}^{(2)} \begin{pmatrix} R_{x(i)} \\ R_{y(i)} \end{pmatrix} - 3K_{ij}^{(3)} \begin{pmatrix} S_{x(i)} \\ S_{y(i)} \end{pmatrix} = \begin{pmatrix} 0 \\ 0 \end{pmatrix},$$

(2.33)

where $\psi_{(x)j}$ and $\psi_{(y)j}$ denote the primary parameters. By collecting the coefficients of the $\delta w(x,y)$ plate deflection and setting their sum to zero in Eq.(2.12) leads to:

$$\delta w: \quad \sum_{i=1}^{k} \nabla \cdot \hat{\mathbf{Q}}_i + q = 0, \tag{2.34}$$

where q is the the external surface load:

$$q = \sum_{i=1}^{k} (q_{b(i)} + q_{t(i)}), \tag{2.35}$$

moreover $\hat{\mathbf{Q}}$ is the effective shear force in the case of Reddy's third-order theory (see later) and $\hat{\mathbf{Q}} = \mathbf{Q}$ for the other theories. Eqs.(2.32)-(2.34) define the invariant form of the equilibrium equations, because independently of the applied theory these equations have the same form. Apparently, the differences among the equilibrium equations of FSDT, SSDT and TSDT are the K_{ij} displacement multiplicator matrix elements and the $\boldsymbol{\psi}_{(p)}$ vector of primary parameters.

2.4.2 Delaminated region

The delaminated region consists of a top and a bottom plate (refer to Figures 2.1, 2.2 and 2.3). Each subplate is modeled by further ESLs. The most essential difference between the delaminated and undelaminated plate regions is that in the delaminated region the in-plane displacements are not coupled at the delamination plane. Therefore, the global membrane displacements u_0, v_0 are replaced by u_{0b}, v_{0b} for ESLs of the bottom plate, moreover by u_{0t}, v_{0t} for the ESLs of the top plate in Eq.(2.8) in accordance with Figures 2.2 and 2.3:

$$\begin{aligned} u_{(i)} &= u_{0b} + \left(K_{ij}^{(0)} + K_{ij}^{(1)} z^{(i)} + K_{ij}^{(2)} [z^{(i)}]^2 + K_{ij}^{(3)} [z^{(i)}]^3\right) \psi_{(x)j}, \quad i = 1..h, \\ v_{(i)} &= v_{0b} + \left(K_{ij}^{(0)} + K_{ij}^{(1)} z^{(i)} + K_{ij}^{(2)} [z^{(i)}]^2 + K_{ij}^{(3)} [z^{(i)}]^3\right) \psi_{(y)j}, \quad i = 1..h, \end{aligned} \tag{2.36}$$

$$\begin{aligned} u_{(i)} &= u_{0t} + \left(K_{ij}^{(0)} + K_{ij}^{(1)} z^{(i)} + K_{ij}^{(2)} [z^{(i)}]^2 + K_{ij}^{(3)} [z^{(i)}]^3\right) \psi_{(x)j}, \quad i = h+1..k, \\ v_{(i)} &= v_{0t} + \left(K_{ij}^{(0)} + K_{ij}^{(1)} z^{(i)} + K_{ij}^{(2)} [z^{(i)}]^2 + K_{ij}^{(3)} [z^{(i)}]^3\right) \psi_{(y)j}, \quad i = h+1..k, \end{aligned} \tag{2.37}$$

where h is the number of ESLs in the bottom plate and j is a summation index, furthermore $w_{(i)}(x,y) = w(x,y)$. Thus, the equilibrium equations of in-plane forces take the form below:

$$\begin{aligned} \delta u_{0b}: \quad & \sum_{i=1}^{h} \nabla \cdot \mathbf{N}_i^{(x,xy)} = 0, \quad \delta u_{0t}: \quad \sum_{i=h+1}^{k} \nabla \cdot \mathbf{N}_i^{(x,xy)} = 0, \\ \delta v_{0b}: \quad & \sum_{i=1}^{h} \nabla \cdot \mathbf{N}_i^{(xy,x)} = 0, \quad \delta v_{0t}: \quad \sum_{i=h+1}^{k} \nabla \cdot \mathbf{N}_i^{(xy,x)} = 0. \end{aligned} \tag{2.38}$$

The form of the other equilibrium equations are the same as those given by Eqs.(2.33)-(2.34).

Finally, it is time to denote that the fundamental solutions of LEFM are singular for problems including cracks (*Anderson (2005); Hills et al. (1996)*). On the contrary, Eq.(2.8) and Eqs.(2.36)-(2.37) do not contain any singular terms, thus the solutions in this work are essentially nonsingular for all of the mechanical fields.

3
The method of two equivalent single layers

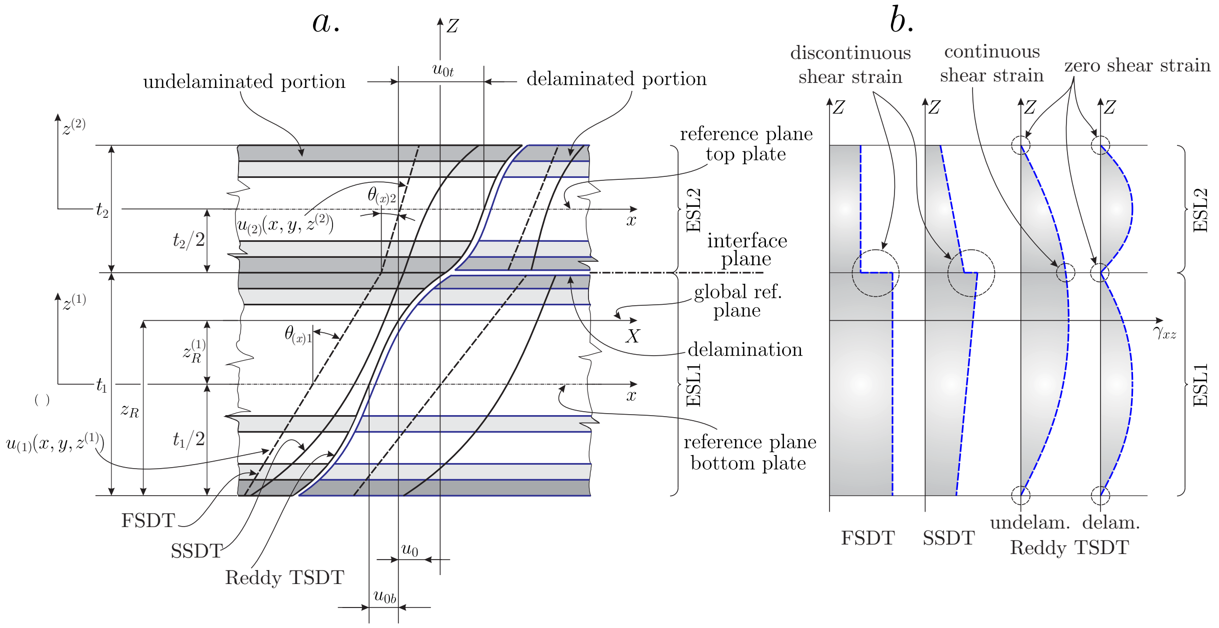

Figure 3.1: Cross sections and deformation of the top (ESL2) and bottom (ESL1) plate elements of a delaminated plate in the Y-Z plane (a). Distribution of the transverse shear strains by FSDT, SSDT and Reddy TSDT (b).

In the case of the method of 2ESLs the plate is divided into two parts by the plane of the delamination. These parts are further divided into two halves along the delamination front perpendicularly to the plane of the plate midsurface resulting in the undelaminated and delaminated portions. This latter fact is represented by the transverse splitting in Figures 3.1. and 3.2 The SEKC is applied to the problem in accordance with Figures 3.1 and 3.2. Using the SEKC defined by Eqs.(2.2)-(2.6) we can eliminate certain parameters from Eq.(2.1), which involves 18 parameters altogether plus the deflections ($w_{(i)}(x, y) = w(x, y)$). This step is called *parameter elimination* (defined in Section 2.2). The parameters to be eliminated are chosen in order to obtain a system of equations, which consists of linearly independent equations. In the subsequent sections the undelaminated and delaminated

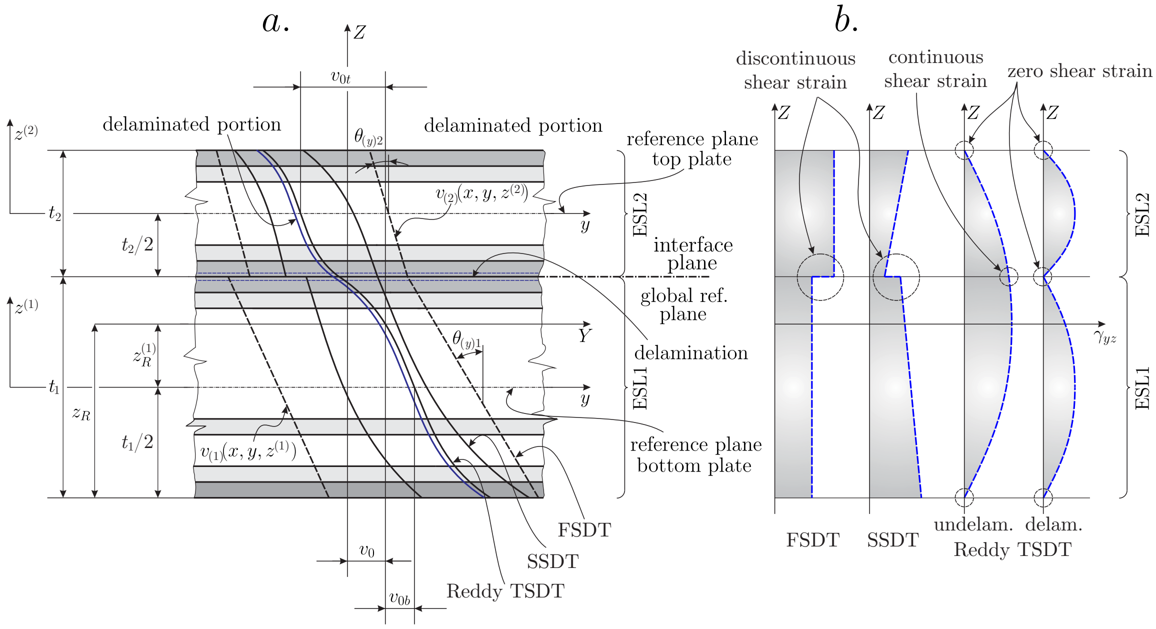

Figure 3.2: Cross sections and deformation of the top (ESL2) and bottom (ESL1) plate elements of a delaminated plate in the Y-Z plane (a). Distribution of the transverse shear strains by FSDT, SSDT and Reddy TSDT (b).

regions are discussed separately. In the first step, the Reddy TSDT displacement field is presented (*Szekrényes (2014c)*), then in the subsequent steps the SSDT *(Szekrényes (2015))* and FSDT *(Szekrényes (2013c))* fields are obtained by the reduction of the Reddy TSDT equations.

3.1 Undelaminated region

The transition zone around the delamination front in the $X-Z$ plane of the composite plate is shown in Figure 3.1a. The through-thickness distribution of the in-plane displacement functions is piecewise cubic for the Reddy TSDT, piecewise quadratic in the case of the SSDT and piecewise linear for FSDT. The corresponding shear strain distributions are shown in Figure 3.1b: it is piecewise quadratic by Reddy TSDT, piecewise linear by SSDT and piecewise constant by FSDT. In Figure 3.2 the $Y-Z$ plane is shown. In accordance with Figures 3.1a and 3.2a, the following conditions are formulated between the two ESLs (continuity of in-plane displacement at the interface planes):

$$(u_{(1)}, v_{(1)}, w_{(1)})\big|_{z^{(1)}=t_1/2} = (u_{(2)}, v_{(2)}, w_{(2)})\big|_{z^{(2)}=-t_2/2}. \tag{3.1}$$

The reference plane belongs to the first ESL, therefore, the following condition is imposed:

$$(u_{(1)}, v_{(1)})\big|_{z^{(1)}=z_R^{(1)}} = (u_0(x,y), v_0(x,y)), \tag{3.2}$$

where the $z_R^{(1)} = t_2/2$, $z_R = 1/2(t_1+t_2)$ in accordance with Figure 3.1a and actually z_R coincides with the global midplane of the model (*Reddy (2004)*). The next set of conditions impose continuous shear strains at the interface plane:

$$(\gamma_{xz(1)}, \gamma_{yz(1)})\big|_{z^{(1)}=t_1/2} = (\gamma_{xz(2)}, \gamma_{yz(2)})\big|_{z^{(2)}=-t_2/2}. \tag{3.3}$$

Finally, in accordance with the basic concept of Reddy plate theory (*Reddy (2004)*) we impose traction-free bottom and top surfaces by (refer to Figures 3.1b and 3.2b):

$$(\gamma_{xz(1)}, \gamma_{yz(1)})\big|_{z^{(1)}=-t_1/2} = (\gamma_{xz(2)}, \gamma_{yz(2)})\big|_{z^{(2)}=t_2/2} = 0. \tag{3.4}$$

In Eq.(2.1) the displacement functions are modified in order to satisfy Eqs.(3.1)-(3.4). In the case of the method of 2ESLs ($i = 1..2$), by applying the FSDT, SSDT and Reddy TSDT theories the in-pane displacement functions can be written as:

$$\begin{aligned} u_{(i)} &= u_0 + \left(K_{ij}^{(0)} + K_{ij}^{(1)} z^{(i)} + K_{ij}^{(2)} [z^{(i)}]^2 + K_{ij}^{(3)} [z^{(i)}]^3\right) \psi_{(x)j}, \quad i = 1..2, \\ v_{(i)} &= v_0 + \left(K_{ij}^{(0)} + K_{ij}^{(1)} z^{(i)} + K_{ij}^{(2)} [z^{(i)}]^2 + K_{ij}^{(3)} [z^{(i)}]^3\right) \psi_{(y)j}, \quad i = 1..2, \\ w_{(i)} &= w(x, y), \quad i = 1..2, \end{aligned} \tag{3.5}$$

where the matrices denoted by K_{ij} are related to the geometry (ESL thicknesses), i refers to the ESL number, the summation index j defines the component in $\boldsymbol{\psi}$, which is the vector of primary parameters, finally $w_{(i)}(x, y) = w(x, y)$ for each ESL.

3.1.1 Reddy's third-order plate theory

Using the conditions above (Eqs.(3.1)-(3.4)) we can eliminate ten parameters from Eq.(2.1), the secondary parameters are: u_{0i}, v_{0i}, $\theta_{(x)2}$, $\theta_{(y)2}$, $\phi_{(x)i}$, $\phi_{(y)i}$ for $i = 1, 2$. The vector of primary parameters is:

$$\boxed{\boldsymbol{\psi}_{(p)} = \begin{pmatrix} \theta_{(p)1} & \lambda_{(p)2} & \lambda_{(p)1} & \frac{\partial w}{\partial p} \end{pmatrix}^T, \quad p{=}x \text{ or } y,} \tag{3.6}$$

where the elements highlighted by the circles are the so-called autocontinuity parameters (see later in Chapter 4.). The calculation of elements of the matrices $K_{ij}^{(0)}$, $K_{ij}^{(1)}$, $K_{ij}^{(2)}$ and $K_{ij}^{(3)}$ are defined in Appendix A.1. The equilibrium equations of Reddy TSDT based on Eq.(3.6) and (2.33) are:

$$\delta u_0 : \sum_{i=1}^{2} \frac{\partial N_{x(i)}}{\partial x} + \frac{\partial N_{xy(i)}}{\partial y} = 0, \quad \delta v_0 : \sum_{i=1}^{2} \frac{\partial N_{xy(i)}}{\partial x} + \frac{\partial N_{y(i)}}{\partial y} = 0, \tag{3.7}$$

for the membrane displacements and:

$$\begin{aligned} \delta\psi_{(x)j} : \sum_{i=1}^{2} K_{ij}^{(0)} \left(\frac{\partial N_{x(i)}}{\partial x} + \frac{\partial N_{xy(i)}}{\partial y}\right) + K_{ij}^{(1)} \left(\frac{\partial M_{x(i)}}{\partial x} + \frac{\partial M_{xy(i)}}{\partial y}\right) + K_{ij}^{(2)} \left(\frac{\partial L_{x(i)}}{\partial x} + \frac{\partial L_{xy(i)}}{\partial y}\right) \\ + K_{ij}^{(3)} \left(\frac{\partial P_{x(i)}}{\partial x} + \frac{\partial P_{xy(i)}}{\partial y}\right) - K_{ij}^{(1)} Q_{x(i)} - 2K_{ij}^{(2)} R_{x(i)} - 3K_{ij}^{(3)} S_{x(i)} = 0, \quad j = 1..3, \\ \delta\psi_{(y)j} : \sum_{i=1}^{2} K_{ij}^{(0)} \left(\frac{\partial N_{xy(i)}}{\partial x} + \frac{\partial N_{y(i)}}{\partial y}\right) + K_{ij}^{(1)} \left(\frac{\partial M_{xy(i)}}{\partial x} + \frac{\partial M_{y(i)}}{\partial y}\right) + K_{ij}^{(2)} \left(\frac{\partial L_{xy(i)}}{\partial x} + \frac{\partial L_{y(i)}}{\partial y}\right) \\ + K_{ij}^{(3)} \left(\frac{\partial P_{xy(i)}}{\partial x} + \frac{\partial P_{y(i)}}{\partial y}\right) - K_{ij}^{(1)} Q_{y(i)} - 2K_{ij}^{(2)} R_{y(i)} - 3K_{ij}^{(3)} S_{y(i)} = 0, \quad j = 1..3, \end{aligned}$$

$$(3.8)$$

with respect to the primary parameters, furthermore the following equation is obtained based on the deflection:

$$\delta w : \sum_{i=1}^{2} \left(\frac{\partial \hat{Q}_{x(i)}}{\partial x} + \frac{\partial \hat{Q}_{y(i)}}{\partial y} \right) + q = 0, \tag{3.9}$$

where $\hat{Q}_x$ and $\hat{Q}_y$ are the equivalent shear forces:

$$\begin{aligned}
\hat{Q}_{x(i)} = &-K_{i4}^{(0)} \left(\frac{\partial N_{x(i)}}{\partial x} + \frac{\partial N_{xy(i)}}{\partial y} \right) - K_{i4}^{(1)} \left(\frac{\partial M_{x(i)}}{\partial x} + \frac{\partial M_{xy(i)}}{\partial y} \right) - K_{i4}^{(2)} \left(\frac{\partial L_{x(i)}}{\partial x} + \frac{\partial L_{xy(i)}}{\partial y} \right) \\
&-K_{i4}^{(3)} \left(\frac{\partial P_{x(i)}}{\partial x} + \frac{\partial P_{xy(i)}}{\partial y} \right) + Q_{x(i)} + 2K_{i4}^{(2)} R_{x(i)} + 3K_{i4}^{(3)} S_{x(i)}, \\
\hat{Q}_{y(i)} = &-K_{i4}^{(0)} \left(\frac{\partial N_{xy(i)}}{\partial x} + \frac{\partial N_{y(i)}}{\partial y} \right) - K_{i4}^{(1)} \left(\frac{\partial M_{xy(i)}}{\partial x} + \frac{\partial M_{y(i)}}{\partial y} \right) - K_{i4}^{(2)} \left(\frac{\partial L_{xy(i)}}{\partial x} + \frac{\partial L_{y(i)}}{\partial y} \right) \\
&-K_{i4}^{(3)} \left(\frac{\partial P_{xy(i)}}{\partial x} + \frac{\partial P_{y(i)}}{\partial y} \right) + Q_{y(i)} + 2K_{i4}^{(2)} R_{y(i)} + 3K_{i4}^{(3)} S_{y(i)}.
\end{aligned} \tag{3.10}$$

The first in Eq.(3.8) states the moment equilibrium (because the fisrt parameter in Eq.(3.6) is a rotation), moreover Eq.(3.9) is the equilibrium equation of equivalent shear forces (derivatives). By taking back the K_{ij} constants into Eqs.(3.8) and the first of (3.9) (with respect to $\psi_{(x)1} = \theta_{(x)1}$ and $\psi_{(y)1} = \theta_{(y)1}$), and subtracting the equivalent shear forces from Eq.(3.8) it is possible to calculate the equivalent bending moments of the undelaminated region:

$$\begin{pmatrix} \hat{M}_x \\ \hat{M}_y \\ \hat{M}_{xy} \end{pmatrix}_{(i)} = \begin{pmatrix} M_x \\ M_y \\ M_{xy} \end{pmatrix}_{(i)} + (K_{i1}^{(0)} - K_{i4}^{(0)}) \begin{pmatrix} N_x \\ N_y \\ N_{xy} \end{pmatrix}_{(i)}, (K_{i1}^{(0)} - K_{i4}^{(0)}) = \begin{cases} -\frac{1}{2}t_2 & \text{if} \quad i = 1, \\ \frac{1}{2}t_1 & \text{if} \quad i = 2. \end{cases} \tag{3.11}$$

Eq.(3.11) is important, because the continuity and boundary conditions can be imposed by using the equivalent bending moments, or stress resultants. The equations of $\delta\psi_{(x)1}$ and $\delta\psi_{(y)1}$ in Eq.(3.8) can be rewritten as:

$$\delta\psi_{(x)1} : \sum_{i=1}^{2} \frac{\partial \hat{M}_{x(i)}}{\partial x} + \frac{\partial \hat{M}_{xy(i)}}{\partial y} - \hat{Q}_{x(i)} = 0, \quad \delta\psi_{(y)1} : \sum_{i=1}^{2} \frac{\partial \hat{M}_{y(i)}}{\partial y} + \frac{\partial \hat{M}_{xy(i)}}{\partial x} - \hat{Q}_{y(i)} = 0. \tag{3.12}$$

3.1.2 Second-order plate theory

In this case $\lambda_{(x)i} = 0$ and $\lambda_{(y)i} = 0$ in Eq.(2.1). Eqs.(3.1)-(3.2) apply, however Eqs.(3.3)-(3.4) are omitted. It should be mentioned that although it is possible to impose the shear strain continuity even in this case, this was not applied in this thesis (*Szekrényes (2015)*).

Therefore we can eliminate four parameters from Eq.(2.1), the secondary parameters are: u_{0i}, v_{0i} for $i = 1, 2$. The vector of primary parameters becomes:

$$\boxed{\boldsymbol{\psi}_{(p)} = \begin{pmatrix} \theta_{(p)1} & \phi_{(p)1} & \theta_{(p)2} & \phi_{(p)2} \end{pmatrix}^T, \quad p = x \text{ or } y.} \tag{3.13}$$

The elements of the matrices $K_{ij}^{(0)}$, $K_{ij}^{(1)}$ and $K_{ij}^{(2)}$ are defined in Appendix A.2. Obviously $K_{ij}^{(3)} = 0$ in this case. The equilibrium of in-plane forces (equations for δu_0 and δv_0) are given by Eq.(3.7). The equilibrium equations with respect to the primary parameters take the forms of:

$$\begin{aligned}
\delta\psi_{(x)j} : & \sum_{i=1}^{2} K_{ij}^{(0)} \left(\frac{\partial N_{x(i)}}{\partial x} + \frac{\partial N_{xy(i)}}{\partial y} \right) + K_{ij}^{(1)} \left(\frac{\partial M_{x(i)}}{\partial x} + \frac{\partial M_{xy(i)}}{\partial y} \right) + K_{ij}^{(2)} \left(\frac{\partial L_{x(i)}}{\partial x} + \frac{\partial L_{xy(i)}}{\partial y} \right) \\
& -K_{ij}^{(1)} Q_{x(i)} - 2K_{ij}^{(2)} R_{x(i)} = 0, \quad j = 1..4, \\
\delta\psi_{(y)j} : & \sum_{i=1}^{2} K_{ij}^{(0)} \left(\frac{\partial N_{xy(i)}}{\partial x} + \frac{\partial N_{y(i)}}{\partial y} \right) + K_{ij}^{(1)} \left(\frac{\partial M_{xy(i)}}{\partial x} + \frac{\partial M_{y(i)}}{\partial y} \right) + K_{ij}^{(2)} \left(\frac{\partial L_{xy(i)}}{\partial x} + \frac{\partial L_{y(i)}}{\partial y} \right) \\
& -K_{ij}^{(1)} Q_{y(i)} - 2K_{ij}^{(2)} R_{y(i)} = 0, \quad j = 1..4.
\end{aligned} \tag{3.14}$$

The last equation becomes:

$$\delta w : \sum_{i=1}^{2} \left(\frac{\partial Q_{x(i)}}{\partial x} + \frac{\partial Q_{y(i)}}{\partial y} \right) + q = 0. \tag{3.15}$$

Because of the fact that the first and third parameters in $\boldsymbol{\psi}$ (Eq.(3.13)) are rotations, the equations for $j = 1, 3$ state the moment equilibrium. Summing the first ($j = 1$) and third ($j = 3$) equations in Eq.(3.14) and taking back the K_{ij} constants in Appendix A.1 results in:

$$\sum_{i=1}^{2} \frac{\partial \hat{M}_{x(i)}}{\partial x} + \frac{\partial \hat{M}_{xy(i)}}{\partial y} - Q_{x(i)} = 0, \quad \sum_{i=1}^{2} \frac{\partial \hat{M}_{y(i)}}{\partial y} + \frac{\partial \hat{M}_{xy(i)}}{\partial x} - Q_{y(i)} = 0, \tag{3.16}$$

where the only difference compared to Eq.(3.12) is that in this case there are no effective shear forces, only equivalent moments that become the same as those by Eq.(3.11):

$$\begin{pmatrix} \hat{M}_x \\ \hat{M}_y \\ \hat{M}_{xy} \end{pmatrix}_{(i)} = \begin{pmatrix} M_x \\ M_y \\ M_{xy} \end{pmatrix}_{(i)} + (K_{i1}^{(0)} + K_{i3}^{(0)}) \begin{pmatrix} N_x \\ N_y \\ N_{xy} \end{pmatrix}_{(i)}, (K_{i1}^{(0)} + K_{i3}^{(0)}) = \begin{cases} -\frac{1}{2}t_2 & \text{if} \quad i = 1, \\ \frac{1}{2}t_1 & \text{if} \quad i = 2. \end{cases} \tag{3.17}$$

The physical meaning of Eq.(3.17) is that the equivalent moments are equal to the sum of the standard bending/twisting moments and the moment of the in-plane normal/shear forces, where the arm of the forces is calculated as the distance between the local and global reference plane of the plate (*Szekrényes (2014d)*).

3.1.3 First-order plate theory

In this case $\phi_{(x)i} = \phi_{(y)i} = 0$, $\lambda_{(x)i} = \lambda_{(y)i} = 0$ in Eq.(2.1). Eqs.(3.1)-(3.2) apply, however Eqs.(3.3)-(3.4) are omitted again (shear strain continuity at the interface plane is not possible to ensure because of the piecewise constant distributions, refer to Figure 3.1b). Thus, we can eliminate only four parameters from Eq.(2.1), the secondary parameters are: u_{0i}, v_{0i} for $i = 1, 2$. The vector of primary parameters is:

$$\boxed{\boldsymbol{\psi}_{(p)} = \begin{pmatrix} \theta_{(p)1} & \theta_{(p)2} \end{pmatrix}^T, \quad p = x \text{ or } y.} \tag{3.18}$$

The elements of the matrices $K_{ij}^{(0)}$ and $K_{ij}^{(1)}$ are defined in Appendix A.3. Apparently $K_{ij}^{(2)} = K_{ij}^{(3)} = 0$ in this case. The in-plane equilibrium is defined by Eq.(3.7). The moment equilibrium equations are:

$$\begin{aligned}
\delta\psi_{(x)j}: \sum_{i=1}^{2} K_{ij}^{(0)} \left(\frac{\partial N_{x(i)}}{\partial x} + \frac{\partial N_{xy(i)}}{\partial y} \right) + K_{ij}^{(1)} \left(\frac{\partial M_{x(i)}}{\partial x} + \frac{\partial M_{xy(i)}}{\partial y} \right) - K_{ij}^{(1)} Q_{x(i)} = 0, \quad j = 1..2,\\
\delta\psi_{(y)j}: \sum_{i=1}^{2} K_{ij}^{(0)} \left(\frac{\partial N_{xy(i)}}{\partial x} + \frac{\partial N_{y(i)}}{\partial y} \right) + K_{ij}^{(1)} \left(\frac{\partial M_{xy(i)}}{\partial x} + \frac{\partial M_{y(i)}}{\partial y} \right) - K_{ij}^{(1)} Q_{y(i)} = 0, \quad j = 1..2.
\end{aligned} \tag{3.19}$$

The equation for δw is equivalent to Eq.(3.15). The equivalent moments can be obtained by taking back the K_{ij} constants given by Appendix A.3 into Eq.(3.19) and subtracting the shear forces:

$$\begin{pmatrix} \hat{M}_x \\ \hat{M}_y \\ \hat{M}_{xy} \end{pmatrix}_{(i)} = \begin{pmatrix} M_x \\ M_y \\ M_{xy} \end{pmatrix}_{(i)} + (K_{i1}^{(0)} + K_{i2}^{(0)}) \begin{pmatrix} N_x \\ N_y \\ N_{xy} \end{pmatrix}_{(i)}, (K_{i1}^{(0)} + K_{i2}^{(0)}) = \begin{cases} -\frac{1}{2}t_2 & \text{if} \quad i = 1, \\ \frac{1}{2}t_1 & \text{if} \quad i = 2, \end{cases} \tag{3.20}$$

that have an important role in the assignment of the boundary and continuity conditions.

3.2 Delaminated region

In the delaminated region (refer to Figures 3.1b and 3.2b) the top and bottom plates are captured by independent ESLs, and thus these plates are modeled by traditional first-, second-order plates and third-order Reddy plates. The displacement field can be given by:

$$\begin{aligned}
u_{(i)} &= u_{0b} + \left(K_{ij}^{(0)} + K_{ij}^{(1)} z^{(i)} + K_{ij}^{(2)} [z^{(i)}]^2 + K_{ij}^{(3)} [z^{(i)}]^3 \right) \psi_{(x)j}, \quad i = 1,\\
v_{(i)} &= v_{0b} + \left(K_{ij}^{(0)} + K_{ij}^{(1)} z^{(i)} + K_{ij}^{(2)} [z^{(i)}]^2 + K_{ij}^{(3)} [z^{(i)}]^3 \right) \psi_{(y)j}, \quad i = 1,\\
u_{(i)} &= u_{0t} + \left(K_{ij}^{(0)} + K_{ij}^{(1)} z^{(i)} + K_{ij}^{(2)} [z^{(i)}]^2 + K_{ij}^{(3)} [z^{(i)}]^3 \right) \psi_{(x)j}, \quad i = 2,\\
v_{(i)} &= v_{0t} + \left(K_{ij}^{(0)} + K_{ij}^{(1)} z^{(i)} + K_{ij}^{(2)} [z^{(i)}]^2 + K_{ij}^{(3)} [z^{(i)}]^3 \right) \psi_{(y)j}, \quad i = 2,\\
w_{(i)} &= w(x, y), \quad i = 1..2,
\end{aligned} \tag{3.21}$$

viz., the global membrane displacement components are zero in this case and j is a summation index. It is important to note that in accordance with Eq.(3.21) the transverse deflections of the top and bottom plates of the delaminated region are identical (constrained mode model, (*Szekrényes (2014c)*)). In other words, the crack opening is eliminated in the plate, and the problem provides essentially mixed-mode II/III fracture without the presence of mode-I (refer to Figure 1.3). The aim is to predict the mechanical fields in the plate as accurately as possible compared to FE calculations. If this is done for mixed-mode II/III, then the model can be extended to general mixed-mode I/II/III case in the course of further research work.

3.2.1 Reddy's third-order plate theory

In this theory the top and bottom plates are traction-free at the top and bottom boundaries (*Reddy (2004)*, refer to Figures 3.1b and 3.2b), thus, from Eq.(3.4) we have:

$$(\gamma_{xz(1)}, \gamma_{yz(1)})\big|_{z^{(1)}=\pm t_1/2} = (\gamma_{xz(2)}, \gamma_{yz(2)})\big|_{z^{(2)}=\pm t_2/2} = 0, \tag{3.22}$$

meaning eight conditions. The secondary parameters are: $\phi_{(x)i}$, $\phi_{(y)i}$, $\lambda_{(x)i}$, $\lambda_{(y)i}$ for $i = 1..2$. The modified displacement field has the same form as that given by Eq.(3.21), the coefficients denoted by K_{ij} are placed in Appendix A.1. The vector of primary parameters becomes:

$$\boxed{\boldsymbol{\psi}_{(p)} = \begin{pmatrix} \theta_{(p)1} & \theta_{(p)2} & \frac{\partial w}{\partial p} \end{pmatrix}^T, \quad p = x \text{ or } y,} \tag{3.23}$$

where $\theta_{(p)2}$ is an autocontinuity parameter. The equilibrium equations with respect to the membrane displacements are:

$$\delta u_{0(i)} : \frac{\partial N_{x(i)}}{\partial x} + \frac{\partial N_{xy(i)}}{\partial y} = 0, \quad \delta v_{0(i)} : \frac{\partial N_{xy(i)}}{\partial x} + \frac{\partial N_{y(i)}}{\partial y} = 0, \quad i = 1(=b), \quad 2(=t). \tag{3.24}$$

The equilibrium equations for the bending and twisting moments are:

$$\delta\psi_{(x)j} : \frac{\partial \hat{M}_{x(j)}}{\partial x} + \frac{\partial \hat{M}_{xy(j)}}{\partial y} - \hat{Q}_{x(j)} = 0, \quad \delta\psi_{(y)j} : \frac{\partial \hat{M}_{y(j)}}{\partial y} + \frac{\partial \hat{M}_{xy(j)}}{\partial x} - \hat{Q}_{y(j)} = 0, \quad j = 1, 2. \tag{3.25}$$

Finally, the equation with respect to δw in accordance with *Reddy (2004)* is:

$$\delta w : \sum_{i=1}^{2} \left\{ \frac{\partial \hat{Q}_{x(i)}}{\partial x} + \frac{\partial \hat{Q}_{y(i)}}{\partial y} - K_{i1}^{(3)} \left(\frac{\partial^2 P_{x(i)}}{\partial x^2} + 2\frac{\partial^2 P_{xy(i)}}{\partial x \partial y} + \frac{\partial^2 P_{y(i)}}{\partial y^2} \right) \right\} + q = 0, \tag{3.26}$$

where the equivalent shear forces are defined as (*Reddy (2004)*):

$$\hat{Q}_{x(i)} = Q_{x(i)} + 3K_{i3}^{(3)} S_{x(i)}, \quad \hat{Q}_{y(i)} = Q_{y(i)} + 3K_{i3}^{(3)} S_{y(i)}, \quad i = 1, 2. \tag{3.27}$$

Finally, the equivalent bending moments become:

$$\begin{pmatrix} \hat{M}_x \\ \hat{M}_y \\ \hat{M}_{xy} \end{pmatrix}_{(i)} = \begin{pmatrix} M_x \\ M_y \\ M_{xy} \end{pmatrix}_{(i)} + K_{i1}^{(3)} \begin{pmatrix} P_x \\ P_y \\ P_{xy} \end{pmatrix}_{(i)}, i = 1, 2. \tag{3.28}$$

3.2.2 Second-order plate theory

In this case $\lambda_{(x)i} = 0$ and $\lambda_{(y)i} = 0$ in Eq.(2.1). No conditions are imposed against the displacement field, and so there are only primary parameters in Eq.(3.21), the vector of primary parameters takes the form below:

$$\boxed{\boldsymbol{\psi}_{(p)} = \begin{pmatrix} \theta_{(p)1} & \phi_{(p)1} & \theta_{(p)2} & \phi_{(p)2} \end{pmatrix}^T, \quad p = x \text{ or } y.} \tag{3.29}$$

The elements of the matrices $K_{ij}^{(0)}$, $K_{ij}^{(1)}$ and $K_{ij}^{(2)}$ are defined in Appendix A.2. Apparently $K_{ij}^{(3)} = 0$ in this case. The membrane force equilibrium is given by Eq.(3.24), the other equilibrium equations are:

$$\begin{aligned} \delta\theta_{(x)i} &: \frac{\partial M_{x(i)}}{\partial x} + \frac{\partial M_{xy(i)}}{\partial y} - Q_{x(i)} = 0, \quad i = 1, 2, \\ \delta\theta_{(y)i} &: \frac{\partial M_{xy(i)}}{\partial x} + \frac{\partial M_{y(i)}}{\partial y} - Q_{y(i)} = 0, \quad i = 1, 2, \end{aligned} \tag{3.30}$$

$$\begin{aligned} \delta\phi_{(x)i} &: \frac{\partial L_{x(i)}}{\partial x} + \frac{\partial L_{xy(i)}}{\partial y} - 2R_{x(i)} = 0, \quad i = 1, 2, \\ \delta\phi_{(y)i} &: \frac{\partial L_{xy(i)}}{\partial x} + \frac{\partial L_{y(i)}}{\partial y} - 2R_{y(i)} = 0, \quad i = 1, 2. \end{aligned} \tag{3.31}$$

Finally, the shear force equilibrium involves:

$$\delta w : \sum_{i=1}^{2} \left(\frac{\partial Q_{x(i)}}{\partial x} + \frac{\partial Q_{y(i)}}{\partial y} \right) + q = 0. \tag{3.32}$$

3.2.3 First-order plate theory

For the FSDT $\phi_{(x)i} = 0$, $\phi_{(y)i} = 0$, $\lambda_{(x)i} = 0$ and $\lambda_{(y)i} = 0$ in Eq.(2.1). Obviously, there are only primary parameters in Eq.(3.21): u_{0i}, v_{0i}, $\theta_{(x)i}$, $\theta_{(y)i}$ for $i = 1, 2$. The vector of primary parameters is:

$$\boxed{\boldsymbol{\psi}_{(p)} = \begin{pmatrix} \theta_{(p)1} & \theta_{(p)2} \end{pmatrix}^T, \; p = x \text{ or } y.} \tag{3.33}$$

The elements of the matrices $K_{ij}^{(0)}$ and $K_{ij}^{(1)}$ are defined in Appendix A.3. In this case $K_{ij}^{(2)} = K_{ij}^{(3)} = 0$. The in-plane force equilibrium involves Eq.(3.24), the moment and shear force equilibrium leads to:

$$\begin{aligned} \delta\theta_{(x)i} &: \frac{\partial M_{x(i)}}{\partial x} + \frac{\partial M_{xy(i)}}{\partial y} - Q_{x(i)} = 0, \quad i = 1, 2, \\ \delta\theta_{(y)i} &: \frac{\partial M_{xy(i)}}{\partial x} + \frac{\partial M_{y(i)}}{\partial y} - Q_{y(i)} = 0, \quad i = 1, 2, \end{aligned} \tag{3.34}$$

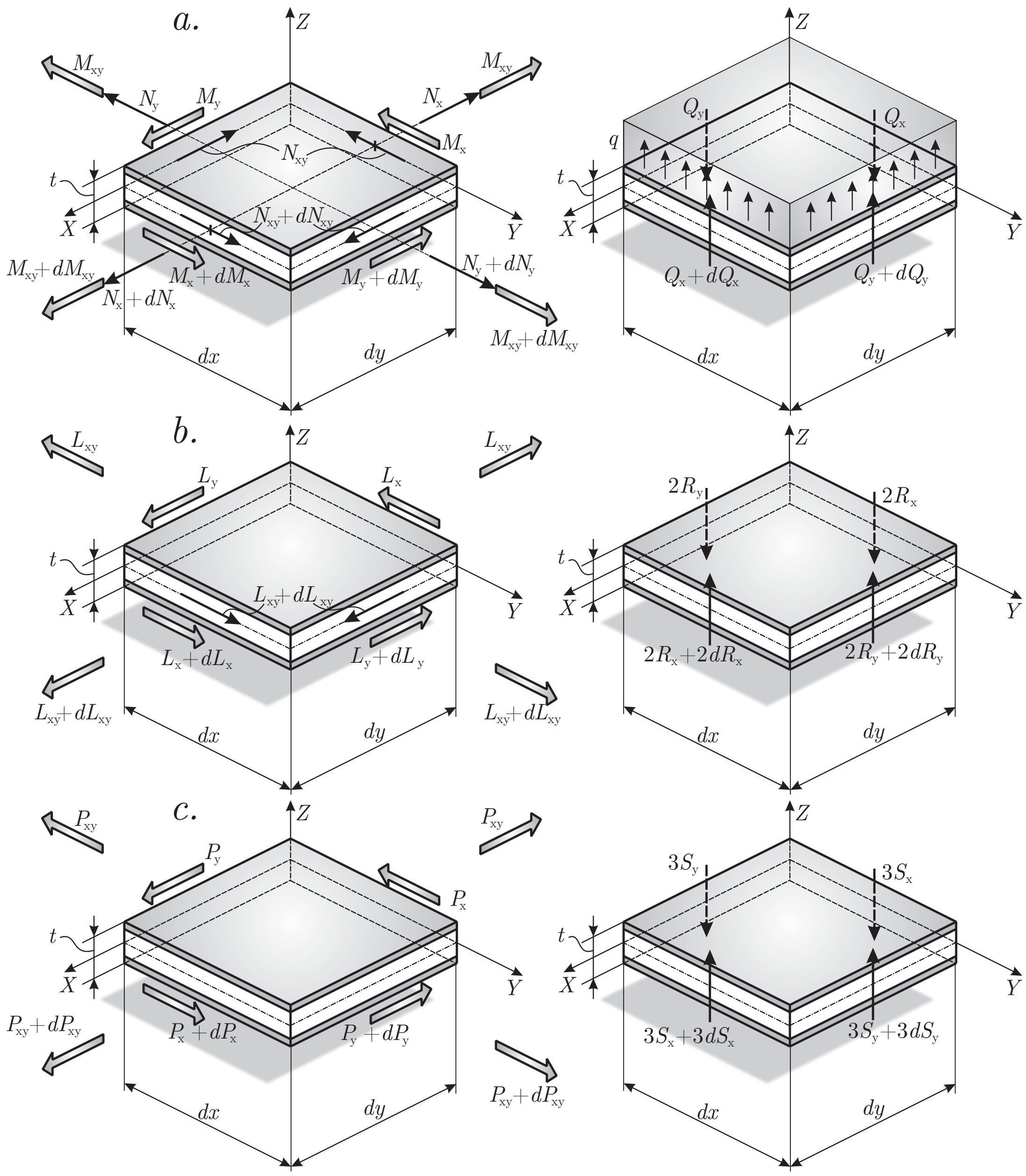

Figure 3.3: Equilibrium of stress resultants of the FSDT (a), SSDT (b) and TSDT (c) for an equivalent single layer.

$$\delta w : \sum_{i=1}^{2} \left(\frac{\partial Q_{x(i)}}{\partial x} + \frac{\partial Q_{y(i)}}{\partial y} \right) + q = 0. \tag{3.35}$$

The equilibrium equations of ESL theories can be obtained by using differential plate elements assuming differential changes of the stress resultants going from one boundary to the other. This scheme is very simple in the case of FSDT as it is shown by Figure 3.3a. For the SSDT Figure 3.3a (moment and shear force equilibrium) should be complemented with Figure 3.3b showing the possible interpretation of the higher-order stress resultants (L and R). Finally, Figure 3.3a, b and c should be considered together if the general TSDT is applied (L, P, R and S), although the equilibrium equations of this theory were not presented, these are documented by *Szekrényes (2014d).*

4

The method of four equivalent single layers

The concept of the method of 4ESLs (developed recently by *Szekrényes (2016a,b)*) is shown in Figures 4.1a and 4.2a. The bottom and top plates are modeled by two ESLs, and thus it is a refinement compared to the method of 2ESLs. It will be shown later that in certain cases it is not enough to apply 2ESLs. The SEKC is applied to the problem shown in Figures 4.1a and 4.2a. Using the conditions defined by Eqs.(2.2)-(2.6) we can eliminate certain parameters from Eq.(2.1), which (for 4 ESLs) involves 34 parameters altogether plus the deflections ($w_{(i)}(x,y) = w(x,y)$). The parameter elimination is carried out similarly to that of the method of 2ESLs. In the subsequent sections the undelaminated and delaminated regions are discussed separately. In the first step, the general TSDT displacement field is presented, then in the subsequent steps the SSDT and FSDT fields are obtained by the reduction of the TSDT equations. The meaning of the transverse splitting in Figure 4.1a

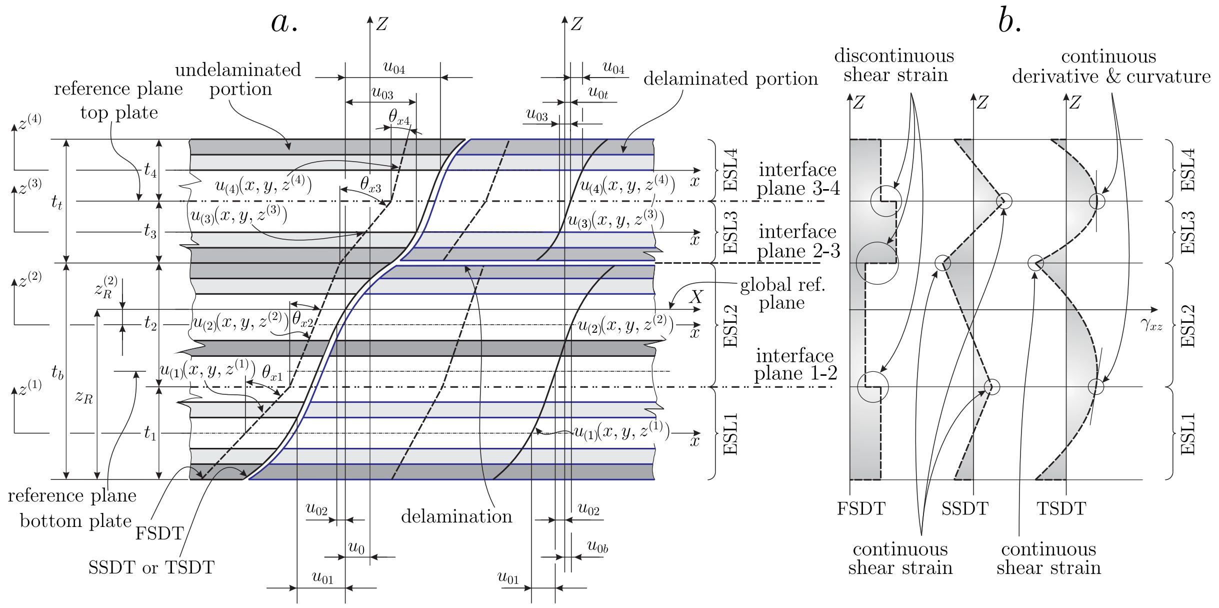

Figure 4.1: Cross sections and deformation of the top (ESL3 and ESL4) and bottom (ESL1 and ESL2) plate elements of a delaminated plate in the X-Z plane (a). Distribution of the transverse shear strains by FSDT, SSDT and TSDT (b).

dc_1254_16

is that different mathematical models are applied in the undelaminated and delaminated regions.

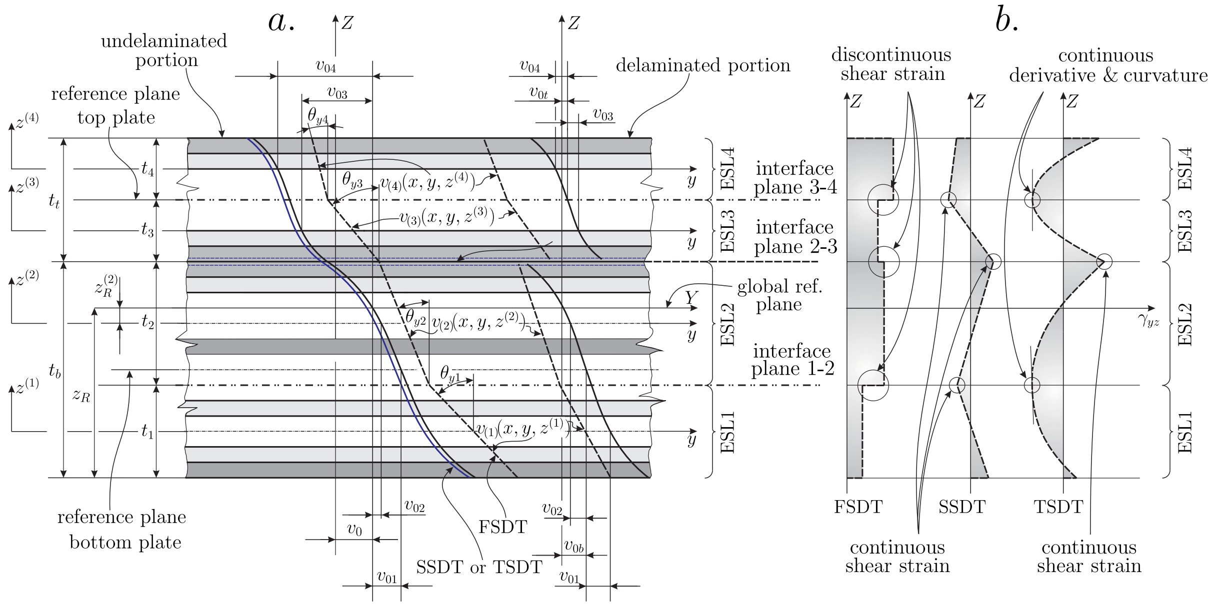

Figure 4.2: Cross sections and deformation of the top (ESL3 and ESL4) and bottom (ESL1 and ESL2) plate elements of a delaminated plate in the Y-Z plane (a). Distribution of the transverse shear strains by FSDT, SSDT and TSDT (b).

4.1 Undelaminated region

The transition zone around the delamination front in the $X - Z$ plane of the composite plate is shown in Figure 4.1a. The distribution of the in-plane displacement functions is piecewise linear by FSDT, quadratic in the case of the SSDT and cubic for the TSDT. The corresponding shear strain distributions are shown in Figure 4.1b: it is piecewise constant by FSDT, piecewise linear by SSDT and piecewise quadratic by TSDT with continuous derivatives and curvatures in the latter case at the perturbation planes. The $Y - Z$ plane is shown in Figure 4.2. In accordance with Figures 4.1a and 4.2a and Eq.(2.2), the following conditions are formulated between the four ESLs (continuity of in-plane displacements at the interface planes):

$$\begin{aligned}
(u_{(1)}, v_{(1)}, w_{(1)})\big|_{z^{(1)}=t_1/2} &= (u_{(2)}, v_{(2)}, w_{(2)})\big|_{z^{(2)}=-t_2/2}\,, \\
(u_{(2)}, v_{(2)}, w_{(2)})\big|_{z^{(2)}=t_2/2} &= (u_{(3)}, v_{(3)}, w_{(3)})\big|_{z^{(3)}=-t_3/2}\,, \\
(u_{(3)}, v_{(3)}, w_{(3)})\big|_{z^{(3)}=t_3/2} &= (u_{(4)}, v_{(4)}, w_{(4)})\big|_{z^{(4)}=-t_4/2}\,.
\end{aligned} \tag{4.1}$$

The reference plane belongs to the second ESL (see Figures 4.1a and 4.2b), therefore, the following condition is imposed (refer to Eq.(2.3)):

$$(u_{(2)}, v_{(2)})\big|_{z^{(2)}=z_R^{(2)}} = (u_0(x,y), v_0(x,y)), \tag{4.2}$$

where $z_R^{(2)} = 1/2(t_3+t_4-t_1)$ in accordance with Figure 4.1a and it gives the position of the global midplane of the model with respect to ESL2. The next set of conditions imposes the continuous shear strains at the interface planes using Eq.(2.4):

$$\begin{aligned}
(\gamma_{xz(1)}, \gamma_{yz(1)})\big|_{z^{(1)}=t_1/2} &= (\gamma_{xz(2)}, \gamma_{yz(2)})\big|_{z^{(2)}=-t_2/2}, \\
(\gamma_{xz(2)}, \gamma_{yz(2)})\big|_{z^{(2)}=t_2/2} &= (\gamma_{xz(3)}, \gamma_{yz(3)})\big|_{z^{(3)}=-t_3/2}, \\
(\gamma_{xz(3)}, \gamma_{yz(3)})\big|_{z^{(3)}=t_3/2} &= (\gamma_{xz(4)}, \gamma_{yz(4)})\big|_{z^{(4)}=-t_4/2}.
\end{aligned} \tag{4.3}$$

As discussed previously, the oscillations in the shear strain distribution can be reduced by ensuring continuous shear strain derivatives at interface planes 1-2 and 3-4 (Eq.(2.5)):

$$\begin{aligned}
\left(\frac{\partial \gamma_{xz(1)}}{\partial z^{(1)}}, \frac{\partial \gamma_{yz(1)}}{\partial z^{(1)}}\right)\bigg|_{z^{(1)}=t_1/2} &= \left(\frac{\partial \gamma_{xz(2)}}{\partial z^{(2)}}, \frac{\partial \gamma_{yz(2)}}{\partial z^{(2)}}\right)\bigg|_{z^{(2)}=-t_2/2}, \\
\left(\frac{\partial \gamma_{xz(3)}}{\partial z^{(3)}}, \frac{\partial \gamma_{yz(3)}}{\partial z^{(3)}}\right)\bigg|_{z^{(3)}=t_3/2} &= \left(\frac{\partial \gamma_{xz(4)}}{\partial z^{(4)}}, \frac{\partial \gamma_{yz(4)}}{\partial z^{(4)}}\right)\bigg|_{z^{(4)}=-t_4/2},
\end{aligned} \tag{4.4}$$

furthermore, by imposing continuous second derivatives of shear strains in the same planes by using the conditions below (Eq.(2.6)):

$$\begin{aligned}
\left(\frac{\partial^2 \gamma_{xz(1)}}{\partial (z^{(1)})^2}, \frac{\partial^2 \gamma_{yz(1)}}{\partial (z^{(1)})^2}\right)\bigg|_{z^{(1)}=t_1/2} &= \left(\frac{\partial^2 \gamma_{xz(2)}}{\partial (z^{(2)})^2}, \frac{\partial^2 \gamma_{yz(2)}}{\partial (z^{(2)})^2}\right)\bigg|_{z^{(2)}=-t_2/2}, \\
\left(\frac{\partial^2 \gamma_{xz(3)}}{\partial (z^{(3)})^2}, \frac{\partial^2 \gamma_{yz(3)}}{\partial (z^{(3)})^2}\right)\bigg|_{z^{(3)}=t_3/2} &= \left(\frac{\partial^2 \gamma_{xz(4)}}{\partial (z^{(4)})^2}, \frac{\partial^2 \gamma_{yz(4)}}{\partial (z^{(4)})^2}\right)\bigg|_{z^{(4)}=-t_4/2}.
\end{aligned} \tag{4.5}$$

To further reduce the number of parameters in the displacement field and to obtain more accurate results, the SSCC is applied at the top and bottom boundaries (Eq.(2.7)):

$$(\gamma_{xz(1)}, \gamma_{yz(1)})\big|_{z^{(1)}=-t_1/2} = (\gamma_{xz(4)}, \gamma_{yz(4)})\big|_{z^{(4)}=t_4/2}. \tag{4.6}$$

The concept of the shear strain control condition (SSCC) is shown in Figure 4.3, where in the undelaminated portion at two points in each cross section the shear strain is identical. Although the SSCC is applicable even in the case of the TSDT it leads to large oscillations in the transverse shear strains (*Szekrényes (2016b)*), therefore it is applied only to the SSDT solution. It is also important to note that the large oscillations in the shear strain distribution take place even if the SSDT solution without the SSCC is applied (*Szekrényes (2016a)*).

In Eq.(2.1) the displacement functions are modified in order to satisfy Eqs.(4.1)-(4.6). In the general sense, by applying the FSDT, SSDT and TSDT theories the displacement functions can be written as:

$$\begin{aligned}
u_{(i)} &= u_0 + \left(K_{ij}^{(0)} + K_{ij}^{(1)} z^{(i)} + K_{ij}^{(2)} [z^{(i)}]^2 + K_{ij}^{(3)} [z^{(i)}]^3\right) \psi_{(x)j}, \quad i = 1..4, \\
v_{(i)} &= v_0 + \left(K_{ij}^{(0)} + K_{ij}^{(1)} z^{(i)} + K_{ij}^{(2)} [z^{(i)}]^2 + K_{ij}^{(3)} [z^{(i)}]^3\right) \psi_{(y)j}, \quad i = 1..4, \\
w_{(i)} &= w(x,y), \quad i = 1..4,
\end{aligned} \tag{4.7}$$

where the matrices denoted by K_{ij} are related to the geometry (ESL thicknesses), i refers to the ESL number, the summation index j defines the component in $\boldsymbol{\psi}$, which is the vector of primary parameters, finally $w(x,y)$ is the transverse deflection and identical for each ESL.

dc_1254_16

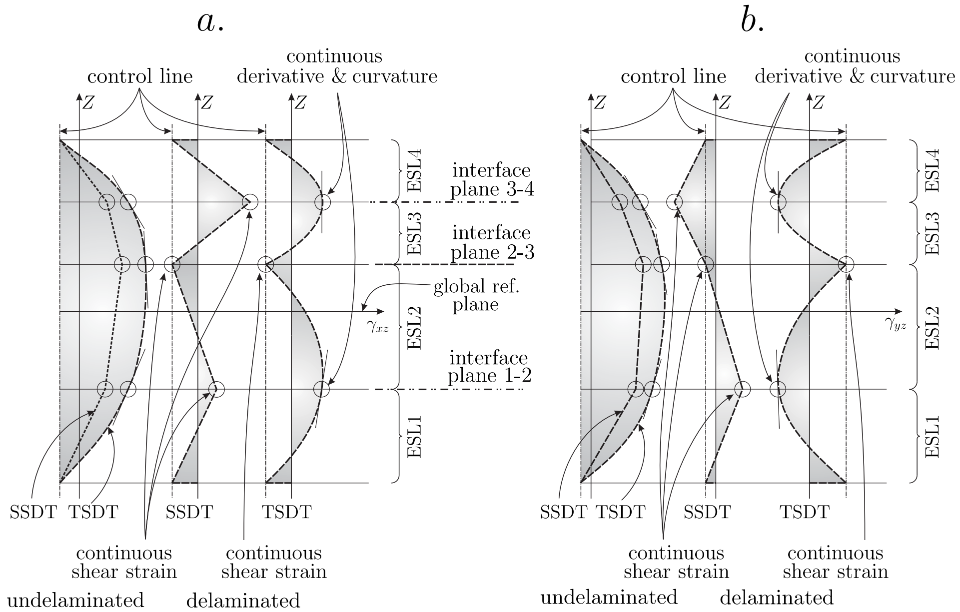

Figure 4.3: The concept of controlled shear strain distribution on the X-Z plane (a) and Y-Z plane (b) in the undelaminated and delaminated regions of the SSDT and TSDT solutions.

4.1.1 Third-order plate theory

Using the conditions above (Eqs.(4.1)-(4.5)) we can eliminate twentytwo parameters from Eq.(2.1), the secondary parameters are: u_{0i}, v_{0i}, $\phi_{(x)i}$, $\phi_{(y)i}$ for $i = 1..4$, $\lambda_{(x)i}$, $\lambda_{(y)i}$ for $i = 1, 2$ and 4. The vector of primary parameters is:

$$\boxed{\boldsymbol{\psi}_{(p)} = \left(\begin{array}{ccccc} \theta_{(p)1} & \theta_{(p)2} & \theta_{(p)3} & \theta_{(p)4} & \lambda_{(p)3} \end{array}\right)^T, \quad p = x \text{ or } y.} \tag{4.8}$$

The elements of the matrices $K_{ij}^{(0)}$, $K_{ij}^{(1)}$, $K_{ij}^{(2)}$ and $K_{ij}^{(3)}$ in Eq.(4.7) are defined in Appendix B.1. The equilibrium equations can be obtained by using Eqs.(2.32)-(2.35) and Eq.(4.8):

$$\begin{aligned} \delta u_0 &: \sum_{i=1}^{4} \frac{\partial N_{x(i)}}{\partial x} + \frac{\partial N_{xy(i)}}{\partial y} = 0, \\ \delta v_0 &: \sum_{i=1}^{4} \frac{\partial N_{xy(i)}}{\partial x} + \frac{\partial N_{y(i)}}{\partial y} = 0, \end{aligned} \tag{4.9}$$

$$\begin{aligned} \delta\psi_{(x)j} :& \sum_{i=1}^{4} K_{ij}^{(0)} \left(\frac{\partial N_{x(i)}}{\partial x} + \frac{\partial N_{xy(i)}}{\partial y}\right) + K_{ij}^{(1)} \left(\frac{\partial M_{x(i)}}{\partial x} + \frac{\partial M_{xy(i)}}{\partial y}\right) + K_{ij}^{(2)} \left(\frac{\partial L_{x(i)}}{\partial x} + \frac{\partial L_{xy(i)}}{\partial y}\right) \\ &+ K_{ij}^{(3)} \left(\frac{\partial P_{x(i)}}{\partial x} + \frac{\partial P_{xy(i)}}{\partial y}\right) - K_{ij}^{(1)} Q_{x(i)} - 2K_{ij}^{(2)} R_{x(i)} - 3K_{ij}^{(3)} S_{x(i)} = 0, \quad j = 1..5, \\ \delta\psi_{(y)j} :& \sum_{i=1}^{4} K_{ij}^{(0)} \left(\frac{\partial N_{xy(i)}}{\partial x} + \frac{\partial N_{y(i)}}{\partial y}\right) + K_{ij}^{(1)} \left(\frac{\partial M_{xy(i)}}{\partial x} + \frac{\partial M_{y(i)}}{\partial y}\right) + K_{ij}^{(2)} \left(\frac{\partial L_{xy(i)}}{\partial x} + \frac{\partial L_{y(i)}}{\partial y}\right) \\ &+ K_{ij}^{(3)} \left(\frac{\partial P_{xy(i)}}{\partial x} + \frac{\partial P_{y(i)}}{\partial y}\right) - K_{ij}^{(1)} Q_{y(i)} - 2K_{ij}^{(2)} R_{y(i)} - 3K_{ij}^{(3)} S_{y(i)} = 0, \quad j = 1..5, \end{aligned}$$

$$(4.10)$$

$$\delta w : \sum_{i=1}^{4} \left(\frac{\partial Q_{x(i)}}{\partial x} + \frac{\partial Q_{y(i)}}{\partial y} \right) + q = 0. \tag{4.11}$$

The first four parameters in $\boldsymbol{\psi}_{(p)}$ are rotations, viz. for each ESL we have a single moment equilibrium equation. By summing the moment equilibrium equations (the first four in Eq.(4.10)) and separating the terms of the stress resultants for each ESL using the constants in Appendix B.1 it is possible to obtain the following equivalent bending and twisting moments:

$$\hat{\mathbf{M}}_i^{(x,y)} = \mathbf{M}_i^{(x,y)} + \sum_{j=1}^{4} K_{ij}^{(0)} \mathbf{N}_i^{(x,y)}, \quad \sum_{j=1}^{4} K_{ij}^{(0)} = \begin{cases} -\ \ \frac{1}{2}(t_2 + t_3 + t_4) & \text{if } i = 1, \\ \quad \frac{1}{2}(t_1 - t_3 - t_4) & \text{if } i = 2, \\ \quad \frac{1}{2}(t_1 + t_2 - t_4) & \text{if } i = 3, \\ \quad \frac{1}{2}(t_1 + t_2 + t_3) & \text{if } i = 4. \end{cases} \tag{4.12}$$

The fifth parameter in $\boldsymbol{\psi}_{(p)}$ is $\lambda_{(p)3}$, which is a parameter related to the third-order displacement field term, therefore from the corresponding equilibrium equation it is possible to obtain the equivalent P stress resultants:

$$\hat{\mathbf{P}}_3^{(x,xy)} = \sum_{i=1}^{4} K_{i5}^{(3)} \mathbf{P}_i^{(x,xy)} + \sum_{i=1}^{4} K_{i5}^{(2)} \mathbf{L}_i^{(x,xy)} + \sum_{i=1}^{4} K_{i5}^{(0)} \mathbf{N}_i^{(x,xy)}. \tag{4.13}$$

It is surprising that neither Eq.(4.11) nor (4.13) contains the standard and higher-order shear forces. The reason for that is Q, R and S are related to the shear strains in accordance with Eq.(2.20), which are always continuous across the transition between the delaminated and undelaminated regions. Note that $K_{i5}^{(1)} = 0, i = 1..4$ (see Appendix B.1), and that is why $\hat{\mathbf{P}}_3^{(x,xy)}$ is independent of the bending and twisting moments.

4.1.2 Second-order plate theory

In this case $\lambda_{(x)i} = 0$ and $\lambda_{(y)i} = 0$ in Eq.(2.1). Eqs.(4.1)-(4.2) apply together with Eq.(4.3) (shear strain continuity), however Eqs.(4.4)-(4.5) are omitted. However, Eq.(4.6) is taken into account (SSCC). Thus, we can eliminate sixteen parameters from Eq.(2.1), the secondary parameters are: u_{0i}, v_{0i} for i=1..4, $\theta_{(x)i}$, $\theta_{(y)i}$, $\phi_{(x)i}$, $\phi_{(y)i}$ for $i = 1$ and 3. The vector of primary parameters becomes:

$$\boxed{\boldsymbol{\psi}_{(p)} = \begin{pmatrix} \theta_{(p)2} & \phi_{(p)2} & \theta_{(p)4} & \phi_{(p)4} \end{pmatrix}^T, \quad p = x \text{ or } y,} \tag{4.14}$$

where $\phi_{(p)2}$ is an autocontinuity parameter. The elements of the matrices $K_{ij}^{(0)}$, $K_{ij}^{(1)}$ and $K_{ij}^{(2)}$ are defined in Appendix B.2. Obviously $K_{ij}^{(3)} = 0$ in this case. The equilibrium equations take the same form as Eq.(4.9)-(4.11) but $j = 1..4$. In accordance with Eq.(4.14) we have a single rotation for the bottom ($\theta_{(p)2}$) and top ($\theta_{(p)4}$) plates, and therefore the first and third equilibrium equations in Eq.(4.10) contain the following equivalent bending moments of the undelaminated region ②:

$$\begin{aligned}
\hat{\mathbf{M}}_{12}^{(x,xy)} &= \sum_{i=1,2}\Big((K_{i1}^{(0)}+K_{i3}^{(0)})\mathbf{N}_i^{(x,xy)}+(K_{i1}^{(1)}+K_{i3}^{(1)})\mathbf{M}_i^{(x,xy)}+(K_{i1}^{(2)}+K_{i3}^{(2)})\mathbf{L}_i^{(x,xy)}\Big),\\
\hat{\mathbf{M}}_{34}^{(x,xy)} &= \sum_{i=3,4}\Big((K_{i1}^{(0)}+K_{i3}^{(0)})\mathbf{N}_i^{(x,xy)}+(K_{i1}^{(1)}+K_{i3}^{(1)})\mathbf{M}_i^{(x,xy)}+(K_{i1}^{(2)}+K_{i3}^{(2)})\mathbf{L}_i^{(x,xy)}\Big).
\end{aligned} \tag{4.15}$$

Using the K_{ij} constants given in Appendix B.2 Eq.(4.15) reduces to:

$$\begin{aligned}
\hat{\mathbf{M}}_{12}^{(x,xy)} &= \mathbf{M}_1^{(x,xy)}-\frac{1}{2}(t_2+t_3+t_4)\mathbf{N}_1^{(x,xy)}+\mathbf{M}_2^{(x,xy)}+\frac{1}{2}(t_1-t_3-t_4)\mathbf{N}_2^{(x,xy)},\\
\hat{\mathbf{M}}_{34}^{(x,xy)} &= \mathbf{M}_3^{(x,xy)}-\frac{1}{2}(t_1+t_2-t_4)\mathbf{N}_3^{(x,xy)}+\mathbf{M}_4^{(x,xy)}+\frac{1}{2}(t_1+t_2+t_3)\mathbf{N}_4^{(x,xy)}.
\end{aligned} \tag{4.16}$$

Comparing Eq.(4.16) to Eq.(4.12) it becomes clear that $\hat{\mathbf{M}}_{12}$ is the sum of $\hat{\mathbf{M}}_1$ and $\hat{\mathbf{M}}_2$, moreover $\hat{\mathbf{M}}_{34}$ is the sum of $\hat{\mathbf{M}}_3$ and $\hat{\mathbf{M}}_4$. The equivalent L stress resultants can be obtained similarly, by taking the second and fourth equations in Eq.(4.10):

$$\begin{aligned}
\hat{\mathbf{L}}_{12}^{(x,xy)} &= \sum_{i=1,2}\Big((K_{i2}^{(0)}+K_{i4}^{(0)})\mathbf{N}_i^{(x,xy)}+(K_{i2}^{(1)}+K_{i4}^{(1)})\mathbf{M}_i^{(x,xy)}+(K_{i2}^{(2)}+K_{i4}^{(2)})\mathbf{L}_i^{(x,xy)}\Big),\\
\hat{\mathbf{L}}_{34}^{(x,xy)} &= \sum_{i=3,4}\Big((K_{i2}^{(0)}+K_{i4}^{(0)})\mathbf{N}_i^{(x,xy)}+(K_{i2}^{(1)}+K_{i4}^{(1)})\mathbf{M}_i^{(x,xy)}+(K_{i2}^{(2)}+K_{i4}^{(2)})\mathbf{L}_i^{(x,xy)}\Big).
\end{aligned} \tag{4.17}$$

4.1.3 First-order plate theory

If the FSDT is applied then $\phi_{(x)i}=0$, $\phi_{(y)i}=0$, $\lambda_{(x)i}=0$ and $\lambda_{(y)i}=0$ in Eq.(2.1). Only Eq.(4.1) is utilized together with Eq.(4.2). The continuity of shear strains cannot be imposed, neither the SSCC. Thus, we can eliminate eight parameters from Eq.(2.1), the secondary parameters are: u_{0i} and v_{0i} for $i=1..4$, The primary parameters are: u_0 and v_0 and $\theta_{(x)i}$, $\theta_{(y)i}$ for $i=1..4$. The vector of primary parameters is:

$$\boxed{\boldsymbol{\psi}_{(p)}=\begin{pmatrix}\theta_{(p)1} & \theta_{(p)2} & \theta_{(p)3} & \theta_{(p)4}\end{pmatrix}^T, \quad p=x \text{ or } y.} \tag{4.18}$$

The elements of $K_{ij}^{(0)}$ and $K_{ij}^{(1)}$ are defined in Appendix B.3. $K_{ij}^{(2)}=0$ and $K_{ij}^{(3)}=0$ in this case. Eqs.(4.9)-(4.11) are valid even for the FSDT, the equivalent moments are given by Eq.(4.12).

4.2 Delaminated region

In the delaminated region (refer to Figures 4.1a and 4.2a) the top and bottom plates are equally modeled by two ESLs, and thus the first and third of Eq.(4.1) still hold in each theory. In accordance with Eq.(4.1) the transverse deflections of the top and bottom plates of the delaminated region are identical (constrained mode model, (*Szekrényes (2014c)*)). The definition of the top and bottom reference planes involve:

$$
\begin{aligned}
(u_{(1)}, v_{(1)})\big|_{z^{(1)}=t_2/2} &= (u_{0b}(x,y), v_{0b}(x,y)), \\
(u_{(3)}, v_{(3)})\big|_{z^{(3)}=t_4/2} &= (u_{0t}(x,y), v_{0t}(x,y)),
\end{aligned}
\tag{4.19}
$$

where u_{0b} and u_{0t} are the global membrane displacements of the bottom and top plates in accordance with Figures 4.1a and 4.2a. Furthermore, the first and third of Eq.(4.3) apply again, as well as Eqs.(4.4)-(4.5). Three more equations are formulated by using the shear strain control conditions (Eq.(2.6)):

$$
\begin{aligned}
(\gamma_{xz(1)}, \gamma_{yz(1)})\big|_{z^{(1)}=-t_1/2} &= (\gamma_{xz(2)}, \gamma_{yz(2)})\big|_{z^{(2)}=t_2/2}, \\
(\gamma_{xz(3)}, \gamma_{yz(3)})\big|_{z^{(3)}=-t_3/2} &= (\gamma_{xz(4)}, \gamma_{yz(4)})\big|_{z^{(4)}=t_4/2}, \\
(\gamma_{xz(1)}, \gamma_{yz(1)})\big|_{z^{(1)}=-t_1/2} &= (\gamma_{xz(4)}, \gamma_{yz(4)})\big|_{z^{(4)}=t_4/2},
\end{aligned}
\tag{4.20}
$$

i.e., instead of imposing traction-free boundaries (as it was done in Section 3.1 using Reddy TSDT) we control the strain distribution by having identical values at the boundaries leading to nine equation sets altogether. The displacement field is given by the following equations:

$$
\begin{aligned}
u_{(i)} &= u_{0b} + \left(K_{ij}^{(0)} + K_{ij}^{(1)} z^{(i)} + K_{ij}^{(2)} [z^{(i)}]^2 + K_{ij}^{(3)} [z^{(i)}]^3\right) \psi_{(x)j}, \quad i = 1..2, \\
v_{(i)} &= v_{0b} + \left(K_{ij}^{(0)} + K_{ij}^{(1)} z^{(i)} + K_{ij}^{(2)} [z^{(i)}]^2 + K_{ij}^{(3)} [z^{(i)}]^3\right) \psi_{(y)j}, \quad i = 1..2, \\
u_{(i)} &= u_{0t} + \left(K_{ij}^{(0)} + K_{ij}^{(1)} z^{(i)} + K_{ij}^{(2)} [z^{(i)}]^2 + K_{ij}^{(3)} [z^{(i)}]^3\right) \psi_{(x)j}, \quad i = 3..4, \\
v_{(i)} &= v_{0t} + \left(K_{ij}^{(0)} + K_{ij}^{(1)} z^{(i)} + K_{ij}^{(2)} [z^{(i)}]^2 + K_{ij}^{(3)} [z^{(i)}]^3\right) \psi_{(y)j}, \quad i = 3..4, \\
w_{(i)} &= w(x,y), \quad i = 1..4,
\end{aligned}
\tag{4.21}
$$

where j is a summation index. The concept of the analysis is to start with the TSDT and to give the SSDT and FSDT equations by the reduction of the TSDT equations.

4.2.1 Third-order plate theory

The first and third in Eq.(4.1) hold, moreover Eq.(4.19) is implied, again the first and third of Eq.(4.3) are utilized together with Eqs.(4.4)-(4.5) leading to 20 conditions altogether. The SSCC by Eq.(4.20) is not implied in this case. The secondary parameters are: u_{0i}, v_{0i}, $\phi_{(x)i}$, $\phi_{(y)i}$ for $i = 1..4$, $\lambda_{(x)i}$, $\lambda_{(y)i}$ for $i = 2$ and 4. The modified displacement field is given by Eq.(4.21) wherein the vector of primary parameters is:

$$
\boxed{\boldsymbol{\psi}_{(p)} = \begin{pmatrix} \theta_{(p)1} & \theta_{(p)2} & \theta_{(p)3} & \theta_{(p)4} & \lambda_{(p)1} & \lambda_{(p)3} \end{pmatrix}^T, \quad p = x \text{ or } y,}
\tag{4.22}
$$

where $\lambda_{(p)1}$ is the autocontinuity parameter. The coefficients denoted by K_{ij} are placed in

Appendix B.1. The equilibrium equations become:

$$\begin{aligned}
&\delta u_{0b}:\sum_{i=1}^{2}\frac{\partial N_{x(i)}}{\partial x}+\frac{\partial N_{xy(i)}}{\partial y}=0,\quad \delta v_{0b}:\sum_{i=1}^{2}\frac{\partial N_{xy(i)}}{\partial x}+\frac{\partial N_{y(i)}}{\partial y}=0,\\
&\delta u_{0t}:\sum_{i=3}^{4}\frac{\partial N_{x(i)}}{\partial x}+\frac{\partial N_{xy(i)}}{\partial y}=0,\quad \delta v_{0t}:\sum_{i=3}^{4}\frac{\partial N_{xy(i)}}{\partial x}+\frac{\partial N_{y(i)}}{\partial y}=0,
\end{aligned}\tag{4.23}$$

$$\begin{aligned}
\delta\psi_{(x)j}:&\sum_{i=1}^{4}K_{ij}^{(0)}\left(\frac{\partial N_{x(i)}}{\partial x}+\frac{\partial N_{xy(i)}}{\partial y}\right)+K_{ij}^{(1)}\left(\frac{\partial M_{x(i)}}{\partial x}+\frac{\partial M_{xy(i)}}{\partial y}\right)+K_{ij}^{(2)}\left(\frac{\partial L_{x(i)}}{\partial x}+\frac{\partial L_{xy(i)}}{\partial y}\right)\\
&+K_{ij}^{(3)}\left(\frac{\partial P_{x(i)}}{\partial x}+\frac{\partial P_{xy(i)}}{\partial y}\right)-K_{ij}^{(1)}Q_{x(i)}-2K_{ij}^{(2)}R_{x(i)}-3K_{ij}^{(3)}S_{x(i)}=0,\quad j=1..6,\\
\delta\psi_{(y)j}:&\sum_{i=1}^{4}K_{ij}^{(0)}\left(\frac{\partial N_{xy(i)}}{\partial x}+\frac{\partial N_{y(i)}}{\partial y}\right)+K_{ij}^{(1)}\left(\frac{\partial M_{xy(i)}}{\partial x}+\frac{\partial M_{y(i)}}{\partial y}\right)+K_{ij}^{(2)}\left(\frac{\partial L_{xy(i)}}{\partial x}+\frac{\partial L_{y(i)}}{\partial y}\right)\\
&+K_{ij}^{(3)}\left(\frac{\partial P_{xy(i)}}{\partial x}+\frac{\partial P_{y(i)}}{\partial y}\right)-K_{ij}^{(1)}Q_{y(i)}-2K_{ij}^{(2)}R_{y(i)}-3K_{ij}^{(3)}S_{y(i)}=0,\quad j=1..6,
\end{aligned}\tag{4.24}$$

$$\delta w:\sum_{i=1}^{4}\left(\frac{\partial Q_{x(i)}}{\partial x}+\frac{\partial Q_{y(i)}}{\partial y}\right)+q=0.\tag{4.25}$$

The equivalent moments are obtained by summing the first four in Eq.(4.24):

$$\hat{\mathbf{M}}_i^{(x,y)}=\mathbf{M}_i^{(x,y)}+\sum_{j=1}^{4}K_{ij}^{(0)}\mathbf{N}_i^{(x,y)},\sum_{j=1}^{4}K_{ij}^{(0)}=\begin{cases}-\ \frac{1}{2}t_2 & \text{if } i=1,\\ \ \frac{1}{2}t_1 & \text{if } i=2,\\ -\ \frac{1}{2}t_4 & \text{if } i=3,\\ \ \frac{1}{2}t_3 & \text{if } i=4.\end{cases}\tag{4.26}$$

The last two parameters in Eq.(4.22) are $\lambda_{(p)1}$ and $\lambda_{(p)3}$, the equivalent P stress resultants can be defined as:

$$\begin{aligned}
\hat{\mathbf{P}}_1^{(x,y)}&=\sum_{i=1}^{4}K_{i5}^{(3)}\mathbf{P}_i^{(x,y)}+\sum_{i=1}^{4}K_{i5}^{(2)}\mathbf{L}_i^{(x,y)}+\sum_{i=1}^{4}K_{i5}^{(0)}\mathbf{N}_i^{(x,y)},\\
\hat{\mathbf{P}}_3^{(x,y)}&=\sum_{i=1}^{4}K_{i6}^{(3)}\mathbf{P}_i^{(x,y)}+\sum_{i=1}^{4}K_{i6}^{(2)}\mathbf{L}_i^{(x,y)}+\sum_{i=1}^{4}K_{i6}^{(0)}\mathbf{N}_i^{(x,y)},
\end{aligned}\tag{4.27}$$

that will be utilized by imposing the continuity conditions. It is important to note that $K_{i5}^{(1)}=K_{i6}^{(1)}=0, i=1..4$.

4.2.2 Second-order plate theory

In this case $\lambda_{(x)i}=0$ and $\lambda_{(y)i}=0$ in Eq.(2.1). The first and third in Eq.(4.1) hold, moreover Eq.(4.19) is implied, again the first and third of Eq.(4.3) is utilized, however Eqs.(4.4)-(4.5) are omitted. The SSCC (Eq.(4.20)) is employed to obtain the modified displacement field. Therefore we can eliminate eighteen parameters from Eqs.(2.36)-(2.37), the secondary parameters are: u_{0i}, v_{0i} for $i = 1..4$, $\theta_{(x)i}$, $\theta_{(y)i}$ for $i = 1, 3$ and $\phi_{(x)i}$, $\phi_{(y)i}$ for $i = 1, 2$ and 3, The vector of primary parameters takes the form of:

$$\boxed{\boldsymbol{\psi}_{(p)} = \left(\begin{array}{ccc} \theta_{(p)2} & \theta_{(p)4} & \phi_{(p)4} \end{array} \right)^T, \quad p = x \text{ or } y.} \tag{4.28}$$

The elements of the matrices $K_{ij}^{(0)}$, $K_{ij}^{(1)}$ and $K_{ij}^{(2)}$ are defined in Appendix B.2. Apparently $K_{ij}^{(3)} = 0$ in this case. Eqs.(4.23)-(4.25) are valid for $j = 1..3$. The equivalent moments are obtained from the first and second of Eq.(4.24):

$$\begin{aligned} \hat{\mathbf{M}}_{12}^{(x,xy)} &= \sum_{i=1,2} \Big((K_{i1}^{(0)} + K_{i2}^{(0)}) \mathbf{N}_i^{(x,xy)} + (K_{i1}^{(1)} + K_{i2}^{(1)}) \mathbf{M}_i^{(x,xy)} + (K_{i1}^{(2)} + K_{i2}^{(2)}) \mathbf{L}_i^{(x,xy)} \Big), \\ \hat{\mathbf{M}}_{34}^{(x,xy)} &= \sum_{i=3,4} \Big((K_{i1}^{(0)} + K_{i2}^{(0)}) \mathbf{N}_i^{(x,xy)} + (K_{i1}^{(1)} + K_{i2}^{(1)}) \mathbf{M}_i^{(x,xy)} + (K_{i1}^{(2)} + K_{i2}^{(2)}) \mathbf{L}_i^{(x,xy)} \Big), \end{aligned} \tag{4.29}$$

furthermore, by using the K_{ij} constants we obtain:

$$\begin{aligned} \hat{\mathbf{M}}_{12}^{(x,xy)} &= \mathbf{M}_1^{(x,xy)} - \frac{1}{2} t_2 \mathbf{N}_1^{(x,xy)} + \mathbf{M}_2^{(x,xy)} + \frac{1}{2} t_1 \mathbf{N}_2^{(x,xy)}, \\ \hat{\mathbf{M}}_{34}^{(x,xy)} &= \mathbf{M}_3^{(x,xy)} - \frac{1}{2} t_4 \mathbf{N}_3^{(x,xy)} + \mathbf{M}_4^{(x,xy)} + \frac{1}{2} t_3 \mathbf{N}_4^{(x,xy)}, \end{aligned} \tag{4.30}$$

which can be obtained by summing the corresponding moments in Eq.(4.26). The equivalent L stress resultant is obtained by the third ($j = 3$) in Eq.(4.24):

$$\hat{\mathbf{L}}_{1234}^{(x,xy)} = \sum_{i=1..4} \Big(K_{i3}^{(0)} \mathbf{N}_i^{(x,xy)} + K_{i3}^{(1)} \mathbf{M}_i^{(x,xy)} + K_{i3}^{(2)} \mathbf{L}_i^{(x,xy)} \Big), \tag{4.31}$$

which plays a key role in the assignment of the continuity and boundary conditions.

4.2.3 First-order plate theory

Similarly to the undelaminated portion we have: $\phi_{(x)i} = 0$, $\phi_{(y)i} = 0$, $\lambda_{(x)i} = 0$ and $\lambda_{(y)i} = 0$ in Eq.(2.1) and Eqs.(2.36)-(2.37). Only the first and third of Eq.(4.1) apply together with Eq.(4.19). The shear strains are approximated by constant distributions in all four ESLs. Thus we can eliminate only eight parameters (u_{0i}, v_{0i} for $i = 1..4$) from Eqs.(2.36)-(2.37). The vector of primary parameters is:

$$\boxed{\boldsymbol{\psi}_{(p)} = \left(\begin{array}{cccc} \theta_{(p)1} & \theta_{(p)2} & \theta_{(p)3} & \theta_{(p)4} \end{array} \right)^T, p = x \text{ or } y.} \tag{4.32}$$

The $K_{ij}^{(0)}$ and $K_{ij}^{(1)}$ elements are defined in Appendix B.3, moreover $K_{ij}^{(2)} = K_{ij}^{(3)} = 0$ in this case. The equilibrium equations are given by Eqs.(4.23)-(4.25) for $j = 1..4$. The equivalent moments are defined by Eq.(4.26).

5
Exact solutions for delaminated Lévy plates by state-space formulation

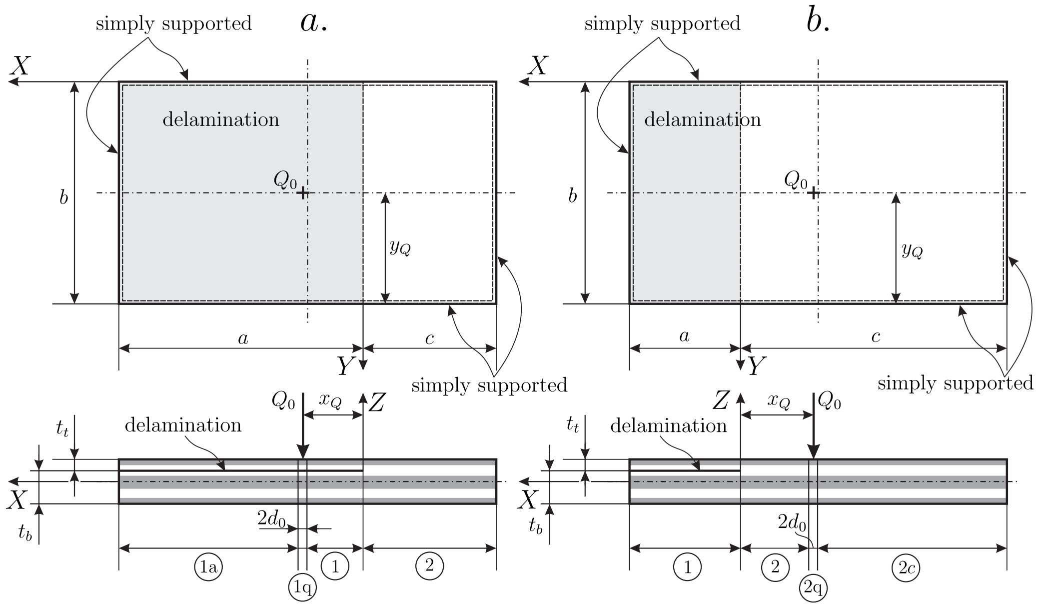

Figure 5.1: Simply supported delaminated composite plates subjected to a concentrated force.

In this chapter exact analytical solutions are developed for laminated orthotropic plates with an asymmetric delamination (i.e., the delamination is not in the midplane) shown in Figures 5.1a and b. The governing equations in terms of the displacement parameters are obtained by using the equilibrium equations developed in Chapters 3 and 4. The plates are loaded by a concentrated force. In accordance with Lévy plate formulation (*Bodaghi and Saidi (2010); Hosseini-Hashemi et al. (2011); Kapuria and Kumari (2012); Thai and Kim (2012)*) at least two opposite edges of the plates should be simply supported. The other two (opposite) edges can be free, built-in or simply supported ones. The basic idea of Lévy plate formulation is that the *primary* displacement parameters, the external load parameter, q in Eq.(2.1), the deflection, $w(x,y)$ and the membrane displacements are expressed by trial functions in the form of:

$$\left\{\begin{array}{c}\psi_{(x)i}(x,y)\\ \psi_{(y)i}(x,y)\end{array}\right\}=\sum_{n=1}^{\infty}\left\{\begin{array}{c}\Phi_{(x)in}(x)\sin\beta y\\ \Phi_{(y)in}(x)\cos\beta y\end{array}\right\},\left\{\begin{array}{c}u(x,y)\\ v(x,y)\\ q(x,y)\\ w(x,y)\end{array}\right\}=\sum_{n=1}^{\infty}\left\{\begin{array}{c}U_n(x)\sin\beta y\\ V_n(x)\cos\beta y\\ Q_n(x)\sin\beta y\\ W_n(x)\sin\beta y\end{array}\right\}. \tag{5.1}$$

Considering the parameters in Eq.(5.1) the trial functions for any ESL in the plate including the undelaminated and delaminated portions are:

$$\left\{\begin{array}{c}\theta_{(x)}(x,y)\\ \theta_{(y)}(x,y)\\ \phi_{(x)}(x,y)\\ \phi_{(y)}(x,y)\\ \lambda_{(x)}(x,y)\\ \lambda_{(y)}(x,y)\end{array}\right\}=\sum_{n=1}^{\infty}\left\{\begin{array}{c}X_n(x)\sin\beta y\\ Y_n(x)\cos\beta y\\ T_{xn}(x)\sin\beta y\\ T_{yn}(x)\cos\beta y\\ Z_{xn}(x)\sin\beta y\\ Z_{yn}(x)\cos\beta y\end{array}\right\},\left\{\begin{array}{c}u_0(x,y)\\ v_0(x,y)\\ u_{0\delta}(x,y)\\ v_{0\delta}(x,y)\\ q(x,y)\\ w(x,y)\end{array}\right\}=\sum_{n=1}^{\infty}\left\{\begin{array}{c}U_{0n}(x)\sin\beta y\\ V_{0n}(x)\cos\beta y\\ U_{0\delta n}(x)\sin\beta y\\ V_{0\delta n}(x)\cos\beta y\\ Q_n(x)\sin\beta y\\ W_n(x)\sin\beta y\end{array}\right\}, \tag{5.2}$$

where $\beta = n\pi/b$, b is the plate width and $\delta = t$ for the top plate, $\delta = b$ for the bottom plate, respectively. By taking back the solution in Eq.(5.2) into the strain field (Eq.(2.10)-(2.11)), then by expressing the stress resultants in accordance with Eqs.(2.19)-(2.20) we can utilize the equilibrium equations given by Eqs.(2.32)-(2.34) and (2.38) to reduce the system of PDEs to system of ODEs, which can be solved by the state-space approach (*Jianqiao (2003)*). The state-space model of the plate system takes the form below (*Jianqiao (2003); Reddy (2004)*):

$$\mathbf{Z}' = \mathbf{TZ} + \mathbf{F}, \tag{5.3}$$

where $\mathbf{Z}$ is the state vector, $\mathbf{T}$ is the system matrix, $\mathbf{F}$ is the vector of particular solutions, the comma means differentiation with respect to x. The general solution of Eq.(5.3) becomes (*Jianqiao (2003)*):

$$\mathbf{Z}(x) = e^{\mathbf{T}x}\left(\mathbf{K} + \int_{x^*}^{x} e^{-\mathbf{T}\xi}\mathbf{F}(\xi)d\xi\right) = \mathbf{G}(x)\mathbf{K} + \mathbf{H}(x), \tag{5.4}$$

where $\mathbf{K}$ is the vector of constants, x^* is the lower integration bound and for problems a and b in Figures 5.1a and 5.1b is given by:

$$x^* = \left\{\begin{array}{cc} x_Q + d_0 & \text{for 1a}\\ x_Q - d_0 & \text{for 1q}\\ 0 & \text{for 1}\\ -c & \text{for 2}\end{array}\right\}\text{problem a}, x^* = \left\{\begin{array}{cc} 0 & \text{for 1}\\ -(x_Q - d_0) & \text{for 2}\\ -(x_Q + d_0) & \text{for 2q}\\ -c & \text{for 2c}\end{array}\right\}\text{problem b}, \tag{5.5}$$

where x_Q and d_0 are given in Figure 5.1. The concept is to substitute the concentrated force with a line load distributed on a small length with $2d_0$. The parameters of the state vector can be expressed through:

$$Z_i^{(d)} = \sum_{j=1}^{r} G_{ij}^{(d)}K_j^{(d)} + H_j^{(d)},\ Z_i^{(ud)} = \sum_{j=1}^{s} G_{ij}^{(ud)}K_j^{(ud)} + H_j^{(ud)}, \tag{5.6}$$

where subscript (d) refers to the delaminated, while (ud) refers the undelaminated plate portion, r and s are the size of vectors and matrices of these parts, respectively. The state-space models are discussed in the sequel for the method of 2ESLs and 4ESLs and in each case the FSDT, SSDT and TSDT quantities are given.

5.1 Generalized continuity conditions

The generalized continuity conditions between regions ① and ② in Figures 5.1a and 5.1b can be written as:

$$\left.\begin{pmatrix} g_\alpha \\ h_\alpha \\ m_\alpha \\ n_\alpha \\ p_\alpha \end{pmatrix}\right|_{x=+0}^{(1)} = \left.\begin{pmatrix} g_\alpha \\ h_\alpha \\ m_\alpha \\ n_\alpha \\ p_\alpha \end{pmatrix}\right|_{x=-0}^{(2)}, \tag{5.7}$$

where g, h, m, n and p denote parameter sets or functions defined in the sequel.

- *The continuity of deflection, its derivatives and the primary parameters* can be defined by a parameter set:

$$g_\alpha^{(l)} = (w, \frac{\partial w}{\partial x}, ..., \psi_{(p)j}; j = 1..\mathrm{Min}(q_l)), \tag{5.8}$$

  where l is the actual region (① or ②) and q_l is the number of parameters in $\psi_{(p)j}$ in both regions. We note that q_l is the total number of parameters in $\psi_{(p)j}$. As an example, for the TSDT model in Eq.(4.8) there are five parameters, on the other hand in Eq.(4.22) we have six, and thus for the TSDT theory with 4ESLs $\mathrm{Min}(q_l) = 5$.

- *The continuity condition of membrane displacement parameters* can be imposed by using the following functions:

$$\begin{aligned} h_\alpha^{(1)} &= \left.\begin{pmatrix} u_{0b} \\ v_{0b} \end{pmatrix} + \sum_{j=1}^{q_1} K_{1j}^{(0)} \begin{pmatrix} \psi_{(x)j} \\ \psi_{(y)j} \end{pmatrix}\right|^{(1)}, h_\alpha^{(2)} = \left.\begin{pmatrix} u_0 \\ v_0 \end{pmatrix} + \sum_{j=1}^{q_2} K_{1j}^{(0)} \begin{pmatrix} \psi_{(x)j} \\ \psi_{(y)j} \end{pmatrix}\right|^{(2)}, \\ m_\alpha^{(1)} &= \left.\begin{pmatrix} u_{0t} \\ v_{0t} \end{pmatrix} + \sum_{j=1}^{q_1} K_{\lambda j}^{(0)} \begin{pmatrix} \psi_{(x)j} \\ \psi_{(y)j} \end{pmatrix}\right|^{(1)}, m_\alpha^{(2)} = \left.\begin{pmatrix} u_0 \\ v_0 \end{pmatrix} + \sum_{j=1}^{q_2} K_{\lambda j}^{(0)} \begin{pmatrix} \psi_{(x)j} \\ \psi_{(y)j} \end{pmatrix}\right|^{(2)}, \end{aligned} \tag{5.9}$$

  where $\lambda = \frac{\omega}{2} + 1$ and ω is even number.

  It will be shown later that the membrane displacement continuity requires the imposition of the conditions above for a single layer in the bottom and a single one in the top plate.

- Since q_l is not always the same number for the delaminated and undelaminated parts of the plate, it is required to define the so-called *autocontinuity condition* (see later) by:

$$n_\alpha^{(l)} = \left.\sum_{j=1}^{q_l} K_{\kappa j}^{(\vartheta)} \begin{pmatrix} \psi_{(x)j} \\ \psi_{(y)j} \end{pmatrix}\right|^{(l)}, \tag{5.10}$$

where $\vartheta = 1, 2, 3$ depending on the vector of primary parameters (see later).

- *The continuity conditions of stress resultants* can be defined by:

$$p_\alpha^{(l)} = \left(\sum_{i=1..k} \mathbf{N}_i^{(x,xy)}, \hat{\mathbf{M}}_1^{(x,xy)} ..., \hat{\mathbf{L}}_1^{(x,xy)} ..., \hat{\mathbf{P}}_1^{(x,y)}, ... \right) \Bigg|^{(l)} . \tag{5.11}$$

The continuity conditions between regions ① - (1q) and (1q) - (1a) for problem ⓐ in Figure 5.1a are imposed by :

$$\begin{aligned} g_\beta^{(1)}\Big|_{x=x_Q-d_0} &= g_\beta^{(1q)}\Big|_{x=x_Q-d_0}, \quad g_\gamma^{(1)}\Big|_{x=x_Q-d_0} = g_\gamma^{(1q)}\Big|_{x=x_Q-d_0}, \\ g_\beta^{(1q)}\Big|_{x=x_Q+d_0} &= g_\beta^{(1a)}\Big|_{x=x_Q+d_0}, \quad g_\gamma^{(1q)}\Big|_{x=x_Q+d_0} = g_\gamma^{(1a)}\Big|_{x=x_Q+d_0}, \end{aligned} \tag{5.12}$$

where the parameter sets are:

$$\begin{aligned} g_\beta^{(l)} &= (w, \frac{\partial w}{\partial x}, ..., u_{0b}, u_{0t}, v_{0b}, v_{0t}, \psi_{(p)j}; j = 1..q_l), \quad p = x, y \\ g_\gamma^{(l)} &= \left(\sum_{i=1..k/2} \mathbf{N}_i^{(x,xy)}, \sum_{i=k/2+1..k} \mathbf{N}_i^{(x,xy)}, \mathbf{M}_i^{(x,xy)} ..., \mathbf{L}_i^{(x,xy)} ..., \mathbf{P}_i^{(x,xy)} ... \right) \Bigg|^{(l)}, \quad i = 1..k. \end{aligned} \tag{5.13}$$

For problem ⓑ in Figure 5.1b the continuity conditions can be imposed in a similar way by using Eqs.(5.7)-(5.12) and changing the evaluation bounds.

5.2 Method of 2ESLs - Reddy TSDT

5.2.1 Undelaminated region

In the case of the Reddy TSDT the state vector contains the parameters of vector $\boldsymbol{\psi}$ (refer to Subsection 3.1.1), the global membrane parameters u_0 and v_0 and the first derivatives of all these parameters, finally the deflection w and its first three derivatives leading to (and using the Lévy solution by Eq.(5.2)):

$$\mathbf{Z}^{(ud)} = \left(U_{0n} U'_{0n} V_{0n} V'_{0n} X_{1n} X'_{1n} Y_{1n} Y'_{1n} Z_{x2n} Z'_{x2n} Z_{y2n} Z'_{y2n} Z_{x1n} Z'_{x1n} Z_{y1n} Z'_{y1n} W_n W'_n W''_n W'''_n \right)^T, \tag{5.14}$$

i.e. the vector $\mathbf{Z}^{(ud)}$ contains 20 elements, moreover the system matrix size is 20×20, matrix $\mathbf{T}$ is placed in Appendix C.1.1 to show its structure and the fact that it contains 90 constants. In the sequel the constants in the system matrix of the undelaminated part are denoted by the "~". The vector $\mathbf{F}$ in Eq.(5.3) is:

$$\mathbf{F}^{(ud)} = \begin{pmatrix} 0 & 0 & 0 & 0 & 0 & 0 & 0 & 0 & 0 & 0 & 0 & 0 & 0 & 0 & 0 & 0 & 0 & 0 & 0 & \tilde{S}_{91} \cdot Q_n \end{pmatrix}^T, \tag{5.15}$$

where $\tilde{S}_{91}$ is a constant and can be determined based on the governing equation for δw (Eq.(3.9)). In accordance with Figure 5.1, for problem ⓐ $Q_n = 0$ because there is no external load in region ②. For problem ⓑ in Figure 5.1 $Q_n = 2\frac{q_0}{b} \sin \beta y_0$ (*Reddy (2004)*), where $q_0 = Q_0/(2d_0)$, Q_0 is the value of the concentrated force.

5.2.2 Delaminated region

The state vector of the Reddy TSDT model of the delaminated part contains the following elements:

$$\mathbf{Z}^{(d)} = \left(U_{0tn}U'_{0tn}V_{0tn}V'_{0tn}X_{2n}X'_{2n}Y_{2n}Y'_{2n}U_{0bn}U'_{0bn}V_{0bn}V'_{0bn}X_{1n}X'_{1n}Y_{1n}Y'_{1n}W_nW'_nW''_nW'''_n\right)^T, \tag{5.16}$$

viz. the size of vector $\mathbf{Z}^{(d)}$ is 20, the system matrix size is 20×20 (similarly to the undelaminated portion). It contains 58 constants, which are denoted by the " $^-$ " symbol. The system matrix can be found in Appendix C.1.1, its structure differs from that of the undelaminated part. Vector $\mathbf{F}$ is:

$$\mathbf{F}^{(d)} = \begin{pmatrix} 0 & 0 & 0 & 0 & 0 & 0 & 0 & 0 & 0 & 0 & 0 & 0 & 0 & 0 & 0 & 0 & 0 & 0 & 0 & \bar{S}_{59} \cdot Q_n \end{pmatrix}^T, \tag{5.17}$$

where $\bar{S}_{59}$ is a constant and can be determined based on the governing equation for δw (Eq.(3.26)). In accordance with Figure 5.1a, for problem a $Q_n = 2\frac{q_0}{b}\sin\beta y_0$ in region 1q, where $q_0 = Q_0/(2d_0)$, Q_0 is the value of the concentrated force. For problem b in Figure 5.1 $Q_n = 0$.

5.2.3 Boundary conditions

The number of B.C.s is always equal to half of the size of the state vector in Eq.(5.3). Only the conditions for problem a in Figure 5.1a are given, for problem b the conditions can be derived in a similar way. The B.C.s can be classified as simply supported, built-in and free edge conditions. For the delaminated region 1a we have:

$$\begin{array}{ll} \text{simply sup.:} & \left\{ \left(w, \frac{\partial^2 w}{\partial x^2}, v_{0b}, v_{0t}, \theta_{(y)1}, \theta_{(y)2}, M_{x(1)}, M_{x(2)}, N_{x(1)}, N_{x(2)}\right)\Big|_{x=a}^{(1a)} = 0, \right. \\ \text{built-in:} & \left\{ \left(w, \frac{\partial w}{\partial x}, u_{0b}, u_{0t}, v_{0b}, v_{0t}, \theta_{(x)1}, \theta_{(y)1}, \theta_{(x)2}, \theta_{(y)2}\right)\Big|_{x=a}^{(1a)} = 0, \right. \\ \text{free edge:} & \left\{ \left(\mathbf{N}_1^{(x,xy)}, \mathbf{N}_2^{(x,xy)}, \mathbf{M}_1^{(x,xy)}, \mathbf{M}_2^{(x,xy)}\right)\Big|_{x=a}^{(1a)} = \mathbf{0}, \left(\frac{\partial^3 w}{\partial x^3}, \sum_{i=1}^{2} Q_{x(i)}\right)\Big|_{x=a}^{(1a)} = 0. \right. \end{array} \tag{5.18}$$

For the undelaminated region 2 we have:

$$\begin{array}{ll} \text{simply sup.:} & \left\{ \left(w, v_0, \theta_{(y)1}, \lambda_{(y)1}, \lambda_{(y)2}, M_{x(1)}, M_{x(2)}, N_{x(1)} + N_{x(2)}, P_{x(1)}, P_{x(2)}\right)\Big|_{x=-c}^{(2)} = 0, \right. \\ \text{built-in:} & \left\{ \left(w, \frac{\partial w}{\partial x}, \sum_{i=1..2} N_{x(i)}, \sum_{i=1..2} N_{xy(i)}, \theta_{(x)1}, \theta_{(y)1}, \lambda_{(x)1}, \lambda_{(y)1}, \lambda_{(x)2}, \lambda_{(y)2}\right)\Big|_{x=-c}^{(2)} = 0, \right. \\ \text{free edge:} & \left\{ \left(\sum_{i=1..2} \mathbf{N}_i^{(x,xy)}, \mathbf{M}_1^{(x,xy)}, \mathbf{P}_1^{(x,xy)}, \mathbf{P}_2^{(x,xy)}\right)\Big|_{x=-c}^{(2)} = \mathbf{0}, \left(\frac{\partial^3 w}{\partial x^3}, \sum_{i=1}^{2} Q_{x(i)}\right)\Big|_{x=-c}^{(2)} = 0. \right. \end{array} \tag{5.19}$$

As it can be seen, at each boundary and each case there are ten conditions, which is exactly the half of the system matrix size of the TSDT model.

5.2.4 Continuity conditions

The parameter sets in Eq.(5.7) for the continuity conditions are defined below.

- The set of deflection, its derivatives and the mutual primary parameters in Eqs.(3.6) and (3.23) is:

$$g_\alpha = (w, \frac{\partial w}{\partial x}, \frac{\partial^2 w}{\partial x^2}, \frac{\partial^3 w}{\partial x^3}, \theta_{(x)1}, \theta_{(y)1}). \tag{5.20}$$

- For the $h_\alpha^{(l)}$ and $m_\alpha^{(l)}$ parameter sets in Eq.(5.9) $q_1 = 3, q_2 = 4$ (refer to Eqs.(3.6) and (3.23)) and $\lambda = 2$ ($\omega = 2$, continuity of membrane displacements).

- The sets of the so-called autocontinuity condition are:

$$n_\alpha^{(2)} = \left(\begin{array}{c} \lambda_{(p)1} \\ \lambda_{(p)2} \end{array} \right)\Bigg|^{(2)}, n_\alpha^{(1)} = \sum_{j=1}^{3} K_{1j}^{(3)} \left(\begin{array}{c} \psi_{(p)j} \\ \psi_{(p)j} \end{array} \right)\Bigg|^{(1)}, \tag{5.21}$$

where $\lambda_{p(1)}$ and $\lambda_{p(2)}$ are the *autocontinuity* parameters (refer to Eqs.(3.6) and (3.23)). Taking back the K_{ij} constants given in Appendix A.1 into the condition above yields the following:

$$\left(\begin{array}{c} \lambda_{(p)1} \\ \lambda_{(p)2} \end{array} \right)\Bigg|^{(2)}_{x=-0} = -\frac{4}{3} \left(\begin{array}{c} \frac{1}{t_1^2}(\theta_{(p)1} + \frac{\partial w}{\partial p}) \\ \frac{1}{t_2^2}(\theta_{(p)2} + \frac{\partial w}{\partial p}) \end{array} \right)\Bigg|^{(1)}_{x=+0}. \tag{5.22}$$

It is clear that there is a parameter in Eq.(3.23) that no conditions are imposed against, and this is $\theta_{(p)2}$. The autocontinuity means that by imposing Eq.(5.22) the continuity of $\theta_{(p)2}$ is satisfied automatically. This can be proven by taking the linear parts in Eq.(2.1) and (2.8) and taking back the K_{ij} constants of the Reddy TSDT solution of the undelaminated region (Appendix A.1):

$$\theta_{(p)2}\big|^{(2)}_{x=-0} = \sum_{j=1}^{4} K_{1j}^{(1)} \psi_{(p)j}\Bigg|^{(2)}_{x=-0} = \left(1 \cdot \theta_{(p)1} - \frac{3}{4} t_2^2 \lambda_{(p)2} + \frac{3}{4} t_1^2 \lambda_{(p)1} + 0 \cdot \frac{\partial w}{\partial p}\right)\Bigg|^{(2)}_{x=-0}. \tag{5.23}$$

Substituting Eq.(5.22) yields:

$$\theta_{(p)2}\big|^{(2)}_{x=-0} = \theta_{(p)2}\big|^{(1)}_{x=+0}. \tag{5.24}$$

In a similar way, by taking the quadratic parts in Eq.(2.1) and (2.8) and taking back the K_{ij} constants we have:

$$\phi_{(p)2}\big|^{(2)}_{x=-0} = \sum_{j=1}^{4} K_{1j}^{(2)} \psi_{(p)j}\Bigg|^{(2)}_{x=-0} = \left(\frac{1}{t_1} \theta_{(p)1} + 0 \cdot \lambda_{(p)2} + \frac{3}{4} t_1 \lambda_{(p)1} + \frac{1}{t_1} \frac{\partial w}{\partial p}\right)\Bigg|^{(2)}_{x=-0}.$$

dc_1254_16

(5.25)

Taking back again Eq.(5.22) results in:

$$\phi_{(p)2}\Big|_{x=-0}^{(2)} = 0. \tag{5.26}$$

Because of the fact that the $K_{ij}^{(2)}$ constants are zero for the delaminated region (see Appendix A.1) we obtain:

$$\phi_{(p)1}\Big|^{(1)} = \sum_{j=1}^{3} K_{1j}^{(2)} \psi_{(p)j}\Bigg|^{(1)} = 0, \tag{5.27}$$

i.e. the autocontinuity is satisfied against the quadratic terms, as well.

- The continuity of stress resultants is ensured by the parameter set below:

$$p_{\alpha}^{(l)} = \left(\sum_{i=1..2} \mathbf{N}_i^{(x,xy)}, \hat{\mathbf{M}}_i^{(x,xy)} \right), \quad i = 1..2. \tag{5.28}$$

- The parameter sets for the continuity between the regions 1-1q and 1a-1q are:

$$\begin{aligned} g_{\beta} &= \left(w, \frac{\partial w}{\partial x}, \frac{\partial^2 w}{\partial x^2}, \frac{\partial^3 w}{\partial x^3}, u_{0b}, u_{0t}, v_{0b}, v_{0t}, \theta_{(x)1}, \theta_{(y)1}, \theta_{(x)2}, \theta_{(y)2} \right), \\ g_{\gamma} &= \left(\mathbf{N}_1^{(x,xy)}, \mathbf{N}_2^{(x,xy)}, \mathbf{M}_1^{(x,xy)}, \mathbf{M}_2^{(x,xy)} \right), \end{aligned} \tag{5.29}$$

totaling 20 conditions.

5.3 Method of 2ESLs - Second-order plate theory

5.3.1 Undelaminated region

In the case of the SSDT the state vector of the undelaminated part contains the parameters of vector $\boldsymbol{\psi}$ (refer to Subsection 3.1.2), the global membrane parameters u_0 and v_0, the deflection w and the first derivatives of all these parameters leading to 22 elements:

$$\mathbf{Z}^{(ud)} = \left(U_{0n}U'_{0n}V_{0n}V'_{0n}X_{2n}X'_{2n}Y_{2n}Y'_{2n}Z_{x2n}Z'_{x2n}Z_{y2n}Z'_{y2n}X_{1n}X'_{1n}Y_{1n}Y'_{1n}Z_{x1n}Z'_{x1n}Z_{y1n}Z'_{y1n}W_nW'_n\right)^T. \tag{5.30}$$

The size of system matrix is 22×22 and it contains 121 constants, it can be found in Appendix C.1.2. Vector $\mathbf{F}$ becomes:

$$\mathbf{F}^{(ud)} = \left(0\ 0\ 0\ 0\ 0\ 0\ 0\ 0\ 0\ 0\ 0\ 0\ 0\ 0\ 0\ 0\ 0\ 0\ 0\ 0\ 0\ \tilde{R}_{122} \cdot Q_n \right)^T, \tag{5.31}$$

where $\tilde{R}_{122}$ is a constant determined based on Eq.(3.15) and Q_n is calculated exactly in the same way as that for the Reddy TSDT.

5.3.2 Delaminated region

In the delaminated region the number of parameters in $\mathbf{Z}$ is 26:

$$\begin{aligned}\mathbf{Z}^{(d)} = \big(& U_{0tn}\ U'_{0tn}\ V_{0tn}\ V'_{0tn}\ X_{2n}\ X'_{2n}\ Y_{2n}\ Y'_{2n}\ T_{x2n}\ T'_{x2n}\ T_{y2n}\ T'_{y2n} \\ & U_{0bn}\ U'_{0bn}\ V_{0bn}\ V'_{0bn}\ X_{1n}\ X'_{1n}\ Y_{1n}\ Y'_{1n}\ T_{x1n}\ T'_{x1n}\ T_{y1n}\ T'_{y1n}\ W_n\ W'_n \big)^T .\end{aligned} \tag{5.32}$$

The structure of matrix $\mathbf{T}$ is shown in Appendix C.1.2, the number of constants is 93. The vector $\mathbf{F}$ is calculated as:

$$\mathbf{F}^{(d)} = \big(0\ 0\ 0\ 0\ 0\ 0\ 0\ 0\ 0\ 0\ 0\ 0\ 0\ 0\ 0\ 0\ 0\ 0\ 0\ 0\ 0\ 0\ 0\ 0\ 0\ \bar{R}_{94} \cdot Q_n \big)^T , \tag{5.33}$$

where $\bar{R}_{94}$ is a constant based on the governing equation of the SSDT solution by Eq.(3.32).

5.3.3 Boundary conditions

The B.C.s for the delaminated region (1a) are:

$$\begin{aligned}
&\text{simply sup.:} && \begin{cases} (w, v_{0b}, v_{0t}, \theta_{(y)1}, \theta_{(y)2}, \phi_{(y)1}, \phi_{(y)2},)\big|_{x=a}^{(1a)} = 0, \\ (N_{x(1)}, N_{x(2)}, M_{x(1)}, M_{x(2)}, L_{x(1)}, L_{x(2)})\big|_{x=a}^{(1a)} = 0, \end{cases} \\
&\text{built-in:} && \begin{cases} (w, u_{0b}, u_{0t}, \theta_{(x)1}, \theta_{(x)2}, \phi_{(x)1}, \phi_{(x)2})\big|_{x=a}^{(1a)} = 0, \\ (v_{0b}, v_{0t}, \theta_{(y)1}, \theta_{(y)2}, \phi_{(y)1}, \phi_{(y)2})\big|_{x=a}^{(1a)} = 0, \end{cases} \\
&\text{free edge:} && \begin{cases} (\mathbf{N}_1^{(x,xy)}, \mathbf{N}_2^{(x,xy)}, \mathbf{M}_1^{(x,xy)}, \mathbf{M}_2^{(x,xy)}, \mathbf{L}_1^{(x,xy)}, \mathbf{L}_2^{(x,xy)})\Big|_{x=a}^{(1a)} = \mathbf{0}, \sum_{i=1}^{2} Q_{x(i)})\Big|_{x=a}^{(1a)} = 0, \end{cases}
\end{aligned} \tag{5.34}$$

where in each case there are thirteen conditions. At the same time, for the undelaminated region (2) we have:

$$\begin{aligned}
&\text{simply sup.:} && \begin{cases} (w, v_0, \theta_{(y)1}, \theta_{(y)2}, \phi_{(y)1}, \phi_{(y)2})\big|_{x=-c}^{(2)} = 0, \\ (\sum_{i=1..2} N_{x(i)}, \hat{M}_{x(1)}, \hat{M}_{x(2)}, \hat{L}_{x(1)}, \hat{L}_{x(2)})\Big|_{x=-c}^{(2)} = 0, \end{cases} \\
&\text{built-in:} && \begin{cases} (w, \sum_{i=1}^{2} N_{x(i)}, \sum_{i=1}^{2} N_{xy(i)}, \theta_{(x)1}, \theta_{(y)1}, \theta_{(x)2}, \theta_{(y)2}, \phi_{(x)1}, \phi_{(y)1}, \phi_{(x)2}, \phi_{(y)2})\Big|_{x=-c}^{(2)} = 0, \end{cases} \\
&\text{free edge:} && \begin{cases} (\sum_{i=1..2} \mathbf{N}_i^{(x,xy)}, \hat{\mathbf{M}}_1^{(x,xy)}, \hat{\mathbf{M}}_2^{(x,xy)}, \hat{\mathbf{L}}_1^{(x,xy)}, \hat{\mathbf{L}}_2^{(x,xy)})\Big|_{x=-c}^{(2)} = \mathbf{0}, \sum_{i=1}^{2} Q_{x(i)}\Big|_{x=-c}^{(2)} = 0, \end{cases}
\end{aligned} \tag{5.35}$$

defining eleven conditions in each case.

5.3.4 Continuity conditions

- The parameter set in order to ensure the continuity of displacement parameters is:

$$g_\alpha = (w, \frac{\partial w}{\partial x}, \theta_{(x)1}, \theta_{(y)1}, \theta_{(x)2}, \theta_{(y)2}, \phi_{(x)1}, \phi_{(y)1}, \phi_{(x)2}, \phi_{(y)2}). \tag{5.36}$$

- To satisfy the continuity of membrane displacements the $h_\alpha^{(l)}$ and $m_\alpha^{(l)}$ parameter sets in Eq.(5.9) involve $q_1 = q_2 = 4$ (refer to Eqs.(3.13) and (3.29)) and $\lambda = 2$ ($\omega = 2$).
- The continuity of stress resultants is imposed by the following set:

$$p_\alpha^{(l)} = \left(\sum_{i=1..2} \mathbf{N}_i^{(x,xy)}, \hat{\mathbf{M}}_i^{(x,xy)}, \hat{\mathbf{L}}_i^{(x,xy)} \right) , \quad i = 1, 2. \tag{5.37}$$

- The continuity between the 1-1q and 1a-1q regions are ensured by the parameter sets of:

$$\begin{aligned} g_\beta &= \left(w, \frac{\partial w}{\partial x}, u_{0b}, u_{0t}, v_{0b}, v_{0t}, \theta_{(x)1}, \theta_{(y)1}, \theta_{(x)2}, \theta_{(y)2}, \phi_{(x)1}, \phi_{(y)1}, \phi_{(x)2}, \phi_{(y)2} \right), \\ g_\gamma &= \left(\mathbf{N}_1^{(x,xy)}, \mathbf{N}_2^{(x,xy)}, \mathbf{M}_1^{(x,xy)}, \mathbf{M}_2^{(x,xy)}, \mathbf{L}_1^{(x,xy)}, \mathbf{L}_2^{(x,xy)} \right). \end{aligned} \tag{5.38}$$

5.4 Method of 2ESLs - First-order plate theory

5.4.1 Undelaminated region

According to the parameters of vector $\boldsymbol{\psi}$ in Subsection 3.1.3 the state vector becomes:

$$\mathbf{Z}^{(ud)} = \left(U_{0n}\ U'_{0n}\ V_{0n}\ V'_{0n}\ X_{2n}\ X'_{2n}\ Y_{2n}\ Y'_{2n}\ X_{1n}\ X'_{1n}\ Y_{1n}\ Y'_{1n}\ W_n\ W'_n \right)^T, \tag{5.39}$$

viz. the vector $\mathbf{Z}$ contains 14 elements, the system matrix size is 14×14 and can be found in Appendix C.1.3. The number of constants in $\mathbf{T}$ is 49. The vector $\mathbf{F}$ is:

$$\mathbf{F}^{(ud)} = \left(\begin{matrix} 0 & 0 & 0 & 0 & 0 & 0 & 0 & 0 & 0 & 0 & 0 & 0 & 0 & \tilde{Q}_{50} \cdot Q_n \end{matrix} \right)^T, \tag{5.40}$$

where $\tilde{Q}_{50}$ is a constant determined on the base of Eq.(3.15) and Q_n is calculated as it is given in Subsection 5.2.1.

5.4.2 Delaminated region

On the base of Subsection 3.2.3 the state vector takes the form of:

$$\mathbf{Z}^{(d)} = \left(U_{0tn}\, U'_{0tn}\, V_{0tn}\, V'_{0tn}\, X_{2n}\, X'_{2n}\, Y_{2n}\, Y'_{2n}\, U_{0bn}\, U'_{0bn}\, V_{0bn}\, V'_{0bn}\, X_{1n}\, X'_{1n}\, Y_{1n}\, Y'_{1n}\, W_n\, W'_n \right)^T, \tag{5.41}$$

as it is seen the vector $\mathbf{Z}$ contains 18 elements, consequently the system matrix size is 18×18 with the structure shown in Appendix C.1.3 and 45 constants. The vector $\mathbf{F}$ is given below:

$$\mathbf{F}^{(d)} = \left(\begin{matrix} 0 & 0 & 0 & 0 & 0 & 0 & 0 & 0 & 0 & 0 & 0 & 0 & 0 & 0 & 0 & 0 & 0 & \bar{Q}_{46} \cdot Q_n \end{matrix} \right)^T, \tag{5.42}$$

where $\bar{Q}_{46}$ is a constant determined by Eq.(3.35) and Q_n was given in Subsection 5.2.2.

5.4.3 Boundary conditions

In the delaminated part (1a) the B.C.s of FSDT are defined as (nine conditions):

$$\begin{aligned}
&\text{simply supported:} && \Big\{ (w, v_{0b}, v_{0t}, \theta_{(y)1}, \theta_{(y)2}, N_{x(1)}, N_{x(2)}, M_{x(1)}, M_{x(2)})\Big|_{x=a}^{(1a)} = 0\,,\\
&\text{built-in:} && \Big\{ (w, u_{0b}, u_{0t}, v_{0b}, v_{0t}, \theta_{(x)1}, \theta_{(y)1}, \theta_{(x)2}, \theta_{(y)2})\Big|_{x=a}^{(1a)} = 0\,,\\
&\text{free edge:} && \Big\{ (\mathbf{N}_1^{(x,xy)}, \mathbf{N}_2^{(x,xy)}, \mathbf{M}_1^{(x,xy)}, \mathbf{M}_2^{(x,xy)}\Big|_{x=a}^{(1a)} = \mathbf{0}, \sum_{i=1}^{2} Q_{x(i)})\Big|_{x=a}^{(1a)} = 0\,.
\end{aligned} \tag{5.43}$$

On the other hand, for the undelaminated region (2) we have seven conditions:

$$\begin{aligned}
&\text{simply supported:} && \Big\{ (w, v_0, \theta_{(y)1}, \theta_{(y)2}, N_{x(1)} + N_{x(2)}, \hat{M}_{x(1)}, \hat{M}_{x(2)})\Big|_{x=-c}^{(2)} = 0\,,\\
&\text{built-in:} && \Big\{ (w, \sum_{i=1..2} N_{x(i)}, \sum_{i=1..2} N_{xy(i)}, \theta_{(x)1}, \theta_{(y)1}, \theta_{(x)2}, \theta_{y2})\Big|_{x=-c}^{(2)} = 0\,,\\
&\text{free edge:} && \Big\{ (\sum_{i=1..2} \mathbf{N}_i^{(x,xy)}, \hat{\mathbf{M}}_1^{(x,xy)}, \hat{\mathbf{M}}_2^{(x,xy)}\Big|_{x=-c}^{(2)} = \mathbf{0}, \sum_{i=1}^{2} Q_{x(i)})\Big|_{x=-c}^{(2)} = 0\,.
\end{aligned} \tag{5.44}$$

5.4.4 Continuity conditions

The parameter set in accordance with Eq.(5.8), Eq.(3.18) and (3.33) is:

$$g_\alpha = (w, \frac{\partial w}{\partial x}, \theta_{(x)1}, \theta_{(y)1}, \theta_{(x)2}, \theta_{(y)2}). \tag{5.45}$$

For the $h_\alpha^{(l)}$ and $m_\alpha^{(l)}$ sets in Eq.(5.9) $q_1 = q_2 = 2$ and $\lambda = 2$ ($\omega = 2$) (continuity of membrane displacements). The set $p_\alpha^{(l)}$ is the same as Eq.(5.28), and finally the sets for Eq.(5.13) are:

$$\begin{aligned}
g_\beta &= \left(w, \frac{\partial w}{\partial x}, u_{0b}, u_{0t}, v_{0b}, v_{0t}, \theta_{(x)1}, \theta_{(y)1}, \theta_{(x)2}, \theta_{(y)2}\right),\\
g_\gamma &= \left(\mathbf{N}_1^{(x,xy)}, \mathbf{N}_2^{(x,xy)}, \mathbf{M}_1^{(x,xy)}, \mathbf{M}_2^{(x,xy)}\right).
\end{aligned} \tag{5.46}$$

5.5 Method of 4ESLs - Third-order plate theory

In the case of the method 4ESLs the number of parameters is in general higher than in the case of the 2ESLs, especially for the TSDT. However, the accuracy of the model is expected to be much better compared to that of the 2ESLs method.

5.5.1 Undelaminated region

According to Eq.(4.7) and Subsection 4.1.1 the state vector of TSDT solution contains 26 elements and becomes:

$$\begin{aligned}
\mathbf{Z}^{(ud)} = (\; & U_{0n} \;\; U_{0n}' \;\; V_{0n} \;\; V_{0n}' \;\; X_{1n} \;\; X_{1n}' \;\; Y_{1n} \;\; Y_{1n}' \;\; X_{2n} \;\; X_{2n}' \;\; Y_{2n} \;\; Y_{2n}' \\
& X_{3n} \;\; X_{3n}' \;\; Y_{3n} \;\; Y_{3n}' \;\; X_{4n} \;\; X_{4n}' \;\; Y_{4n} \;\; Y_{4n}' \;\; T_{x3n} \;\; T_{x3n}' \;\; T_{y3n} \;\; T_{y3n}' \;\; W_n \;\; W_n' \;)^T .
\end{aligned} \tag{5.47}$$

dc_1254_16

The system matrix dimension is 26 × 26 and placed in Appendix C.2.1. The number of constant in $\mathbf{T}$ is 89. The vector of external loads takes the following form:

$$\mathbf{F}^{(ud)} = \left(0\ 0\ 0\ 0\ 0\ 0\ 0\ 0\ 0\ 0\ 0\ 0\ 0\ 0\ 0\ 0\ 0\ 0\ 0\ 0\ 0\ 0\ 0\ 0\ 0\ \tilde{S}_{90} \cdot Q_n \right)^T, \tag{5.48}$$

where $\tilde{S}_{90}$ is a constant based on Eq.(4.11) and Q_n is defined in Subsection 5.2.1.

5.5.2 Delaminated region

In Eq.(4.22) there are twelve parameters, the state vector can be given as:

$$\begin{aligned}\mathbf{Z}^{(d)} = (&U_{0bn}\, U'_{0bn}\, V_{0bn}\, V'_{0bn}\, X_{1n}\, X'_{1n}\, Y_{1n}\, Y'_{1n}\, X_{2n}\, X'_{2n}\, Y_{2n}\, Y'_{2n}\, T_{x1n}\, T'_{x1n}\, T_{y1n}\, T'_{y1n}\\ &U_{0tn}\, U'_{0tn}\, V_{0tn}\, V'_{0tn}\, X_{3n}\, X'_{3n}\, Y_{3n}\, Y'_{3n}\, X_{4n}\, X'_{4n}\, Y_{4n}\, Y'_{4n}\, T_{x3n}\, T'_{x3n}\, T_{y3n}\, T'_{y3n}\, W_n\, W'_n)^T,\end{aligned} \tag{5.49}$$

i.e. the system matrix dimension is 34 × 34, its structure involving 85 constants is shown in Appendix C.2.1. The vector of external loads takes the form of:

$$\mathbf{F}^{(d)} = \left(0\ 0\ 0\ 0\ 0\ 0\ 0\ 0\ 0\ 0\ 0\ 0\ 0\ 0\ 0\ 0\ 0\ 0\ 0\ 0\ 0\ 0\ 0\ 0\ 0\ 0\ 0\ 0\ 0\ 0\ 0\ 0\ 0\ \bar{S}_{86} \cdot Q_n \right)^T, \tag{5.50}$$

where $\bar{S}_{86}$ is a constant based on TSDT (Eq.(4.25)). Q_n is given in Subsection 5.2.2.

5.5.3 Boundary conditions

The B.C.s of the problem in Figure 5.1a are determined through the displacement parameters and stress resultants in accordance with the following for the delaminated region 1a:

$$\begin{aligned}
&\text{- simply sup.:} && \begin{cases} (w, v_{0b}, v_{0t}, \theta_{(y)1}, \theta_{(y)2}, \theta_{(y)3}, \theta_{(y)4}, \lambda_{(y)1}, \lambda_{(y)3})\big|_{x=a}^{(1a)} = 0, \\ \left(\sum_{i=1}^{2} N_{x(i)}, \sum_{i=3}^{4} N_{x(i)}, M_{x(1)}, M_{x(2)}, M_{x(3)}, M_{x(4)}, P_{x(1)}, P_{x(3)}\right)\Big|_{x=a}^{(1a)} = 0, \end{cases}\\
&\text{- built-in:} && \begin{cases} (w, u_{0b}, u_{0t}, \theta_{(x)1}, \theta_{(x)2}, \theta_{(x)3}, \theta_{(x)4}, \lambda_{(x)1}, \lambda_{(x)3})\big|_{x=a}^{(1a)} = 0, \\ (v_{0b}, v_{0t}, \theta_{(y)1}, \theta_{(y)2}, \theta_{(y)3}, \theta_{(y)4}, \lambda_{(y)1}, \lambda_{(y)3})\big|_{x=a}^{(1a)} = 0, \end{cases}\\
&\text{- free edge:} && \begin{cases} (\hat{\mathbf{M}}_1^{(x,xy)}, \hat{\mathbf{M}}_2^{(x,xy)}, \hat{\mathbf{M}}_3^{(x,xy)}, \hat{\mathbf{M}}_4^{(x,xy)}, \hat{\mathbf{P}}_1^{(x,y)}, \hat{\mathbf{P}}_3^{(x,y)})\Big|_{x=a}^{(1a)} = \mathbf{0}, \\ \left(\sum_{i=1..2} \mathbf{N}_i^{(x,xy)}, \sum_{i=3..4} \mathbf{N}_i^{(x,xy)}\right)\Big|_{x=a}^{(1)} = \mathbf{0}, \ \sum_{i=1..4} Q_{x(i)}\Big|_{x=a}^{(1a)} = 0, \end{cases}
\end{aligned} \tag{5.51}$$

and for the undelaminated region 2:

$$\begin{aligned}
&\text{- simply sup.:} && \begin{cases} (w, v_0, \theta_{(y)1}, \theta_{(y)2}, \theta_{(y)3}, \theta_{(y)4}, \lambda_{(y)3})\big|_{x=-c}^{(2)} = 0, \\ \left(\sum_{i=1}^{4} N_{x(i)}, M_{x(1)}, M_{x(2)}, M_{x(3)}, M_{x(4)}, P_{x(3)}\right)\Big|_{x=-c}^{(2)} = 0, \end{cases}\\
&\text{- built-in:} && \begin{cases} \left(w, \sum_{i=1..4} N_{x(i)}, \theta_{(x)1}, \theta_{(x)2}, \theta_{(x)3}, \theta_{(x)4}, \lambda_{(x)3}\right)\Big|_{x=-c}^{(2)} = 0, \\ \left(\sum_{i=1..4} N_{xy(i)}, \theta_{(y)1}, \theta_{(y)2}, \theta_{(y)3}, \theta_{(y)4}, \lambda_{(y)3}\right)\Big|_{x=-c}^{(2)} = 0, \end{cases}\\
&\text{- free edge:} && \begin{cases} (\hat{\mathbf{M}}_1^{(x,xy)}, \hat{\mathbf{M}}_2^{(x,xy)}, \hat{\mathbf{M}}_3^{(x,xy)}, \hat{\mathbf{M}}_4^{(x,xy)}, \hat{\mathbf{P}}_3^{(x,y)})\Big|_{x=-c}^{(2)} = \mathbf{0}, \\ \sum_{i=1..4} \mathbf{N}_i^{(x,xy)}\Big|_{x=-c}^{(2)} = \mathbf{0}, \ \sum_{i=1..4} Q_{x(i)}\Big|_{x=-c}^{(2)} = 0. \end{cases}
\end{aligned} \tag{5.52}$$

5.5.4 Continuity conditions between regions (1) and (2)

The conditions between regions ① and ② (refer to Figure 5.1a) involve the continuity of the displacement parameters and stress resultants. In the sequel, the continuity of the displacement field and stress resultants are discussed separately using the parameter sets in Eq.(5.7).

5.5.4.1 Continuity of displacement parameters

In the case of the general TSDT the continuity of the in-plane displacement is ensured only if the constant, linear, quadratic and cubic terms in Eqs.(2.8) and (2.36)-(2.37) are exactly the same in the delamination front ($x = 0$) in each ESL. Because of the parameter elimination based on the SEKC it is not possible to match directly the constant, quadratic and cubic terms in the displacement function from layer by layer. Only the continuity of *primary parameters* can be defined between each ESL. In spite of that the continuity of the remaining membrane, linear, quadratic and cubic terms can be ensured indirectly (automatically) if certain conditions are met. In fact this feature of the problem has already been shown in Subsection 5.2.4 in the course of the Reddy TSDT, however, here a more general description is given. The requirements of *automatic continuity* are formulated in the form of a theorem. We define the following set of parameters to satisfy the first in Eq.(5.7):

$$g_\alpha = (w, \frac{\partial w}{\partial x}, \theta_{(x)1}, \theta_{(y)1}, \theta_{(x)2}, \theta_{(y)2}, \theta_{(x)3}, \theta_{(y)3}, \theta_{(x)4}, \theta_{(y)4}\lambda_{(x)3}, \lambda_{(y)3}), \tag{5.53}$$

which contains the deflection, slope and the *mutual primary parameters* in Eq.(4.8) and (4.22) as a necessary condition. However the first in Eq.(5.7) is not a sufficient condition. The sufficient conditions are presented through a theorem.

5.5.4.2 The theorem of autocontinuity (AC theorem)

AC theorem: If the displacement fields in the form of Eqs.(2.8) and (2.36)-(2.37) in a laminated plate with delamination is developed by using the SEKC requirements and $N_d \in \mathbb{N}$ and $N_{ud} \in \mathbb{N}$ are the numbers of eliminated parameters in the delaminated and undelaminated parts, respectively, and $N_d \neq N_{ud}$, then the total continuity of the first-, second- and third-order terms in the in-plane displacement functions of each ESL in the delaminated and undelaminated plate parts - apart from those imposed by the first of Eq.(5.7) (*mutual primary parameters*) - can be ensured by imposing the continuity of $|N_d - N_{ud}| \in \mathbb{N}$ number of parameters. These parameters are the *autocontinuity* (or simply *AC*) *parameters*, which are at the same time *primary parameters* too. The autocontinuity is satisfied only if along the interface planes (interface planes $1-2$ and $3-4$ in Figures 4.1 and 4.2) except for the delamination plane (Figures 2.2 and 2.3) the same conditions are imposed in the delaminated and undelaminated regions. Along the delamination plane (interface $2-3$ in Figures 4.1 and 4.2) different conditions can be applied. Figure 5.2a shows a case when the autocontinuity between the delaminated and undelaminated parts is satisfied, Figure 5.2b indicates a case when dissimilar conditions are imposed at interface 3-4 leading to a discontinuous displacement field in the top plates.

Proof: In the case of the TSDT model $N_d = 20$, $N_{ud} = 22$ (refer to Subsections 4.1.1 and 4.2.1), so the number of AC parameters is $|N_d - N_{ud}| = 2$. The AC parameters can be assigned based on the vector of primary parameters: the comparison of the $\boldsymbol{\psi}_{(p)}$ vectors in

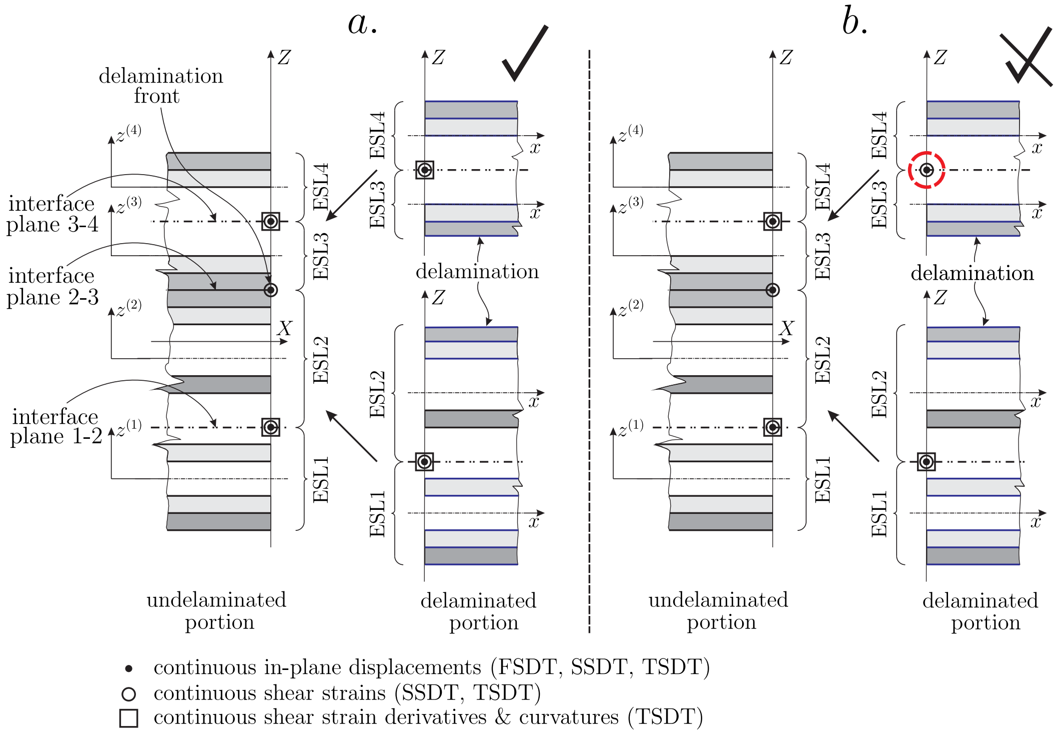

Figure 5.2: Illustration of the theorem of autocontinuity: similar (a) and dissimilar (b) conditions are imposed at interface planes 1-2 and 3-4 of the delaminated and undelaminated parts.

Subsections 4.1.1 and 4.2.1 (Eqs.(4.8) and (4.22)) reveals that the AC parameters are $\lambda_{(x)1}$ and $\lambda_{(y)1}$ in the delaminated region. The comparison of the displacement field (Eqs.(4.7) and (4.21)) for the undelaminated and delaminated regions using the K_{ij} constants in Appendix B.1 results in the following sufficient conditions:

$$\lambda_{(p)1}\Big|_{x=+0}^{(1)} = \sum_{j=1..5} K_{3j}^{(3)} \psi_{(p)j}\Big|_{x=-0}^{(2)}, \quad p = x, y. \tag{5.54}$$

The former conditions ensure the continuity of the cubic terms in the displacement fields of regions 1 and 2 at $x = 0$ (Figure 5.2a). Considering the fact that the parameters in g_α by Eq.(5.53) are continuous between regions 1 and 2 and by using the matrix elements given in Appendix B.1 (TSDT) it is possible to have the following expression for $\lambda_{(p)1}$ at $x = +0$:

$$\lambda_{(p)1}\Big|_{x=+0}^{(1)} = \frac{4}{3}\left(\frac{1}{t_1+t_2}\left[\frac{\theta_{(p)1}}{t_1+2t_2} - \frac{\theta_{(p)2}}{t_2}\right] + \frac{(2t_3+t_4)\theta_{(p)3} - t_3\theta_{(p)4}}{t_2(t_3+t_4)(t_1+2t_2)}\right) + \frac{(2t_3+t_4)t_3\lambda_{(p)3}}{t_2(t_1+2t_2)}\Bigg|_{x=-0}^{(2)}. \tag{5.55}$$

Taking the former condition back into the quadratic part of the displacement field given by Eq.(4.7) of each ESL of the undelaminated part 2 yields the following at $x = -0$:

$$\sum_{j=1..5}\left(K_{1j}^{(2)}\psi_{(p)j}\right)\Bigg|_{x=-0}^{(2)} = \left(\frac{1}{(t_1+t_2)}\left[-\frac{(3t_2+2t_1)\theta_{(p)1}}{(t_1+2t_2)} + \frac{(t_1+2t_2)\theta_{(p)2}}{t_2}\right]\right.$$
$$\left. - \frac{(2t_3+t_4)\theta_{(p)3} - t_3\theta_{(p)4}}{t_2(t_3+t_4)(t_1+2t_2)}\right) + \frac{(2t_3+t_4)t_3\lambda_{(p)3}}{t_2(t_1+2t_2)}\Bigg|_{x=-0}^{(2)}, \tag{5.56}$$

$$\sum_{j=1..5}\left(K^{(2)}_{2j}\psi_{(p)j}\right)\Bigg|^{(2)}_{x=-0}=\left(\frac{-1}{(t_1+t_2)}\left[\frac{t_2\theta_{(p)1}}{(t_1+2t_2)}+\frac{t_1\theta_{(p)2}}{t_2}\right]+\right.$$
$$\left.+\frac{(t_1+t_2)((2t_3+t_4)\theta_{(p)3}-t_3\theta_{(p)4})}{t_2(t_3+t_4)(t_1+2t_2)}\right)+\frac{3}{4}\frac{(2t_3+t_4)(t_1+t_2)t_3\lambda_{(p)3}}{t_2(t_1+2t_2)}\Bigg|^{(2)}_{x=-0}, \tag{5.57}$$

$$\sum_{j=1..5}\left(K^{(2)}_{3j}\psi_{(p)j}\right)\Bigg|^{(2)}_{x=-0}=\frac{-\theta_{(p)3}+\theta_{(p)4}}{(t_3+t_4)}-\frac{3}{4}(t_3+t_4)\lambda_{(p)3}\Bigg|^{(2)}_{x=-0}, \tag{5.58}$$

$$\sum_{j=1..5}\left(K^{(2)}_{4j}\psi_{(p)j}\right)\Bigg|^{(2)}_{x=-0}=\frac{-\theta_{(p)3}+\theta_{p(4)}}{(t_3+t_4)}+\frac{3}{4}(t_3+t_4)\lambda_{(p)3}\Bigg|^{(2)}_{x=-0}. \tag{5.59}$$

Simultaneously, by taking back Eq.(5.55) into the displacement functions of every ESLs of the delaminated part 1 defined by Eq.(4.21) we have at $x=+0$:

$$\sum_{j=1..6}\left(K^{(2)}_{1j}\psi_{(p)j}\right)\Bigg|^{(1)}_{x=+0}=\left(\frac{1}{(t_1+t_2)}\left[-\frac{(3t_2+2t_1)\theta_{(p)1}}{(t_1+2t_2)}+\frac{(t_1+2t_2)\theta_{(p)2}}{t_2}\right]\right.$$
$$\left.-\frac{(2t_3+t_4)\theta_{(p)3}-t_3\theta_{(p)4}}{t_2(t_3+t_4)(t_1+2t_2)}\right)+\frac{(2t_3+t_4)t_3\lambda_{(p)3}}{t_2(t_1+2t_2)}\Bigg|^{(1)}_{x=+0}, \tag{5.60}$$

$$\sum_{j=1..6}\left(K^{(2)}_{2j}\psi_{(p)j}\right)\Bigg|^{(1)}_{x=+0}=\left(\frac{-1}{(t_1+t_2)}\left[\frac{t_2\theta_{(p)1}}{(t_1+2t_2)}+\frac{t_1\theta_{(p)2}}{t_2}\right]+\right.$$
$$\left.+\frac{(t_1+t_2)((2t_3+t_4)\theta_{(p)3}-t_3\theta_{(p)4})}{t_2(t_3+t_4)(t_1+2t_2)}\right)+\frac{3}{4}\frac{(2t_3+t_4)(t_1+t_2)t_3\lambda_{(p)3}}{t_2(t_1+2t_2)}\Bigg|^{(1)}_{x=+0}, \tag{5.61}$$

$$\sum_{j=1..6}\left(K^{(2)}_{3j}\psi_{(p)j}\right)\Bigg|^{(1)}_{x=-0}=\frac{-\theta_{(p)3}+\theta_{(p)4}}{(t_3+t_4)}-\frac{3}{4}(t_3+t_4)\lambda_{(p)3}\Bigg|^{(1)}_{x=-0}, \tag{5.62}$$

$$\sum_{j=1..6}\left(K^{(2)}_{4j}\psi_{(p)j}\right)\Bigg|^{(1)}_{x=+0}=\frac{-\theta_{(p)3}+\theta_{(p)4}}{(t_3+t_4)}+\frac{3}{4}(t_3+t_4)\lambda_{(p)3}\Bigg|^{(1)}_{x=+0}. \tag{5.63}$$

Obviously, the right-hand sides of Eqs.(5.56)-(5.59) and Eqs.(5.60)-(5.63) in pairs are the same. Considering the continuity of the parameters in Eq.(5.53) by the first of Eq.(5.7) it can be seen that the continuity of the quadratic term in the displacement functions of regions 1 and 2 is automatically satisfied. The same proof has been given for the Reddy TSDT in Subsection 5.2.4. We note that in accordance with Subsections 3.1.1 and 3.2.1 $N_{ud}=8$ and $N_d=4$, and so four conditions were imposed by Eq.(5.22). Despite there are more autocontinuity parameters than $|N_d-N_{ud}|$, only $|N_d-N_{ud}|$ number of conditions should be imposed. In other words, out of $\lambda_{(p)2},\lambda_{(p)1},\theta_{(p)2}$ (6 conditions) we have to choose four.

dc_1254_16

Consequence (of the AC theorem): If the continuity of linear terms (rotations) in the displacement field in each ESL given by Eqs.(2.8) and (2.36)-(2.37) are continuous between region ① and ②, moreover the continuity of quadratic and cubic terms of each ESL is imposed using the AC parameters (Eq.(5.54)), then the continuity of the membrane displacement components between the top plates (as well as the bottom plates) of the delaminated and undelaminated regions can be ensured by imposing the equality between the membrane (constant) displacement terms of only a single ESL in the delaminated part ① and a single one in the undelaminated part ②, but not every ESLs. The ESLs can be chosen optionally, however the chosen ESLs should be in the same through-thickness position in the delaminated and undelaminated plate regions. In this case the continuity of the membrane parts in the other ESLs is satisfied automatically. The consequence of the theorem is expressed by Eq.(5.9). In the TSDT we choose the first (in the bottom layer) and third (in top layer, i.e. $\lambda = 3$ and $\omega = 4$ in Eq.(5.9)) ESLs to impose the continuity of the membrane displacements using the equations below:

$$\begin{aligned}
&\left.\left(\begin{array}{c} u_{0b} \\ v_{0b} \end{array}\right) + \sum_{j=1..6} K_{1j}^{(0)} \left(\begin{array}{c} \psi_{(x)j} \\ \psi_{(y)j} \end{array}\right)\right|_{x=+0}^{(1)} = \left.\left(\begin{array}{c} u_{0} \\ v_{0} \end{array}\right) + \sum_{j=1..5} K_{1j}^{(0)} \left(\begin{array}{c} \psi_{(x)j} \\ \psi_{(y)j} \end{array}\right)\right|_{x=-0}^{(2)}, \\
&\left.\left(\begin{array}{c} u_{0t} \\ v_{0t} \end{array}\right) + \sum_{j=1..6} K_{3j}^{(0)} \left(\begin{array}{c} \psi_{(x)j} \\ \psi_{(y)j} \end{array}\right)\right|_{x=+0}^{(1)} = \left.\left(\begin{array}{c} u_{0} \\ v_{0} \end{array}\right) + \sum_{j=1..5} K_{3j}^{(0)} \left(\begin{array}{c} \psi_{(x)j} \\ \psi_{(y)j} \end{array}\right)\right|_{x=-0}^{(2)}.
\end{aligned} \tag{5.64}$$

Eq.(5.64) is the fourth condition in Eq.(5.7) ($h_\alpha^{(l)}$ and $m_\alpha^{(l)}$). The autocontinuity theorem is also valid for the SSDT. The only difference is that the $K_{ij}^{(3)}$ constants are zero.

5.5.4.3 Continuity of stress resultants

The continuity conditions can be defined based on the equivalent stress resultants by Eqs.(4.12)-(4.13) and by Eqs.(4.26)-(4.27):

$$p_\alpha^{(l)} = (\sum_{i=1..4} \mathbf{N}_i^{(x,xy)}, \hat{\mathbf{M}}_i^{(x,xy)}, \hat{\mathbf{P}}_3^{(x,y)}) \mid^{(l)}, \quad i = 1..4. \tag{5.65}$$

5.5.5 Continuity between regions (1)-(1q) and (1q)-(1a)

The continuity between regions ① - (1q) and (1q)-(1a) (see Figure 5.1a) can be imposed by defining the sets of parameters below:

$$\begin{aligned}
g_\beta &= (u_{0b}, u_{0t}, v_{0b}, v_{0t}, w, \frac{\partial w}{\partial x}, \theta_{(x)i}, \theta_{(y)i}, \lambda_{(x)1}, \lambda_{(y)1}, \lambda_{(x)3}, \lambda_{(y)3}), \quad i = 1..4, \\
g_\gamma &= \left(\sum_{i=1..2} \mathbf{N}_i^{(x,xy)}, \sum_{i=3..4} \mathbf{N}_i^{(x,xy)}, \hat{\mathbf{M}}_i^{(x,xy)}, \mathbf{P}_1^{(x,xy)}, \mathbf{P}_3^{(x,xy)}\right), \quad i = 1..4.
\end{aligned} \tag{5.66}$$

The summary of the equations results in: Eq.(5.51)-(5.52) means 30 B.C.s, Eqs.(5.53), (5.54), (5.64) and (5.65) yield 30 conditions between regions ① and ②. Eq.(5.66) provides 2×34 conditions. That means 30+30+34+34=128 conditions altogether in the case of the TSDT solution of problem ⓐ in Figure 5.1a. Problem ⓑ in Figure 5.1b can be solved similarly, therefore the details are not given. The B.C.s and the C.C.s for the FSDT and SSDT models can be defined similarly, these are discussed in the sequel.

Definition: *Over-constrained plate model.* If the displacement fields given by Eqs.(2.8) and (2.36)-(2.37) are developed by using the SEKC requirements and the resulting equilibrium equations by the basic theory of elasticity, as well as the solution of the corresponding boundary value problem do not make it possible to provide the continuity of the *equivalent* bending ($\hat{M}_x$) and twisting moments ($\hat{M}_{xy}$), between each ESL, moreover the sum of in-plane normal (N_x) and shear forces (N_{xy}) of the delaminated and undelaminated plate regions, then the model becomes over-constrained. The result of the over-constraining is the bad estimation of the displacement, strain and stress fields.

Definition: *Well-constrained plate model.* If the solution of the boundary value problem (the number of constants in the solutions functions) makes it possible to provide the continuity of the of the *equivalent* bending ($\hat{M}_x$) and twisting moments ($\hat{M}_{xy}$) between each ESL, moreover the sum of in-plane normal (N_x) and shear forces (N_{xy}) of the delaminated and undelaminated plate regions, then the model is well-constrained.

The models proposed in this thesis are well-constrained models. If we impose even the dynamic B.C.s (*Szekrényes (2014c)*), then in the delaminated portion there are four traction-free surfaces, leading to eight further conditions. Moreover in the undelaminated part, there are two traction-free surfaces involving four dynamic B.C.s. Due to these conditions the number of parameters that should be eliminated from Eqs.(4.7) and (4.21) leads to an over-constrained model with incorrect results (similar to the locking phenomenon (*Reddy (2004)*)), although the autocontinuity is satisfied even in this case. These aspects are also true for the SSDT solution. That is the reason for why the dynamic boundary conditions are not imposed at the traction-free surfaces of the plate.

5.6 Method of 4ESLs - Second-order plate theory

5.6.1 Undelaminated region

According to Eq.(4.14) the state vector of SSDT solution contains the following 22 elements:

$$\mathbf{Z}^{(ud)} = \left(U_{0n}U'_{0n}V_{0n}V'_{0n}X_{2n}X'_{2n}Y_{2n}Y'_{2n}T_{x2n}T'_{x2n}T_{y2n}T'_{y2n}X_{4n}X'_{4n}Y_{4n}Y'_{4n}T_{x4n}T'_{x4n}T_{y4n}T'_{y4n}W_nW'_n\right)^T. \tag{5.67}$$

The vector of external loads takes the following form:

$$\mathbf{F}^{(ud)} = \left(0\ 0\ 0\ 0\ 0\ 0\ 0\ 0\ 0\ 0\ 0\ 0\ 0\ 0\ 0\ 0\ 0\ 0\ 0\ 0\ 0\ \tilde{R}_{122}\cdot Q_n \right)^T, \tag{5.68}$$

where $\tilde{R}_{122}$ is a constant determined by (Eq.(4.11)) and Q_n is defined in Subsection 5.2.1. The system matrix $\mathbf{T}^{(ud)}$ is a 22×22 one and its structure is exactly the same as that of the SSDT with 2ESLs, placed in Appendix C.1.2.

5.6.2 Delaminated region

In Eq.(4.28) there are six parameters, considering the membrane displacements and the deflection as further parameters, the state vector can be defined as:

$$\mathbf{Z}^{(d)} = \left(U_{0bn}U'_{0bn}V_{0bn}V'_{0bn}X_{2n}X'_{2n}Y_{2n}Y'_{2n}T_{x2n}T'_{x2n}T_{y2n}T'_{y2n}U_{0tn}U'_{0tn}V_{0tn}V'_{0tn}X_{4n}X'_{4n}Y_{4n}Y'_{4n}W_nW'_n\right)^T.$$

(5.69)

The vector of external loads takes the form of:

$$\mathbf{F}^{(d)} = \left(0\ 0\ 0\ 0\ 0\ 0\ 0\ 0\ 0\ 0\ 0\ 0\ 0\ 0\ 0\ 0\ 0\ 0\ 0\ 0\ 0\ \tilde{S}_{90} \cdot Q_n \right)^T, \tag{5.70}$$

where $\bar{S}_{90}$ is a constant based on the state space model of the SSDT solution (using Eq.(4.25)). It can be seen that in this case the size of the system matrices is the same for the undelaminated part as the delaminated one ($\mathbf{T}^{(d)}$, 22×22), even the structures are the same (see the matrix of the undelaminated part for the 2ESLs solution in Appendix C.1.2).

5.6.3 Boundary conditions

The B.C.s of the SSDT solution can be determined based on Subsection 4.2.2 and are summarized as follows in the delaminated part 1a (refer to Figure 5.1a):

$$\begin{array}{ll}
\text{simply supported:} & \left\{\begin{array}{l} (w, v_{0b}, v_{0t}, \theta_{(y)2}, \theta_{(y)4}, \phi_{(y)4})\big|_{x=a}^{(1a)} = 0, \\ (\sum\limits_{i=1}^{2} N_{x(i)}, \sum\limits_{i=3}^{4} N_{x(i)}, \hat{M}_{x(12)}, \hat{M}_{x(34)}, L_{x(4)})^{(1a)}\Big|_{x=a} = 0, \end{array}\right. \\
\text{built-in:} & \left\{\begin{array}{l} (w, u_{0b}, u_{0t}, \theta_{(x)2}, \theta_{(x)4}, \phi_{(x)4})\big|_{x=a}^{(1a)} = 0, \\ (v_{0b}, v_{0t}, \theta_{(y)2}, \theta_{(y)4}, \phi_{(y)4})\big|_{x=a}^{(1a)} = 0, \end{array}\right. \\
\text{free edge:} & \left\{\begin{array}{l} (\hat{\mathbf{M}}_{12}^{(x,xy)}, \hat{\mathbf{M}}_{34}^{(x,xy)}, \hat{\mathbf{L}}_{1234}^{(x,y)})\Big|_{x=a}^{(1a)} = \mathbf{0}, \\ (\sum\limits_{i=1..2} \mathbf{N}_i^{(x,xy)}, \sum\limits_{i=3..4} \mathbf{N}_i^{(x,xy)})\Big|_{x=a}^{(1)} = \mathbf{0}, \sum\limits_{i=1..4} Q_{x(i)}\Big|_{x=a}^{(1a)} = 0. \end{array}\right.
\end{array} \tag{5.71}$$

According to Subsection 4.1.2 the B.C.s of the undelaminated part 2 are (Figure 5.1a):

$$\begin{array}{ll}
\text{simply supported:} & \left\{\begin{array}{l} (w, v_0, \theta_{(y)2}, \phi_{(y)2}, \theta_{(y)4}, \phi_{(y)4})\big|_{x=-c}^{(2)} = 0, \\ (\sum\limits_{i=1}^{4} N_{x(i)}, \hat{M}_{x(12)}, \hat{M}_{x(34)}, L_{x(2)}, L_{x(4)})^{(2)}\Big|_{x=-c} = 0, \end{array}\right. \\
\text{built-in:} & \left\{\begin{array}{l} (w, \sum\limits_{i=1..4} N_{x(i)}, \theta_{(x)2}, \phi_{(x)2}, \theta_{(x)4}, \phi_{(x)4})\Big|_{x=-c}^{(2)} = 0, \\ (\sum\limits_{i=1..4} N_{xy(i)}, \theta_{(y)2}, \phi_{(y)2}, \theta_{(y)4}, \phi_{(y)4})\Big|_{x=-c}^{(2)} = 0, \end{array}\right. \\
\text{free edge:} & \left\{\begin{array}{l} (\hat{\mathbf{M}}_{12}^{(x,xy)}, \hat{\mathbf{M}}_{34}^{(x,xy)}, \hat{\mathbf{L}}_{12}^{(x,y)}, \hat{\mathbf{L}}_{34}^{(x,y)})\Big|_{x=-c}^{(2)} = \mathbf{0}, \\ \sum\limits_{i=1..4} \mathbf{N}_i^{(x,xy)}\Big|_{x=-c}^{(2)} = \mathbf{0}, \sum\limits_{i=1..4} Q_{x(i)}\Big|_{x=-c}^{(2)} = 0. \end{array}\right.
\end{array} \tag{5.72}$$

5.6.4 Continuity conditions

The parameter sets for Eq.(5.7) based on Eqs.(4.14)-(4.17) become:

$$\begin{aligned} g_\alpha^{(l)} &= (w, \frac{\partial w}{\partial x}, \theta_{(x)2}, \theta_{(y)2}, \phi_{(x)2}, \phi_{(y)2}, \theta_{(x)4}, \theta_{(y)4})|^{(l)}, \\ p_\alpha^{(l)} &= (\hat{\mathbf{M}}_{12}^{(x,xy)}, \hat{\mathbf{M}}_{34}^{(x,xy)}, \hat{\mathbf{L}}_{1234}^{(x,y)}, \sum_{i=1..4} \mathbf{N}_i^{(x,xy)})\ |^{(l)}. \end{aligned} \tag{5.73}$$

The continuity of the membrane displacement is imposed by Eq.(5.9), wherein $q_1 = 3$ and $q_2 = 4$ and $\lambda = 3$ ($\omega = 4$). Moreover, the continuity of the second-order terms is imposed by (*autocontinuity condition*):

$$\phi_{(p)2}\Big|_{x=-0}^{(2)} = \sum_{j=1..3} K_{2j}^{(2)} \psi_{(p)j}\Big|_{x=+0}^{(1)}, \quad p = x, y. \tag{5.74}$$

The continuity between regions 1-1q and 1q-1a (see Figure 5.1a) can be imposed by defining the sets of parameters below:

$$\begin{aligned} g_\beta &= (u_{0b}, u_{0t}, v_{0b}, v_{0t}, w, \frac{\partial w}{\partial x}, \theta_{(x)2}, \theta_{(y)2}, \theta_{(x)4}, \theta_{(y)4}, \phi_{(x)4}, \phi_{(y)4}), \\ g_\gamma^{(l)} &= (\hat{\mathbf{M}}_{12}^{(x,xy)}, \hat{\mathbf{M}}_{34}^{(x,xy)}, \hat{\mathbf{L}}_{1234}^{(x,y)}, \sum_{i=1..2} \mathbf{N}_i^{(x,xy)}, \sum_{i=3..4} \mathbf{N}_i^{(x,xy)}) \mid^{(l)}, \end{aligned} \tag{5.75}$$

where $\hat{\mathbf{L}}_{1234}^{(x,y)} = \hat{\mathbf{L}}_{12}^{(x,y)} + \hat{\mathbf{L}}_{34}^{(x,y)}$ in accordance with Eq.(4.17).

5.7 Method of 4ESLs - First-order plate theory

5.7.1 Undelaminated region

According to Eq.(4.18) and Subsection 4.1.3 the state vector of the FSDT solution contains 22 elements and becomes:

$$\mathbf{Z}^{(ud)} = \left(U_{0n}U'_{0n}V_{0n}V'_{0n}X_{1n}X'_{1n}Y_{1n}Y'_{1n}X_{2n}X'_{2n}Y_{2n}Y'_{2n}X_{3n}X'_{3n}Y_{3n}Y'_{3n}X_{4n}X'_{4n}Y_{4n}Y'_{4n}W_nW'_n\right)^T. \tag{5.76}$$

The vector of external loads takes the following form:

$$\mathbf{F}^{(ud)} = \left(\begin{array}{cccccccccccccccccccccc} 0 & 0 & 0 & 0 & 0 & 0 & 0 & 0 & 0 & 0 & 0 & 0 & 0 & 0 & 0 & 0 & 0 & 0 & 0 & 0 & 0 & \tilde{R}_{122} \cdot Q_n \end{array}\right)^T, \tag{5.77}$$

where $\tilde{R}_{122}$ is a constant based on Eq.(4.11) and Q_n is defined in Subsection 5.2.1. The system matrix $\mathbf{T}^{(ud)}$ has the same structure and size (22×22) as the one for the SSDT solution by the method of 2ESLs. This matrix is placed in Appendix C.1.2.

5.7.2 Delaminated region

In Eq.(4.32) there are eight parameters, considering the membrane displacements and the deflection as further parameters, the state vector can be defined as:

$$\begin{aligned} \mathbf{Z}^{(d)} = \big(& U_{0bn}\ U'_{0bn}\ V_{0bn}\ V'_{0bn}\ X_{1n}\ X'_{1n}\ Y_{1n}\ Y'_{1n}\ X_{2n}\ X'_{2n}\ Y_{2n}\ Y'_{2n} \\ & U_{0tn}\ U'_{0tn}\ V_{0tn}\ V'_{0tn}\ X_{3n}\ X'_{3n}\ Y_{3n}\ Y'_{3n}\ X_{4n}\ X'_{4n}\ Y_{4n}\ Y'_{4n}\ W_n\ W'_n \big)^T, \end{aligned} \tag{5.78}$$

The vector of external loads takes the form of:

$$\mathbf{F}^{(d)} = \left(0\ 0\ 0\ 0\ 0\ 0\ 0\ 0\ 0\ 0\ 0\ 0\ 0\ 0\ 0\ 0\ 0\ 0\ 0\ 0\ 0\ 0\ 0\ 0\ 0\ \bar{R}_{94} \cdot Q_n\right)^T, \tag{5.79}$$

where $\bar{R}_{94}$ is a constant based on the state space model of the TSDT solution (Eq.(4.25)). The matrix $\mathbf{T}^{(d)}$ has again the same structure and size (26×26) as the one for the SSDT and can be found in Appendix C.1.2.

dc_1254_16

5.7.3 Boundary conditions

The B.C.s of the FSDT model can be determined based on Subsection 4.2.3 and are summarized as follows in the delaminated part 1a (refer to Figure 5.1a):

$$
\begin{aligned}
&\text{simply supported:} && \begin{cases} (w, v_{0b}, v_{0t}, \theta_{(y)1}, \theta_{(y)2}, \theta_{(y)3}, \theta_{(y)4})\big|_{x=a}^{(1a)} = 0, \\ (\sum_{i=1}^{2} N_{x(i)}, \sum_{i=3}^{4} N_{x(i)}, M_{x(1)}, M_{x(2)}, M_{x(3)}, M_{x(4)})^{(1a)}\Big|_{x=a} = 0, \end{cases} \\
&\text{built-in:} && \begin{cases} (w, u_{0b}, u_{0t}, \theta_{(x)1}, \theta_{(x)2}, \theta_{(x)3}, \theta_{(x)4})\big|_{x=a}^{(1a)} = 0, \\ (v_{0b}, v_{0t}, \theta_{(y)1}, \theta_{(y)2}, \theta_{(y)3}, \theta_{(y)4})\big|_{x=a}^{(1a)} = 0, \end{cases} \\
&\text{free edge:} && \begin{cases} (\hat{\mathbf{M}}_1^{(x,xy)}, \hat{\mathbf{M}}_2^{(x,xy)}, \hat{\mathbf{M}}_3^{(x,xy)}, \hat{\mathbf{M}}_4^{(x,xy)})\Big|_{x=a}^{(1a)} = \mathbf{0}, \\ (\sum_{i=1..2} \mathbf{N}_i^{(x,xy)}, \sum_{i=3..4} \mathbf{N}_i^{(x,xy)})\Big|_{x=a}^{(1a)} = \mathbf{0}, \sum_{i=1..4} Q_{x(i)}\Big|_{x=a}^{(1a)} = 0. \end{cases}
\end{aligned}
\tag{5.80}
$$

In accordance with Subsection 4.1.3 the B.C.s of the undelaminated part 2 are (Figure 5.1a):

$$
\begin{aligned}
&\text{simply supported:} && \begin{cases} (w, v_0, \theta_{(y)1}, \theta_{(y)2}, \theta_{(y)3}, \theta_{(y)4})\big|_{x=-c}^{(2)} = 0, \\ (\sum_{i=1}^{4} N_{x(i)}, M_{x(1)}, M_{x(2)}, M_{x(3)}, M_{x(4)})^{(2)}\Big|_{x=-c} = 0, \end{cases} \\
&\text{built-in:} && \begin{cases} (w, \sum_{i=1..4} N_{x(i)}, \theta_{(x)1}, \theta_{(x)2}, \theta_{(x)3}, \theta_{(x)4})\Big|_{x=-c}^{(2)} = 0, \\ (\sum_{i=1..4} N_{xy(i)}, \theta_{(y)1}, \theta_{(y)2}, \theta_{(y)3}, \theta_{(y)4})\Big|_{x=-c}^{(2)} = 0, \end{cases} \\
&\text{free edge:} && \begin{cases} (\hat{\mathbf{M}}_1^{(x,xy)}, \hat{\mathbf{M}}_2^{(x,xy)}, \hat{\mathbf{M}}_3^{(x,xy)}, \hat{\mathbf{M}}_4^{(x,xy)})\Big|_{x=-c}^{(2)} = \mathbf{0}, \\ \sum_{i=1..4} \mathbf{N}_i^{(x,xy)}\Big|_{x=-c}^{(2)} = \mathbf{0}, \sum_{i=1..4} Q_{x(i)}\Big|_{x=-c}^{(2)} = 0. \end{cases}
\end{aligned}
\tag{5.81}
$$

5.7.4 Continuity conditions

The parameter set for Eq.(5.7) based on Eqs.(4.18) and (4.32) becomes:

$$
\begin{aligned}
g_\alpha &= (w, \frac{\partial w}{\partial x}, \theta_{(x)1}, \theta_{(y)1}, \theta_{(x)2}, \theta_{(y)2}, \theta_{(x)3}, \theta_{(y)3}, \theta_{(x)4}, \theta_{(y)4}), \\
p_\alpha^{(l)} &= (\hat{\mathbf{M}}_i^{(x,xy)}, \sum_{i=1..4} \mathbf{N}_i^{(x,xy)}) \mid^{(l)}, \quad i = 1..4.
\end{aligned}
\tag{5.82}
$$

The continuity of the membrane displacements is satisfied through Eq.(5.9), wherein for the FSDT solution $q_1 = q_2 = 4$ and $\lambda = 3$ $(\omega = 4)$. Finally, the continuity between regions 1-1q and 1q-1a (see Figure 5.1a) can be imposed by:

$$
\begin{aligned}
g_\beta &= (u_{0b}, u_{0t}, v_{0b}, v_{0t}, w, \frac{\partial w}{\partial x}, \theta_{(x)i}, \theta_{(y)i}), \quad i = 1..4, \\
g_\gamma &= \left(\hat{M}_{xi}, \sum_{i=1..2} N_{xi}, \sum_{i=3..4} N_{xi}, \hat{M}_{xyi}, \sum_{i=1..2} N_{xyi}, \sum_{i=3..4} N_{xyi} \right), \quad i = 1..4.
\end{aligned}
\tag{5.83}
$$

6 Results - displacement and stress

6.1 Geometry, material, load and finite element model

In this section laminated orthotropic composite plates with simply supported B.C.s and two different geometries are analyzed in accordance with Figures 5.1a and 5.1b. The data of problem ⓐ depicted in Figure 5.1a are: $a = 105$ mm (delamination length), $c = 45$ mm (undelaminated length), $b = 100$ and 160 mm (plate widths), $t_t + t_b = 4.5$ mm (plate thickness), $Q_0 = 1000$ N, $x_Q = 31$ mm, $y_Q = 50$ mm and $y_Q = 80$ mm (point of action coordinates of Q_0), $d_0 = 1$ mm. For problem ⓑ in Figure 5.1b the data are: $a = 55$ mm (delamination length), $c = 35$ mm (undelaminated length), $b = 60$ and 90 mm (plate widths), $t_t + t_b = 4.5$ mm (plate thickness), $Q_0 = 10000$ N, $x_Q = 11$ mm, $y_Q = 30$ mm and $y_Q = 45$ mm (point of action coordinates of Q_0), $d_0 = 1$ mm. The problem was solved by replacing the concentrated load by distributed force on the distance of $2d_0$. The plate is made out of a carbon/epoxy material, the lay-up of the undelaminated part was $[\pm 45^f/0/\pm 45^f_2/\bar{0}]_S$ (superscript f means that the ply is woven fabric). A single layer was 0.5 mm thick, refer to Figure 2.1. The properties (moduli and Poisson's ratios) of the individual laminae are given by Table 6.1 (*Kollár and Springer (2003)*). Four different positions of the delamination was studied, these were assigned as cases I, II, III and IV and are shown in Figure 2.1. The computation was performed in the code MAPLE (*Garvan (2002); Kamerich (2011)*) in accordance with the following points. The stiffness matrices of each single layer of the plate were determined based on the elastic properties of the laminae given in Table 6.1 using Eq.(2.22). The problems in Figures 5.1a and 5.1b were solved by varying the number of terms (N) in the trial function by creating a for-do cycle. Based on the displacement parameters the stress resultants and the stresses were calculated. The convergence of the results was analyzed and it was found that after the 13^{th} trial function term there was no change in the displacement field, stresses, forces and energy release rates.

In order to verify the analytical results finite element (FE) analyses were carried out. The 3D finite element models of the plate with different delamination positions were created in the code ANSYS 12 using 8 node linear SOLID elements. The model for problem ⓑ is shown in Figure 6.1. The global element size was 2 mm × 2 mm × 0.5 mm. In the vicinity of the crack tip a refined mesh was constructed including trapezoid shape elements. The

dc_1254_16

Table 6.1: Elastic properties of single carbon/epoxy composite laminates.

	E_x [GPa]	E_y [GPa]	E_z [GPa]	G_{yz} [GPa]	G_{xz} [GPa]	G_{xy} [GPa]	ν_{yz} [-]	ν_{xz} [-]	ν_{xy} [-]
$\pm 45^f$	16.39	16.39	16.4	5.46	5.46	16.4	0.5	0.5	0.3
0	148	9.65	9.65	4.91	4.66	3.71	0.27	0.25	0.3

Z displacements of the contact nodes over the delaminated surface were imposed to be the same. The displacements in the Z direction were constrained at the edges of the model, the X and Y displacements were constrained in order to eliminate the rigid body motion of the model. The enlarged views in the vicinity of the delamination front are also shown in Figure 6.1. The position of the delamination was varied in the through thickness direction, these were assigned as cases I, II, III and IV. The mode-II and mode-III ERRs were calculated by the virtual crack closure technique (VCCT) (e.g.: *Bonhomme et al. (2010); Raju et al. (1988)*). The scheme and the relevant equations can be found in Appendix D. The size of the crack tip elements were $\Delta x = 0.25$ mm, $\Delta y = 2.0$ mm and $\Delta z = 0.25$ mm. The delamination tip elements and the global mesh resolution were chosen in accordance with recommendations of the literature (*Johnston et al. (2014); Mehrabadi (2014); Raju et al. (1988)*). The main aspect is that Δx and Δz should be between the one quarter and one

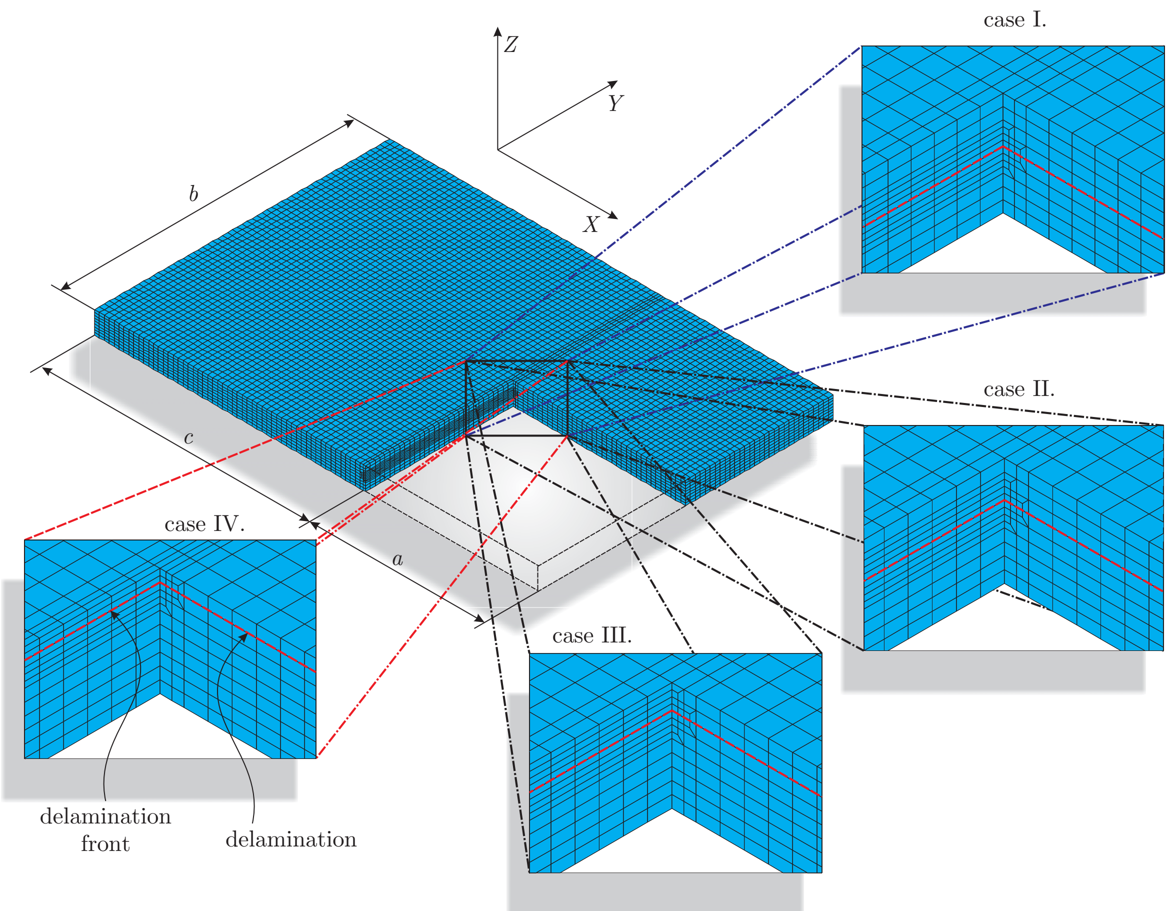

Figure 6.1: 3D FE model of a delaminated composite plate (problem b in Figure 5.1b).

dc_1254_16

half of the thickness of a single layer (0.5 mm, refer to Figure 2.1 and Figure D.1). In this case convergent results can be expected for the ERRs. For the determination of G_{II} and G_{III} along the delamination front a so-called MACRO was written in the ANSYS Design and Parametric Language (ADPL). The MACRO gets the nodal forces and displacements at the crack tip and at each pair of nodes, respectively. Then by defining the size of crack tip elements it determines and plots the ERRs at each node along the delamination front.

6.2 Method of 2ESLs

6.2.1 Solution of problem (a)

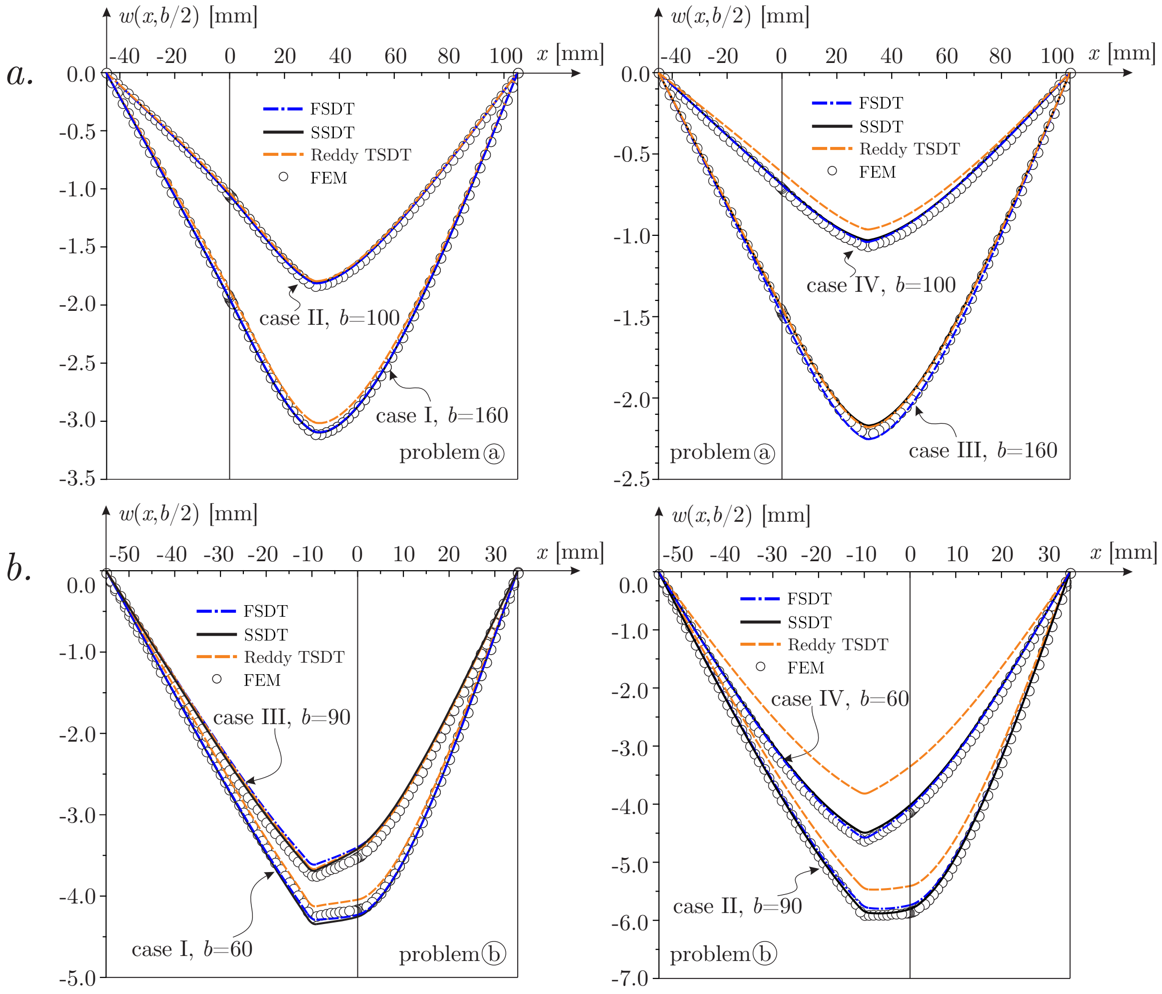

Figure 6.2: Comparison of deflections at $Y = b/2$ calculated from FE analysis, FSDT, SSDT and Reddy TSDT using 2ESLs for problem ⓐ and ⓑ in Figure 5.1 (Compare to Fig. 6.21).

In this subsection the analytical and numerical results are compared to each other. The analyses were carried out by using the present TSDT (Reddy), SSDT and FSDT solutions, respectively. Four cases were investigated (cases I-IV, refer to Figure 2.1), simultaneously two different plate widths were applied. The corresponding geometry and lay-up are always indicated in the legend of the subsequent figures.

In Figure 6.2 the deflections calculated by the FE model and the FSDT, SSDT and Reddy TSDT are plotted. The displacements were determined along the middle line ($Y = b/2$, refer to Figure 5.1) of the plates. For problem ⓐ it is seen that the Reddy TSDT involves a little

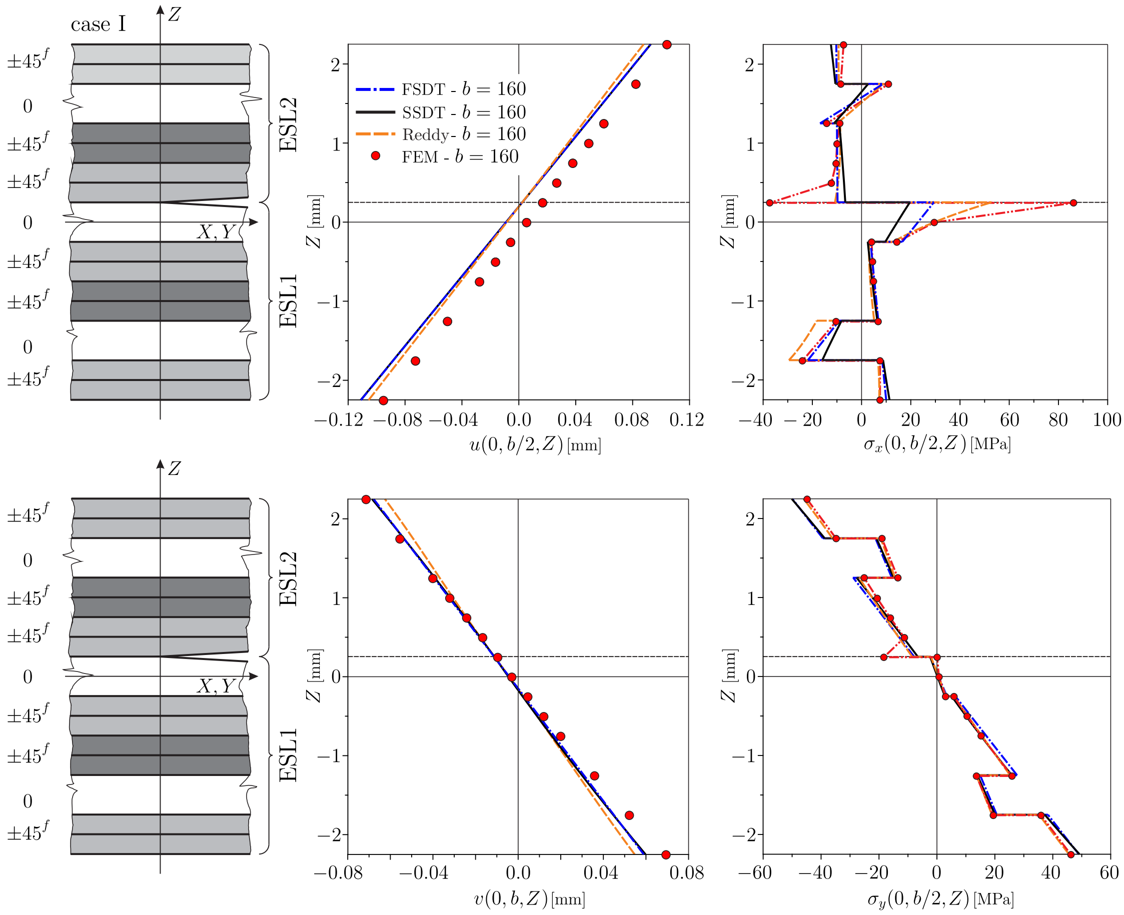

Figure 6.3: Distribution of the in-plane displacements (u, v) and normal stresses (σ_x, σ_y) over the thickness, problem ⓐ in Figure 5.1, case I, $b = 160$ mm (Compare to Fig. 6.22).

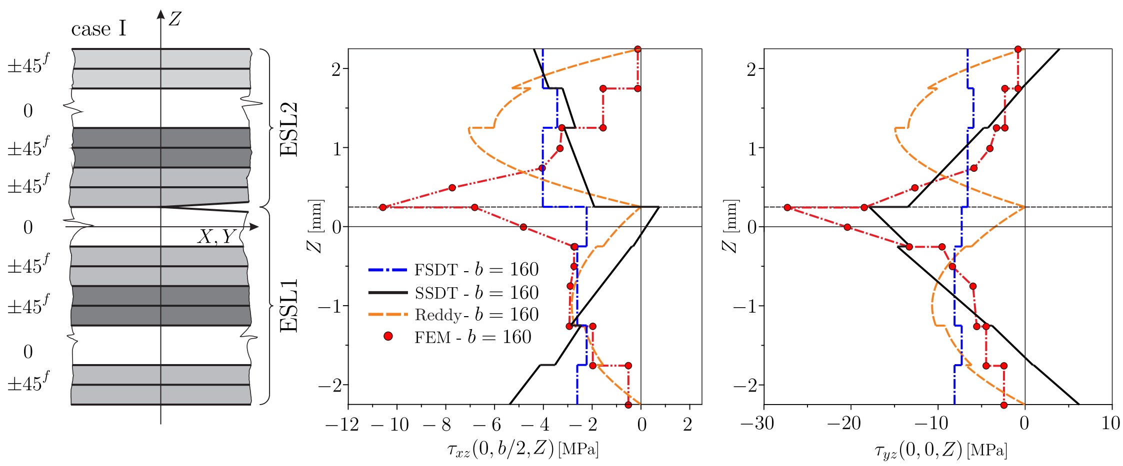

Figure 6.4: Distribution of the shear stresses (τ_{xz}, τ_{yz}) over the thickness, problem ⓐ in Figure 5.1, case I, $b = 160$ mm. Solution by constitutive equations (Compare to Fig. 6.23).

stiffening (i.e. locking) and the displacements are below those by FE solution, on the contrary the FSDT and SSDT solutions agree well with the numerical set of points.

Figure 6.3 depicts further results for case I with b=160 mm. The in-plane displacements and the stresses were evaluated at cross sections located on the delamination front (refer to the legends again). It can be seen in Figure 6.3 that the displacement distributions agree very well, in contrast the stress distributions by the Reddy TSDT, SSDT and FSDT do

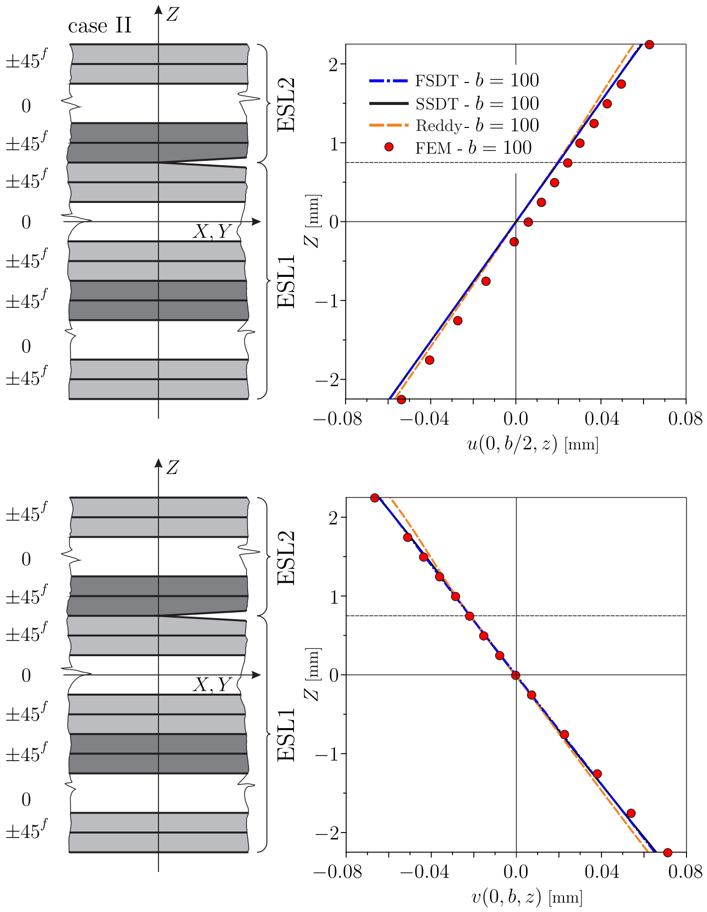

Figure 6.5: Distribution of the in-plane displacements (u, v) and normal stresses (σ_x, σ_y) over the thickness, problem ⓐ in Figure 5.1, case II, $b = 100$ mm (Compare to Fig. 6.24).

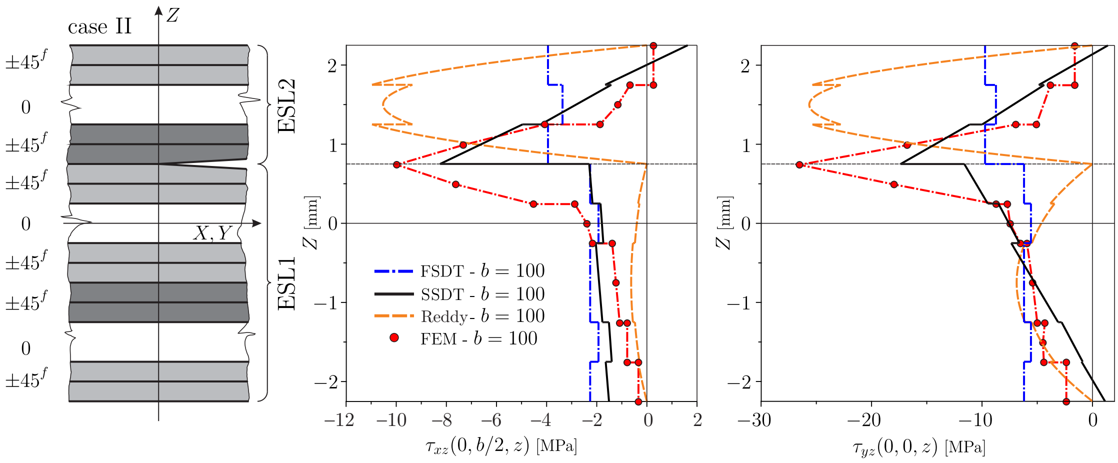

Figure 6.6: Distribution of the shear stresses (τ_{xz}, τ_{yz}) over the thickness, problem ⓐ in Figure 5.1, case II, $b = 100$ mm. Solution by constitutive equations (Compare to Fig. 6.25).

not contain a so significant peak than that the FE solution gives. This aspect takes place in each case and can be explained by the singular nature of the FE stress field around the delamination tip: it is well-known that by increasing the mesh resolution the stresses become higher and higher. On the contrary the analytical solution is nonsingular and can be considered as a better solution than the FE one. An immediate observation in Figure 6.3 is that there is a misalignment between the numerically and analytically determined u

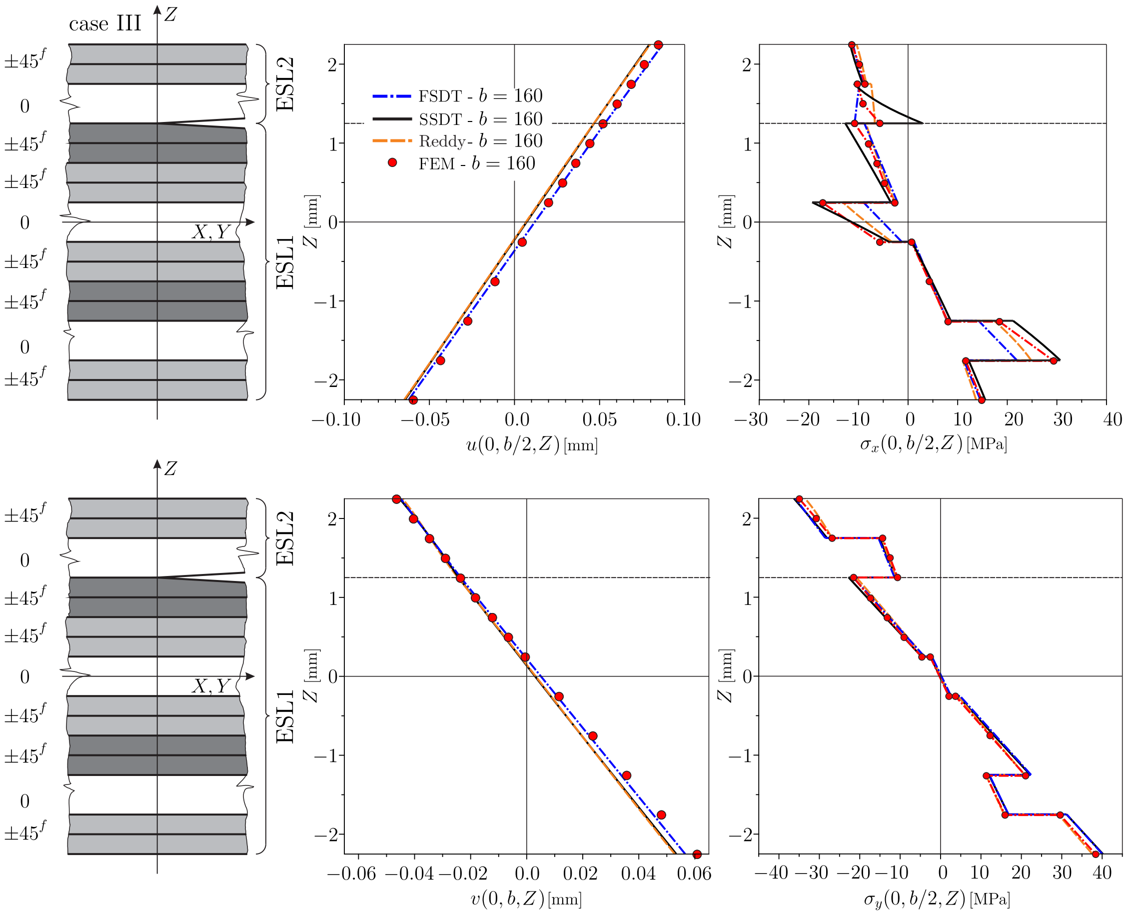

Figure 6.7: Distribution of the in-plane displacements (u, v) and normal stresses (σ_x, σ_y) over the thickness, problem a in Figure 5.1, case III, $b = 160$ mm (Compare to Fig. 6.26).

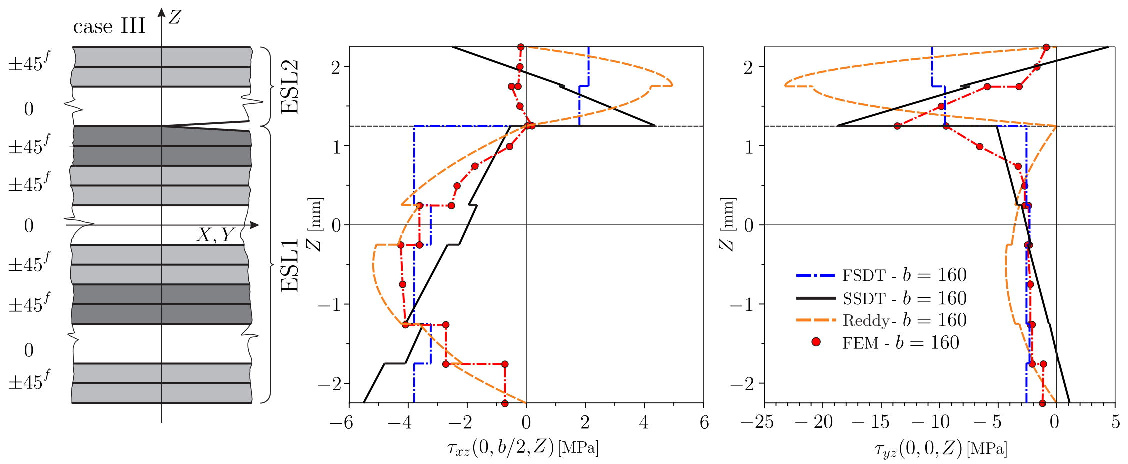

Figure 6.8: Distribution of the shear stresses (τ_{xz}, τ_{yz}) over the thickness, problem a in Figure 5.1, case III, $b = 160$ mm. Solution by constitutive equations (Compare to Fig.6.27).

and v displacement distributions, more clearly, the intersection point of the displacement distributions by FEM are not the same as that of the analytical solution. It has to be mentioned that we can compare only the slope of the solutions, because the intersection point with the horizontal axis slightly depends upon the boundary conditions related to the in-plane displacements. The rigid body motion of the plate in the $X - Y$ plane (refer to Figure 6.1) can be eliminated in several different ways, e.g. in the present analysis the

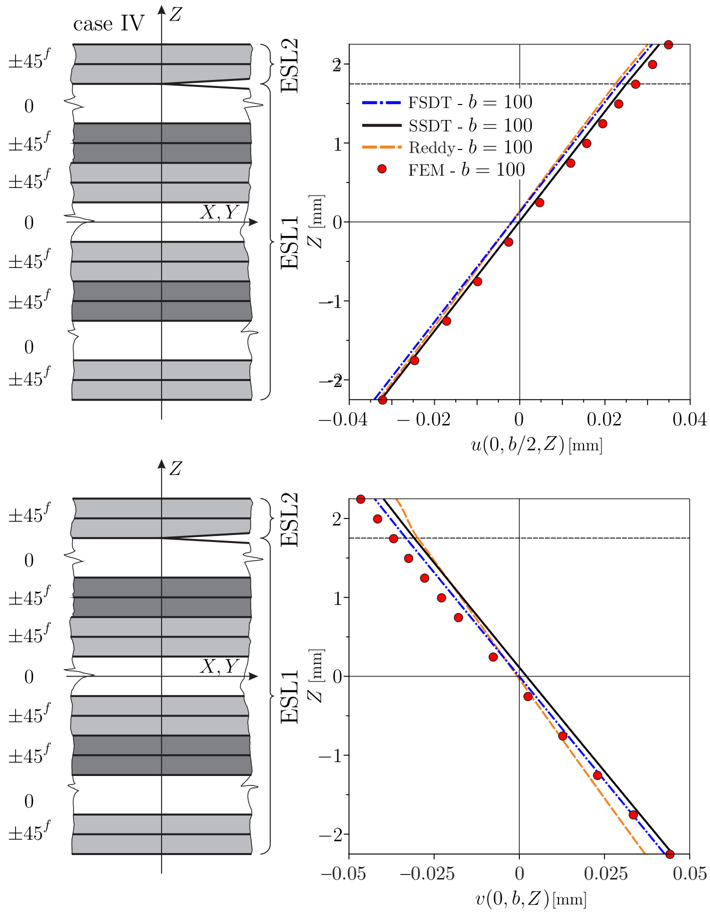

Figure 6.9: Distribution of the in-plane displacements (u, v) and normal stresses (σ_x, σ_y) over the thickness, problem ⓐ in Figure 5.1, case IV, $b = 100$ mm (Compare to Fig. 6.28).

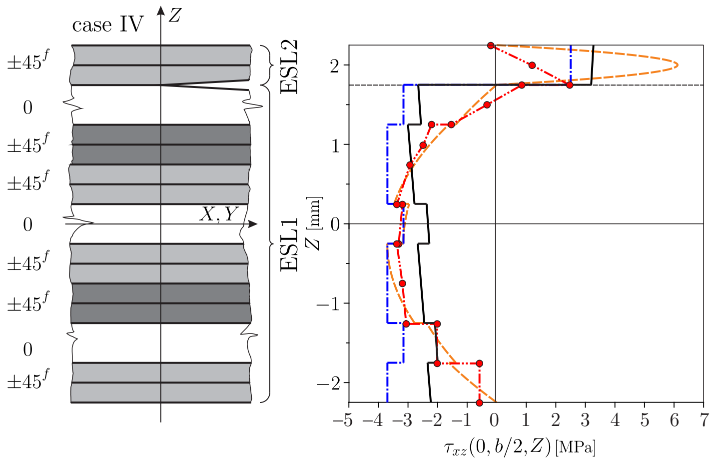

Figure 6.10: Distribution of the shear stresses (τ_{xz}, τ_{yz}) over the thickness, problem ⓐ in Figure 5.1, case IV, $b = 100$ mm. Solution by constitutive equations (Compare to Fig. 6.29).

following conditions were imposed: $X = a, Y = 0, Z = -(t_t + t_b)/2 : u = 0, v = 0$ and $X = a, Y = b, Z = -(t_t + t_b)/2 : u = 0$. In the case of the normal stresses σ_x and σ_y the average stress was calculated, which means that the stress in region ① at $x = +0$ and the one in region ② at $x = -0$ were added and divided by two. For σ_x the FE solution indicates a peak in the plane of the delamination, the peak by Reddy TSDT solution is significantly less. The FSDT approximation is quite similar to the Reddy TSDT for case I. For σ_y each

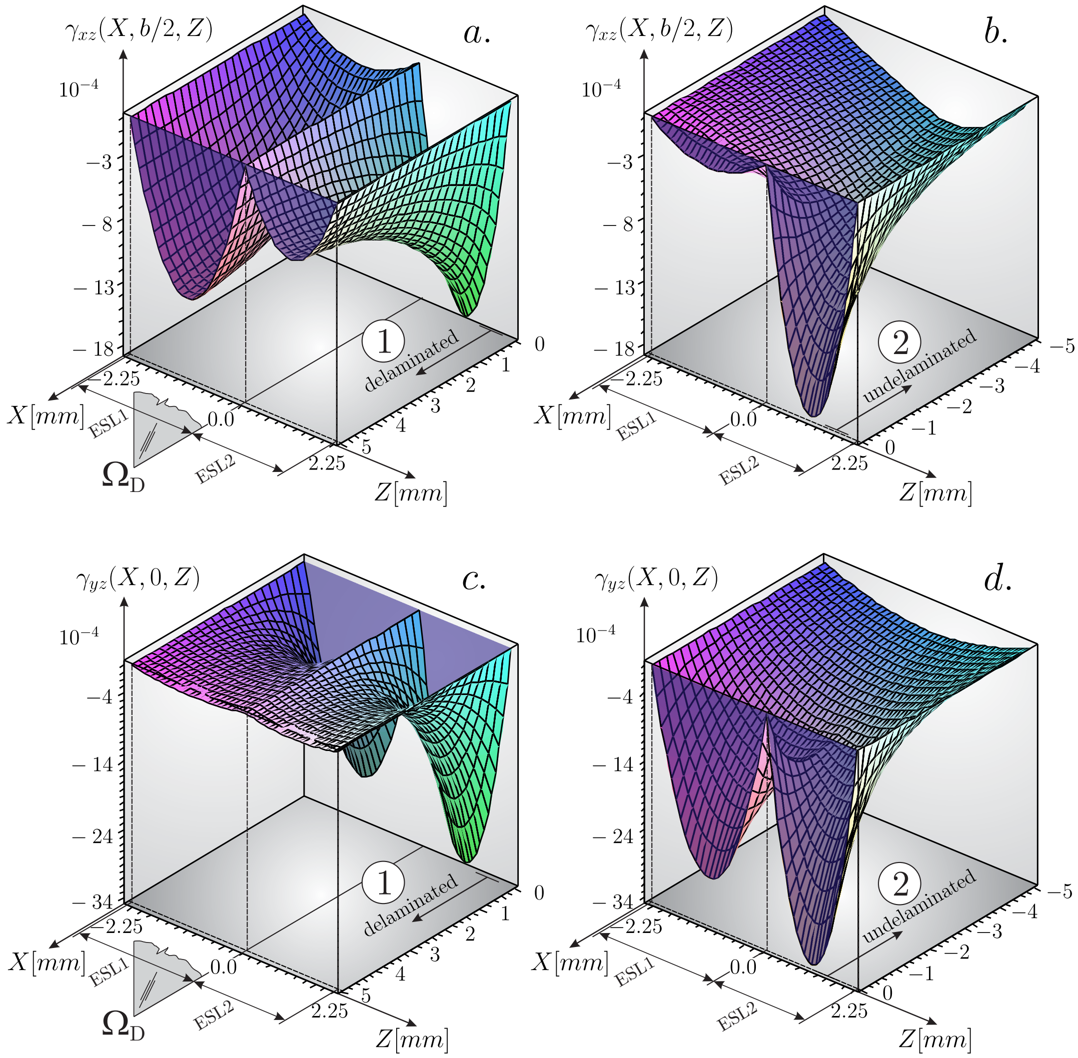

Figure 6.11: Distribution of the shear strains γ_{xz} ((a) and (b)) and γ_{yz} ((c) and (d)) by Reddy TSDT at the transition between the delaminated and undelaminated regions at Y=$b/2$ and Y=0 (case I, b=100 mm), Ω_D is the delamination plane (Compare to Fig. 6.30).

solution agrees more or less.

The approximation of shear stresses is again very contradictory as it is shown in Figure 6.4. This solution was obtained by the analytical models directly, called as the solution by constitutive equations. The FE solution shows a peak in the delamination plane. The major difference between the analytical solutions is that the shear stress by FSDT and SSDT does not vanish at the top and bottom boundaries (the traction-free condition is violated). In contrast, the Reddy TSDT does satisfy the dynamic boundary conditions, the shear strains (and so the stresses) vanish even at the delamination tip. Although there are differences, the area under the curves is approximately the same, which is in fact proportional to the shear force.

The further cases (II, III and IV) are presented in Figures 6.5-6.10. In Figure 6.5 the three analytical solutions agree very well with respect to each field in case II. The shear stresses by constitutive equations are plotted in Figure 6.6. The conclusions are similar to those for case I. Apparently, the shear stresses are better approximated by Reddy TSDT than by SSDT and FSDT and it is the only solution that satisfies the dynamic conditions.

In case III (Figure 6.7) the displacements and the normal stresses agree well again,

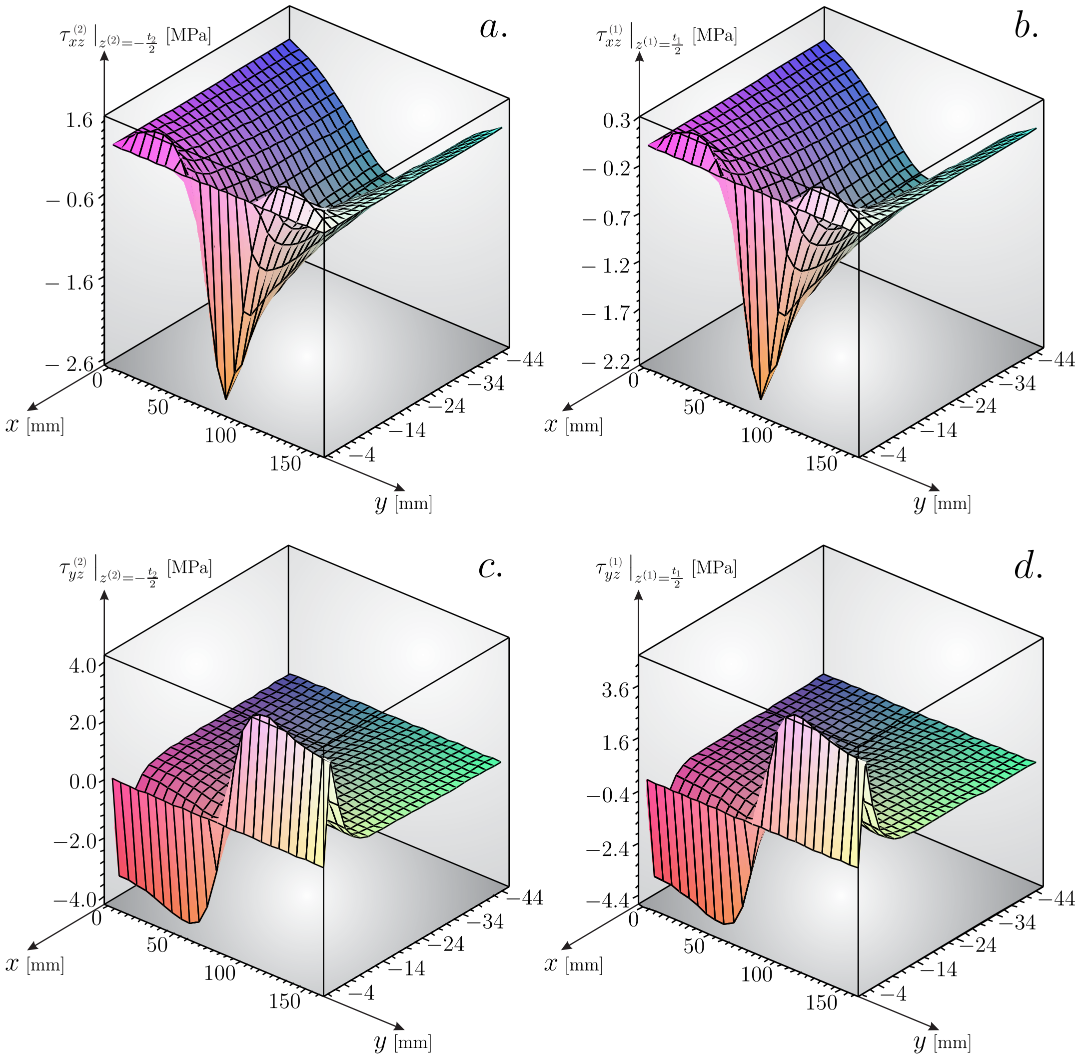

Figure 6.12: Distribution of the interlaminar shear stress by Reddy TSDT for case I, b=160 mm, $\tau_{xz}^{(2)}$ (a), $\tau_{xz}^{(1)}$ (b), $\tau_{yz}^{(2)}$ (c) and $\tau_{yz}^{(1)}$ (d) (Compare to Fig. 6.31).

however in Figure 6.8 the direction of τ_{xz} from Reddy TSDT, SSDT and FSDT in the top plate does not agree with the FE result. The stiffening effect in Reddy TSDT is clearly seen in Figure 6.9 regarding u and v, even the stresses are better predicted by the FDST and SSDT theories. Apart from that in case IV (Figure 6.10) the shear stresses are a little bit overpredicted in the top plate again by each theory.

Figure 6.11 plots the distribution of the shear strains by Reddy TSDT in the neighborhood of the delamination tip in case I if b = 100 mm. As expected the shear strains change suddenly at the transition between the delaminated and undelaminated plate portions. It has to be mentioned that the condition of shear strain continuity (Eq.(3.3)) in the delamination plane of the undelaminated part is very important to obtain accurate ERR distributions (see later). In the case of the FSDT the shear strains (and so the stresses) are discontinuous in the through-thickness direction, this leads to significant errors if the delamination gets closer to the top boundary surface of the plate. The results are similar in case III (see Appendix E), as well. The distributions of the interlaminar shear stresses (τ_{xz} and τ_{yz}) calculated by Reddy TSDT in the delamination plane of the undelaminated region are plotted in Figure 6.12 for case I with b=160 mm. Satisfying the basic concepts of Reddy plates the shear stresses vanish along the delamination tip, which is followed by a sudden

dc_1254_16

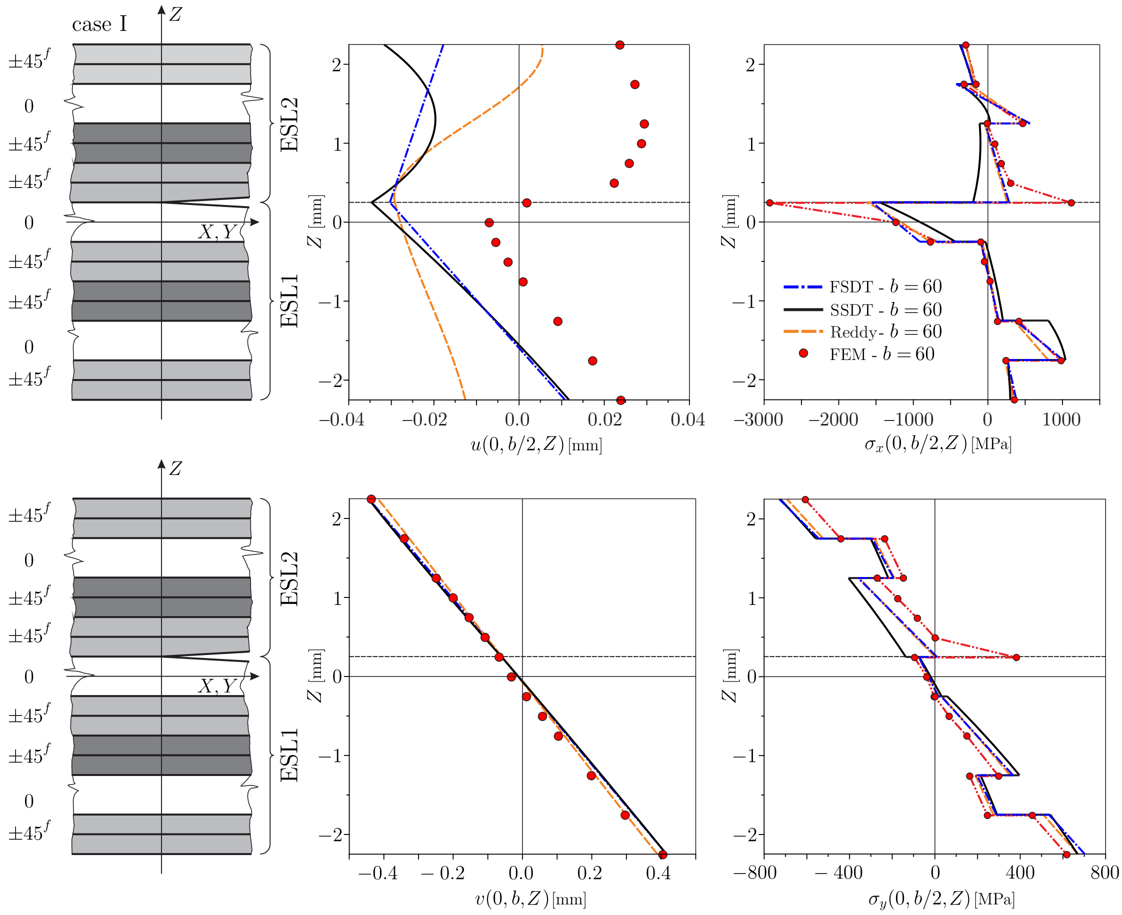

Figure 6.13: Distribution of the in-plane displacements (u, v) and normal stresses (σ_x, σ_y) over the thickness, problem b in Figure 5.1, case I, $b = 60$ mm (Compare to Fig. 6.32).

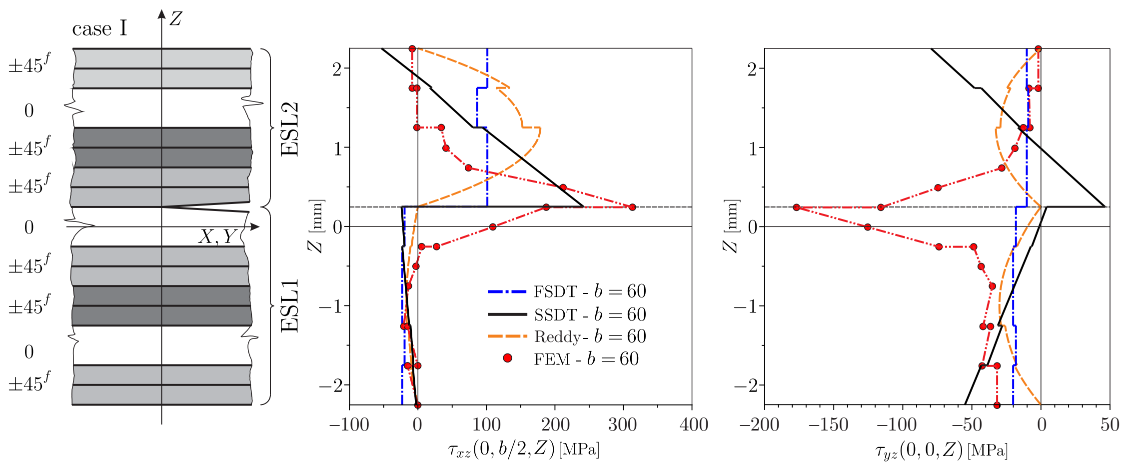

Figure 6.14: Distribution of the shear stresses (τ_{xz}, τ_{yz}) over the thickness, problem b in Figure 5.1, case I, $b = 60$ mm. Solution by constitutive equations (Compare to Fig. 6.33).

increase and a subsequent decay. Although it is possible to obtain these distributions by the FE model too, the post-processing (plotting) would be a lengthy process, the analytical solution is more reasonable in this case, especially because of the singular (and so the not invariant) nature of the FE solution.

dc_1254_16

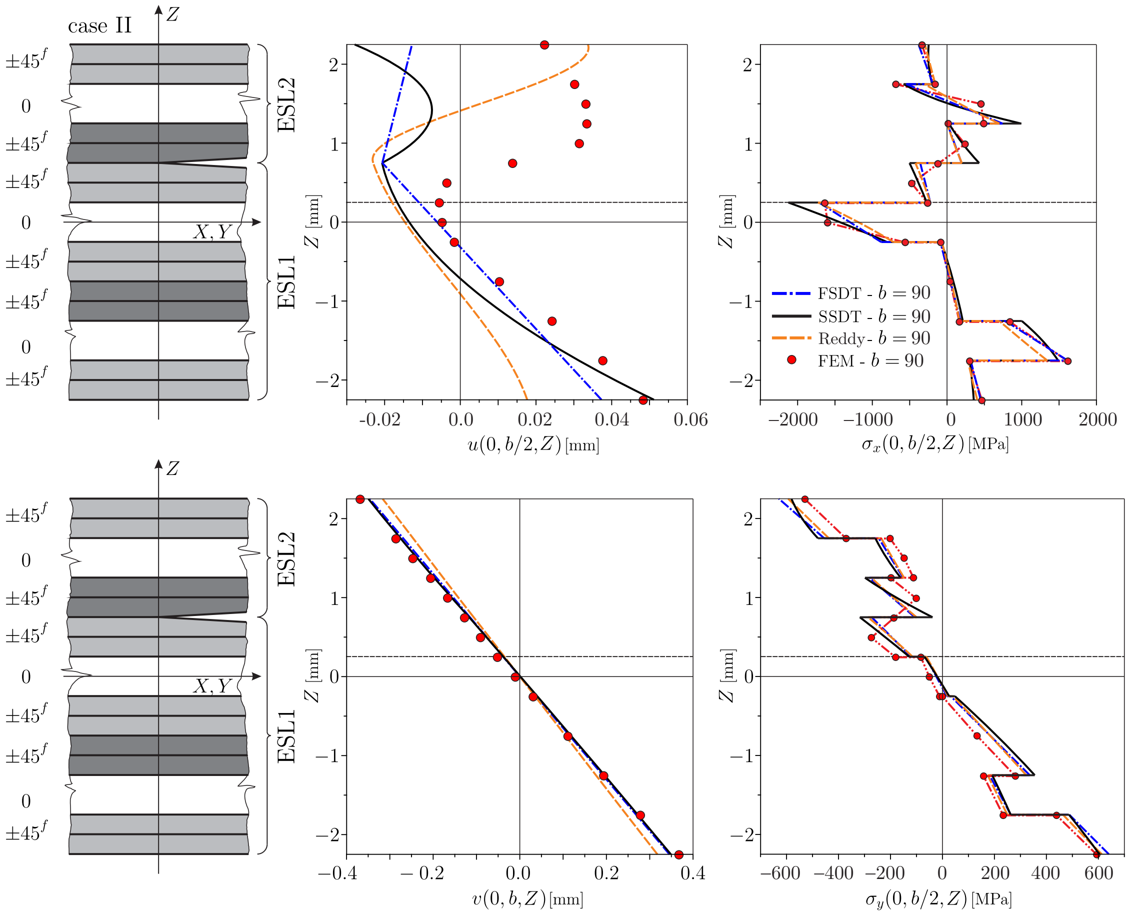

Figure 6.15: Distribution of the in-plane displacements (u, v) and normal stresses (σ_x, σ_y) over the thickness, problem (b) in Figure 5.1, case II, $b = 90$ mm (Compare to Fig. 6.34).

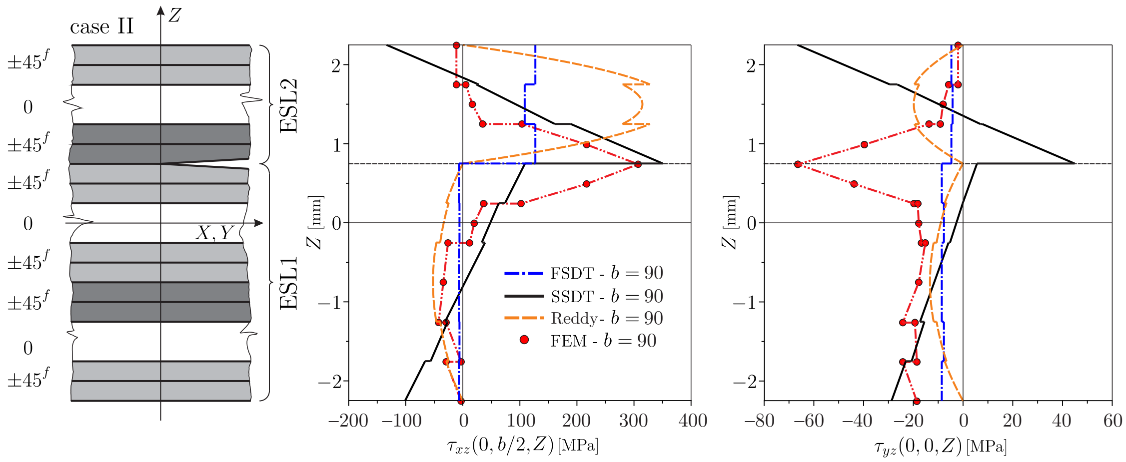

Figure 6.16: Distribution of the shear stresses (τ_{xz}, τ_{yz}) over the thickness, problem (b) in Figure 5.1, case II, $b = 90$ mm. Solution by constitutive equations (Compare to Fig. 6.35).

6.2.2 Solution of problem (b)

The problem (b) in Figure 5.1b is also solved by the present analytical models. For problem (a) the FSDT and SSDT analytical solution agreed very well with the FE solution, the Reddy TSDT showed some stiffening. The main aim to solve problem (b) is to assess the accuracy of the models for a plate with smaller size and shorter delamination, respectively. Since each

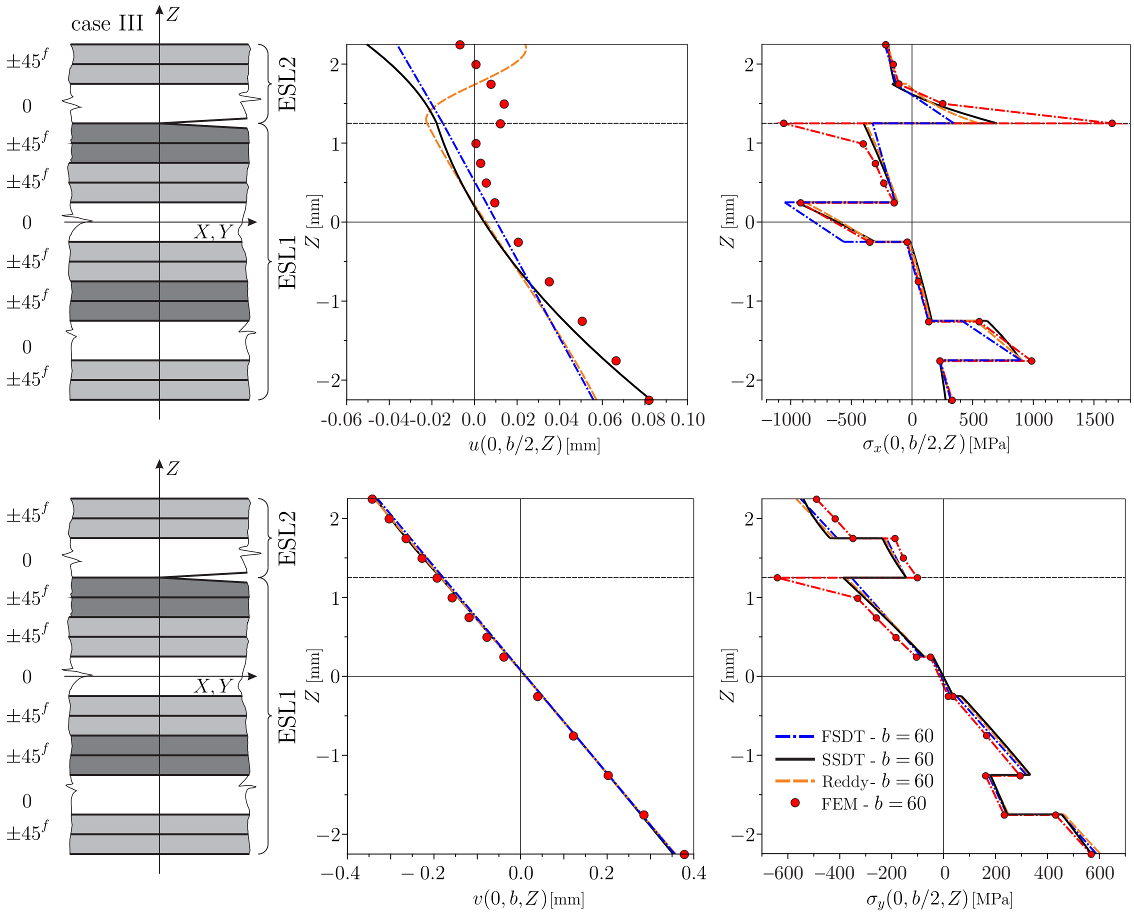

Figure 6.17: Distribution of the in-plane displacements (u, v) and normal stresses (σ_x, σ_y) over the thickness, problem (b) in Figure 5.1, case III, $b = 60$ mm (Compare to Fig. 6.36).

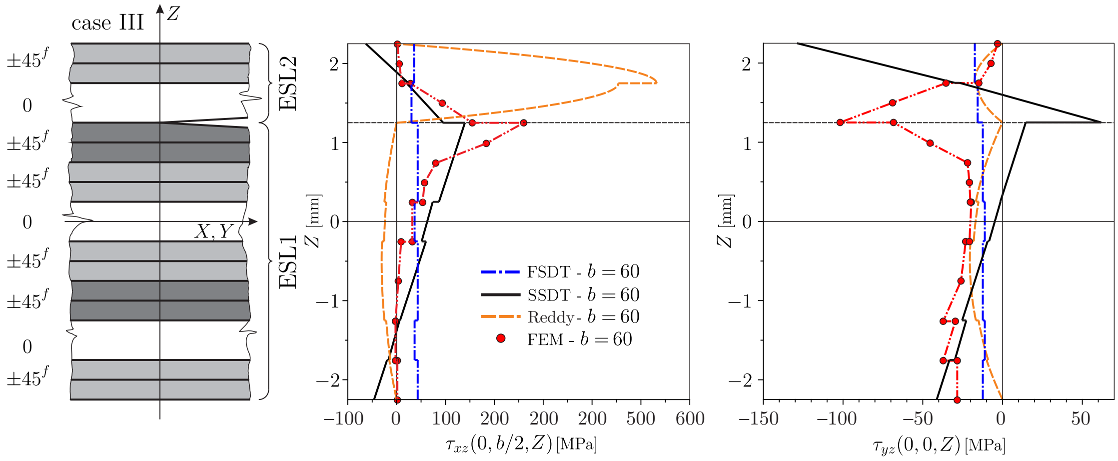

Figure 6.18: Distribution of the shear stresses (τ_{xz}, τ_{yz}) over the thickness, problem (b) in Figure 5.1, case III, $b = 60$ mm. Solution by constitutive equations (Compare to Fig. 6.37).

theory is capable to model thick plates it is expected to find them suitable even for problem (b).

For problem (b) the deflections are plotted in Figure 6.2b: the locking phenomenon is significant in the case of Reddy TSDT, especially for case IV. The FSDT and SSDT solutions seem to be more reliable. Figure 6.13 presents the displacements and stresses in case I. It is clear that the perturbation because of the delamination is significantly stronger than

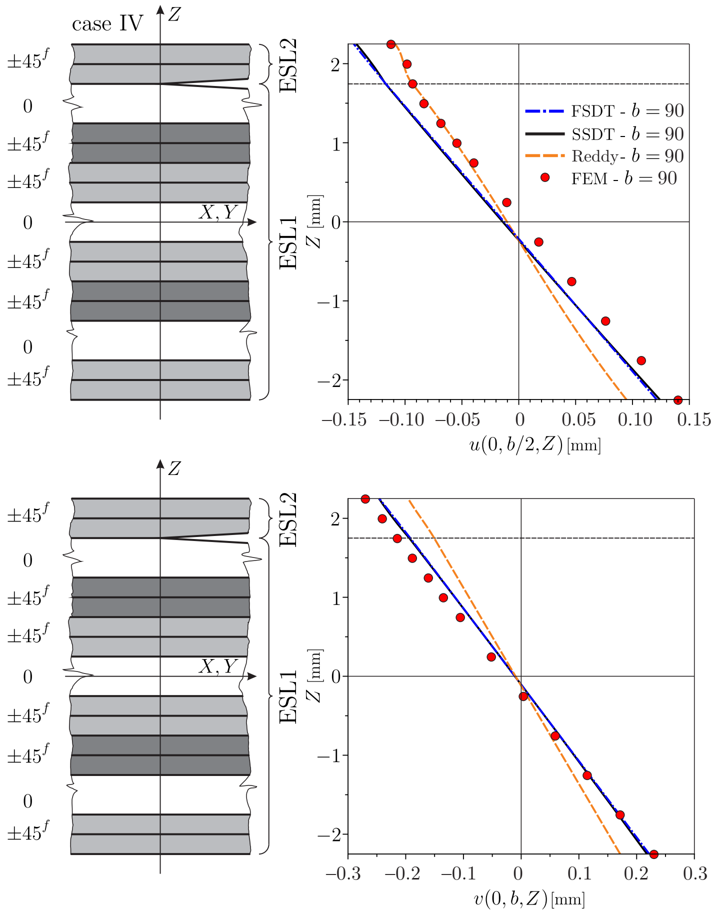

Figure 6.19: Distribution of the in-plane displacements (u, v) and normal stresses (σ_x, σ_y) over the thickness, problem ⓑ in Figure 5.1, case IV, $b = 90$ mm (Compare to Fig. 6.38).

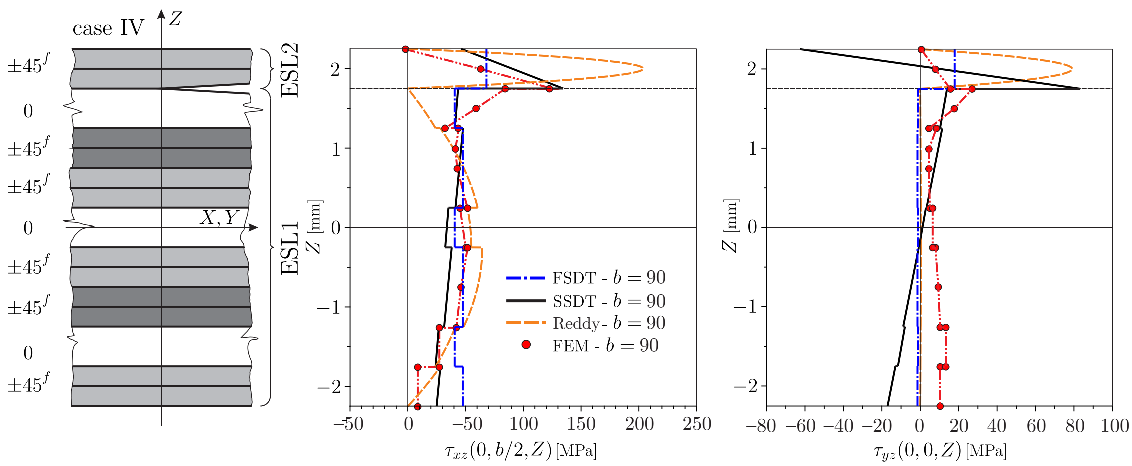

Figure 6.20: Distribution of the shear stresses (τ_{xz}, τ_{yz}) over the thickness, problem ⓑ in Figure 5.1, case IV, $b = 90$ mm. Solution by constitutive equations (Compare to Fig. 6.39).

in problem ⓐ. The SSDT is the best in approximating the shape of the FE solution for u, however, the curve obtained by Reddy theory approximates better the values of the FE solution over the whole plate thickness. Similarly to problem ⓐ, the v displacement component is well approximated by the analytical models. The difference between the stresses by analytical models is not significant, the FE model provides a peak in the plane of the delamination.

dc_1254_16

The shear stress distributions from constitutive equations are plotted in Figure 6.14 for case I. Similarly to problem ⓐ each theory provides a good prediction of both shear stress components. The major conclusions for cases II-IV are the following. In case II (Figure 6.15) and cases III (Figure 6.17) the perturbation of the u displacement is significant, however it decreases significantly in case IV (Figure 6.19). The v component is excellently approximated by each theory, it can also be observed that Reddy TSDT becomes a little bit inaccurate in cases III and IV for u. Considering the normal stresses the peak appears in the plane of the delamination in accordance with the FE model, however each theory predicts more or less similar distributions. Regarding the shear stresses (Figures 6.16, 6.18 and 6.20), it is evident that the analytical solutions approximate the area under the curve of the FE solution but not the aspect of the FE distribution. It is the peak stress and the mesh resolution that governs the distribution by the FE solution.

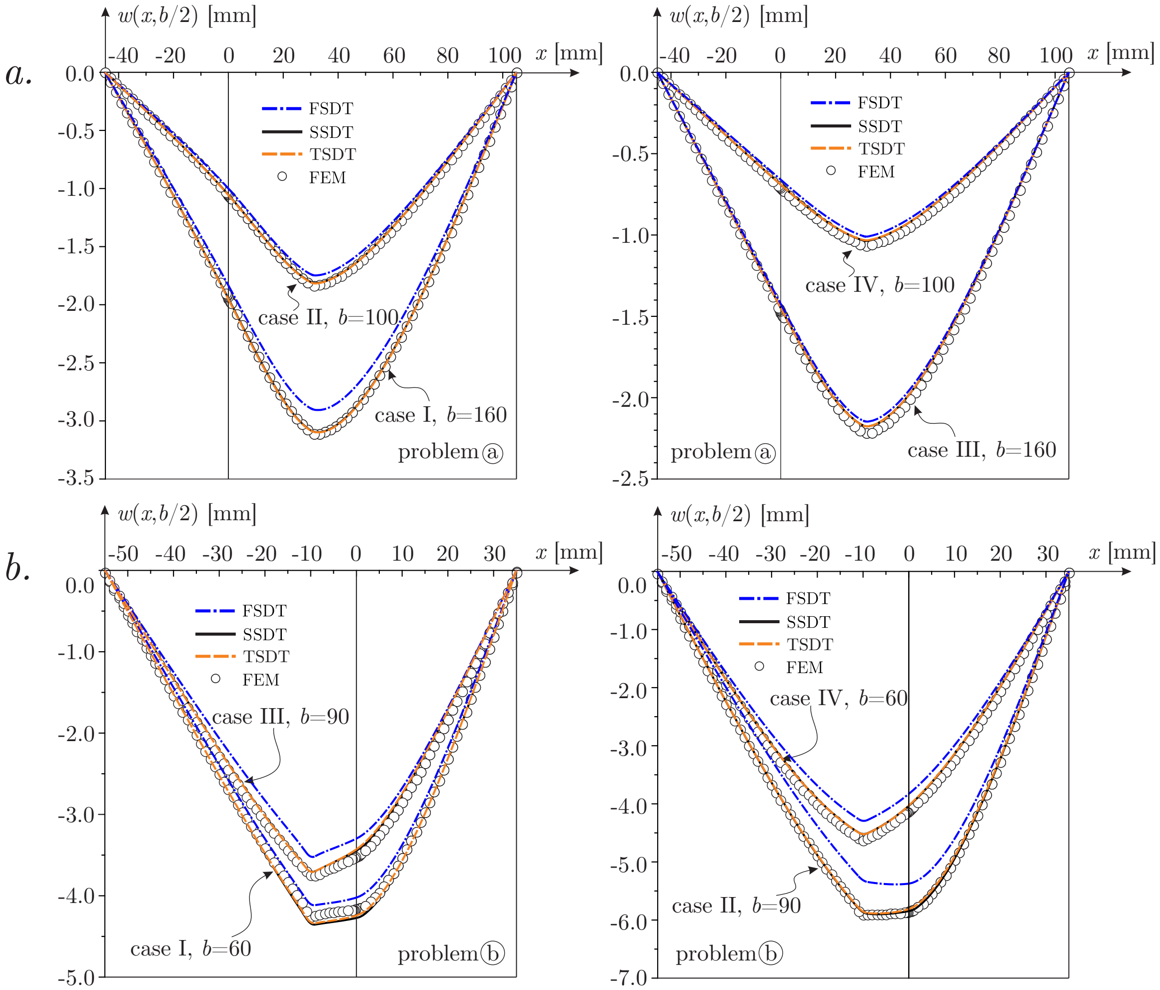

Figure 6.21: Comparison of deflections at $Y = b/2$ calculated from FE analysis, FSDT, SSDT and TSDT using 4ESLs for problem ⓐ and ⓑ in Figure 5.1 (Compare to Fig. 6.2).

6.3 Method of 4ESLs

6.3.1 Solution of problem (a)

The deflections calculated by using the method of 4ESLs for problem ⓐ are shown in Figure 6.21a. In each case the result of the SSDT and TSDT agrees excellently with the FE

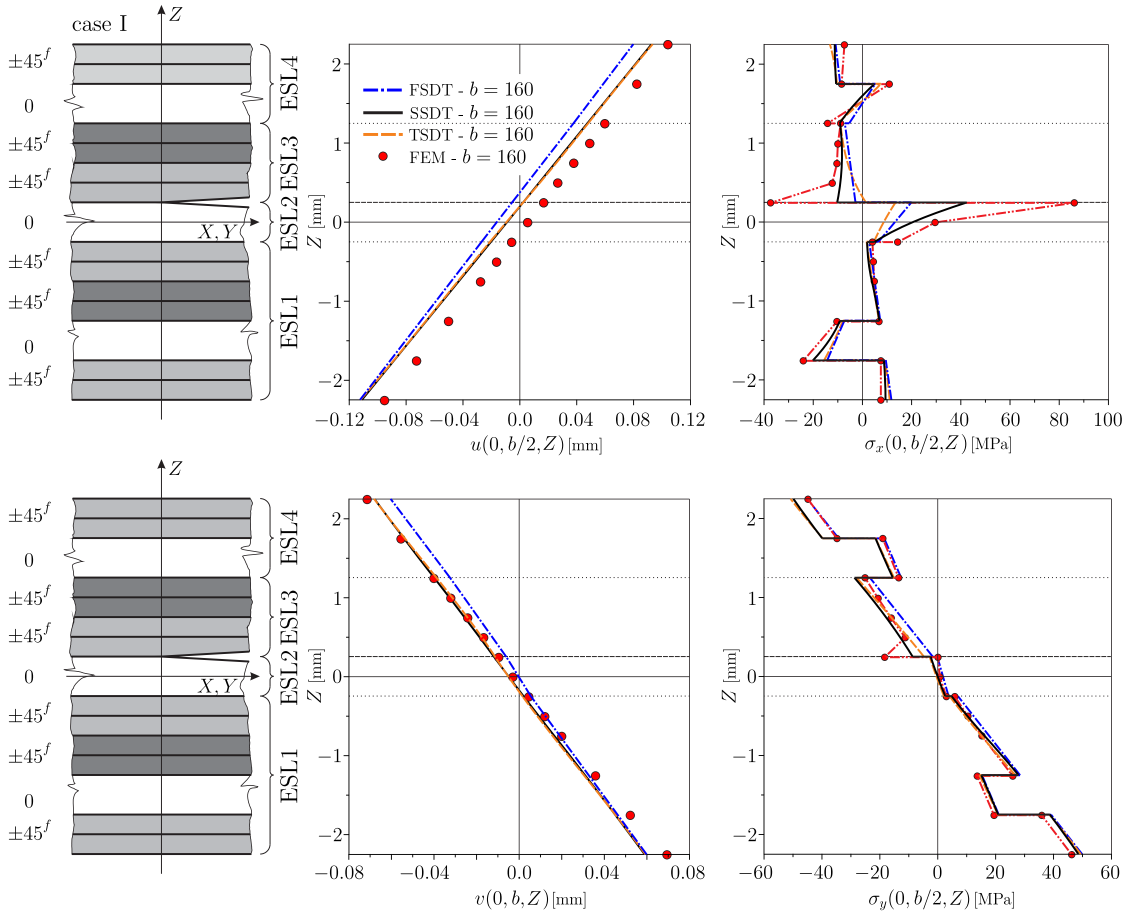

Figure 6.22: Distribution of the in-plane displacements (u, v) and normal stresses (σ_x, σ_y) over the thickness, problem ⓐ in Figure 5.1a, case I, $b = 160$ mm (Compare to Fig. 6.3).

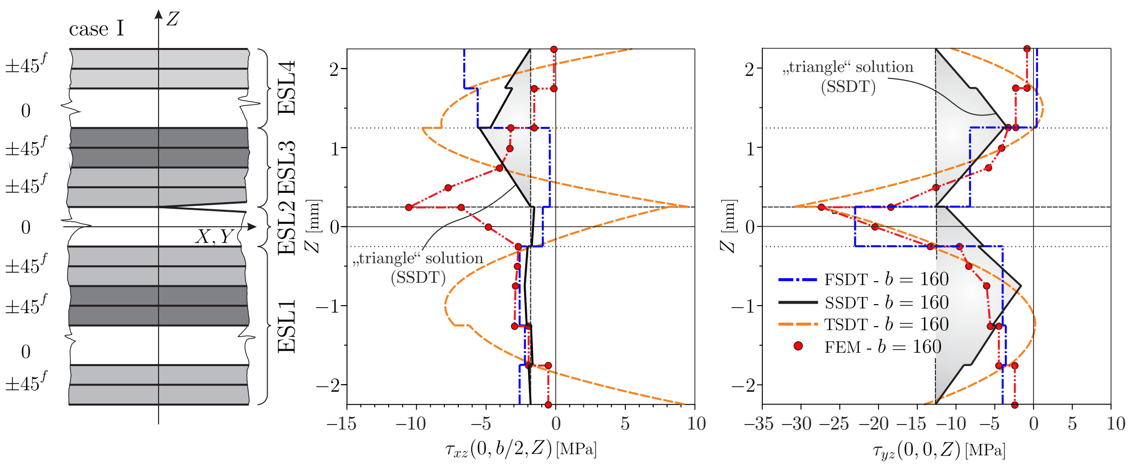

Figure 6.23: Distribution of the shear stresses (τ_{xz}, τ_{yz}) over the thickness, problem ⓐ in Figure 5.1, case I, $b = 160$ mm. Solution by constitutive equations (Compare to Fig. 6.4).

solution. It is surprising, but in this case it is the FSDT solution that involves some locking phenomenon, especially in case I.

Figure 6.22 shows the distribution of the in-plane displacements u and v and normal stresses σ_x, σ_y at specified cross sections at the delamination front for case I, when the delamination is nearby the midplane. The results of the FSDT, SSDT, TSDT and FE solutions are presented applying the method of 4ESLs. The displacement curves show very

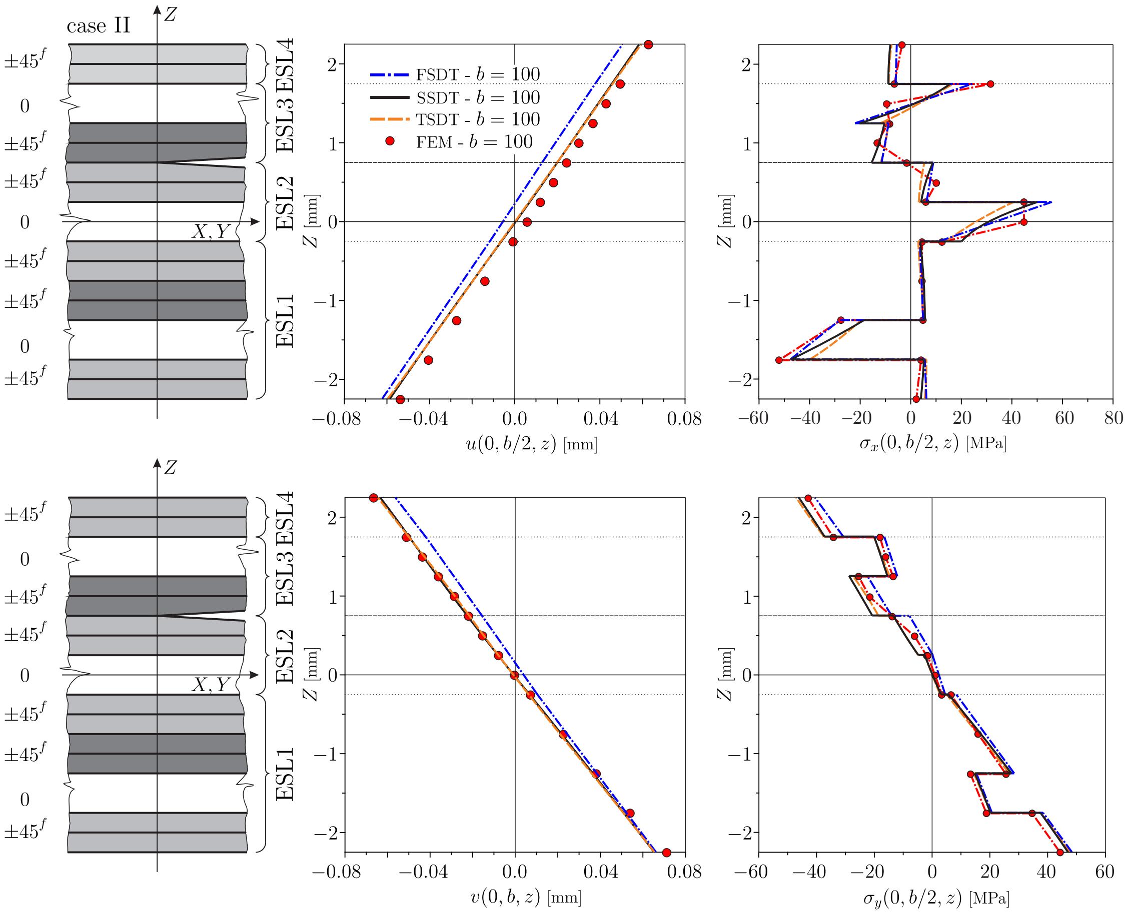

Figure 6.24: Distribution of the in-plane displacements (u, v) and normal stresses (σ_x, σ_y) over the thickness, problem ⓐ in Figure 5.1, case II, $b = 100$ mm (Compare to Fig. 6.5).

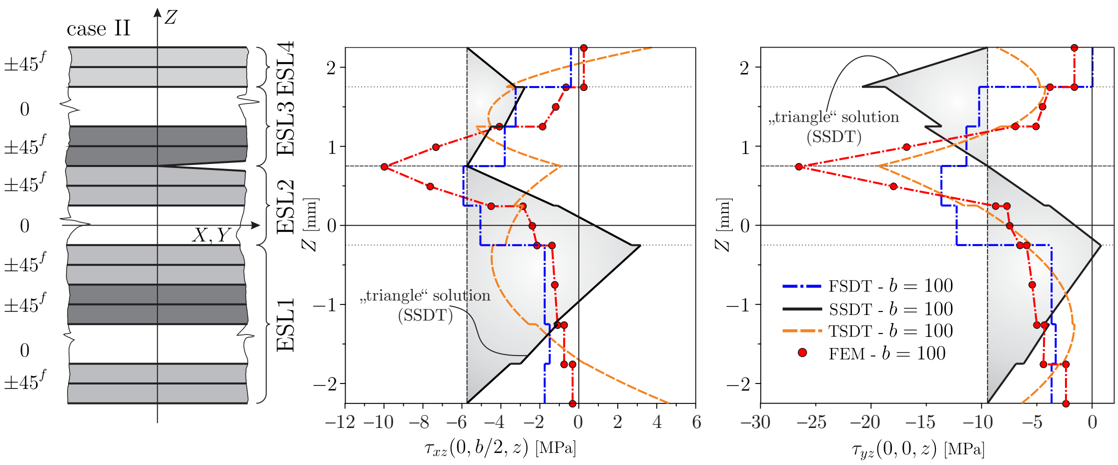

Figure 6.25: Distribution of the shear stresses (τ_{xz}, τ_{yz}) over the thickness, problem ⓐ in Figure 5.1, case II, $b = 100$ mm. Solution by constitutive equations (Compare to Fig. 6.6).

moderate nonlinearity, it can be seen that considering both components the TSDT and SSDT provide the best fit to the numerical results. In contrast it is the SSDT that approximates the normal stresses (σ_x and σ_y) in the best way, especially the peak in the plane of the delamination. Regarding the shear stresses in Figure 6.23 the TSDT provides the highest accuracy in τ_{yz} compared to the FE results. For τ_{xz} the SSDT is definitely the best. It has to be mentioned that the SSDT solution becomes overperturbated without the SSCC,

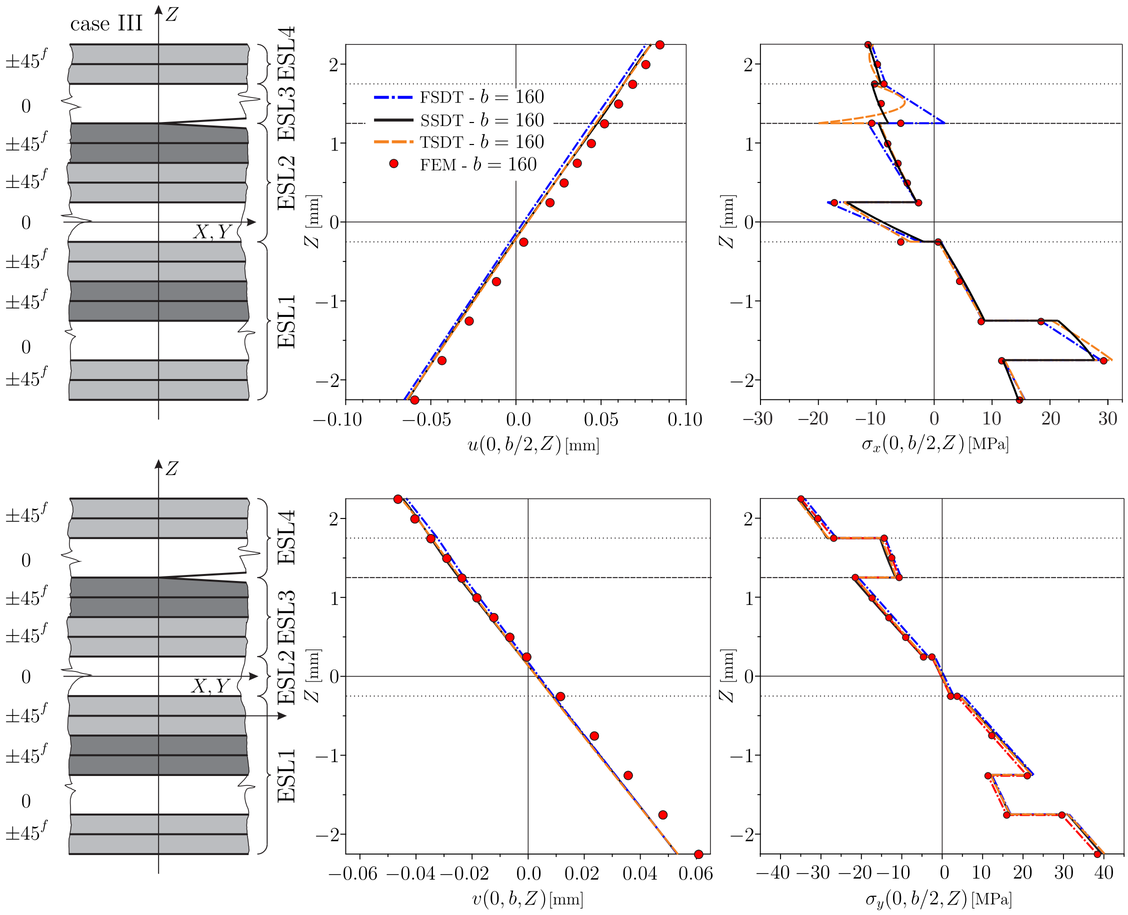

Figure 6.26: Distribution of the in-plane displacements (u, v) and normal stresses (σ_x, σ_y) over the thickness, problem ⓐ in Figure 5.1, case III, $b = 160$ mm (Compare to Fig. 6.7).

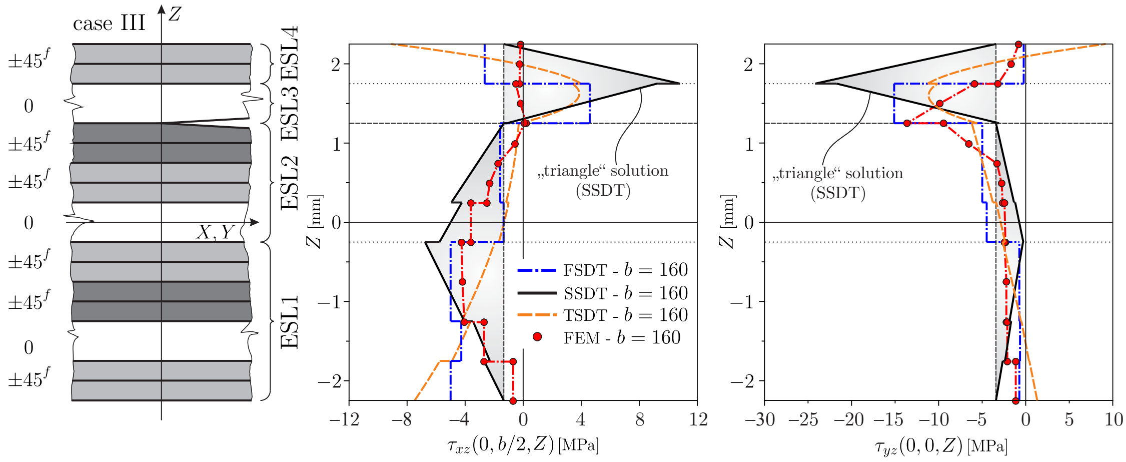

Figure 6.27: Distribution of the shear stresses (τ_{xz}, τ_{yz}) over the thickness, problem ⓐ in Figure 5.1, case III, $b = 160$ mm. Solution by constitutive equations (Compare to Fig. 6.8).

i.e. large fluctuations can take place in the through thickness distribution of τ_{xz} and τ_{yz} (*Szekrényes (2016b)*). In the case of the shear stresses, each theory approximates well the area under the distribution by FEM. The SSDT solution with SSCC is called the "triangle" solution because the shear strain distributions are triangles in the delaminated region (refer to Figure 6.30).

The distributions of case II are presented in Figure 6.24. Again, the TSDT and SSDT

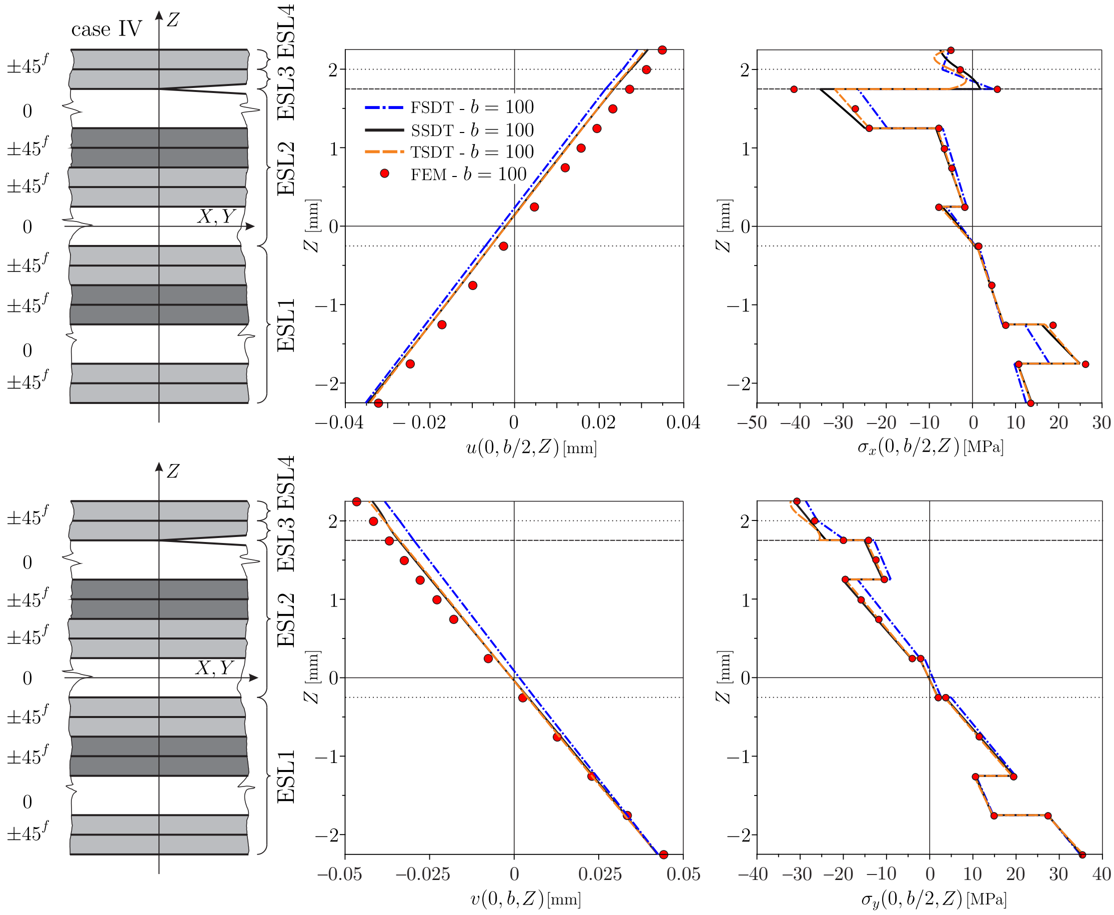

Figure 6.28: Distribution of the in-plane displacements (u, v) and normal stresses (σ_x, σ_y) over the thickness, problem ⓐ in Figure 5.1, case IV, $b = 100$ mm (Compare to Fig. 6.9).

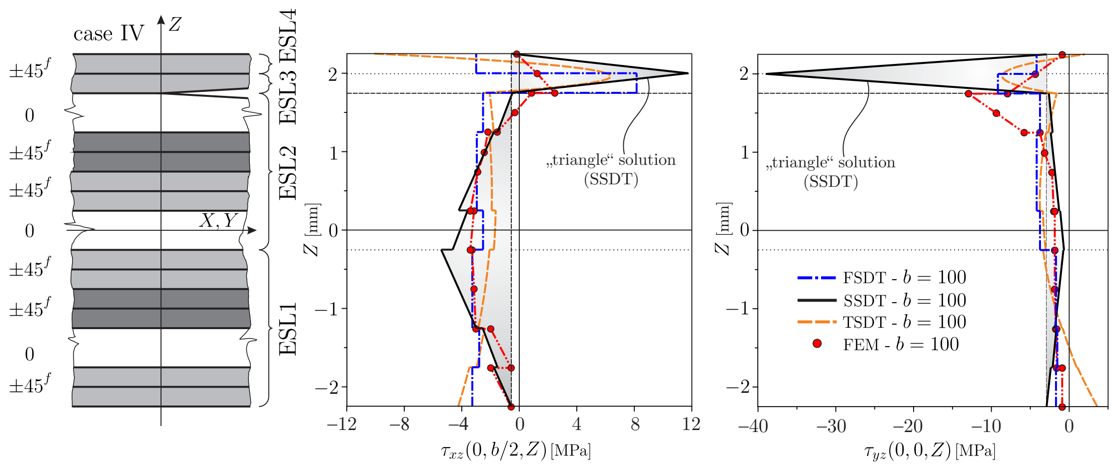

Figure 6.29: Distribution of the shear stresses (τ_{xz}, τ_{yz}) over the thickness, problem ⓐ in Figure 5.1, case IV, $b = 100$ mm. Solution by constitutive equations (Compare to Fig. 6.10).

provide the best fit to the displacement distributions by FEM. However, this time it is FSDT that fits the normal stresses in the best way. The TSDT and FSDT approximate the shear stresses in Figure 6.25 well, the SSDT result is also good.

Cases III and IV - when the delamination is located closer to the top surface of the plate - are demonstrated through Figures 6.26-6.29. Briefly summarizing the results, it can be seen that the SSDT provides very similar results for the shear stresses to those calculated

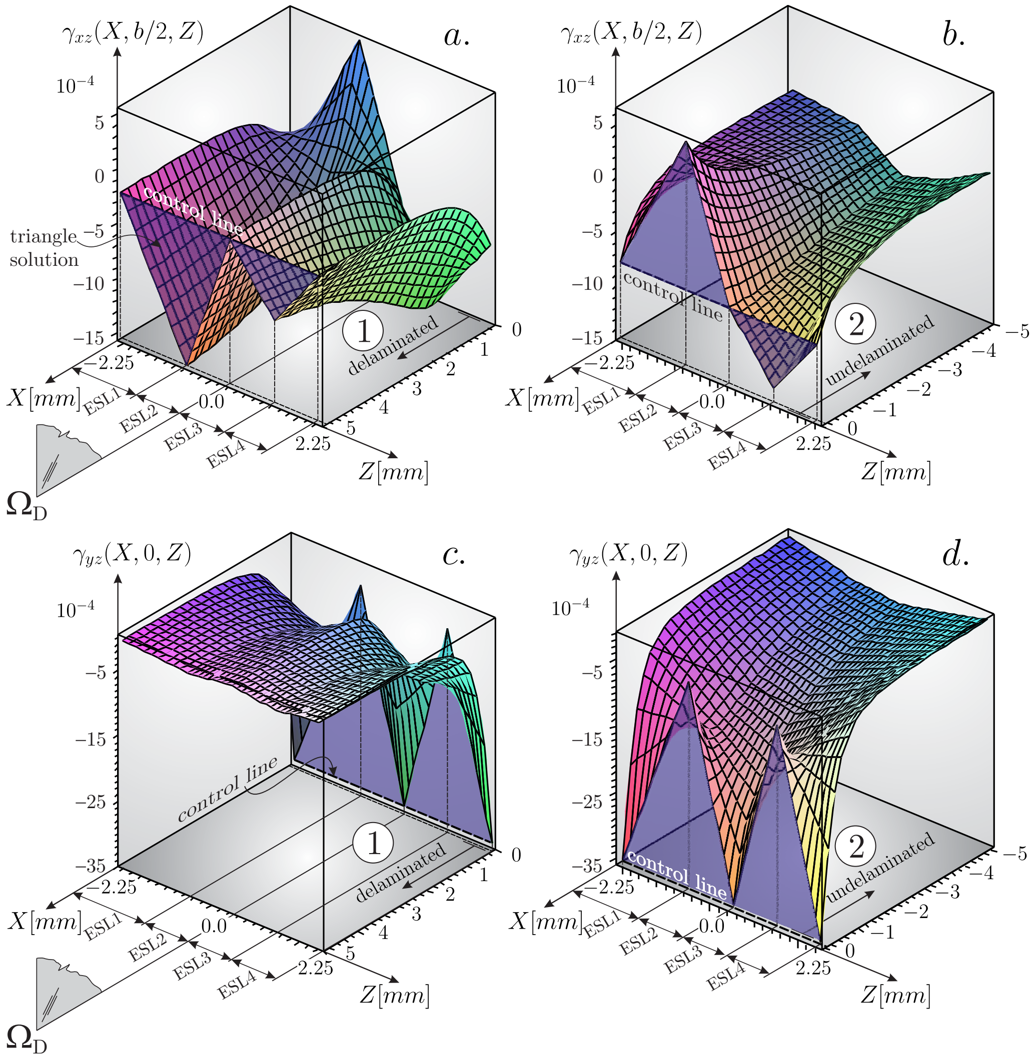

Figure 6.30: Distribution of the shear strains γ_{xz} ((a) and (b)) and γ_{yz} ((c) and (d)) by SSDT at the transition between the delaminated and undelaminated regions at $Y=b/2$ and $Y=0$ (case I, b=100 mm), Ω_D is the delamination plane (Compare to Fig. 6.11).

by Reddy TSDT plotted in Figures 6.8 and 6.10. On the other hand the FSDT and TSDT are still very reasonable to approximate the mechanical fields. Overall, the most accurate results are obtained by the TSDT and SSDT models.

In Figure 6.30 the shear strain distributions in the transition between regions 1 and 2 are plotted. Case I is investigated with the plate width of b = 100 mm, and so the results are comparable to those presented in Figure 6.11 by using the Reddy TSDT and the method of 2ESLs. Based on Figure 6.30 it is concluded that the SSCC is in fact the alternative of the dynamic boundary conditions, without the appearance of the stiffening in the deflection (refer to Figures 6.2 and 6.21). The SSDT without the SSCC was utilized by *Szekrényes (2016b)* and in cases III and IV large oscillations in the mechanical fields were observed, thus the SSCC has a key role in this respect. The distribution of the interlaminar shear stresses at the interface plane between ESL2 and ESL3 is shown in Figure 6.31 for case I and b = 160 mm. Again, the comparison with Figure 6.12 (calculated by Reddy TSDT, method of 2ESLs) reveals that the two approximations predict different stress values, even though the distributions are similar. For case III the shear strain and interlaminar stress distributions are presented in Appendix E.

dc_1254_16

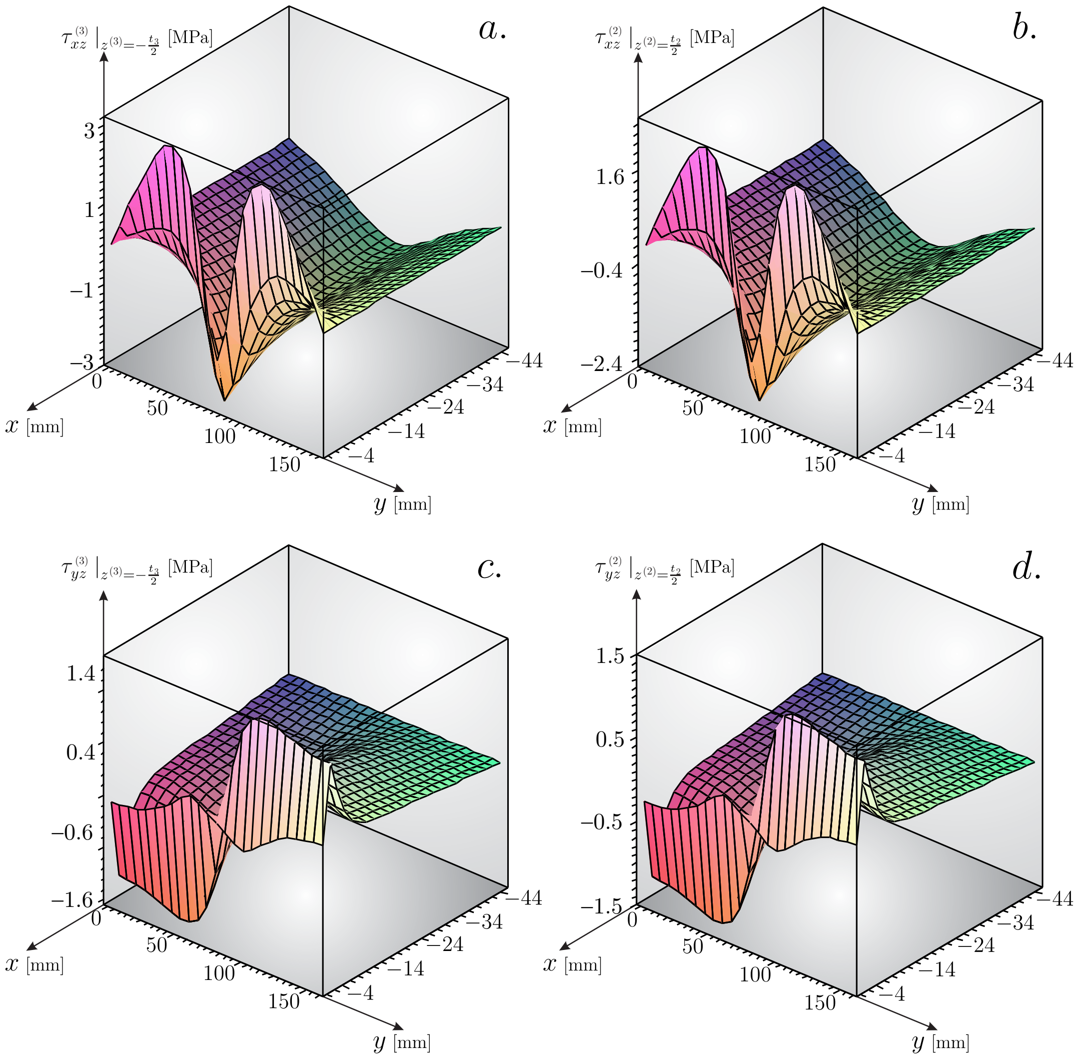

Figure 6.31: Distribution of the interlaminar shear stress by SSDT for case I, b=160 mm, $\tau_{xz}^{(3)}$ (a), $\tau_{xz}^{(2)}$ (b), $\tau_{yz}^{(3)}$ (c) and $\tau_{yz}^{(2)}$ (d) (Compare to Fig. 6.12).

6.3.2 Solution of problem (b)

The results of problem b in Figure 5.1b are shown in Figures 6.32-6.39. It is shown that in this example because of the smaller plate dimensions and the shorter crack length the perturbation in the mechanical fields is significantly more intense than in problem a. The results in case I are displayed in Figure 6.32. An immediate observation is that the u displacement by FEM is inaccurately predicted by all of the theories, or neither one of the theories capture well the FE solution. Nevertheless, it has to be emphasized that the load of problem b is Q_0=10000 N, i.e. ten times higher than that of problem a. Thus, smaller displacements and - as Figure 6.32 shows - significantly higher stresses are obtained. In case I the normal stress, σ_y is again better predicted by the SSDT than FSDT and TSDT, however for σ_x the FSDT is the best. Moreover with respect to the shear stress τ_{xz} plotted in Figure 6.33 the FSDT seems to be the best, the TSDT and SSDT give also reasonable results. On the contrary τ_{yz} is badly estimated by both (SSDT, TSDT) theories. The higher perturbation of the system is the reason for the latter discrepancy compared to the FE results. The subsequent cases II, III and IV are presented in Figures 6.34-6.39. The conclusions are in fact the same as those for problem a. It can be stated that considering both problems and all the four cases it is not to easy to choose an optimal solution. The FSDT provides

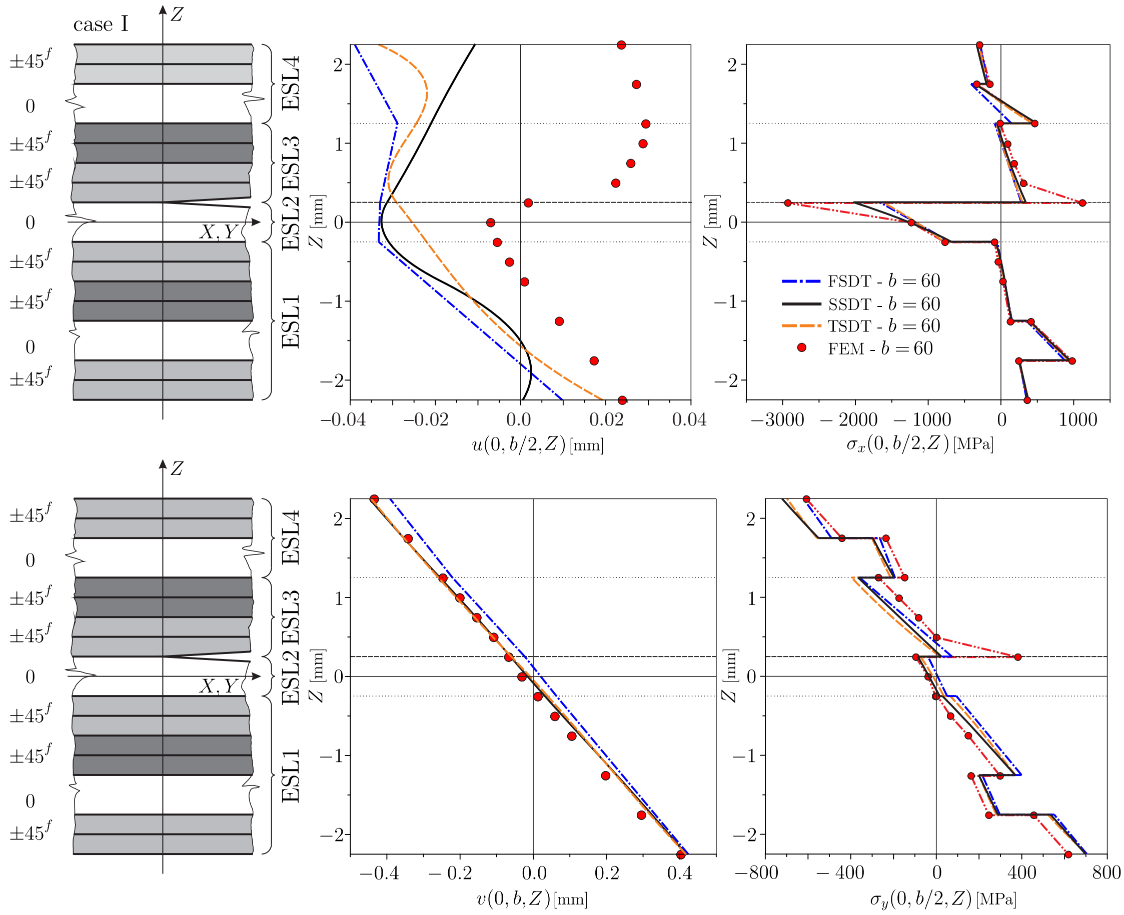

Figure 6.32: Distribution of the in-plane displacements (u, v) and normal stresses (σ_x, σ_y) over the thickness, problem b in Figure 5.1, case I, $b = 60$ mm (Compare to Fig. 6.13).

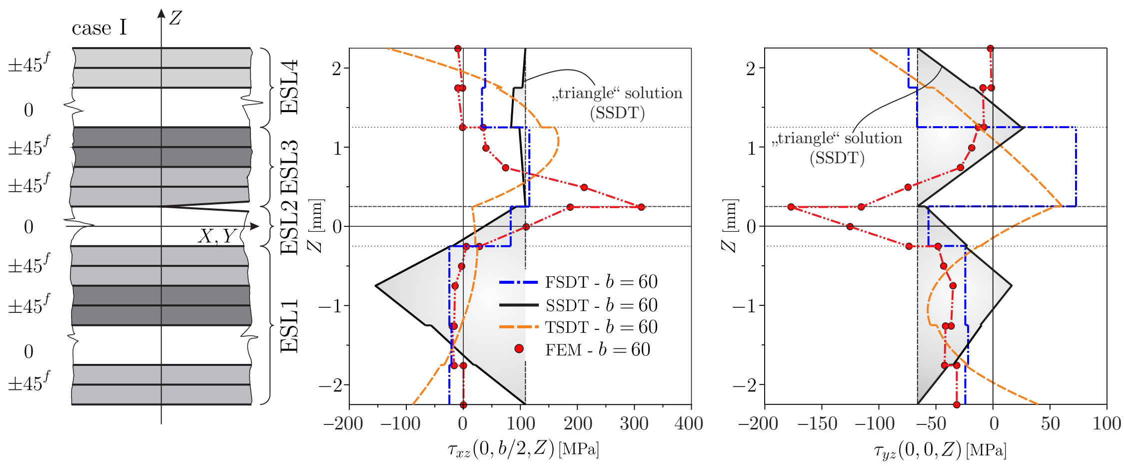

Figure 6.33: Distribution of the shear stresses (τ_{xz}, τ_{yz}) over the thickness, problem b in Figure 5.1, case I, $b = 60$ mm. Solution by constitutive equations (Compare to Fig. 6.14).

the highest error in the approximation of the deflection (Figure 6.21), at the same time the SSDT and TSDT perform excellently in this respect. The in-plane displacements and stresses are similar by all the three theories. The results of the method of 2ESLs and 4ESLs can be compared to each other based on the figure captions: each caption refers to the "pair" of the actual solution.

It is important to highlight the basic differences among the FE and the higher-order

dc_1254_16

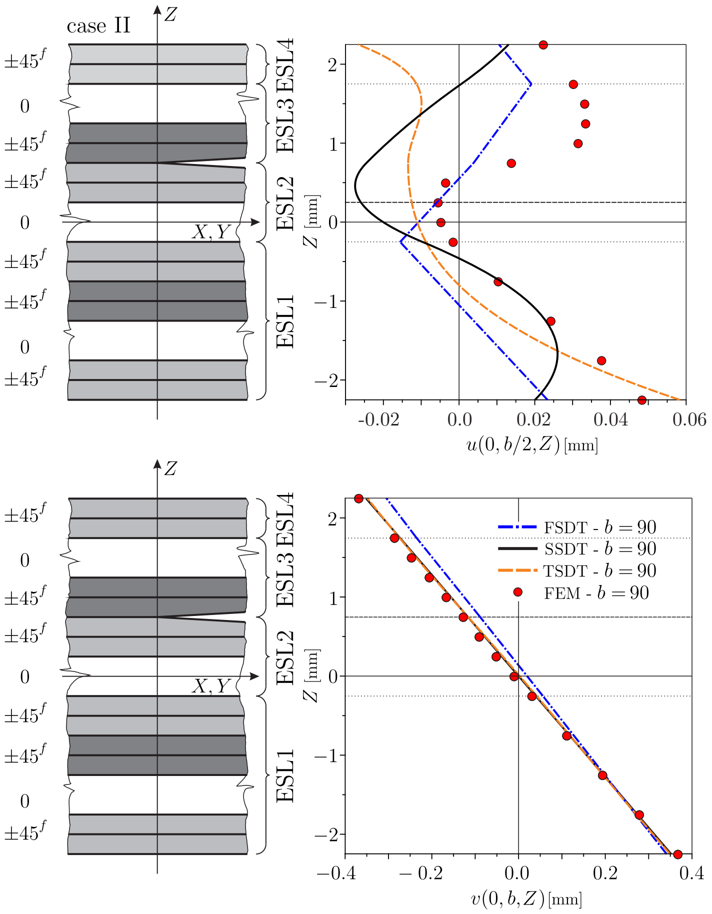

Figure 6.34: Distribution of the in-plane displacements (u, v) and normal stresses (σ_x, σ_y) over the thickness, problem (b) in Figure 5.1, case II, $b = 90$ mm (Compare to Fig. 6.15).

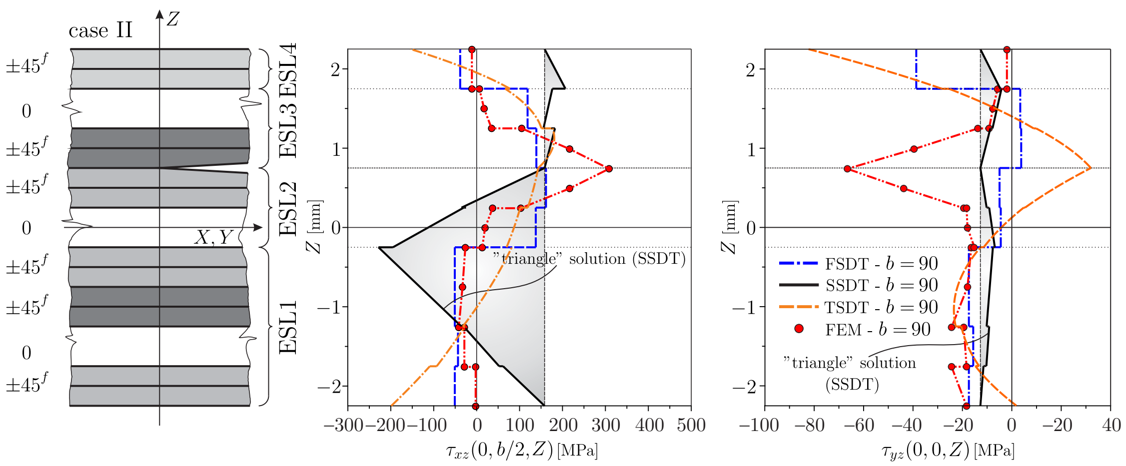

Figure 6.35: Distribution of the shear stresses (τ_{xz}, τ_{yz}) over the thickness, problem (b) in Figure 5.1, case II, $b = 90$ mm. Solution by constitutive equations (Compare to Fig. 6.16).

plate models. The FE model is based on the 3D approximation of the original continuum mechanics problem. The solution is directly obtained for the nodal displacements based on the stiffness equation. On the contrary the plate models are based on the equilibrium of the stress resultants (and their derivatives), that are calculated by integrating the stress distributions over the thickness. Eventually, the latter is a 2D approximation. On the base of the solution for the displacement parameters we calculate back the through-thickness

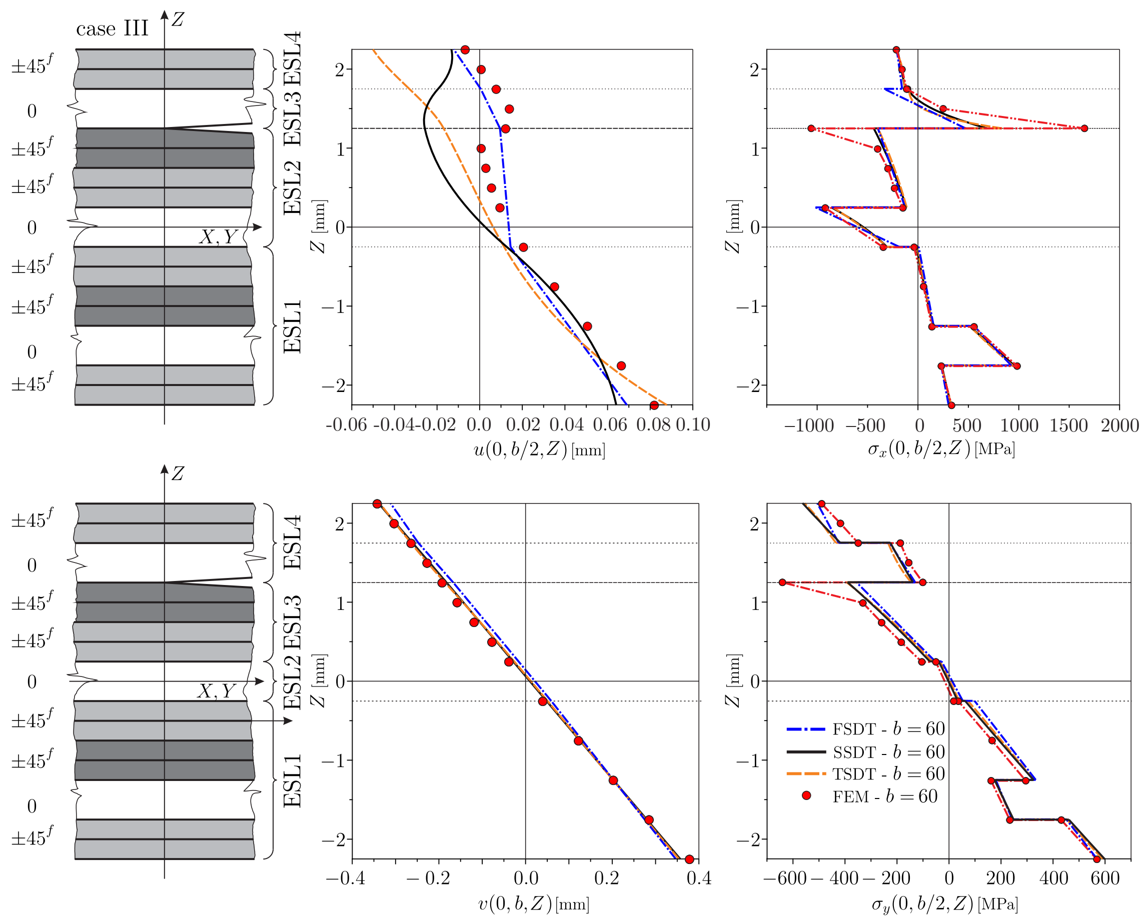

Figure 6.36: Distribution of the in-plane displacements (u, v) and normal stresses (σ_x, σ_y) over the thickness, problem ⓑ in Figure 5.1, case III, $b = 60$ mm (Compare to Fig. 6.17).

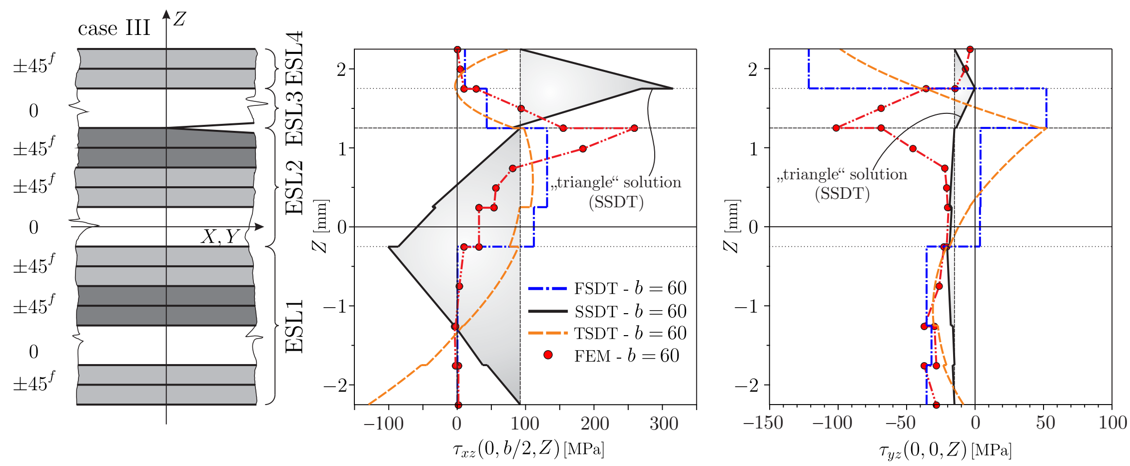

Figure 6.37: Distribution of the shear stresses (τ_{xz}, τ_{yz}) over the thickness, problem ⓑ in Figure 5.1, case III, $b = 60$ mm. Solution by constitutive equations (Compare to Fig. 6.18).

distributions, that depend on the SEKC conditions. However, based on the results of problem ⓑ (i.e., when the plate dimensions are relatively small) the perturbation because of the delamination can lead to significant differences between the numerically and analytically calculated u displacements and shear stress distributions. In spite of that the distributions of the other quantities (v, σ_x, σ_y) are well approximated. However, to choose a suitable analytical model that can be the candidate for development of a plate/shell finite element it

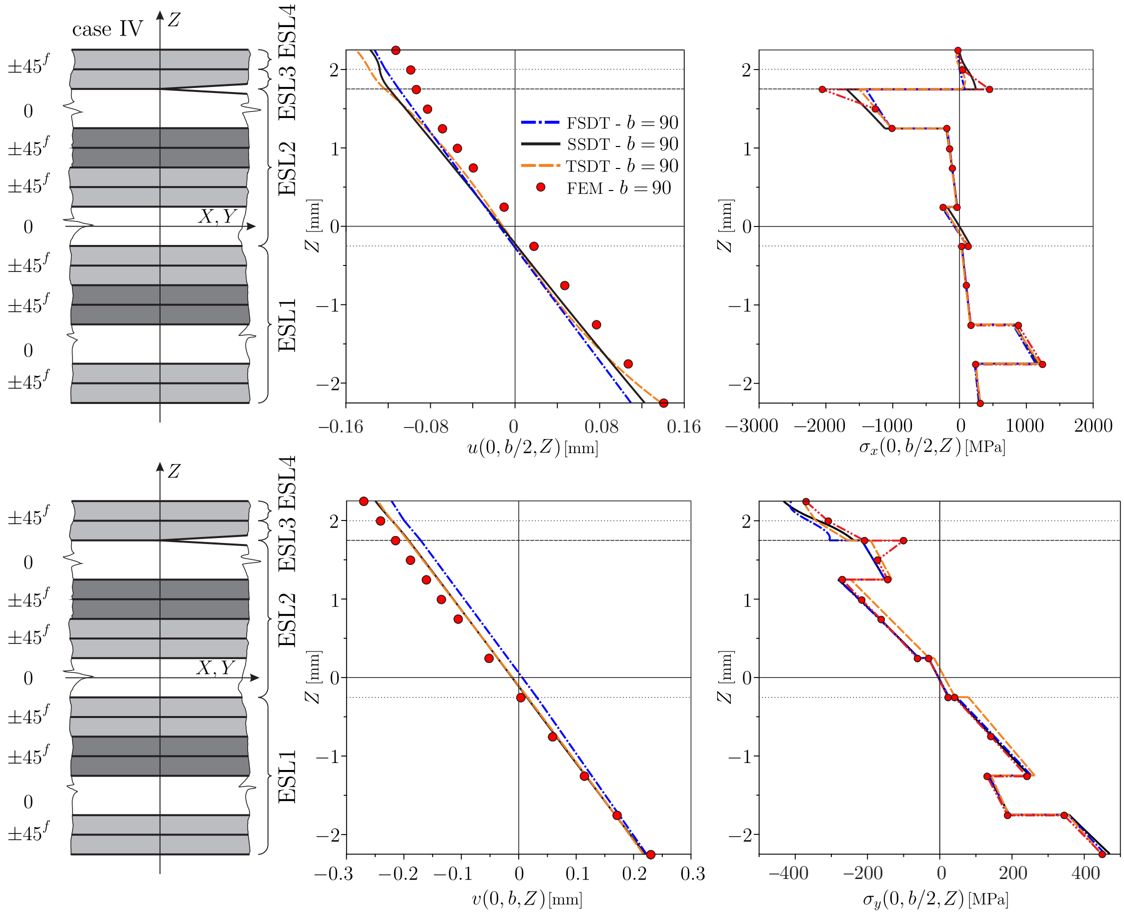

Figure 6.38: Distribution of the in-plane displacements (u, v) and normal stresses (σ_x, σ_y) over the thickness, problem (b) in Figure 5.1, case IV, $b = 90$ mm (Compare to Fig. 6.19).

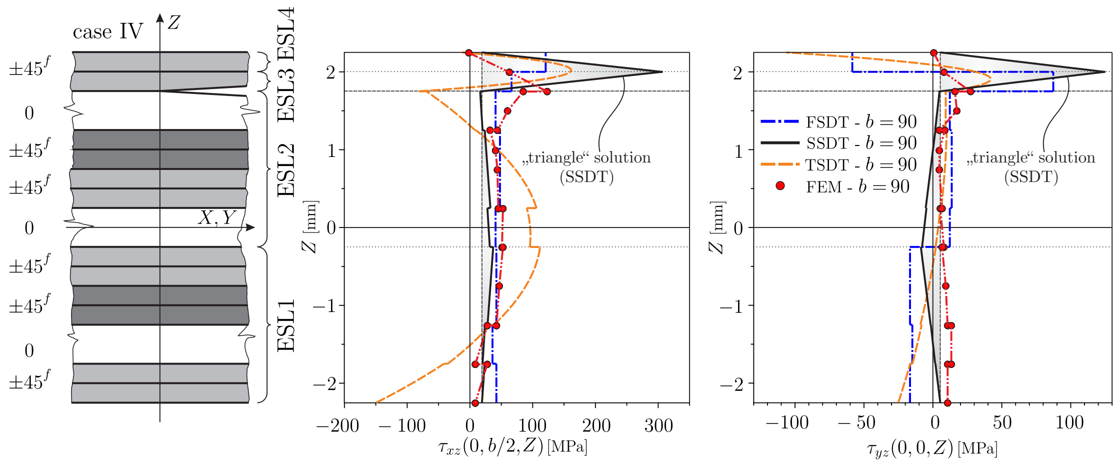

Figure 6.39: Distribution of the shear stresses (τ_{xz}, τ_{yz}) over the thickness, problem (b) in Figure 5.1, case IV, $b = 60$ mm. Solution by constitutive equations (Compare to Fig. 6.20).

is required to assess the accuracy in approximating the energy release rates, as well. This is carried out in the next chapter.

7
Energy release rates and mode mixity

7.1 J-integral calculation in delaminated composite plates

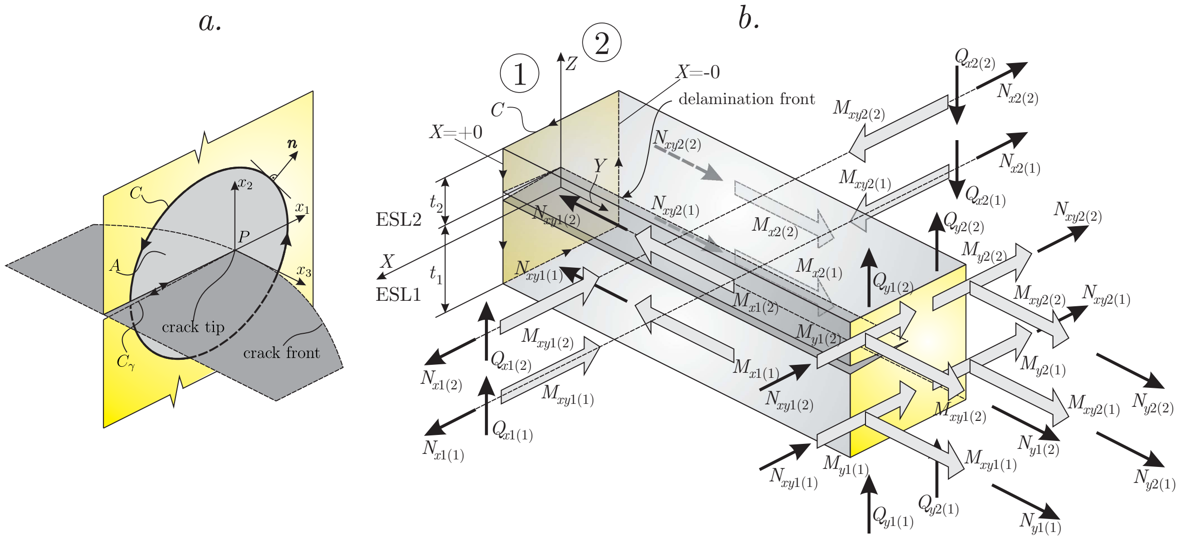

Figure 7.1: Reference system and parameters for the 3D J-integral (a). The stress resultants by FSDT (method of 2ESLs) in regions 1 and 2 in the case of a zero-area path (b).

The J-integral was originally developed by *Cherepanov (1967)* and *Rice (1968)* to characterize strain concentrations in plane problems including cracks and notches. For 2D fracture problems the J-integral was applied recently in several papers *(Mladensky and Rizov (2014, 2013b); Rizov and Mladensky (2015, 2016))*. Earlier, it was extended to three dimensional problems too. The general definition of the 3D J-integral is (*Rigby and Aliabadi (1998); Shivakumar and Raju (1992)*):

$$J_m = \int\limits_C (\mathcal{W} n_m - \sigma_{ij} u_{i,m} n_j) ds + \int\limits_A (\mathcal{W}\delta_{m3} - \sigma_{i3} u_{i,m})_{,3} dA, \; m = 1, 2, 3, \tag{7.1}$$

where in accordance with Figure 7.1a C is a closed contour containing the delamination tip, $\mathcal{W}$ is the strain energy density, n_m is the outward normal vector, σ_{ij} is the stress tensor, u_i is the displacement vector, s is the arc length coordinate along contour C, δ_{ij} is the Kronecker symbol and A is the area enclosed by contour C. The strain energy density for shear deformable plates (refer to Eq.(2.17)) can be written as (*Reddy (2004)*):

$$\mathcal{W} = \frac{1}{2}\int_0^{\varepsilon_{ij}} \sigma_{ij} d\varepsilon_{ij} = \frac{1}{2}(\sigma_x\varepsilon_x + \sigma_y\varepsilon_y + \tau_{xy}\gamma_{xy} + \tau_{xz}\gamma_{xz} + \tau_{yz}\gamma_{yz}). \tag{7.2}$$

We calculate the J-integrals for a delaminated composite plate by applying a zero-area path, i.e. in Eq.(7.1) the area A becomes zero, and so the last term vanishes. Since the J-integral is path independent (*Rice (1968)*) this gives the same result as any other appropriate contour. The zero-area path is shown in Figure 7.1b together with the stress resultants acting on both sides of the delamination if the FSDT is applied using the method of 2ESLs. In our case $x_1 = x$, $x_2 = z^{(i)}$ and $x_3 = y$. It is also important to highlight that because of the zero area-path vector $\mathbf{n}$ is always parallel to the X axis in Figure 7.1b, thus J_1 is the only nonzero term and $J_2 = J_3 = 0$. We calculate the first term in Eq.(7.1) by integrating between k number of ESLs. By using Eqs.(2.10)-(2.11) we have:

$$\begin{aligned}
\int_C \mathcal{W} n_1 ds = \frac{1}{2}\sum_{i=1}^{k}\int_{t_i/2}^{-t_i/2} &\{\sigma_{x1(i)}(\varepsilon^{(0)}_{x1(i)} + \varepsilon^{(1)}_{x1(i)} z^{(i)} + \varepsilon^{(2)}_{x1(i)}[z^{(i)}]^2 + \varepsilon^{(3)}_{x1(i)}[z^{(i)}]^3) + \\
&\sigma_{y1(i)}(\varepsilon^{(0)}_{y1(i)} + \varepsilon^{(1)}_{y1(i)} z^{(i)} + \varepsilon^{(2)}_{y1(i)}[z^{(i)}]^2 + \varepsilon^{(3)}_{y1(i)}[z^{(i)}]^3) \\
&\tau_{xy1(i)}(\gamma^{(0)}_{xy1(i)} + \gamma^{(2)}_{xy1(i)} z^{(i)} + \gamma^{(2)}_{xy1(i)}[z^{(i)}]^2 + \gamma^{(3)}_{xy1(i)}[z^{(i)}]^3) + \\
&\tau_{xz1(i)}(\gamma^{(0)}_{xz1(i)} + \gamma^{(2)}_{xz1(i)} z^{(i)} + \gamma^{(2)}_{xz1(i)}[z^{(i)}]^2) + \\
&\tau_{yz1(i)}(\gamma^{(0)}_{yz1(i)} + \gamma^{(2)}_{yz1(i)} z^{(i)} + \gamma^{(2)}_{yz1(i)}[z^{(i)}]^2)\}\, dz^{(i)}\big|_{x=+0} \\
+\frac{1}{2}\sum_{i=1}^{k}\int_{-t_i/2}^{t_i/2} &\{\sigma_{x2(i)}(\varepsilon^{(0)}_{x2(i)} + \varepsilon^{(1)}_{x2(i)} z^{(i)} + \varepsilon^{(2)}_{x2(i)}[z^{(i)}]^2 + \varepsilon^{(3)}_{x2(i)}[z^{(i)}]^3) + \\
&\sigma_{y2(i)}(\varepsilon^{(0)}_{y2(i)} + \varepsilon^{(1)}_{y2(i)} z^{(i)} + \varepsilon^{(2)}_{y2(i)}[z^{(i)}]^2 + \varepsilon^{(3)}_{y2(i)}[z^{(i)}]^3) \\
&\tau_{xy2(i)}(\gamma^{(0)}_{xy2(i)} + \gamma^{(2)}_{xy2(i)} z^{(i)} + \gamma^{(2)}_{xy2(i)}[z^{(i)}]^2 + \gamma^{(3)}_{xy2(i)}[z^{(i)}]^3) + \\
&\tau_{xz2(i)}(\gamma^{(0)}_{xz2(i)} + \gamma^{(2)}_{xz2(i)} z^{(i)} + \gamma^{(2)}_{xz2(i)}[z^{(i)}]^2) + \\
&\tau_{yz2(i)}(\gamma^{(0)}_{yz2(i)} + \gamma^{(2)}_{yz2(i)} z^{(i)} + \gamma^{(2)}_{yz2(i)}[z^{(i)}]^2)\}\, dz^{(i)}\big|_{x=-0},
\end{aligned} \tag{7.3}$$

where subscript 1 and 2 refers to the delaminated region ① and undelaminated region ② and the stresses are calculated in accordance with Eq.(2.17). For the second term in Eq.(7.1) we apply the following displacement field for the i^{th} ESL:

$$\begin{aligned}
u_{p(i)} &= u^{(0)}_{p(i)} + u^{(1)}_{p(i)} z^{(i)} + u^{(2)}_{p(i)}[z^{(i)}]^2 + u^{(3)}_{p(i)}[z^{(i)}]^3, \\
v_{p(i)} &= v^{(0)}_{p(i)} + v^{(1)}_{p(i)} z^{(i)} + v^{(2)}_{p(i)}[z^{(i)}]^2 + v^{(3)}_{p(i)}[z^{(i)}]^3, \\
w_{p(i)} &= w,
\end{aligned} \tag{7.4}$$

where the different terms can be identified based on Eq.(2.8) for the undelaminated part ② ($p = 2$) and based on Eqs.(2.36)-(2.37) for the delaminated part ① ($p = 1$). Thus, the second term in Eq.(7.1) becomes:

$$
\begin{aligned}
&\int_C (\sigma_{ij} u_{i,1} n_j) ds = \int_C (\sigma_x \frac{\partial u}{\partial x} + \tau_{xy} \frac{\partial v}{\partial x} + \tau_{xz} \frac{\partial w}{\partial x}) ds = \\
&\sum_{i=1}^{k} \int_{t_i/2}^{-t_i/2} \{\sigma_{x1(i)} (\frac{\partial u_{1(i)}^{(0)}}{\partial x} + \frac{\partial u_{1(i)}^{(1)}}{\partial x} z^{(i)} + \frac{\partial u_{1(i)}^{(2)}}{\partial x} [z^{(i)}]^2 + \frac{\partial u_{1(i)}^{(3)}}{\partial x} [z^{(i)}]^3) + \\
&\qquad \tau_{xy1(i)} (\frac{\partial v_{1(i)}^{(0)}}{\partial x} + \frac{\partial v_{1(i)}^{(1)}}{\partial x} z^{(i)} + \frac{\partial v_{1(i)}^{(2)}}{\partial x} [z^{(i)}]^2 + \frac{\partial v_{1(i)}^{(3)}}{\partial x} [z^{(i)}]^3) + \tau_{xz1(i)} \frac{\partial w_1}{\partial x} \Big\} dz^{(i)} \Big|_{x=+0} \\
&+ \sum_{i=1}^{k} \int_{-t_i/2}^{t_i/2} \{\sigma_{x2(i)} (\frac{\partial u_{2(i)}^{(0)}}{\partial x} + \frac{\partial u_{2(i)}^{(1)}}{\partial x} z^{(i)} + \frac{\partial u_{2(i)}^{(2)}}{\partial x} [z^{(i)}]^2 + \frac{\partial u_{2(i)}^{(3)}}{\partial x} [z^{(i)}]^3) + \\
&\qquad \tau_{xy2(i)} (\frac{\partial v_{2(i)}^{(0)}}{\partial x} + \frac{\partial v_{2(i)}^{(1)}}{\partial x} z^{(i)} + \frac{\partial v_{2(i)}^{(2)}}{\partial x} [z^{(i)}]^2 + \frac{\partial v_{2(i)}^{(3)}}{\partial x} [z^{(i)}]^3) + \tau_{xz2(i)} \frac{\partial w_2}{\partial x} \Big\} dz^{(i)} \Big|_{x=-0} .
\end{aligned}
\tag{7.5}
$$

By applying Eq.(2.9) to Eq.(7.4) and taking back Eqs.(7.3) and (7.5) into Eq.(7.1) yields:

$$
\begin{aligned}
J_1 = &\frac{1}{2} \sum_{i=1}^{k} \int_{t_i/2}^{-t_i/2} \{-\sigma_{x1(i)} (\varepsilon_{x1(i)}^{(0)} + \varepsilon_{x1(i)}^{(1)} z^{(i)} + \varepsilon_{x1(i)}^{(2)} [z^{(i)}]^2 + \varepsilon_{x1(i)}^{(3)} [z^{(i)}]^3) + \\
&\sigma_{y1(i)} (\varepsilon_{y1(i)}^{(0)} + \varepsilon_{y1(i)}^{(1)} z^{(i)} + \varepsilon_{y1(i)}^{(2)} [z^{(i)}]^2 + \varepsilon_{y1(i)}^{(3)} [z^{(i)}]^3) + \\
&\tau_{xy1(i)} (\left(\frac{\partial u_{1(i)}^{(0)}}{\partial y} - \frac{\partial v_{1(i)}^{(0)}}{\partial x} \right) + \left(\frac{\partial u_{1(i)}^{(1)}}{\partial y} - \frac{\partial v_{1(i)}^{(1)}}{\partial x} \right) z^{(i)} + \\
&\left(\frac{\partial u_{1(i)}^{(2)}}{\partial y} - \frac{\partial v_{1(i)}^{(2)}}{\partial x} \right) [z^{(i)}]^2 + \left(\frac{\partial u_{1(i)}^{(3)}}{\partial y} - \frac{\partial v_{1(i)}^{(3)}}{\partial x} \right) [z^{(i)}]^3) + \\
&\tau_{xz1(i)} (\gamma_{xz1(i)}^{(0)} + \gamma_{xz1(i)}^{(2)} z^{(i)} + \gamma_{xz1(i)}^{(2)} [z^{(i)}]^2 - 2 \frac{\partial w_1}{\partial x}) + \\
&\tau_{yz1(i)} (\gamma_{yz1(i)}^{(0)} + \gamma_{yz1(i)}^{(2)} z^{(i)} + \gamma_{yz1(i)}^{(2)} [z^{(i)}]^2)\} \, dz^{(i)} \Big|_{x=+0} \\
+ &\frac{1}{2} \sum_{i=1}^{k} \int_{-t_i/2}^{t_i/2} \{-\sigma_{x2(i)} (\varepsilon_{x2(i)}^{(0)} + \varepsilon_{x2(i)}^{(1)} z^{(i)} + \varepsilon_{x2(i)}^{(2)} [z^{(i)}]^2 + \varepsilon_{x2(i)}^{(3)} [z^{(i)}]^3) + \\
&\sigma_{y2(i)} (\varepsilon_{y2(i)}^{(0)} + \varepsilon_{y2(i)}^{(1)} z^{(i)} + \varepsilon_{y2(i)}^{(2)} [z^{(i)}]^2 + \varepsilon_{y2(i)}^{(3)} [z^{(i)}]^3) + \\
&\tau_{xy2(i)} (\left(\frac{\partial u_{2(i)}^{(0)}}{\partial y} - \frac{\partial v_{2(i)}^{(0)}}{\partial x} \right) + \left(\frac{\partial u_{2(i)}^{(1)}}{\partial y} - \frac{\partial v_{2(i)}^{(1)}}{\partial x} \right) z^{(i)} + \\
&\left(\frac{\partial u_{2(i)}^{(2)}}{\partial y} - \frac{\partial v_{2(i)}^{(2)}}{\partial x} \right) [z^{(i)}]^2 + \left(\frac{\partial u_{2(i)}^{(3)}}{\partial y} - \frac{\partial v_{2(i)}^{(3)}}{\partial x} \right) [z^{(i)}]^3) + \\
&\tau_{xz2(i)} (\gamma_{xz2(i)}^{(0)} + \gamma_{xz2(i)}^{(2)} z^{(i)} + \gamma_{xz2(i)}^{(2)} [z^{(i)}]^2 - 2 \frac{\partial w_2}{\partial x}) + \\
&\tau_{yz2(i)} (\gamma_{yz2(i)}^{(0)} + \gamma_{yz2(i)}^{(2)} z^{(i)} + \gamma_{yz2(i)}^{(2)} [z^{(i)}]^2)\} \, dz^{(i)} \Big|_{x=-0} .
\end{aligned}
\tag{7.6}
$$

Utilizing the definition of stress resultants by Eq.(2.18) and considering that the plate is modeled by k number of ESLs leads to the following:

$$\begin{aligned}
J_1 = \frac{1}{2}\sum_{i=1}^{k} \{ & (N_{x1(i)}\, \varepsilon^{(0)}_{x1(i)}\Big|_{x=+0} - N_{x2(i)}\, \varepsilon^{(0)}_{x2(i)}\Big|_{x=-0}) - (N_{y1(i)}\, \varepsilon^{(0)}_{y1(i)}\Big|_{x=+0} - N_{y2(i)}\, \varepsilon^{(0)}_{y2(i)}\Big|_{x=-0}) + \\
& (M_{x1(i)}\, \varepsilon^{(1)}_{x1(i)}\Big|_{x=+0} - M_{x2(i)}\, \varepsilon^{(1)}_{x2(i)}\Big|_{x=-0}) - (M_{y1(i)}\, \varepsilon^{(1)}_{y1(i)}\Big|_{x=+0} - M_{y2(i)}\, \varepsilon^{(2)}_{y2(i)}\Big|_{x=-0}) + \\
& (L_{x1(i)}\, \varepsilon^{(2)}_{x1(i)}\Big|_{x=+0} - L_{x2(i)}\, \varepsilon^{(2)}_{x2(i)}\Big|_{x=-0}) - (L_{y1(i)}\, \varepsilon^{(2)}_{y1(i)}\Big|_{x=+0} - L_{y2(i)}\, \varepsilon^{(2)}_{y2(i)}\Big|_{x=-0}) + \\
& (P_{x1(i)}\, \varepsilon^{(3)}_{x1(i)}\Big|_{x=+0} - P_{x2(i)}\, \varepsilon^{(3)}_{x2(i)}\Big|_{x=-0}) - (P_{y1(i)}\, \varepsilon^{(3)}_{y1(i)}\Big|_{x=+0} - P_{y2(i)}\, \varepsilon^{(3)}_{y2(i)}\Big|_{x=-0}) - \\
& (N_{xy1(i)}\, \hat{\gamma}^{(0)}_{xy1(i)}\Big|_{x=+0} - N_{xy2(i)}\, \hat{\gamma}^{(0)}_{xy2(i)}\Big|_{x=-0}) - (M_{xy1(i)}\, \hat{\gamma}^{(1)}_{xy1(i)}\Big|_{x=+0} - M_{xy2(i)}\hat{\gamma}^{(1)}_{xy2(i)}\Big|_{x=-0}) + \\
& (L_{xy1(i)}\, \hat{\gamma}^{(2)}_{xy1(i)}\Big|_{x=+0} - L_{xy2(i)}\, \hat{\gamma}^{(2)}_{xy2(i)}\Big|_{x=-0}) - (P_{xy1(i)}\, \hat{\gamma}^{(3)}_{xy1(i)}\Big|_{x=+0} - P_{xy2(i)}\, \hat{\gamma}^{(3)}_{xy2(i)}\Big|_{x=-0}) + \\
& (Q_{x1(i)}\left(\gamma^{(0)}_{xz1(i)} - 2\frac{\partial w_{1(i)}}{\partial x}\right)\Big|_{x=+0} - Q_{x2(i)}\left(\gamma^{(0)}_{xz2(i)} - 2\frac{\partial w_{2(i)}}{\partial x}\right)\Big|_{x=-0}) + \\
& (Q_{y1(i)}\, \gamma^{(0)}_{yz1(i)}\Big|_{x=+0} - Q_{y2(i)}\, \gamma^{(0)}_{yz2(i)}\Big|_{x=-0}) + \\
& (R_{x1(i)}\, \gamma^{(1)}_{xz1(i)}\Big|_{x=+0} - R_{x2(i)}\, \gamma^{(1)}_{xz2(i)}\Big|_{x=-0}) + (R_{y1(i)}\, \gamma^{(1)}_{yz1(i)}\Big|_{x=+0} - R_{y2(i)}\, \gamma^{(1)}_{yz2(i)}\Big|_{x=-0}) + \\
& (S_{x1(i)}\, \gamma^{(2)}_{xz1(i)}\Big|_{x=+0} - S_{x2(i)}\, \gamma^{(2)}_{xz2(i)}\Big|_{x=-0}) + (S_{y1(i)}\, \gamma^{(2)}_{yz1(i)}\Big|_{x=+0} - S_{y2(i)}\, \gamma^{(2)}_{yz2(i)}\Big|_{x=-0}) \}.
\end{aligned} \tag{7.7}$$

7.2 Mode partitioning of the total J-integral in Lévy plates

Considering the fact that we applied a zero-area path and the shear forces (Q_x, Q_y), higher-order stress resultants (R_x, R_y, S_x and S_y), the corresponding shear strains and the first derivative of the deflection are continuous at the transition between regions 1 and 2 (refer to Eq.(5.53)) the J-integral can be simplified significantly. The result can be written in the form of:

$$J_1 = J_{II} + J_{III}, \tag{7.8}$$

where J_{II} is the mode-II, J_{III} is the mode-III J-integral (refer to Figure 1.3). The task of mode separation can be carried out very simply for Lévy plates by taking back the solutions by Eq.(5.2) into the strain components by Eqs.(2.10)-(2.11) and the stress resultants by Eqs.(2.19)-(2.20). This leads to terms related to $sin^2(\beta y)$ and $cos^2(\beta y)$, respectively. Mode separation in this special case is very simple: terms containing $sin^2(\beta y)$ contribute to the mode-II, terms containing $cos^2(\beta y)$ are associated to the mode-III J-integral. Thus, we have:

$$\begin{aligned}
J_{II} = \frac{1}{2}\sum_{i=1}^{k} \Big\{ & (N_{x1(i)}\, \varepsilon^{(0)}_{x1(i)}\Big|_{x=+0} - N_{x2(i)}\, \varepsilon^{(0)}_{x2(i)}\Big|_{x=-0}) - (N_{y1(i)}\, \varepsilon^{(0)}_{y1(i)}\Big|_{x=+0} - N_{y2(i)}\, \varepsilon^{(0)}_{y2(i)}\Big|_{x=-0}) + \\
& (M_{x1(i)}\, \varepsilon^{(1)}_{x1(i)}\Big|_{x=+0} - M_{x2(i)}\, \varepsilon^{(1)}_{x2(i)}\Big|_{x=-0}) - (M_{y1(i)}\, \varepsilon^{(1)}_{y1(i)}\Big|_{x=+0} - M_{y2(i)}\, \varepsilon^{(2)}_{y2(i)}\Big|_{x=-0}) + \\
& (L_{x1(i)}\, \varepsilon^{(2)}_{x1(i)}\Big|_{x=+0} - L_{x2(i)}\, \varepsilon^{(2)}_{x2(i)}\Big|_{x=-0}) - (L_{y1(i)}\, \varepsilon^{(2)}_{y1(i)}\Big|_{x=+0} - L_{y2(i)}\, \varepsilon^{(2)}_{y2(i)}\Big|_{x=-0}) + \\
& (P_{x1(i)}\, \varepsilon^{(3)}_{x1(i)}\Big|_{x=+0} - P_{x2(i)}\, \varepsilon^{(3)}_{x2(i)}\Big|_{x=-0}) - (P_{y1(i)}\, \varepsilon^{(3)}_{y1(i)}\Big|_{x=+0} - P_{y2(i)}\, \varepsilon^{(3)}_{y2(i)}\Big|_{x=-0}) \Big\},
\end{aligned} \tag{7.9}$$

$$\begin{aligned}
J_{III} = -\frac{1}{2}\sum_{i=1}^{k} \Big\{ & (N_{xy1(i)}\, \hat{\gamma}^{(0)}_{xy1(i)}\Big|_{x=+0} - N_{xy2(i)}\, \hat{\gamma}^{(0)}_{xy2(i)}\Big|_{x=-0}) + \\
& (M_{xy1(i)}\, \hat{\gamma}^{(1)}_{xy1(i)}\Big|_{x=+0} - M_{xy2(i)}\, \hat{\gamma}^{(1)}_{xy2(i)}\Big|_{x=-0}) + \\
& (L_{xy1(i)}\, \hat{\gamma}^{(2)}_{xy1(i)}\Big|_{x=+0} - L_{xy2(i)}\, \hat{\gamma}^{(2)}_{xy2(i)}\Big|_{x=-0}) + \\
& (P_{xy1(i)}\, \hat{\gamma}^{(3)}_{xy1(i)}\Big|_{x=+0} - P_{xy2(i)}\, \hat{\gamma}^{(3)}_{xy2(i)}\Big|_{x=-0}) \Big\},
\end{aligned} \tag{7.10}$$

where:

$$\hat{\gamma}^{(q)}_{xyp(i)} = \frac{\partial u^{(q)}_{p(i)}}{\partial y} - \frac{\partial v^{(q)}_{p(i)}}{\partial x}, \quad p = 1 \text{ or } 2,\ q = 0, 1, 2, 3, \tag{7.11}$$

are the so-called conjugate shear strains. In Eqs.(7.9)-(7.10) $k = 2$ for the method of 2ESLs, and $k = 4$ for the method of 4ESLs. Eqs.(7.9)-(7.10) are valid upto third-order plates, however, it is easy to generalize for nth order plates. It is important to note that Eqs.(7.9)-(7.10) agree with the concept of *Rigby and Aliabadi (1998)*. As it can be seen the mode-II J-integral is contributed by N_x, N_y, M_x, M_y, L_x, L_y, P_x and P_y, on the other hand the mode-III J-integral contains N_{xy}, M_{xy}, L_{xy} and P_{xy}. In the sequel the results of the method of 2ESLs (FSDT, SSDT, Reddy TSDT) and 4ESLs (FSDT, SSDT, TSDT) are presented and compared to the results of FE analysis obtained by using the VCCT method (Appendix D). It is important to note that although the code ANSYS is capable to determine the J-integral numerically, it is not available for orthotropic materials. Therefore, the only alternative to calculate the ERRs in ANSYS is the VCCT using the models described in Section 6.1 (Figure 6.1). It is well-known that under static conditions and for a linear elastic material the J-integral is equivalent to the energy release rate, i.e.: $G_{II} = J_{II}$ and $G_{III} = J_{III}$.

7.3 J-integrals and mode mixity by the method of 2ESLs

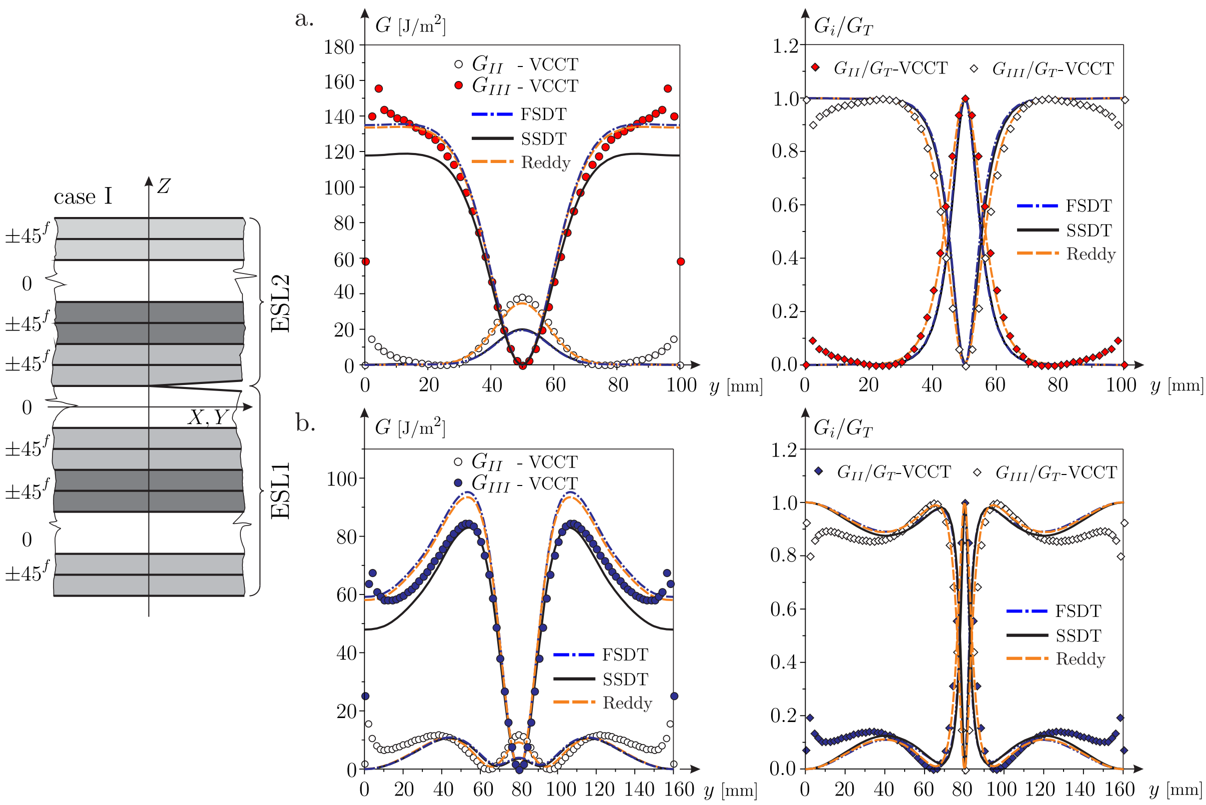

Figure 7.2: Distribution of the ERRs and mode mixity along the delamination front, problem a in Figure 5.1, case I. Plate widths: b=100 mm (a), b=160 mm (b) (Compare to Fig. 7.10).

The ERR and the mode mixity are presented through Figures 7.2 and 7.5 for problem a in Figure 5.1a and through Figures 7.6-7.9 for problem b in Figure 5.1b. In each figure

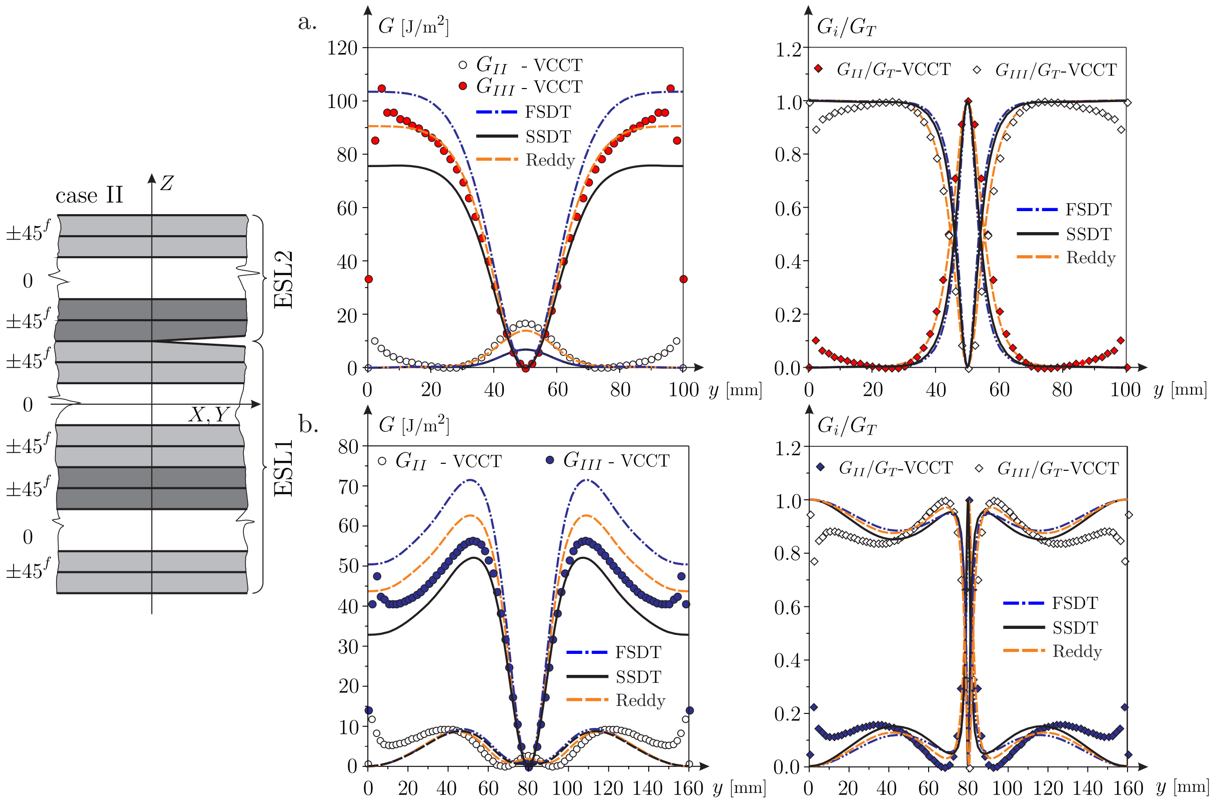

Figure 7.3: Distribution of the ERRs and mode mixity along the delamination front, problem ⓐ in Figure 5.1, case II. Plate widths: b=100 mm (a), b=160 mm (b) (Compare to Fig. 7.11).

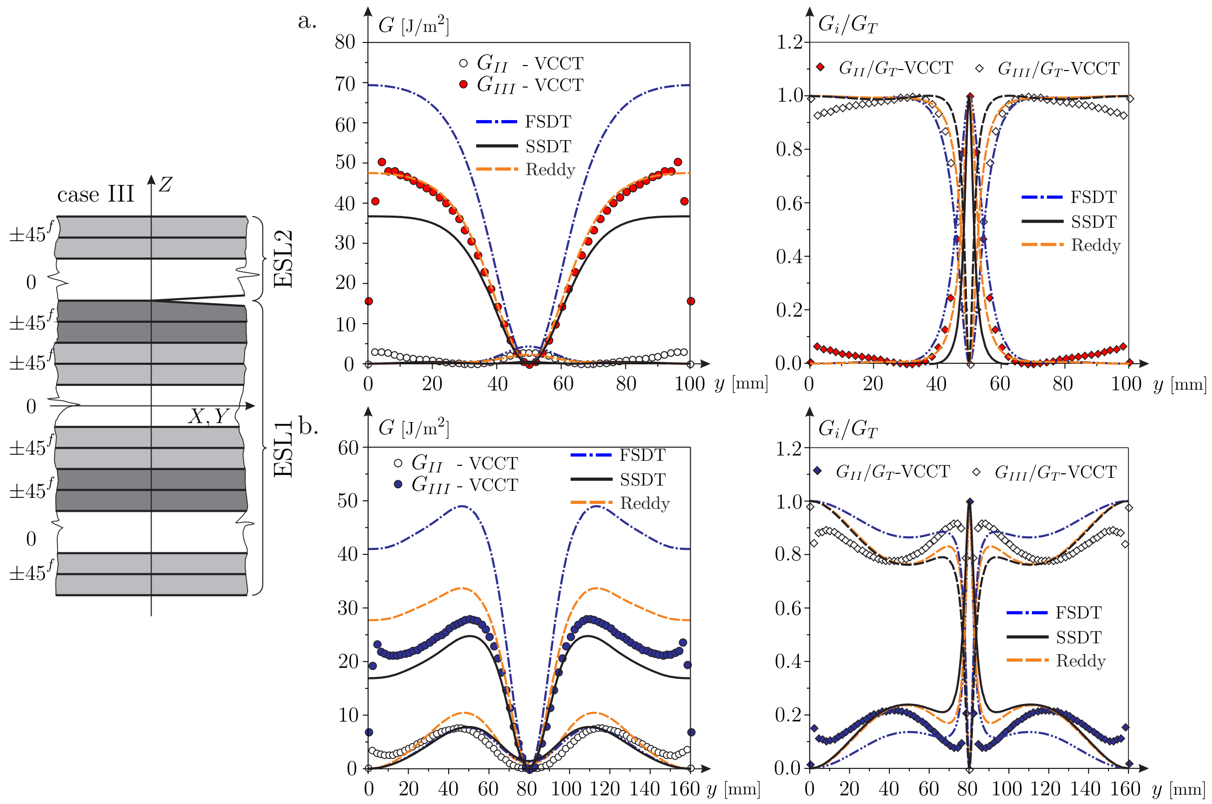

Figure 7.4: Distribution of the ERRs and mode mixity along the delamination front, problem ⓐ in Figure 5.1, case III. Plate widths: b=100 mm (a), b=160 mm (b) (Compare to Fig.7.12).

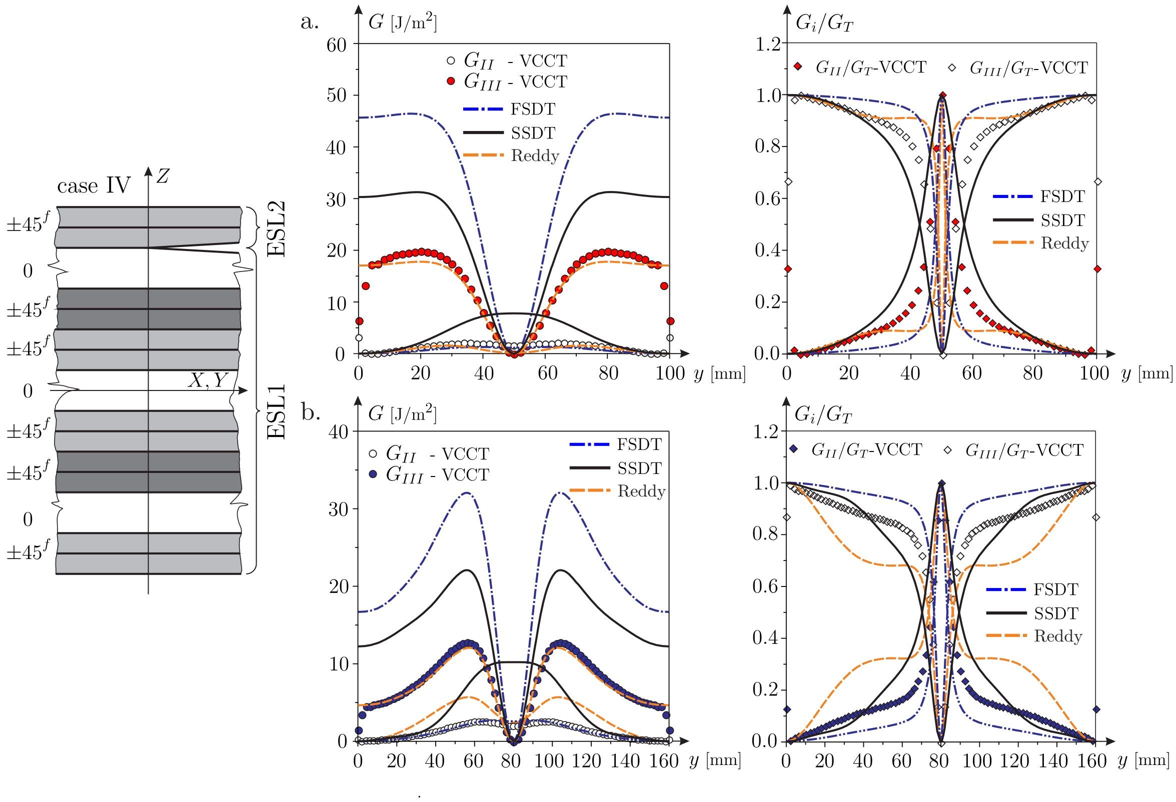

Figure 7.5: Distribution of the ERRs and mode mixity along the delamination front, problem ⓐ in Figure 5.1, case IV. Plate widths: b=100 mm (a), b=160 mm (b) (Compare to Fig.7.13).

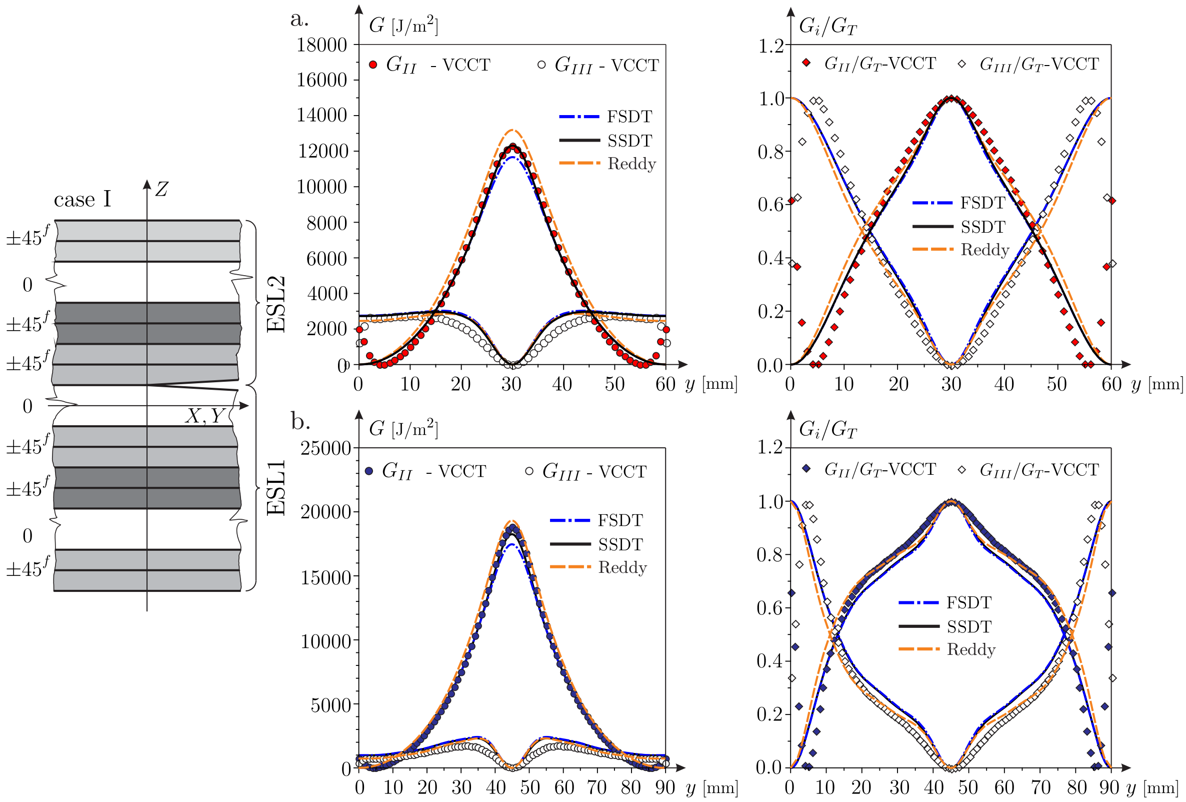

Figure 7.6: Distribution of the ERRs and mode mixity along the delamination front, problem ⓑ in Figure 5.1, case I. Plate widths: b=60 mm (a), b=90 mm (b) (Compare to Fig. 7.14).

dc_1254_16

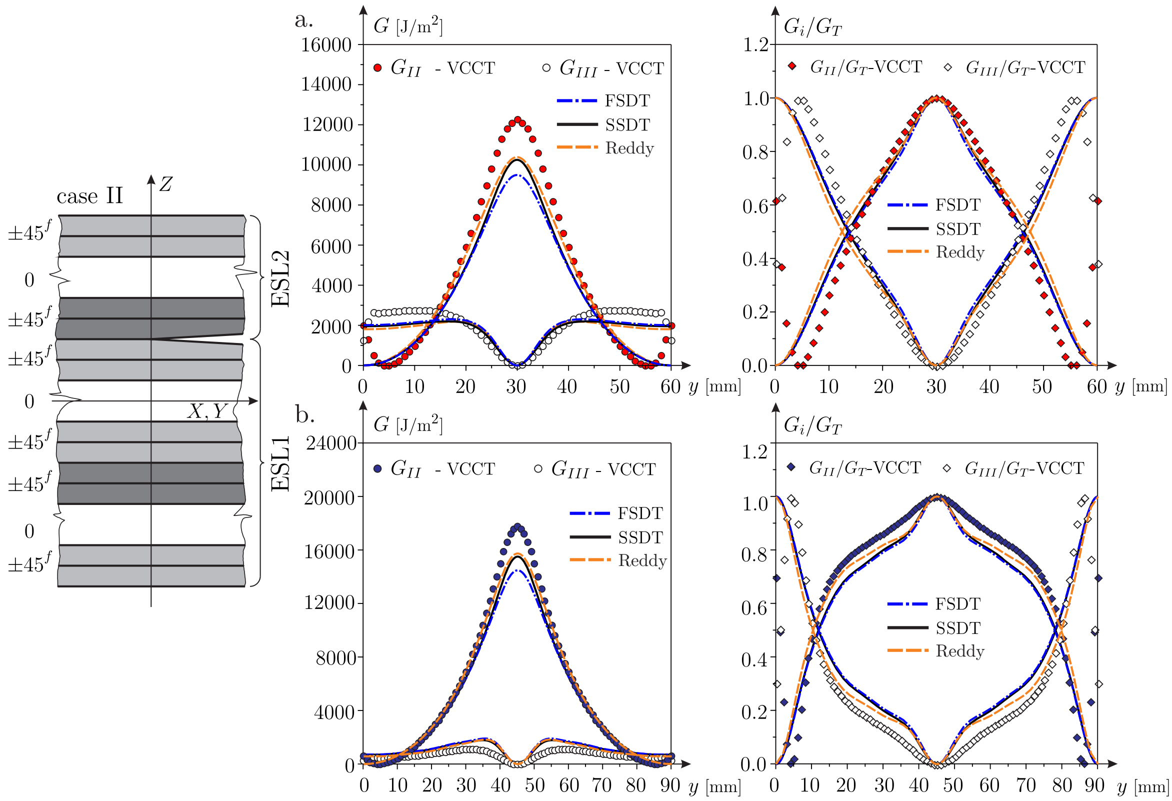

Figure 7.7: Distribution of the ERRs and mode mixity along the delamination front, problem (b) in Figure 5.1, case II. Plate widths: b=60 mm (a), b=90 mm (b) (Compare to Fig. 7.15).

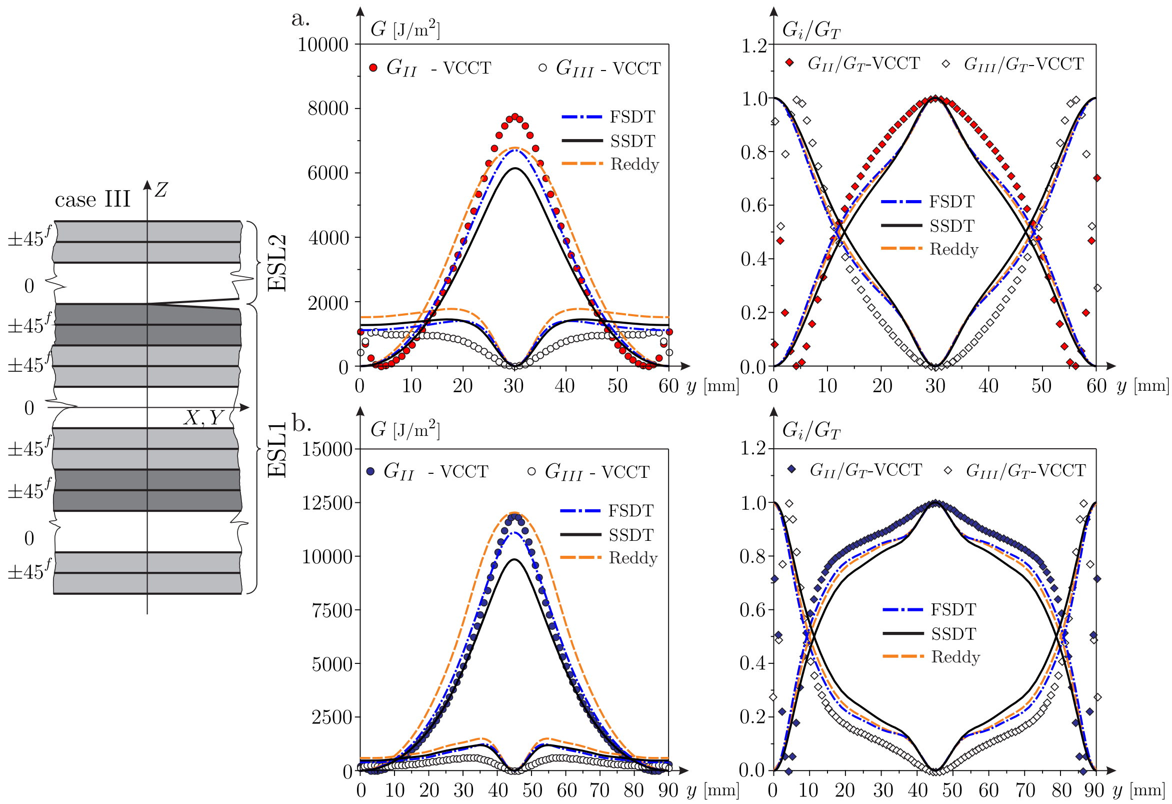

Figure 7.8: Distribution of the ERRs and mode mixity along the delamination front, problem (b) in Figure 5.1, case III. Plate widths: b=60 mm (a), b=90 mm (b) (Compare to Fig. 7.16).

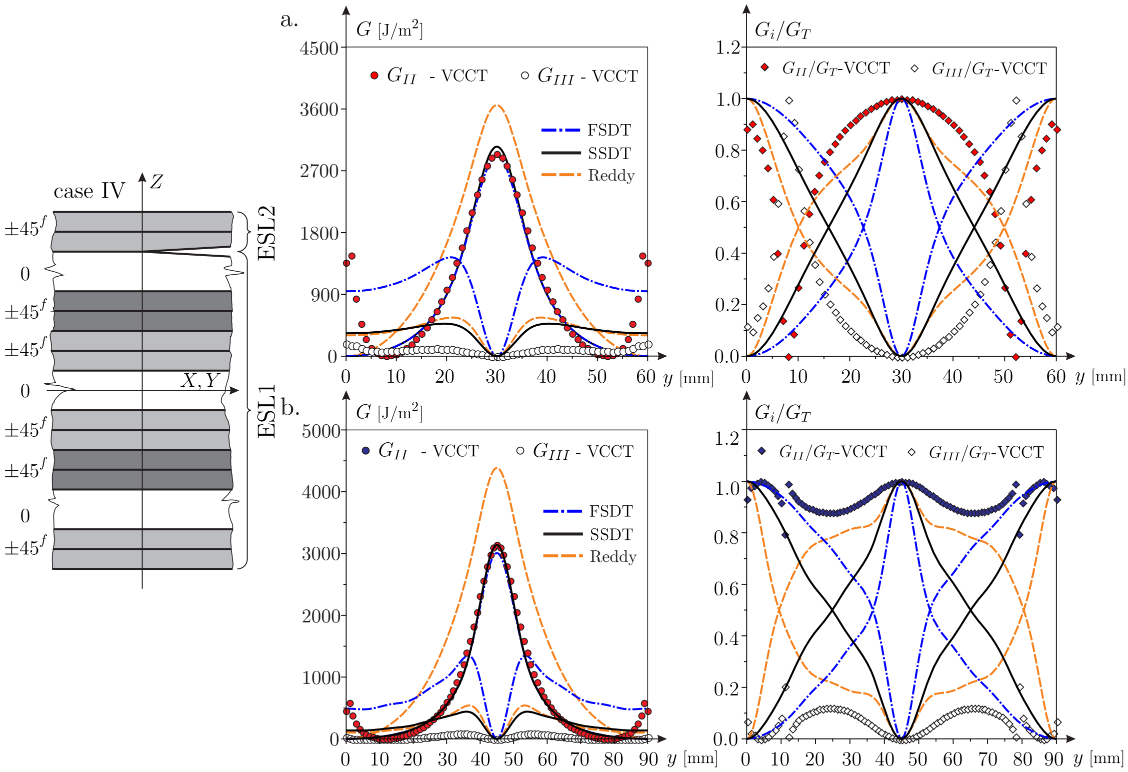

Figure 7.9: Distribution of the ERRs and mode mixity along the delamination front, problem (b) in Figure 5.1, case IV. Plate widths: b=60 mm (a), b=90 mm (b) (Compare to Fig. 7.17).

$G_T = G_{II} + G_{III}$ is the total ERR. The solution by the VCCT, Reddy TSDT (*Szekrényes (2014c)*), SSDT (*Szekrényes (2015)*) and the corresponding FSDT (*Szekrényes (2013c)*) results are compared to each other. The material is the same as that in Chapter 6 (Table 6.1). In Figure 7.2a it can be seen that for case I the FSDT and SSDT solutions underpredict G_{II}, moreover the FSDT agrees quite well with the Reddy TSDT in the case of G_{III}, in this respect the SSDT is worst if b = 100 mm. On the contrary, the Reddy TSDT agrees excellently with the numerical results for both components. Figure 7.2b presents the results for the wider plate, this time the SSDT performs better, even though the Reddy TSDT and FSDT provide good agreement, as well. It is important to highlight that the agreement between analysis and numerical calculation is the worst at and nearby the edges (if $y = 0$ or $y = b$), it is clear that the analytical models do not take the edge effects into account. So the agreement is investigated along the delamination front except for the edge regions. In case II, presented in Figure 7.3, the same conclusions hold. Based on Figures 7.4 and 7.5 for cases III and IV (i.e. when the bottom plate thickness is larger) it is shown that the FSDT overpredicts, the SSDT underpredicts/overpredicts significantly the mode-III ERR, simultaneously, the mode-II ERR by Reddy TSDT agrees better with the numerical results. The major difference between the FSDT, SSDT and Reddy TSDT solutions is the shear strain continuity at the interface plane and the satisfaction of the dynamic B.C. in the latter case. That is the reason for the differences presented in Figures 7.4 and 7.5. In accordance with Figures 7.4 and 7.5, the FSDT seems to be inaccurate in cases III and IV for both plate widths. Eventually, the SSDT and especially the Reddy TSDT approach quite well both ERR components for each plate width in case III (Figure 7.4), but if b=160 mm, then the mode-II ERR is dissimilar to the FE solution at the edges. Compared to the VCCT results, the mode-III ERR is approximated very well by Reddy TSDT, on the contrary the SSDT solution becomes inaccurate in case IV (Figure 7.5). The fracture is mode-III dominated in

dc_1254_16

problem ⓐ.

Figures 7.6-7.9 demonstrate the ERR and mode mixity distributions for problem ⓑ. Similar results were obtained to those presented in Figures 7.2-7.5, however the fracture is mode-II dominated, and so the mode-II ERR agrees better with the numerical results. Running through on cases I, II, III and IV, the conlusions are that the FSDT gives correct results only in cases I and II, in case III the overprediction of the mode-III ERR becomes moderate, while in case IV the estimation of G_{III} is not acceptable. The SSDT and Reddy TSDT perform very well compared to the FSDT. Considering all of the cases the Reddy TSDT is definitely the best solution for problem ⓐ with b = 100 mm, however if b = 160 mm the overall performance of the SSDT solution is better.

The final conclusion is that the FSDT is applicable only to those cases, when the delamination is not far from the midplane of the plate. The SSDT solves the problem better in case IV than Reddy TSDT, however, considering all of the cases the Reddy TSDT would be the best choice among the models based on the method of 2ESLs. However, we should not forget about the locking effect taking place in the deflection and shown in Figure 6.2. Also, it is clear, that the presence of the delamination induces complex deformations along the delamination front, which could be better captured by higher-order plate theories than FSDT. This consequence has already been confirmed in recent papers (*Szekrényes (2013b, 2014b,d)*). It can be seen based on the results, that case IV is the critical case, when the accuracy of the method of 2ESLs is not satisfactory. Therefore in the sequel the results of the method of 4ESLs are presented.

7.4 J-integrals and mode mixity by the method of 4ESLs

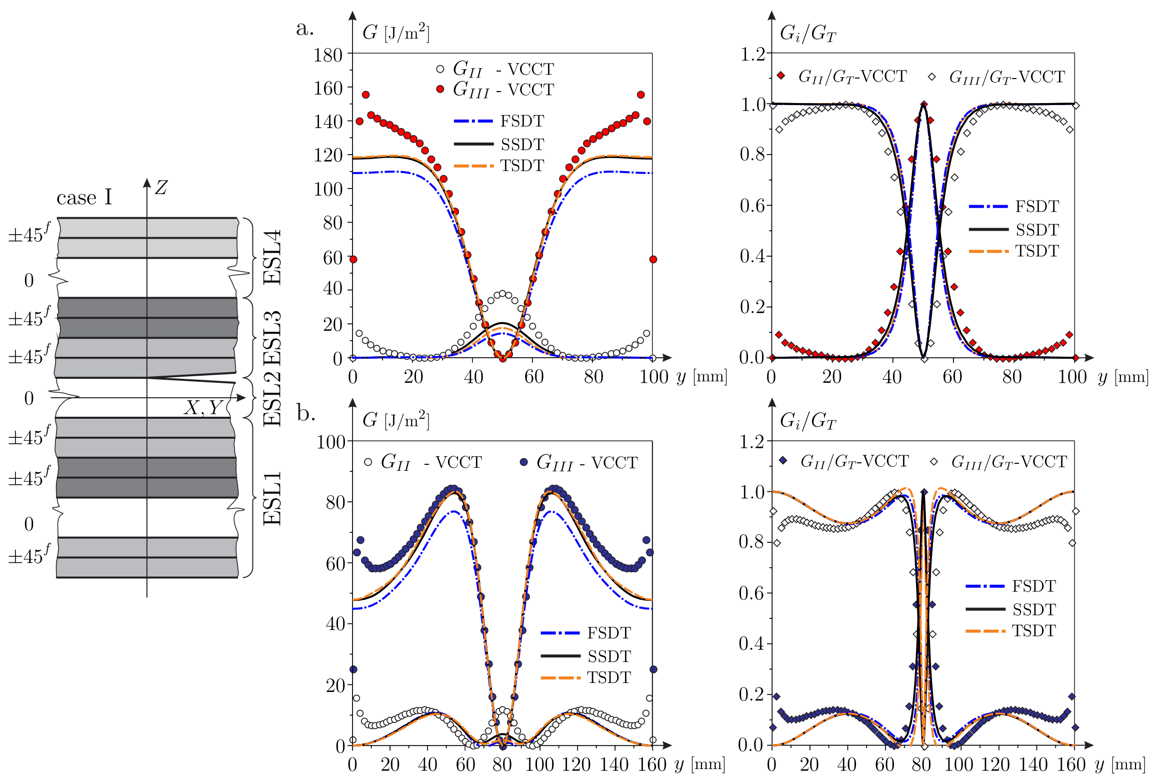

Figure 7.10: Distribution of the ERRs and mode mixity along the delamination front, problem ⓐ in Figure 5.1, case I. Plate widths: b=100 mm(a), b=160 mm(b) (Compare to Fig.7.2).

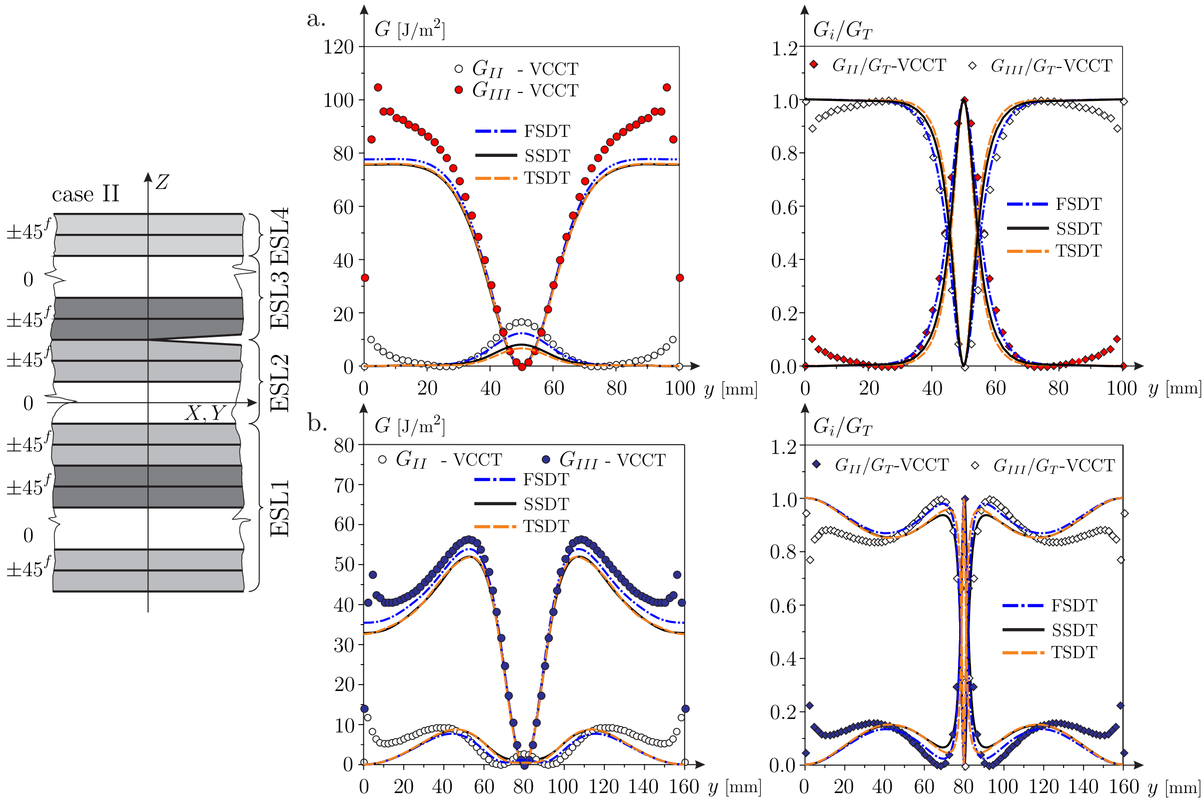

Figure 7.11: Distribution of the ERRs and mode mixity along the delamination front, problem ⓐ in Figure 5.1, case II. Plate widths: b=100 mm(a), b=160 mm(b)(Compare to Fig.7.3).

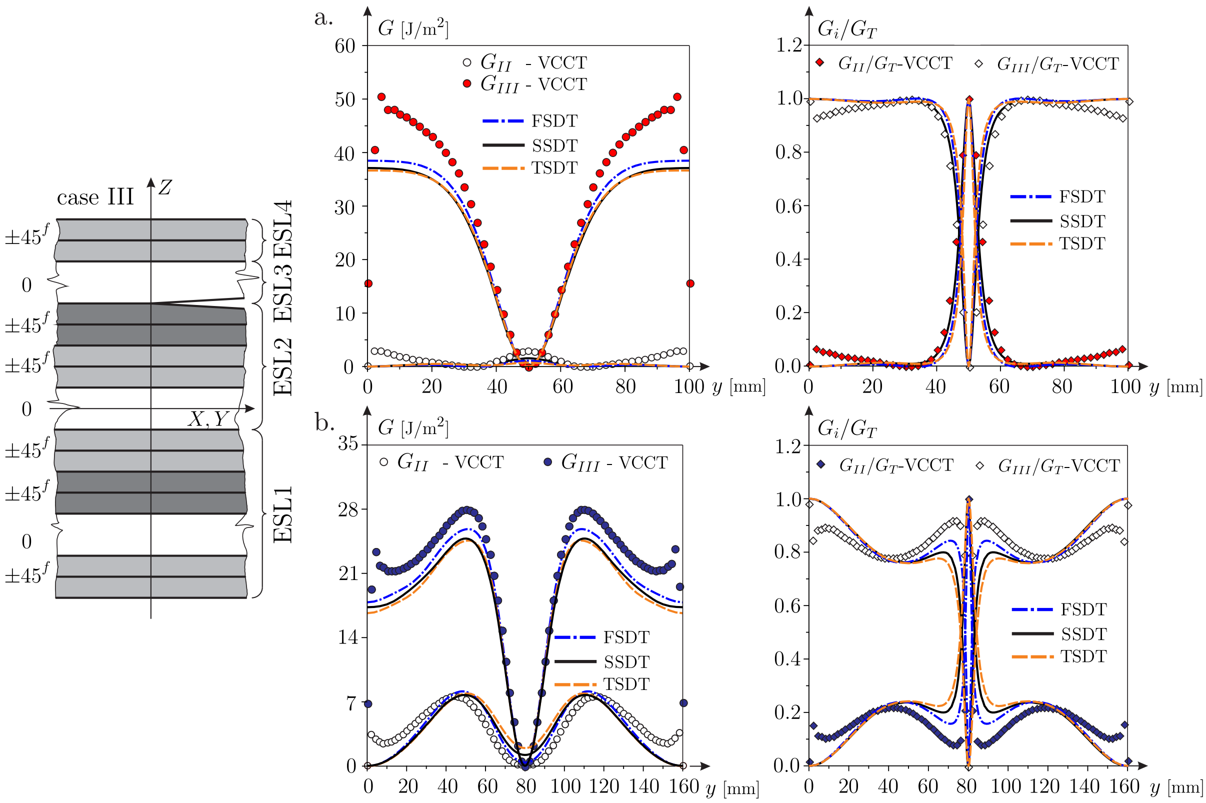

Figure 7.12: Distribution of the ERRs and mode mixity along the delamination front, problem ⓐ in Figure 5.1, case III. Plate widths: b=100 mm(a),b=160 mm(b)(Compare to Fig.7.4).

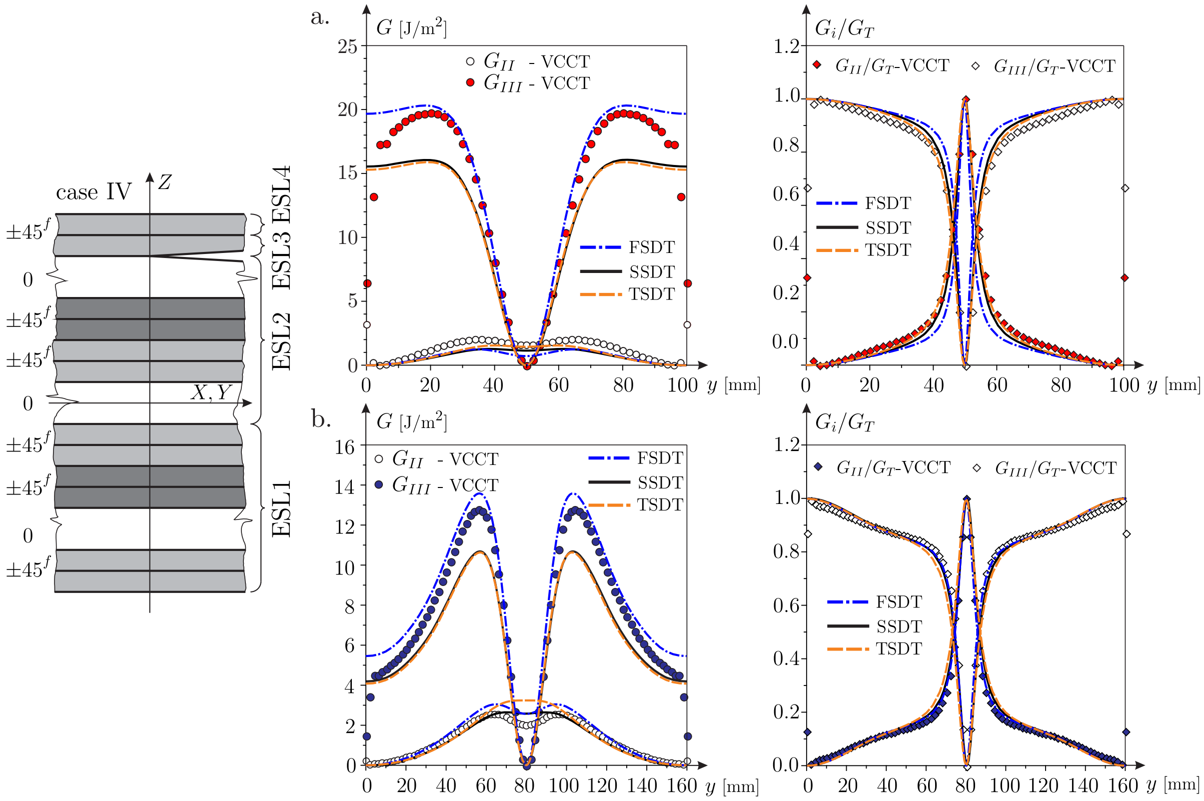

Figure 7.13: Distribution of the ERRs and mode mixity along the delamination front, problem ⓐ in Figure 5.1, case IV. Plate widths: b=100 mm(a),b=160 mm(b)(Compare to Fig.7.5).

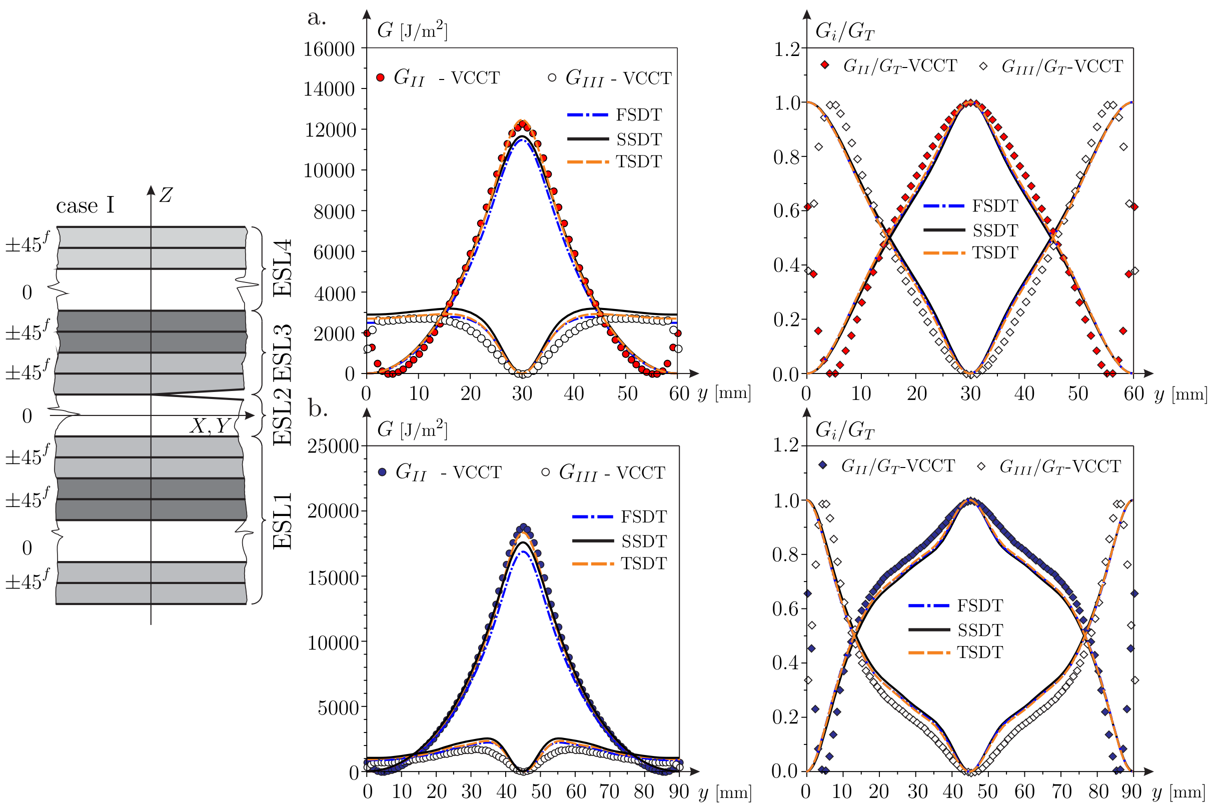

Figure 7.14: Distribution of the ERRs and mode mixity along the delamination front, problem ⓑ in Figure 5.1, case I. Plate widths: b=60 mm(a), b=90 mm(b)(Compare to Fig.7.6).

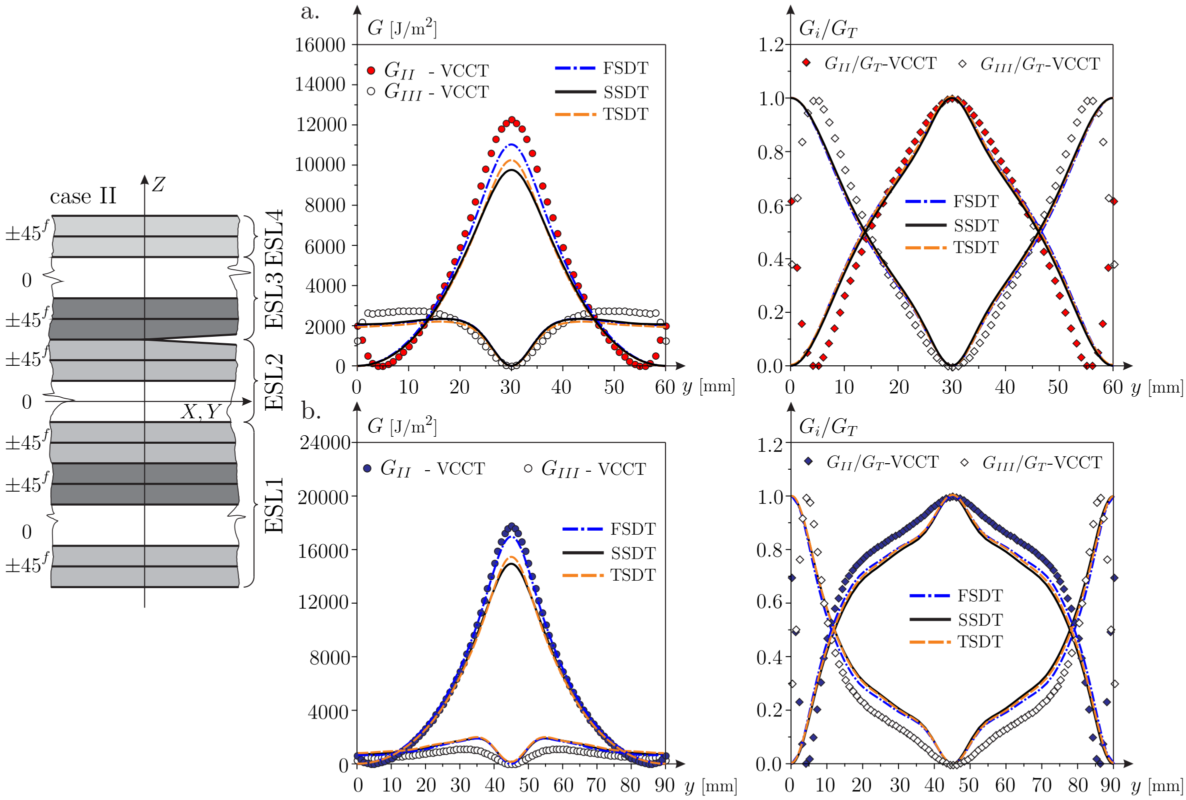

Figure 7.15: Distribution of the ERRs and mode mixity along the delamination front, problem (b) in Figure 5.1, case II. Plate widths: b=60 mm(a), b=90 mm(b)(Compare to Fig.7.7).

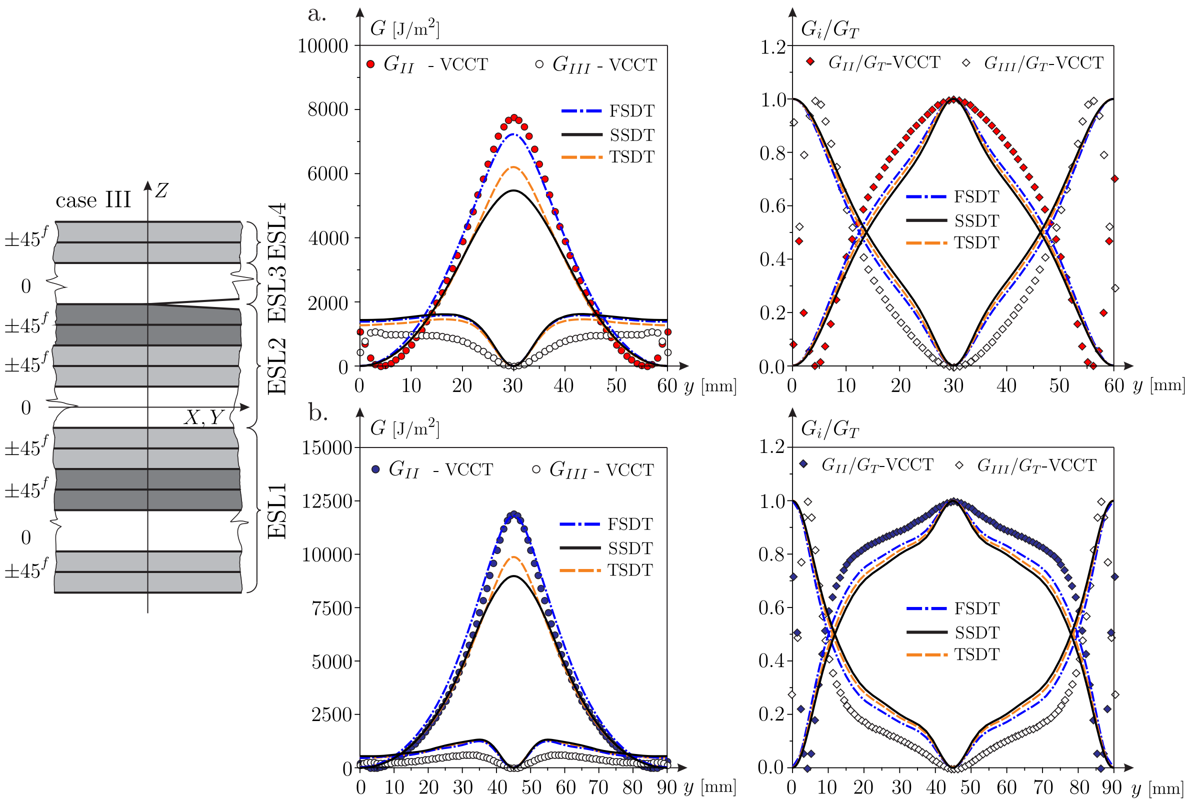

Figure 7.16: Distribution of the ERRs and mode mixity along the delamination front, problem (b) in Figure 5.1, case III. Plate widths: b=60 mm(a), b=90 mm(b)(Compare to Fig.7.8).

dc_1254_16

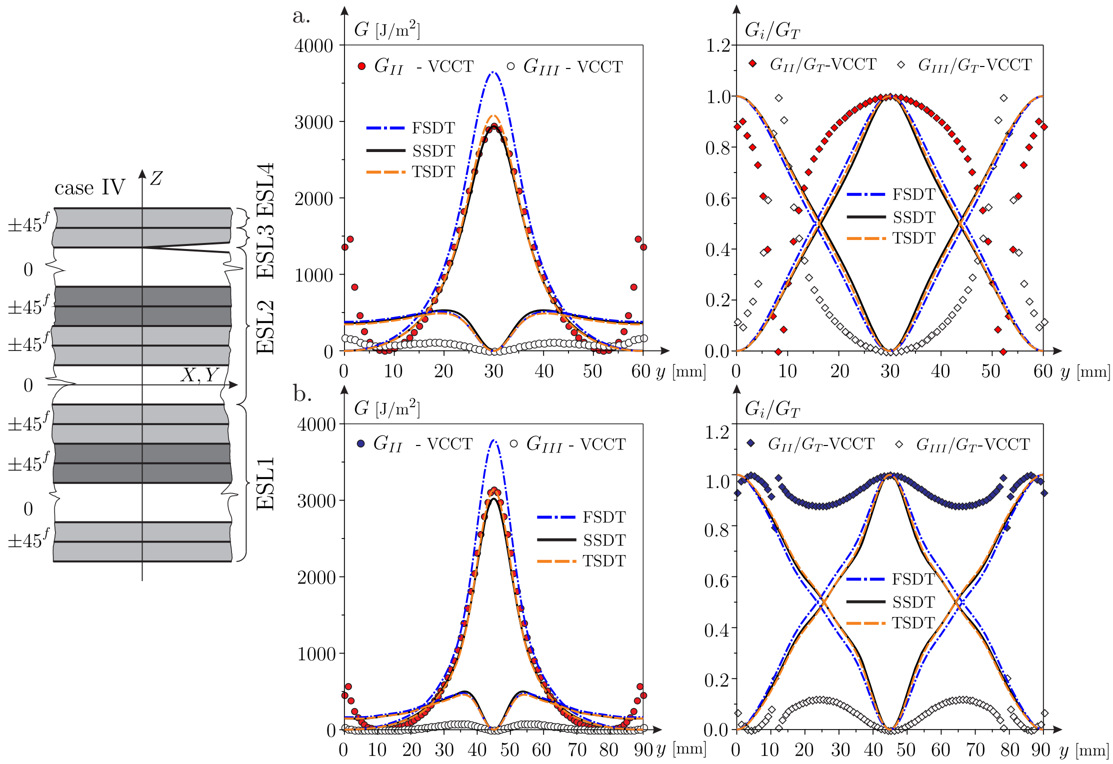

Figure 7.17: Distribution of the ERRs and mode mixity along the delamination front, problem (b) in Figure 5.1, case IV. Plate widths: b=60 mm(a), b=90 mm(b)(Compare to Fig.7.9).

The ERR ($G_{II} = J_{II}$, $G_{III} = J_{III}$) and mode mixity distributions are plotted in Figures 7.10-7.13 for problem (a) in Figure 5.1 using the method of 4ESLs. In Figures 7.10 and 7.11 cases I and II are presented for both plate widths (b = 100 and b = 160 mm). The symbols show the results of the FE calculations by the VCCT (*Bonhomme et al. (2010); Mehrabadi (2014)*), the curves represent the analytical solutions. The results of case I show that compared to the FE model the mode-II ERR is underpredicted by the FSDT and TSDT models if b = 100 mm. Although the SSDT still shows underprediction, it is obvious that it provides the best agreement with the numerical model. The mode-III ERR is captured better by the TSDT and SSDT than by FSDT. The mode mixities ($G_T = G_{II} + G_{III}$) are well predicted by each theory (b = 100 mm). If the plate width is b = 160 mm then again the SSDT and TSDT are definitely the best choices, although the FSDT theory also performs well. In case II (Figure 7.11) it is shown that the FSDT performs better than the other two theories for both plate widths. Figure 7.12 shows the results in case III for both plate widths. In case III (top half of Figure 7.12) if b = 100 mm the three theories provide similar distributions compared to the FE results. For b = 160 mm the FSDT follows better the ERRs and the mode mixity than the SSDT and TSDT. In case IV (Figure 7.13) it is the FSDT that can be ranked as the best solution for both plate widths, at the same time the SSDT and TSDT theories provide similar accuracy. It is again surprising that in case IV the FSDT is slightly better than the TSDT in the estimation of the ERRs, even the mode ratios are better predicted by FSDT. Considering all of the cases (I-IV) in Figures 7.10 and 7.13 (problem (a)) it is concluded that the FSDT approximates the numerical results with the highest accuracy among the three theories considered.

The results for problem (b) in Figure 5.1 are displayed in Figures 7.14-7.17. It has to be mentioned that the perturbation of the displacement and stress fields is significantly more intense than in the case of problem (a), even the size of the plate is smaller. Therefore the agreement with the FE results is expected to be worst than in problem ⓐ. The layout of these figures is the same as that for Figures 7.10-7.13. Briefly speaking, in case I (Figure 7.14) the SSDT overestimates slightly the mode-III ERR for both plate widths ($b = 60$ mm and $b = 90$ mm), while the FSDT and TSDT perform with similar accuracy. Nevertheless each theory overpredicts the mode-III ERR a little. In case II (Figure 7.15) the performance of all three theories is similar, but the FSDT seems to be the best. Figures 7.16 and 7.17 show the results for cases III and IV. In case III (Figure 7.16) the FSDT theory seems to be the best choice, while in case IV the SSDT and TSDT are definitely better than FSDT in approximating G_{II}. Obviously each theory is suitable to calculate the ERRs and mode ratios. The results of the method of 2ESLs and 4ESLs are comparable based on the figure captions.

Based on the results obtained it can be concluded that the accurate description of the displacement and stress fields is very important to obtain ERR and mode mixity distributions with high accuracy. Moreover each theory gives finite stresses, that is why the stress field is nonsingular in each cases. The comparison of the shear stress distributions in Figures 6.23, 6.25, 6.27, 6.29, 6.33, 6.35, 6.37 and 6.39 to the ERR and mode mixity distributions in Figures 7.10-7.17 indicates that the better the approximation of shear stresses is, the higher the accuracy of the approximation of the ERRs is. Although it is also noteworthy that the J-integrals do not depend directly on the shear and higher-order forces (Q, R and S, refer to Eqs.(7.9)- (7.10)), only indirectly through the equilibrium equations. The final conclusion is that for problem ⓐ the FSDT theory gives the best approximation of the numerical results, however the inaccurate approximation of the deflections should be kept in mind, shown in Figure 6.2. In contrast, for problem ⓑ the FSDT and TSDT theories should be highlighted, especially in case IV. However, the approximation of the deflection by FSDT plotted in Figure 6.21 involves more significant errors than those appearing for problem ⓐ.

Table 7.1: Ranking of the results of the applied plate theories for G_{II} and G_{III} with respect to the agreement with the VCCT results for problem ⓐ.

B.C.s: simply supported			2ESLs				4ESLs			
Theory			FSDT	SSDT	Reddy	Figure	FSDT	SSDT	TSDT	Figure
Size of $\mathbf{T}^{(d)}$		case	18×18	26×26	20×20		26×26	22×22	34×34	
Size of $\mathbf{T}^{(ud)}$			14×14	22×22	20×20		22×22	22×22	26×26	
Problem ⓐ b=100 mm	G_{II}	I.	2.	3.	1.	7.2	3.	1.	2.	7.10
		II.	2.	2.	1.	7.3	1.	2.	3.	7.11
		III.	2.	3.	1.	7.4	2.	1.	3.	7.12
		IV.	2.	3.	1.	7.5	3.	2.	1.	7.13
	G_{III}	I.	1.	3.	2.	7.2	3.	2.	1.	7.10
		II.	2.	3.	1.	7.3	1.	3.	2.	7.11
		III.	3.	2.	1.	7.4	1.	2.	3.	7.12
		IV.	3.	2.	1.	7.5	1.	2.	3.	7.13
Problem ⓐ b=160 mm	G_{II}	I.	3.	2.	1.	7.2	3.	1.	2.	7.10
		II.	3.	2.	1.	7.3	1.	3.	2.	7.11
		III.	2.	1.	3.	7.4	1.	2.	3.	7.12
		IV.	1.	3.	2.	7.5	2.	1.	3.	7.13
	G_{III}	I.	3.	1.	2.	7.2	3.	2.	1.	7.10
		II.	3.	1.	2.	7.3	1.	2.	3.	7.11
		III.	3.	1.	2.	7.4	1.	2.	3.	7.12
		IV.	3.	2.	1.	7.5	1.	2.	3.	7.13

dc_1254_16

7.5 Ranking of the applied plate theories

The performance of the developed analytical models with respect to the agreement with the ERRs by the VCCT results for problems a and b are ranked in Tables 7.1 and 7.2. The main viewpont of ranking is the degree of agreement of the results by the actual theory with the results of the VCCT for G_{II} and G_{III} along the whole delamination front of the plates. In Table 7.1 the results of problem a are ranked, the relevant figures are also referred to. The best one is the Reddy TSDT (method of 2ESLs) if $b = 100$ mm and the SSDT if $b = 160$ mm. Considering the slightly inaccurate deflections by Reddy TSDT in Figure 6.2 the overall winner is the SSDT using the method of 2ESLs. The results of the method of 4ESLs in Table 7.1 shows that the FSDT provides the best approximation, however as it was mentioned before, the deflections in Figure 6.21 are better captured by the SSDT and TSDT. Considering this fact and the system matrix sizes shown by Table 7.1 in each case, the SSDT is declared as the winner for the solution of problem a.

Table 7.2: Ranking of the results of the applied plate theories for G_{II} and G_{III} with respect to the agreement with the VCCT results for problem b.

B.C.s: simply supported			2ESLs				4ESLs			
Theory		case	FSDT	SSDT	Reddy TSDT	Figure	FSDT	SSDT	TSDT	Figure
Problem b, b=60 mm	G_{II}	I.	2.	1.	3.	7.6	3.	2.	1.	7.14
		II.	3.	2.	1.	7.7	1.	3.	2.	7.15
		III.	2.	3.	1.	7.8	1.	3.	2.	7.16
		IV.	2.	1.	3.	7.9	3.	1.	2.	7.17
	G_{III}	I.	3.	2.	1.	7.6	1.	3.	2.	7.14
		II.	1.	2.	3.	7.7	2.	3.	1.	7.15
		III.	1.	2.	3.	7.8	2.	3.	1.	7.16
		IV.	3.	1.	2.	7.9	2.	3.	1.	7.17
Problem b, b=90 mm	G_{II}	I.	3.	1.	2.	7.6	3.	2.	1.	7.14
		II.	3.	2.	1.	7.7	1.	3.	2.	7.15
		III.	1.	3.	2.	7.8	1.	3.	2.	7.16
		IV.	1.	2.	3.	7.9	3.	2.	1.	7.17
	G_{III}	I.	3.	2.	1.	7.6	1.	3.	2.	7.14
		II.	3.	2.	1.	7.7	1.	2.	3.	7.15
		III.	1.	2.	3.	7.8	1.	3.	2.	7.16
		IV.	3.	1.	2.	7.9	3.	2.	1.	7.17

For problem b the ranking is presented in Table 7.2. If the method of 2ESLs is applied, then the Reddy TSDT would be the best, however, the approximation of the deflection is even worst than in the case of problem a (see Figure 6.2). Even though the FSDT has more 1^{st} ranks than the SSDT, the FSDT has more 3^{rd} places as well. Thus for both plate widths the SSDT is the optimal solution. Based on a similar logical concept if the method of 4ESLs is applied again it is the SSDT that can be declared as the best solution based on Table 7.2. It has to be mentioned that the TSDT has more 1^{st} places than the SSDT, but the difference between the SSDT and TSDT is marginal, moreover the system matrix sizes are significantly higher for the TSDT as it is highlighted in Table 7.1. Thus, the overall winner is the SSDT theory for both the method of 2ESLs and 4ESLs and for problem a and b as well. Therefore, the SSDT model can be recommended to develop plate and shell finite elements for the nonsingular delamination modeling in laminated composite plates.

8
Summary

In this thesis the delamination in composite plates was investigated assuming mixed-mode II/III fracture conditions and straight delamination fronts. Based on these assumptions the general equations of delaminated orthotropic composite plates were presented. The so-called semi-layerwise technique was developed for the modeling of plates with optional number of layers. The in-plane displacement functions in each equivalent single layer were captured by general third-order functions, at the same time the transverse deflection was captured by a single term, i.e. the plates were assumed to be shear deformable, but transversely inextensible. The kinematic continuity between the equivalent single layers was established by the system of exact kinematic conditions. The basic aspect is that the set of conditions are related to the through-thickness direction. This set of conditions includes the continuity of in-plane displacements, the location of the global reference plane, the continuity of shear strains, their first and second derivatives, and finally the so-called shear strain control condition. The latter condition is an alternative of the dynamic boundary condition against the shear stresses, however, the shear strain is not zero at the traction-free surfaces, but at several (at least two) points the value of the shear strain is imposed to be the same.

With the aid of the kinematic conditions the number of parameters in the displacement functions was reduced significantly. A general expression was defined for the modified displacement field by introducing the vector of primary parameters and the displacement multiplicator matrix containing constants. The strain and stress fields were derived based on the modified displacement field and by using the basic equations of elasticity. The equilibrium equations of the delaminated and undelaminated parts were derived by means of the principle of virtual work. Using the general description the method of two equivalent single layers was developed. In accordance with this approximation the delaminated plate is divided into two subplates (top and bottom) by the plane of the delamination. Three theories were utilized in order to show the performance of the model: the first- and second-order shear deformable plate theories and Reddy third-order theory. In each case the equilibrium equations were derived for the undelaminated and delaminated regions of the plate based on the vector of primary parameters. The so-called equivalent stress resultants were derived, as well. As a next step the method of four equivalent single layers was proposed, which is a refinement compared to the method of two equivalent single layers. In this respect the first-, second- and third-order plate theories were applied. The whole plate was divided into four parts, so apart from the delamination plane further two interface planes (or perturbation planes) were generated. The vector of primary parameters, equilibrium equations and equivalent stress resultants were derived even in this case.

To exemplify the performance of the developed models layered simply supported plates subjected to a concentrated load were considered. The problems were solved by developing the system of governing partial differential equations by the Lévy plate formulation. The mathematical solution was obtained by the state-space approach. For the method of two equivalent single layers the boundary and continuity conditions were given. It was shown that for the Reddy third-order theory the number of parameters that continuity conditions are required against is not the same for the undelaminated as for the delaminated part. Therefore, the so-called autocontinuity condition was defined. The boundary and continuity conditions were also documented for the method of four equivalent single layers. The autocontinuity condition was given in the form of a theorem and even the proof and consequence of the theorem was provided. The continuity conditions were formulated in a general way, through different parameter sets. These sets included the continuity of the deflection, its derivatives and the primary parameters, the continuity of membrane displacements, the autocontinuity condition and finally the stress resultants. The sets were defined for each theory. Even the state space models were detailed together with the structure of the state vector, the vector of external loads and the system matrix.

In the results section composite plates with nine layers and four cases were investigated with respect to the position of the delamination in the transverse direction. The deflection, in-plane displacements, the normal and shear stresses were evaluated and were compared to each other and to the results of 3D finite element analysis. It was shown that the Reddy third-order theory involves some stiffening in the deflection, although the in-plane displacements and the stresses are accurately described by this theory. On the other hand the method of four equivalent single layers showed that some stiffening takes place in the deflection by the first-order plate theory, in spite of that the other functions are reasonably approximated.

Considering the fracture mechanical point of view the 3D J-integral was applied to the mixed-mode II/III problem and the total J-integral was separated into mode-II and mode-III components. It was shown that the J-integral can be calculated by the stress resultants and the strain field components by applying a zero-area path around the delamination tip. Eventually, the distribution of J_{II} and J_{III} was determined along the delamination front. The results of the analytical models were compared to those by the virtual crack closure technique. The agreement among the analytical models and the numerical results were assessed and in each case the models were ranked, as well. It was concluded that considering all the fields and the J-integrals the SSDT theory is the optimal choice for the delamination modeling of composite plates. This conclusion holds equally in the case of the methods of two and four equivalent layers. Even though it is reasonable to apply rather the method of four equivalent single layers because it provides a better description of the mechanical fields than the method of two equivalent single layers. The theses related to this work are summarized as follows.

8.1 Novel scientific results - Theses

Thesis 1.

a. I have given the definition of the semi-layerwise plate model for delaminated plates. The concept is that a laminated composite plate consisting of N_l number of layers is modeled by N_{ESL} number of equivalent single layers and $N_{ESL} < N_l$. The planes between the adjacent equivalent single layers are the interface or perturbation planes. Out of the perturbation planes a single one has to be located in the plane of the delamination.

(b.) I have formulated the system of exact kinematic conditions for the modeling of delaminated composite plates built-up by N_{ESL} number of third-order equivalent single layers. The system of exact kinematic conditions is the set of conditions related to the kinematic continuity in the transverse direction between the equivalent single layers of a semi-layerwise plate model. The set of conditions consists of the following elements:

- continuity of in-plane and transverse displacement components,
- the definition of the global membrane displacement components at the reference plane,
- continuity of transverse shear strains and their first and second derivatives at the interface planes,
- the shear strain control condition.

The system of exact kinematic conditions can be implemented into any plate theory. For shear deformable but transversely inextensible plates the system of exact kinematic conditions is the set of conditions against the in-plane displacement components, their first, second and third derivatives with respect to the local transverse coordinates.

- **Related publications**: *Szekrényes (2013b,c, 2016a).*

Thesis (2.)

I have shown that the displacement field satisfying the system of exact kinematic conditions in the i^{th} equivalent single layer of a semi-layerwise plate model can be given as:

$$
\begin{aligned}
u_{(i)} &= u_0^* + \left(K_{ij}^{(0)} + K_{ij}^{(1)} z^{(i)} + K_{ij}^{(2)} [z^{(i)}]^2 + K_{ij}^{(3)} [z^{(i)}]^3\right) \psi_{(x)j}, \quad i = q..s,\\
v_{(i)} &= v_0^* + \left(K_{ij}^{(0)} + K_{ij}^{(1)} z^{(i)} + K_{ij}^{(2)} [z^{(i)}]^2 + K_{ij}^{(3)} [z^{(i)}]^3\right) \psi_{(y)j}, \quad i = q..s,\\
w_{(i)} &= w, \quad i = 1..k.
\end{aligned}
$$

where in the third-order functions $\psi_{(p)j}$ ($p = x$ or y) is the vector of primary parameters, K_{ij} is the displacement multiplicator matrix, moreover the following hold for the

$$
\left.\begin{array}{l}
\text{undelaminated region}\\
\text{delaminated region, bottom plate}\\
\text{delaminated region, top plate}
\end{array}\right\} \Rightarrow \left\{\begin{array}{lll}
(u_0^*, v_0^*) = (u_0, v_0)\,, & q = 1, & s = k,\\
(u_0^*, v_0^*) = (u_{0b}, v_{0b})\,, & q = 1, & s = h,\\
(u_0^*, v_0^*) = (u_{0t}, v_{0t})\,, & q = h+1, & s = k,
\end{array}\right.
$$

where k is the total number of equivalent single layers, h is the number of equivalent single layers in the bottom plate. The membrane displacements u_0 v_0, u_{0b}, v_{0b}, u_{0t}, v_{0t} and the w deflection are typically primary parameters. The further primary parameters of the system can be chosen in order to have a system of algebraic equations based on the system of exact kinematic conditions built-up by linearly independent equations. Based on the principle of virtual work I have derived the invariant form the equilibrium equations for third-order plates. I have shown the form of the equilibrium equations if the method of two and four equivalent single layers is applied. I have shown that by summing the convenient equilibrium equations it is possible to derive the vectors of equivalent stress resultants, like equivalent moments $\hat{\mathbf{M}}^{(x,xy)}$, equivalent $\hat{\mathbf{L}}^{(x,xy)}$ and $\hat{\mathbf{P}}^{(x,xy)}$ stress resultants. The equivalent stress resultants play a key role in assigning the boundary and continuity conditions of the boundary value problems.

- **Related publications**: *Szekrényes (2014b, 2016a,b).*

Thesis 3.

a. I have shown that the generalized continuity conditions between the delaminated (1) and undelaminated (2) regions of third-order orthotropic composite Lévy plates can be written as:

$$\left.\begin{pmatrix} g_\alpha \\ h_\alpha \\ m_\alpha \\ n_\alpha \\ p_\alpha \end{pmatrix}\right|_{x=+0}^{(1)} = \left.\begin{pmatrix} g_\alpha \\ h_\alpha \\ m_\alpha \\ n_\alpha \\ p_\alpha \end{pmatrix}\right|_{x=-0}^{(2)},$$

where g_α is a parameter set containing the deflection, its derivatives depending on the applied theory, and the components of $\psi_{(p)j}$, h_α and m_α are parameter sets for the membrane part of the displacement field, n_α is the set of autocontinuity condition and p_α is a parameter set containing the standard and equivalent stress resultants.

b. I have derived the theorem of autocontinuity. The autocontinuity theorem states that the total continuity of the displacement field of the delaminated and undelaminated regions at the mutual cross section of third-order orthotropic composite Lévy plates apart from the continuity of the $g_\alpha, h_\alpha, m_\alpha$ and p_α sets can be ensured by imposing the continuity of $|N_d - N_{ud}| \in \mathbb{N}$ number of parameters, where N_d and N_{ud} are the numbers of eliminated parameters in the delaminated and undelaminated regions. The former parameters are the *autocontinuity parameters*, that are at the same time *primary parameters* too. The autocontinuity is satisfied only if along the interfaces between the equivalent single layers the same conditions are imposed in the delaminated and undelaminated regions. Along the delamination plane different conditions can be applied. I have given a proof of the autocontinuity theorem for the third-order plate model with the method of four equivalent single layers and the Reddy third-order theory including the method of two equivalent single layers. The consequence of the theorem has also been given resulting in the reduction of the number of continuity conditions against the membrane parts of the displacement fields.

- **Related publications**: *Szekrényes (2015, 2016a,b).*

Thesis 4.

I have determined the closed-from expressions for the 3D J-integral in third-order delaminated composite Lévy plates under mixed-mode II/III fracture condition consisting of optional (k) number of equivalent single layers. I have shown that the general expression can be reduced by applying a zero-area path containing the delamination tip. It was shown that the J-integral can be calculated by using the stress resultants and the strain field components calculated at the mutual section of the undelaminated and delaminated regions of the plate. I have decomposed the total J-integral into J_{II} (mode-II) and J_{III} (mode-III) components in delaminated orthotropic Lévy plates. Moreover, I have shown that the mode-II J-integral is contributed by N_x, N_y (in-plane plate forces), M_x, M_y (bending moments), L_x, L_y, P_x and P_y (higher-order stress resultants), on the other hand the mode-III J-integral contains N_{xy} (in-plane shear force), M_{xy} (twisting moment), L_{xy} and P_{xy} (higher-order stress resultants). This result is in agreement with the basic concept published in the literature. I have also defined the so-called conjugate shear strain. The expressions of J_{II} and J_{III} have been applied to simply supported delaminated first,- second- and third-order delaminated plates.

- **Related publications**: *Szekrényes (2014a,c,d).*

Thesis 5.

a. I have applied the method of two equivalent single layers to problems involving the bending of simply supported orthotropic composite plates containing a through-width delamination with straight front. The solution was obtained by the first-, second-order and third-order Reddy theories. I have determined the mechanical fields in simply supported delaminated plates with different geometrical parameters and I have compared the results of the analytical models to those by 3D finite element analysis. I have shown that the Reddy third-order theory involves some stiffening (locking) leading to inaccuracies in the approximation of the plate deflection. I have also applied the method of four equivalent single layers to the plate problems mentioned before using the first-, second- and third-order plate theories. The stiffening effect in the first-order plate model was shown.

b. Considering the results for the mechanical fields and the J-integral by the methods of two and four equivalent single layers I have made the ranking of the different plate theories regarding their accuracy. The primary viewpoint was the agreement of the transverse deflection and the distribution of the J-integral over the delamination front with the finite element results. The agreement of the in-plane displacement and the stress distributions compared to the finite element results was only a secondary viewpoint. Based on the ranking of the plate theories I have concluded that considering the accuracy and the model size the optimal solution of the problems discussed is the second-order plate theory, which can be the candidate to develop a plate/shell finite element for the modeling of laminated composites with delamination.

- **Related publications**: *Szekrényes (2013b, 2014d, 2016a).*

8.2 Application possibilities of the results

The results presented in this thesis can be applied equally in the field of experimental and research engineering according to the following.

- The models presented can be used to develop beam, plate and shell finite elements or can be implemented into isogeometric analysis, which can replace the computationally expensive 3D modeling of cracks and delaminations in laminated composite thin- and thick-walled structures.
- The models can be applied to fracture mechanical plate specimens (e.g. the edge cracked torsion (ECT, *Marat-Mendes and Freitas (2009)*) or the 4-point bending plate (4PBP, *Mehrabadi (2014)*)) to derive analytical (closed-form) solutions.
- The method of 2ESLs and 4ESLs can be applied to free vibration problem of delaminated beams, plates and shells. The significance of the novel formulations is that it is possible to determine the stress resultants in the top and bottom plates separately. Recently it was shown that the free vibration in delaminated composite beams (*Szekrényes (2014, 2015)*) and plates (*Szekrényes (2015)*) is the source of parametric excitation. The models can also be applied to the stability (buckling) analysis of laminated structures with delaminations.
- The models can be complemented with the effect of normal deformation in order to improve the accuracy. Instead of using shear strain continuity between the interface plane shear stress continuity can be employed.
- The developments can implemented into sandwich and functionally graded beam, plate and shell theories including delaminations and cracks.

References

Adams, D.F., Carlsson, L.A., Pipes, R.B., 2000. Experimental characterization of advanced composite materials. CRC Press, Boca Raton London New York Washington, D.C.. Third edition.

Ahn, J.S., Kim, Y.W., Woo, K.S., 2013. Analysis of circular free edge effect in composite laminates by p-convergent global-local model. *International Journal of Mechanical Sciences* 66, 149–155.

Anderson, T.L., 2005. Fracture Mechanics - Fundamentals and Applications. CRC Press, Taylor & Francis Group, Boca Raton, London, New York, Singapore. Third edition.

Argüelles, A., Viña, J., Canteli, A.F., Bonhomme, J., 2011. Influence of resin type on the delamination behavior of carbon fiber reinforced composites under mode-II loading. *International Journal of Damage Mechanics* 20, 963–977.

Arrese, A., Carbajal, N., Vargas, G., Mujika, F., 2010. A new method for determining mode II R-curve by the end-notched flexure test. *Engineering Fracture Mechanics* 77, 51–70.

Batista, M., 2012. Comparison of Reissner, Mindlin and Reddy plate models with exact three dimensional solution for simply supported isotropic and transverse inextensible rectangular plate. *Meccanica* 47, 257–268.

Bennati, S., Colleluori, M., Corigliano, D., Valvo, P.S., 2009. An enhanced beam-theory model of the asymmetric double cantilever beam (ADCB) test for composite laminates. *Composites Science and Technology* 69, 1735–1745.

Bennati, S., Fisicaro, P., Valvo, P.S., 2013a. An enhanced beam-theory model of the mixed-mode bending (MMB) test - Part I: Literature review and mechanical model. *Meccanica* 48, 443–462.

Bennati, S., Fisicaro, P., Valvo, P.S., 2013b. An enhanced beam-theory model of the mixed-mode bending (MMB) test - Part II: Applications and results. *Meccanica* 48, 465–484.

Bodaghi, M., Saidi, A.R., 2010. Lévy-type solution for buckling analysis of thick functionally graded rectangular plates based on the higher-order shear deformation plate. *Applied Mathematical Modelling* 34, 3659–3673.

Bonhomme, J., Argüelles, A., Castrillo, M.A., Viña, J., 2010. Computational models for mode I composite fracture failure: the virtual crack closure technique versus the two-step extension method. *Meccanica* 45, 297–304.

Bruno, D., Greco, F., Lonetti, P., 2003. A coupled interface-multilayer approach for mixed mode delamination and contact analysis in laminated composites. *International Journal of Solids and Structures* 40, 7245 – 7268.

Bruno, D., Greco, F., Lonetti, P., 2005. A 3D delamination modelling technique based on plate and interface theories for laminated structures. *European Journal of Mechanics A/Solids* 24, 127–149.

Budzik, M.K., Jumel, J., Salem, N.B., Shanahan, M.E.R., 2013. Instrumented end notched flexure - crack propagation and process zone monitoring Part II: Data reduction and experimental. *International Journal of Solids and Structures* 50, 310–319.

Burlayenko, V.N., Sadowski, T., 2012. A numerical study of the dynamic response of sandwich plates initially damaged by low-velocity impact. *Computational Materials Science* 52, 212–216.

Cherepanov, G., 1967. Crack propagation in continuous media: {PMM} vol. 31, no. 3, 1967, pp. 476488. *Journal of Applied Mathematics and Mechanics* 31, 503 – 512.

Cherepanov, G.P., 1997. Methods of Fracture Mechanics: Solid Matter Physics. Kluwer Academic Publishers, Dordrecht, Boston, London.

Chou, P.C., Pagano, N.J., 1967. Elasticity - Tensor, dyadic, and engineering approaches. D. Van Nostrand Company, Inc., Princeton, New Jersey, Toronto, London.

Christoforou, A.P., Elsharkawy, A.A., Guedoua, L.H., 2008. An inverse solution for low-velocity impact in composite plates. *Computers & Structures* 86, 988–996.

Davidson, B.D., Sediles, F.O., 2011. Mixed-mode I-II-III delamination toughness determination via a shear-torsion-bending test. *Composites Part A: Applied Science and Manufacturing* 42, 589–603.

Davidson, B.D., Sediles, F.O., Humphrey, K.D., 2010. A shear-torsion-bending test for mixed-mode I-II-III delamination toughness determination, in: 25th Technical Conference of the American Society for Composites and 14th US-Japan Conference on Composite Materials, 20-22 September 2010, Dayton, Ohio, USA, pp. 1001–1020.

Davidson, B.D., Yu, L., Hu, H., 2000. Determination of energy release rate and mode mix in three-dimensional layered structures using plate theory. *International Journal of Fracture* 105, 81–104.

Fernández, M.V., Moura, M.F.S.F., da Silva A T Marques, L.F.M., 2013. Mixed-mode fatigue/fracture characterization of composite bonded joints using the single-leg bending test. *Composites Part A: Applied Science and Manufacturing* 44, 63–69.

Ferreira, A.J.M., Roque, C.M.C., Carrera, E., Cinefra, M., Polit, O., 2011. Two higher order zig-zag theories for the accurate analysis of bending, vibration and buckling response of laminated plates by radial basis functions collocation and a unified formulation. *Journal of Composite Materials* 45, 2523–2536.

Ganapathy, S., Rao, K., 1998. Failure analysis of laminated composite cylindrical/spherical shell panels subjected to low-velocity impact. *Computers & Structures* 68, 627–641.

Garvan, F., 2002. The Maple Book. Chapman & Hall/CRC, Boca Raton, London, New York, Washington D.C.

Goodmiller, G., TerMaath, S., 2014. Investigation of composite patch performance under low-velocity impact loading, in: 55th AIAA/ASME/ASCE/AHS/SC Structures, Structural Dynamics, and Materials Conference. National Harbor, Maryland, USA.

Hamed, M.A., Nosier, A., Farrahi, G.H., 2006. Separation of delamination modes in composite beams with symmetric delaminations. *Materials and Design* 27, 900–910.

Hills, D.A., Kelly, P.A., Dai, D.N., Korsunsky, A.M., 1996. Solution of Crack Problems, The Distributed Dislocation Technique. Kluwer Academic Publishers, Dordrecht, Boston, London.

Ho, S.L., Tay, A.A.O., 2011. A numerical analysis of penny-shaped delaminations in an encapsulated silicon module, in: Proceedings - Electronic Components and Technology Conference, pp. 1115 – 1121.

Hosseini-Hashemi, S., Fadaee, M., Taher, H.R.D., 2011. Exact solutions for free flexural vibration of Lévy-type rectangular thick plates via third-order shear deformation plate

dc_1254_16

theory. *Applied Mathematical Modelling* 35, 708–727.

Islam, M.M., Kapania, R.K., 2011. Delamination growth using cohesive zone model for adhesive bonding under compression, in: Proulx, T. (Ed.), Experimental and Applied Mechanics, Springer New York. pp. 527–536.

Izadi, M., Tahani, M., 2010. Analysis of interlaminar stresses in general cross-ply laminates with distributed piezoelectric actuators. *Composite Structures* , 757–768.

Jianqiao, Y., 2003. Laminated Composite Plates and Shells - 3D modelling. Springer, London, Berlin, Heidelberg, New York, Hong Kong, Milan, Paris, Tokyo.

Johnston, A., Davidson, B., Simon, K., 2014. Assessment of split-beam-type tests for mode III delamination toughness determination. *International Journal of Fracture* 185, 31–48.

Johnston, A.L., Davidson, B.D., Simon, K.K., 2012. Evaluation of new test methods for the determination of G_{IIIc} of laminated polymeric composites, in: 27th Annual Technical Conference of the American Society for Composites 2012, Held Jointly with 15th Joint US-Japan Conference on Composite Materials and ASTM-D30 Meeting, pp. 120–139.

Jumel, J., Budzik, M.K., Salem, N.B., Shanahan, M.E.R., 2013. Instrumented end notched flexure - crack propagation and process zone monitoring. Part I: Modelling and analysis. *International Journal of Solids and Structures* 50, 297–309.

Jumel, J., Budzik, M.K., Shanahan, M.E.R., 2011a. Beam on elastic foundation with anticlastic curvature: Application to analysis of mode I fracture tests. *Engineering Fracture Mechanics* 78, 3253–3269.

Jumel, J., Budzik, M.K., Shanahan, M.E.R., 2011b. Process zone in the single cantilever beam under transverse loading. part I: Theoretical analysis. *Theoretical and Applied Fracture Mechanics* 56, 7–12.

Kamerich, E., 2011. A guide to Maple. Springer Science & Business Media, New York, Berlin, Heidelberg.

Kapuria, S., Kumari, P., 2012. Boundary layer effects in Levy-type rectangular piezoelectric composite plates using a coupled efficient layerwise theory. *European Journal of Mechanics - A/Solids* 36, 122–140.

Kenane, M., Benmedakhene, S., Azari, Z., 2010. Fracture and fatigue study of unidirectional glass/epoxy laminate under different mode of loading. *Fatigue and Fracture of Engineering Materials and Structures* 33, 285–293.

Kiani, M., Shiozaki, H., Motoyama, K., 2013. Using experimental data to improve crash modeling for composite materials, in: Conference Proceedings of the Society for Experimental Mechanics Series, pp. 215–226. 2012 Annual Conference on Experimental and Applied Mechanics; Costa Mesa, CA; United States; 11-14 June, 2012.

Kim, S., Kim, J.S., Yoon, H., 2011. Experimental and numerical investigations of mode I delamination behaviors of woven fabric composites with carbon, kevlar and their hybrid fibers. *International Journal of Precision Engineering and Manufacturing* 12, 321–329.

Kollár, L.P., Springer, G.S., 2003. Mechanics of Composite Structures. Cambridge University Press, Cambridge, New York, Melbourne, Madrid, Cape Town, Singapore, São Paolo.

Kondo, A., Sato, Y., Suemasu, H., Aoki, Y., 2011. Fracture resistance of carbon/epoxy composite laminates under mixed-mode II and III failure and its dependence on fracture morphology. *Advanced Composite Materials* 20, 405–418.

Kondo, A., Sato, Y., Suemasu, H., Gouzu, K., Aoki, Y., 2010. Characterization of fracture resistance of carbon/epoxy composite laminates during mixed-mode II and III stable damage propagation. *Journal of the Japan Society for Composite Materials* 36, 179–188.

Kumar, Y., Lal, R., 2012. Vibrations of nonhomogeneous orthotropic rectangular plates with bilinear thickness variation resting on winkler foundation. *Meccanica* 47, 893–915.

Kutnar, A., Kamke, F.A., Nairn, J.A., Sernek, M., 2008. Mode II fracture behavior of bonded viscoelastic thermal compressed wood. *Wood and Fiber Science* 40, 362–373.

Lee, L.J., Tu, D.W., 1993. *J* integral for delaminated composite laminates. *Composites Science and Technology* 47, 185–192.

Levinson, M., 1980. An accurate, simple theory of the statics and dynamics of elastic plates. *Mechanics Research Communications* 7, 343–350.

Marat-Mendes, R., de Freitas, M., 2013. Fractographic analysis of delamination in glass/fibre epoxy composites. *Journal of Composite Materials* 47, 1437–1448.

Marat-Mendes, R.M., Freitas, M.M., 2009. Characterisation of the edge crack torsion (ECT) test for the measurement of the mode III interlaminar fracture toughness. *Engineering Fracture Mechanics* 76, 2799–2809.

Mehrabadi, F.A., 2013. Analysis of pure mode III and mixed mode (III+ II) interlaminar crack growth in polymeric woven fabrics. *Materials & Design* 44, 429–437.

Mehrabadi, F.A., 2014. The use of ECT and 6PBP tests to evaluate fracture behavior of adhesively bonded steel/epoxy joints under mode-III and mixed mode III/II. *Applied Adhesion Science* 2, 1–15.

Mehrabadi, F.A., Khosravan, M., 2013. Mode III interlaminar fracture in woven glass/epoxy composite laminates. *World Academy of Science, Engineering and Technology* 73, 479–483.

Miura, M., Shindo, Y., Takeda, T., Narita, F., 2012. Interlaminar fracture characterization of woven glass/epoxy composites under mixed-mode II/III loading conditions at cryogenic temperatures. *Engineering Fracture Mechanics* 96, 615–625.

Mladensky, A., Rizov, V., 2014. Non-linear fracture study of single cantilever beam specimen. *ZAMM - Zeitschrift für Angewandte Mathematik und Mechanik* , 1–13DOI 10.1002/zamm.201400104.

Mladensky, A.S., Rizov, V., 2013a. Analysis of mixed mode II/III crack in bilayered composite beam. *Journal of Theoretical and Applied Mechanics* 42, 41–52.

Mladensky, A.S., Rizov, V., 2013b. Analytical investigation of nonlinear interlaminar fracture in trilayered polymer composite beam under mode II crack loading conditions using the J-integral approach. *Archive of Applied Mechanics* 83, 1637–1658.

de Morais, A.B., Pereira, A.B., 2008. Mixed mode II + III interlaminar fracture of carbon/epoxy laminates. *Composites Science and Technology* 68, 2022–2027.

de Morais, A.B., Pereira, A.B., 2009. Mode III interlaminar fracture of carbon/epoxy laminates using a four-point bending plate test. *Composites Part A - Applied Science and Manufacturing* 40, 1741–1746.

de Morais, A.B., Pereira, A.B., de Moura, M.F.S.F., 2011. Mode III interlaminar fracture of carbon/epoxy laminates using the six-point edge crack torsion (6ECT). *Composites Part A: Applied Science and Manufacturing* 42, 1793–1799.

de Moura, M.F.S.F., Fernandez, M.V.C., de Morais, A.B., Campilho, R.D.S.G., 2009. Numerical analysis of the edge crack torsion test for mode III interlaminar fracture of composite laminates. *Engineering Fracture Mechanics* 76, 469–478.

Nikbakht, M., Choupani, N., 2008. Fracture toughness characterization of carbon-epoxy composite using Arcan specimen. *World Academy of Science, Engineering and Technology* 41, 738–744.

Nikbakht, M., Choupani, N., Hosseini, S.R., 2010. 2D and 3D interlaminar fracture assessment under mixed-mode loading conditions. *Materials Science and Engineering A* 516, 162–168.

Ovesy, H., Totounferoush, A., Ghannadpour, S., 2015. Dynamic buckling analysis of delaminated composite plates using semi-analytical finite strip method. *Journal of Sound and Vibration* 343, 131–143.

Panda, S.K., Singh, B.N., 2009. Nonlinear free vibration of spherical shell panel using higher order shear deformation theory - A finite element approach. *International Journal of Pressure Vessels and Piping* 86, 373–383.

Panda, S.K., Singh, B.N., 2011. Large amplitude free vibration analysis of thermally postbuckled composite doubly curved panel using nonlinear FEM. *Finite Elements in Analysis and Design* 47, 378–386.

Peng, L., Zhang, J., Zhao, L., Bao, R., Yang, H., Fei, B., 2011. Mode I delamination growth of multidirectional composite laminates under fatigue loading. *Journal of Composite Materials* 45, 1077–1090.

Pereira, A.B., de Morais, A.B., 2009. Mixed-mode I + III interlaminar fracture of carbon/epoxy laminates. *Composites Part A: Applied Science and Manufacturing* 40, 518–523.

Pereira, A.B., de Morais, A.B., de Moura, M.F.S.F., 2011. Design and analysis of a new six-point edge crack torsion (6ECT) specimen for mode III interlaminar fracture characterisation. *Composites Part A: Applied Science and Manufacturing* 42, 131–139.

Petrolito, J., 2014. Vibration and stability analysis of thick orthotropic plates using hybrid-Trefftz elements. *Applied Mathematical Modelling* 38, 5858–5869.

Phillips, L.N. (Ed.), 1989. Design with Advanced Composite Materials. Springer-Verlag, The Design Council, Berlin, Heidelberg, New York, London, Paris, Tokyo.

Qing, G., Liu, Y., Li, D., 2011. A semi-analytical model for the energy release rate analyses of composite laminates with a delamination. *Finite Elements in Analysis and Design* 47, 1017 – 1024.

Raju, I., jr Crews, J., Aminpour, M., 1988. Convergence of strain energy release rate components for edge-delaminated composite laminates. *Engineering Fracture Mechanics* 30, 383–396.

Reddy, J.N., 2004. Mechanics of laminated composite plates and shells - Theory and analysis. CRC Press, Boca Raton, London, New York, Washington D.C.

Rice, J.R., 1968. A path independent integral and the approximate analysis of strain concentration by notches and cracks. *Journal of Applied Mechanics* 35, 379–386.

Rigby, R.H., Aliabadi, M.H., 1998. Decomposition of the mixed-mode J-integral - revisited. *International Journal of Solids and Structures* 35, 2073–2099.

Rizov, V., Mladensky, A., 2015. Elastic-plastic analysis of asymmetric double cantilever beam specimen. *International Journal of Mechanical Sciences* 92, 44 – 51.

Rizov, V., Mladensky, A., 2016. Non-linear fracture analysis of cantilever beam opened notch specimen. *Applied Mathematical Modelling* 40, 4220 – 4230.

Rizov, V., Mladensky, A.S., 2012. Analysis of mode II crack in bilayered composite beam. *Journal of Theoretical and Applied Mechanics* 42, 67–78.

Rizov, V., Shindo, Y., Horiguchi, K., Narita, F., 2006. Mode III interlaminar fracture behaviour of glass fiber reinforced polymer woven laminates at 293 to 4 K. *Applied Composite Materials* 13, 287–304.

dc_1254_16

Rizov, V., Shipsha, A., Zenkert, D., 2005. Indentation study of foam core sandwich composite panels. *Composite Structures* 69, 95–102.

Romhany, G., Szebenyi, G., 2012. Interlaminar fatigue crack growth behavior of MWCNT/carbon fiber reinforced hybrid composites monitored via newly developed acoustic emission method. *Express Polymer Letters* 6, 572–580.

Saeedi, N., Sab, K., Caron, J.F., 2012a. Delaminated multilayered plates under uniaxial extension. part I: Analytical analysis using a layerwise stress approach. *International Journal of Solids and Structures* 49, 3711–3726.

Saeedi, N., Sab, K., Caron, J.F., 2012b. Delaminated multilayered plates under uniaxial extension. part II: Efficient layerwise mesh strategy for the prediction of delamination onset. *International Journal of Solids and Structures* 49, 3727–3740.

Sahoo, S.S., Singh, V.K., Panda, S.K., 2016. Nonlinear fexural analysis of shallow carbon/epoxy laminated composite curved panels: experimental and numerical investigation. *Journal of Engineering Mechanics* 142.

Salem, N.B., Budzik, M.K., Jumel, J., Shanahan, M.E.R., Lavelle, F., 2013. Investigation of the crack front process zone in the double cantilever beam test with backface strain monitoring technique. *Engineering Fracture Mechanics* 98, 272–283.

Sankar, B.V., Sonik, V., 1995. Pointwise energy release rate in delaminated plates. *AIAA Journal* 33, 1312–1318.

Sarvestani, H.Y., Sarvestani, M.Y., 2012. Free-edge stress analysis of general composite laminates under extension, torsion and bending. *Applied Mathematical Modelling* 36, 1570–1588.

Shivakumar, K.N., Raju, I.S., 1992. An equivalent domain integral method for three-dimensional mixed-mode fracture problems. *Engineering Fracture Mechanics* 42, 935–959.

da Silva, L.F.M., Estevez, V.H.C., Chavez, F.J.P., 2011. Fracture toughness of a structural adhesive under mixed mode loadings. *Materialwissenschaft und Werkstofftechnik* 42, 460–470.

Singh, V.K., Panda, S.K., 2014. Nonlinear free vibration analysis of single/doubly curved composite shallow shell panels. *Thin-Walled Structures* 85, 431–349.

Sorensen, L., Botsis, J., Gmür, T., Cugnoni, J., 2007. Delamination detection and characterisation of bridging tractions using long FBG optical sensors. *Composites Part A - Applied Science and Manufacturing* 38, 2087–2096.

Suemasu, H., Kondo, A., Gozu, K., Aoki, Y., 2010. Novel test method for mixed mode II and III interlaminar fracture toughness. *Advanced Composite Materials* 19, 349–361.

Suemasu, H., Tanikado, Y., 2012. Delamination propagation behavior and the fracture toughness of composite laminates under shear fracture mode, in: 27th Annual Technical Conference of the American Society for Composites 2012, Held Jointly with 15th Joint US-Japan Conference on Composite Materials and ASTM-D30 Meeting, pp. 367–379.

Szekrényes, A., 2007. Delamination fracture analysis in the G_{II}-G_{III} plane using prestressed composite beams. *International Journal of Solids and Structures* 44, 3359–3378.

Szekrényes, A., 2007. Improved analysis of unidirectional composite delamination specimens. *Mechanics of Materials* 39, 953–974.

Szekrényes, A., 2009a. Improved analysis of the modified split-cantilever beam for mode III fracture. *International Journal of Mechanical Sciences* 51, 682–693.

Szekrényes, A., 2009b. Interlaminar fracture analysis in the G_I-G_{III} plane using prestressed transparent composite beams. *Composites Part A - Applied Science and Manufacturing*

40, 1621–1631.

Szekrényes, A., 2011. Interlaminar fracture analysis in the G_I-G_{II}-G_{III} space using prestressed transparent composite beams. *Journal of Reinforced Plastics and Composites* 30, 1655–1669.

Szekrényes, A., 2012. Interlaminar fracture analysis in the G_{II}-G_{III} plane using prestressed transparent composite beams. *Composites Part A - Applied Science and Manufacturing* 43, 95–103.

Szekrényes, A., 2014. Coupled flexural-longitudinal vibration of delaminated composite beams with local stability analyis. *Journal of Sound and Vibration* 333, 5141–5164.

Szekrényes, A., 2015. Natural vibration-induced parametric excitation in delaminated Kirchhoff plates. *Journal of Composite Materials* , 1–28, DOI:0021998315603111.

Szekrényes, A., 2015. A special case of parametrically excited systems: free vibration of delaminated composite beams. *European Journal of Mechanics A/Solids* 49, 82–105.

Talha, M., Singh, B., 2010. Static response and free vibration analysis of FGM plates using higher order shear deformation theory. *Applied Mathematical Modelling* 34, 3991–4011.

Thai, H.T., Choi, D.H., 2013. Analytical solutions of refined plate theory for bending, buckling and vibration analyses of thick plates. *Applied Mathematical Modelling* 37, 8310–8323.

Thai, H.T., Kim, S.E., 2012. Lévy-type solution for free vibration analysis of orthotropic plates based on two variable refined plate theory. *Applied Mathematical Modelling* 36, 3870–3882.

Wang, C., Zhang, H., Shi, G., 2012. 3-D finite element simulation of impact damage of laminated plates using solid-shell interface elements. *Applied Mechanics and Materials* 130-132, 766–770.

Yoshihara, H., Satoh, A., 2009. Shear and crack tip deformation correction for the double cantilever beam and three-point end-notched flexure specimens for mode I and mode II fracture toughness measurement of wood. *Engineering Fracture Mechanics* 76, 335–346.

Zammit, A.D., Feih, S., Orifici, A.C., 2011. 2D numerical investigation of pre-tension on low velocity impact damage of sandwich structures, in: 18^{th} International Conference on Composite Materials (ICCM18), pp. 1–6. 21-26 August, Jeju International Convention Center, Jeju Island, SOUTH KOREA.

Zhang, J., Fox, B.L., 2007. Manufacturing influence on the delamination fracture behavior of the T800H/3900-2 carbon fiber reinforced polymer composites. *Materials and Manufacturing Processes* 22, 768–772.

Zhou, W., Liang, X., Li, Y., You, S., Liu, R., Chai, H., Lv, Z., 2013. Acoustic emission monitoring for delaminated composites under bending damage failure condition. *Applied Mechanics and Materials* 310, 51–54.

Zou, Z., Reid, S., Soden, P., Li, S., 2001. Mode separation of energy release rate for delamination in composite laminates using sublaminates. *International Journal of Solids and Structures* 38, 2597 – 2613.

Publications in the topic of the thesis

Szekrényes, A., 2012. Interlaminar stresses and energy release rates in delaminated orthotropic composite plates. *International Journal of Solids and Structures* 49, 2460–2470.

Szekrényes, A., 2013a. Interface crack between isotropic Kirchhoff plates. *Meccanica* 48, 507–526.

Szekrényes, A., 2013b. Interface fracture in orthotropic composite plates using second-order shear deformation theory. *International Journal of Damage Mechanics* 22, 1161–1185.

Szekrényes, A., 2013c. The system of exact kinematic conditions and application to delaminated first-order shear deformable composite plates. *International Journal of Mechanical Sciences* 77, 17–29.

Szekrényes, A., 2014a. Analysis of classical and first-order shear deformable cracked orthotropic plates. *Journal of Composite Materials* 48, 1441–1457.

Szekrényes, A., 2014b. Application of Reddy's third-order theory to delaminated orthotropic composite plates. *European Journal of Mechanics A/Solids* 43, 9–24.

Szekrényes, A., 2014c. Bending solution of third-order orthotropic Reddy plates with asymmetric interfacial crack. *International Journal of Solids and Structures* 51, 2598–2619.

Szekrényes, A., 2014d. Stress and fracture analysis in delaminated orthotropic composite plates using third-order shear deformation theory. *Applied Mathematical Modelling* 38, 3897–3916.

Szekrényes, A., 2015. Antiplane-inplane shear mode delamination between two second-order shear deformable composite plates. *Mathematics and Mechanics of Solids* , 1–24, DOI:10.1177/1081286515581871.

Szekrényes, A., 2016a. Nonsingular crack modelling in orthotropic plates by four equivalent single layers. *European Journal of Mechanics A/Solids* 55, 73–99.

Szekrényes, A., 2016b. Semi-layerwise analysis of laminated plates with nonsingular delamination - the theorem of autocontinuity. *Applied Mathematical Modelling* 40, 1344–1371.

A

Matrix elements (K_{ij}) - Method of 2ESLs

A.1 Reddy's third-order plate theory

In this Appendix the K_{ij} constants of the model presented in Subections 3.1.1 and 3.2.1 are listed.

A.1.1 Undelaminated region

The displacement components in the x direction for the Reddy TSDT are:

$$\begin{aligned} u_{(1)} &= u_0 + u_{01} + \theta_{(x)1} z^{(1)} + \phi_{(x)1} \left[z^{(1)}\right]^2 + \lambda_{(x)1} \left[z^{(1)}\right]^3, \\ u_{(2)} &= u_0 + u_{02} + \theta_{(x)2} z^{(2)} + \phi_{(x)2} \left[z^{(2)}\right]^2 + \lambda_{(x)2} \left[z^{(2)}\right]^3, \end{aligned} \tag{A.1}$$

The shear strains by Eq.(2.9) are:

$$\begin{aligned} \gamma_{xz(1)} &= \frac{\partial u_{(1)}}{\partial z^{(1)}} + \frac{\partial w}{\partial x} = \theta_{(x)1} + 2\phi_{(x)1} z^{(1)} + 3\lambda_{(x)1} \left[z^{(1)}\right]^2 + \frac{\partial w}{\partial x}, \\ \gamma_{xz(2)} &= \frac{\partial u_{(2)}}{\partial z^{(2)}} + \frac{\partial w}{\partial x} = \theta_{(x)2} + 2\phi_{(x)2} z^{(2)} + 3\lambda_{(x)2} \left[z^{(2)}\right]^2 + \frac{\partial w}{\partial x}. \end{aligned} \tag{A.2}$$

We apply the SEKC to the displacement functions and shear strains. It is important that the conditions are the same for the v displacement component, as well. Thus, the condition by Eq.(3.1) results in:

$$u_0 + u_{01} + \frac{1}{2}\theta_{(x)1} t_1 + \frac{1}{4}\phi_{(x)1} t_1^2 + \frac{1}{8}\lambda_{(x)1} t_1^3 = u_0 + u_{02} - \frac{1}{2}\theta_{(x)2} t_2 + \frac{1}{4}\phi_{(x)2} t_2^2 - \frac{1}{8}\lambda_{(x)2} t_2^3. \tag{A.3}$$

The application of Eq.(3.2) provides:

$$u_{01} + \theta_{(x)1} z_R^{(1)} + \phi_{(x)1} \left[z_R^{(1)}\right]^2 + \lambda_{(x)1} \left[z_R^{(1)}\right]^3 = 0. \tag{A.4}$$

The shear strain continuity imposed by Eq.(3.3) yields:

$$\theta_{(x)2} - \phi_{(x)2}t_2 + \frac{3}{4}\lambda_{(x)2}t_2^2 + \frac{\partial w}{\partial x} = \theta_{(x)1} + \phi_{(x)1}t_1 + \frac{3}{4}\lambda_{(x)1}t_1^2 + \frac{\partial w}{\partial x} = 0. \tag{A.5}$$

Finally, based on Eq.(3.4) the traction-free bottom and top surfaces involve:

$$\begin{aligned} &\theta_{(x)1} - \phi_{(x)1}t_1 + \frac{3}{4}\lambda_{(x)1}t_1^2 + \frac{\partial w}{\partial x} = 0, \\ &\theta_{(x)2} + \phi_{(x)2}t_2 + \frac{3}{4}\lambda_{(x)2}t_2^2 + \frac{\partial w}{\partial x} = 0. \end{aligned} \tag{A.6}$$

Eqs.(A.3)-(A.6) mean a linear algebraic system of equations, wherein the unknowns are: u_{01}, u_{02}, $\theta_{(x)2}$, $\phi_{(x)1}$ and $\phi_{(x)2}$, i.e. the secondary parameters. The solution for these parameters in terms of the primary parameters is:

$$u_{01} = \underbrace{-\frac{z_R^{(1)}}{t_b}(t_1 + z_R^{(1)})}_{K_{11}^{(0)}}\,\theta_{(x)1} \underbrace{-\frac{\left(z_R^{(1)}\right)^2}{4}(3t_1 + 4z_R^{(1)})}_{K_{13}^{(0)}}\,\lambda_{(x)1} \underbrace{-\frac{\left(z_R^{(1)}\right)^2}{t_1}}_{K_{14}^{(0)}}\,\frac{\partial w}{\partial x}, \tag{A.7}$$

$$\begin{aligned} u_{02} = &\underbrace{\frac{1}{4t_1}(3t_1(t_1+t_2) - 4z_R^{(1)}(z_R^{(1)} + t_1))}_{K_{21}^{(0)}}\,\theta_{(x)1} \underbrace{-\frac{1}{4}t_2^3}_{K_{22}^{(0)}}\,\lambda_{(x)2} + \\ &\underbrace{\left\{\frac{1}{16}(5t_1^3 + 9t_2t_1^2) - \left(z_R^{(1)}\right)^2(\frac{3}{4}t_1 - z_R^{(1)})\right\}}_{K_{23}^{(0)}}\,\lambda_{(x)1} + \underbrace{\frac{1}{4t_1}(t_1^2 + t_2t_1 - 4\left(z_R^{(1)}\right)^2)}_{K_{24}^{(0)}}\,\frac{\partial w}{\partial x}, \end{aligned} \tag{A.8}$$

$$\theta_{(x)2} = \underbrace{1}_{K_{21}^{(1)}}\cdot\theta_{(x)1} \underbrace{-\frac{3}{4}t_2^2}_{K_{22}^{(1)}}\,\lambda_{(x)2} + \underbrace{\frac{3}{4}t_1^2}_{K_{23}^{(1)}}\,\lambda_{(x)1}, \tag{A.9}$$

$$\phi_{(x)1} = \underbrace{\frac{1}{t_1}}_{K_{11}^{(2)}}\,\theta_{(x)1} + \underbrace{\frac{3}{4}t_1}_{K_{13}^{(2)}}\,\lambda_{(x)1} + \underbrace{\frac{1}{t_1}}_{K_{14}^{(2)}}\,\frac{\partial w}{\partial x}, \tag{A.10}$$

$$\phi_{(x)2} = \underbrace{-\frac{1}{t_2}}_{K_{21}^{(2)}}\,\theta_{(x)1} \underbrace{-\frac{3}{4}\frac{t_1^2}{t_2}}_{K_{23}^{(2)}}\,\lambda_{(x)1} \underbrace{-\frac{1}{t_2}}_{K_{24}^{(2)}}\,\frac{\partial w}{\partial x}. \tag{A.11}$$

The K_{ij} coefficients in Eq.(3.5) can be determined by applying Eq.(2.1) for two ESLs and taking back the results of Eqs.(A.7)-(A.11), and finally making a comparison to Eq.(3.5). The coefficients denoted K_{ij} are collected based on the vector of primary parameters defined by Eq.(3.6), some of the coefficients are also indicated within Eqs.(A.7)-(A.11). Therefore, the coefficients for the Reddy TSDT are:

$$K_{11}^{(0)} = -\frac{z_R^{(1)}}{t_1}(t_1 + z_R^{(1)}), \quad K_{12}^{(0)} = 0, \quad K_{13}^{(0)} = -\frac{\left(z_R^{(1)}\right)^2}{4}(3t_1 + 4z_R^{(1)}), \quad K_{14}^{(0)} = -\frac{\left(z_R^{(1)}\right)^2}{t_1}, \tag{A.12}$$

$$K_{21}^{(0)} = \frac{1}{4t_1}(3t_1(t_1 + t_2) - 4z_R^{(1)}(z_R^{(1)} + t_1)), \quad K_{22}^{(0)} = -\frac{1}{4}t_2^3, \tag{A.13}$$

$$K_{23}^{(0)} = \frac{1}{16}(5t_1^3 + 9t_2t_1^2) - \left(z_R^{(1)}\right)^2(\frac{3}{4}t_1 + z_R^{(1)}), \quad K_{24}^{(0)} = \frac{1}{4t_1}(t_1^2 + t_2t_1 - 4\left(z_R^{(1)}\right)^2) \tag{A.14}$$

$$K_{11}^{(1)} = 1, \quad K_{12}^{(1)} = K_{13}^{1} = K_{14}^{1} = 0, \quad K_{21}^{(1)} = 1, \quad K_{22}^{(1)} = -\frac{3}{4}t_2^2, \quad K_{23}^{(1)} = \frac{3}{4}t_1^2, \quad K_{24}^{(1)} = 0, \tag{A.15}$$

$$K_{11}^{(2)} = \frac{1}{t_1}, \quad K_{12}^{(2)} = 0, \quad K_{13}^{(2)} = \frac{3}{4}t_1, \quad K_{14}^{(2)} = \frac{1}{t_1}, \quad K_{21}^{(2)} = -\frac{1}{t_2}, \quad K_{22}^{(2)} = 0, \tag{A.16}$$

$$K_{23}^{(2)} = -\frac{3t_1^2}{4t_2}, \quad K_{24}^{(2)} = -\frac{1}{t_2}, \quad K_{11}^{(3)} = K_{12}^{(3)} = 0, \quad K_{13}^{(3)} = 1, \quad K_{14}^{(3)} = 0, \tag{A.17}$$

$$K_{21}^{(3)} = 0, \quad K_{22}^{(3)} = 1, \quad K_{23}^{(3)} = K_{24}^{(3)} = 0, \tag{A.18}$$

where $z_R^{(1)} = t_2/2$. The determination of the K_{ij} coefficients for the delaminated part and for the other theories works in the same way, and therefore only the results are given.

A.1.2 Delaminated region

$$K_{11}^{(0)} = K_{12}^{(0)} = K_{13}^{(0)} = K_{21}^{(0)} = K_{22}^{(0)} = K_{23}^{(0)} = 0, \tag{A.19}$$

$$K_{11}^{(1)} = 1, \quad K_{12}^{(1)} = K_{13}^{(1)} = K_{21}^{(1)} = 0, \quad K_{22}^{(1)} = 1, \quad K_{23}^{(1)} = 0, \tag{A.20}$$

$$K_{11}^{(2)} = K_{12}^{(2)} = K_{13}^{(2)} = K_{21}^{(2)} = K_{22}^{(2)} = K_{23}^{(2)} = 0, \tag{A.21}$$

$$K_{11}^{(3)} = -\frac{4}{3t_1^2}, K_{12}^{(3)} = 0, \quad K_{13}^{(3)} = -\frac{4}{3t_1^2}, \quad K_{21}^{(3)} = 0, \quad K_{22}^{(3)} = -\frac{4}{3t_2^2}, \quad K_{23}^{(3)} = -\frac{4}{3t_2^2}. \tag{A.22}$$

A.2 Second-order plate theory

In this Appendix the K_{ij} constants of the SSDT model presented in Subsections 3.1.2 and 3.2.2 are given.

A.2.1 Undelaminated region

$$K_{11}^{(0)} = -z_R^{(1)}, \quad K_{12}^{(0)} = -\left(z_R^{(1)}\right)^2, \quad K_{13}^{(0)} = K_{14}^{(0)} = 0, \tag{A.23}$$

$$K_{21}^{(0)} = -z_R^{(1)} - \frac{1}{2}t_1, \quad K_{22}^{(0)} = \frac{1}{4}(t_1 - 2z_R^{(1)})(t_1 + 2z_R^{(1)}), \quad K_{23}^{(0)} = -\frac{1}{2}t_2, \quad K_{24}^{(0)} = -\frac{1}{4}t_2^2, \tag{A.24}$$

$$K_{11}^{(1)} = 1, \quad K_{12}^{(1)} = K_{13}^{(1)} = K_{14}^{(1)} = 0, \quad K_{21}^{(1)} = K_{22}^{(1)} = 0, \quad K_{23}^{(1)} = 1, \quad K_{24}^{(1)} = 0, \tag{A.25}$$

$$K_{11}^{(2)} = 0, \quad K_{12}^{(2)} = 1, \quad K_{13}^{(2)} = K_{14}^{(2)} = 0, \quad K_{21}^{(2)} = K_{22}^{(2)} = K_{23}^{(2)} = 0, \quad K_{24}^{(2)} = 1. \tag{A.26}$$

dc_1254_16

A.2.2 Delaminated region

$$K_{11}^{(0)} = K_{12}^{(0)} = K_{13}^{(0)} = K_{14}^{(0)} = K_{21}^{(0)} = K_{22}^{(0)} = K_{23}^{(0)} = K_{24}^{(0)} = 0, \tag{A.27}$$

$$K_{11}^{(1)} = 1, \quad K_{12}^{(1)} = K_{13}^{(1)} = K_{14}^{(1)} = 0 = K_{21}^{(1)} = K_{22}^{(1)} = 0, K_{23}^{(1)} = 1, \quad K_{24}^{(1)} = 0, \tag{A.28}$$

$$K_{11}^{(2)} = 0, \quad K_{12}^{(2)} = 1, \quad K_{13}^{(2)} = K_{14}^{(2)} = K_{21}^{(2)} = K_{22}^{(2)} = K_{23}^{(2)} = 0, \quad K_{24}^{(2)} = 1. \tag{A.29}$$

A.3 First-order plate theory

This Appendix contains the K_{ij} constants of the FSDT model presented in Subsections 3.1.3 and 3.2.3.

A.3.1 Undelaminated region

$$K_{11}^{(0)} = -\frac{1}{2}t_1, \quad K_{12}^{(0)} = -z_R^{(1)} - \frac{1}{2}t_2, \quad K_{21}^{(0)} = 0, \quad K_{22}^{(0)} = -z_R^{(1)}, \tag{A.30}$$

$$K_{11}^{(1)} = 1, \quad K_{12}^{(1)} = K_{21}^{(1)} = 0, \quad K_{22}^{(1)} = 1. \tag{A.31}$$

A.3.2 Delaminated region

$$K_{11}^{(0)} = K_{12}^{(0)} = K_{21}^{(0)} = K_{22}^{(0)} = 0, \quad K_{11}^{(1)} = 1, \quad K_{12}^{(1)} = K_{21}^{(1)} = 0, \quad K_{22}^{(1)} = 1. \tag{A.32}$$

B

Matrix elements (K_{ij}) - Method of 4ESLs

B.1 Third-order plate theory

This Appendix collects the K_{ij} matrix elements for the third-order plate theory presented in Subsections 4.1.1 and 4.2.1.

B.1.1 Undelaminated region

$$K_{11}^{(0)} = -\frac{1}{12}\frac{(t_1+t_2+2z_R^{(2)})(5t_2^2+7t_1t_2-10z_R^{(2)}t_2+8(z_R^{(2)})^2+2t_1^2-4z_R^{(2)}t_1)}{(t_1+2t_2)(t_1+t_2)}, \tag{B.1}$$

$$K_{12}^{(0)} = -\frac{1}{12}\frac{(t_1+t_2+2z_R^{(2)})^2(t_1+4t_2-4z_R^{(2)})^2}{t_2(t_1+t_2)}, \tag{B.2}$$

$$K_{13}^{(0)} = \frac{1}{12}\frac{(t_1+t_2+2z_R^{(2)})^2(t_1+t_2-4z_R^{(2)})(2t_3+t_4)}{t_2(t_1+2t_2)(t_3+t_4)}, \tag{B.3}$$

$$K_{14}^{(0)} = -\frac{1}{12}\frac{(t_1+t_2+2z_R^{(2)})^2(t_1+t_2-4z_R^{(2)})t_3}{t_2(t_1+2t_2)(t_3+t_4)}, \tag{B.4}$$

$$K_{15}^{(0)} = \frac{1}{16}\frac{(t_1+t_2+2z_R^{(2)})^2(t_1+t_2-4z_R^{(2)})t_3(2t_3+t_4)}{t_2(t_1+2t_2)}, \tag{B.5}$$

$$K_{21}^{(0)} = \frac{1}{3}\frac{(3t_2-4z_R^{(2)})(z_R^{(2)})^2}{(t_1+2t_2)(t_1+t_2)}, K_{22}^{(0)} = -\frac{1}{3}\frac{(3t_1t_2-3t_1z_R^{(2)}-4(z_R^{(2)})^2+3t_2^2)z_R^{(2)}}{t_2(t_1+t_2)}, \tag{B.6}$$

dc_1254_16

$$K_{23}^{(0)} = -\frac{1}{3}\frac{(2t_3+t_4)(3t_1+3t_2+4z_R^{(2)})(z_R^{(2)})^2}{t_2(t_3+t_4)(t_1+2t_2)}, K_{24}^{(0)} = \frac{1}{3}\frac{(3t_1+3t_2+4z_R^{(2)})t_3(z_R^{(2)})^2}{t_2(t_3+t_4)(t_1+2t_2)}, \tag{B.7}$$

$$K_{25}^{(0)} = -\frac{1}{4}\frac{t_3(2t_3+t_4)(3t_1+3t_2+4z_R^{(2)})(z_R^{(2)})^2}{t_2(t_1+2t_2)}, \tag{B.8}$$

$$K_{31}^{(0)} = -\frac{1}{12}\frac{(t_2+4z_R^{(2)})(t_2-2z_R^{(2)})^2}{(t_1+2t_2)(t_1+t_2)}, K_{32}^{(0)} = \frac{1}{12}\frac{(t_2-2z_R^{(2)})^2(3t_1+4t_2+4z_R^{(2)})}{t_2(t_1+2t_2)}, \tag{B.9}$$

$$K_{33}^{(0)} = \frac{(10t_3+5t_4)t_2^3+(3t_1t_4+6t_1t_3+12t_4t_3+18t_3^2)t_2^2+(-(12t_4+24t_3)(z_R^{(2)})^2}{12t_2(t_3+t_4)(t_1+2t_2)}$$
$$+\frac{(6t_1t_4t_3+9t_1t_3^2)t_2-4(z_R^{(2)})^2(2t_1+t_2)(3t_1+z_R^{(2)})}{12t_2(t_3+t_4)(t_1+2t_2)}, \tag{B.10}$$

$$K_{34}^{(0)} = -\frac{t_3}{12}\frac{(5t_2^3+(3t_1+6t_3)t_2^2+(3t_1t_3-12(z_R^{(2)})^2)t_2-4(z_R^{(2)})^2(4z_R^{(2)}+3t_1)}{t_2(t_1+2t_2)(t_3+t_4)}, \tag{B.11}$$

$$K_{35}^{(0)} = \frac{t_3}{16}\left(\frac{(10t_3+5t_4)t_2^3+(6t_1t_3+10t_3^2+3t_1t_4+6t_4t_3)t_2^2+(-(12t_4+24t_3)(z_R^{(2)})^2}{t_2(t_3+t_4)(t_1+2t_2)}\right.$$
$$\left.+\frac{3t_1t_4t_3+5t_1t_3^2)t_2-4(z_R^{(2)})^2(2t_3+t_4)(3t_1+4z_R^{(2)})}{t_2(t_3+t_4)(t_1+2t_2)}\right), \tag{B.12}$$

$$K_{41}^{(0)} = -\frac{1}{12}\frac{(t_2+4z_R^{(2)})(t_2-2z_R^{(2)})^2}{(t_1+2t_2)(t_1+t_2)}, K_{42}^{(0)} = \frac{1}{12}\frac{(4t_2+3t_1+4z_R^{(2)})(t_2-4z_R^{(2)})^2}{t_2(t_1+t_2)}, \tag{B.13}$$

$$K_{43}^{(0)} = \frac{(2t_3+t_4)(5t_2^3+3(4t_3+t_1+2t_4)t_2^2+3(t_1t_4+t_1t_3-4(z_R^{(2)})^2)t_2-4(z_R^{(2)})^2(4z_R^{(2)}+3t_1)}{12t_2(t_1+2t_2)(t_3+t_4)}, \tag{B.14}$$

$$K_{44}^{(0)} = -\frac{1}{12}\frac{5t_2^3t_3+3(t_1t_3-4t_4t_3-2t_4^2)t_2^2+3(-t_1t_4^2-2t_1t_3t_4-4t_3(z_R^{(2)})^2)t_2}{t_2(t_1+2t_2)(t_3+t_4)}$$
$$-\frac{1}{12}\frac{4t_3(z_R^{(2)})^2(4z_R^{(2)}+3t_1)}{t_2(t_1+2t_2)(t_3+t_4)}, \tag{B.15}$$

$$K_{45}^{(0)} = \frac{(2t_3+t_4)(5t_2^3t_3+(3t_1t_3-2t_3t_4+4t_3^2-2t_4^2)t_2^2}{16t_2(t_1+2t_2)}+$$
$$+\frac{(2t_1t_3^2-t_1t_3t_4-12t_3(z_R^{(2)})^2-t_1t_4^2)t_2-4t_3(z_R^{(2)})^2(4z_R^{(2)}+3t_1)}{16t_2(t_1+2t_2)}, \tag{B.16}$$

$$K_{11}^{(1)} = 1, K_{12}^{(1)} = K_{13}^{(1)} = K_{14}^{(1)} = K_{15}^{(1)} = 0, K_{21}^{(1)} = 0, K_{22}^{(1)} = 1, K_{23}^{(1)} = K_{24}^{(1)} = K_{25}^{(1)} = 0,$$
$$K_{31}^{(1)} = K_{32}^{(1)} = 0, K_{33}^{(1)} = 1, K_{34}^{(1)} = K_{35}^{(1)} = 0, K_{41}^{(1)} = K_{42}^{(1)} = K_{43}^{(1)} = 0, K_{44}^{(1)} = 1, K_{45}^{(1)} = 0, \tag{B.17}$$

$$K_{11}^{(2)} = -\frac{(3t_2+2t_1)}{(t_1+2t_2)(t_1+t_2)}, K_{12}^{(2)} = -\frac{(t_1+2t_2)}{t_2(t_1+t_2)}, K_{13}^{(2)} = -\frac{(2t_3+t_4)(t_1+t_2)}{t_2(t_3+t_4)(t_1+2t_2)}, \tag{B.18}$$

$$K_{14}^{(2)} = -\frac{(t_1+t_2)t_3}{t_2(t_1+2t_2)(t_3+t_4)}, K_{15}^{(2)} = -\frac{3}{4}\frac{t_3(2t_3+t_4)(t_1+t_2)}{t_2(t_1+2t_2)}, \tag{B.19}$$

$$K_{21}^{(2)} = -\frac{t_2}{(t_1+2t_2)(t_1+t_2)}, K_{22}^{(2)} = -\frac{t_1}{t_2(t_1+t_2)}, \tag{B.20}$$

$$K_{23}^{(2)} = -K_{13}^{(2)}, K_{24}^{(2)} = -K_{14}^{(2)}, K_{25}^{(2)} = -K_{15}^{(2)}, \tag{B.21}$$

$$K_{33}^{(2)} = -\frac{1}{(t_3+t_4)}, K_{34}^{(2)} = \frac{1}{(t_3+t_4)}, K_{35}^{(2)} = -\frac{3}{4}(t_3+t_4), \tag{B.22}$$

$$K_{43}^{(2)} = K_{33}^{(2)}, K_{44}^{(2)} = K_{34}^{(2)}, K_{45}^{(2)} = -K_{35}^{(2)}, \tag{B.23}$$

$$K_{11}^{(3)} = K_{21}^{(3)} = \frac{4}{3(t_1+2t_2)(t_1+t_2)}, K_{12}^{(3)} = K_{22}^{(3)} = -\frac{4}{3t_2(t_1+t_2)}, \tag{B.24}$$

$$K_{13}^{(3)} = K_{23}^{(3)} = \frac{4}{3}\frac{2t_3+t_4}{t_2(t_1+2t_2)(t_3+t_4)}, K_{14}^{(3)} = K_{24}^{(3)} = -\frac{4}{3}\frac{t_3}{t_2(t_1+2t_2)(t_3+t_4)}, \tag{B.25}$$

$$K_{15}^{(3)} = K_{25}^{(3)} = \frac{(2t_3+t_4)t_3}{t_2(t_1+2t_2)}, K_{35}^{(3)} = K_{45}^{(3)} = 1, \tag{B.26}$$

where $z_R^{(2)} = 1/2(t_3+t_4-t_1)$ is the coordinate of the global reference plane in the local coordinate system of ESL2 (refer to Figure 4.1).

B.1.2 Delaminated region

$$K_{11}^{(0)} = -\frac{1}{4}\frac{t_2(2t_1+t_2)}{(t_1+t_2)}, K_{12}^{(0)} = -\frac{1}{4}\frac{t_2^2}{(t_1+t_2)}, \tag{B.27}$$

$$K_{13}^{(0)} = K_{14}^{(0)} = 0, K_{15}^{(0)} = \frac{1}{16}(3t_1+t_2)t_2^2, K_{16}^{(0)} = 0, \tag{B.28}$$

$$K_{21}^{(0)} = \frac{1}{4}\frac{t_1^2}{(t_1+t_2)}, K_{22}^{(0)} = \frac{1}{4}\frac{t_1(t_1+2t_2)}{(t_1+t_2)}, \tag{B.29}$$

$$K_{23}^{(0)} = K_{24}^{(0)} = 0, K_{25}^{(0)} = -\frac{1}{16}(t_1+3t_2)t_1^2, K_{26}^{(0)} = 0, \tag{B.30}$$

$$K_{31}^{(0)} = K_{32}^{(0)} = 0, K_{33}^{(0)} = -\frac{1}{4}\frac{t_4(2t_3+t_4)}{(t_3+t_4)}, K_{34}^{(0)} = -\frac{1}{4}\frac{t_4^2}{(t_3+t_4)}, \tag{B.31}$$

$$K_{35}^{(0)} =, K_{36}^{(0)} = \frac{1}{16}(3t_3+t_4)t_4^2, \tag{B.32}$$

$$K_{41}^{(0)} = K_{42}^{(0)} = 0, K_{43}^{(0)} = \frac{1}{4}\frac{t_3^2}{(t_3+t_4)}, K_{44}^{(0)} = \frac{1}{4}\frac{t_3(t_3+2t_4)}{(t_3+t_4)}, \tag{B.33}$$

$$K_{45}^{(0)} = 0, K_{46}^{(0)} = -\frac{1}{16}(t_3+3t_4)t_2^2, \tag{B.34}$$

$$K_{11}^{(1)} = 1, K_{12}^{(1)} = K_{13}^{(1)} = K_{14}^{(1)} = K_{15}^{(1)} = K_{16}^{(1)} = 0, \tag{B.35}$$

$$K_{21}^{(1)} = 0, K_{22}^{(1)} = 1, K_{23}^{(1)} = K_{24}^{(1)} = K_{25}^{(1)} = K_{26}^{(1)} = 0, \tag{B.36}$$

$$K_{31}^{(1)} = K_{32}^{(1)} = 0, K_{33}^{(1)} = 1, K_{34}^{(1)} = K_{35}^{(1)} = K_{36}^{(1)} = 0, \tag{B.37}$$

$$K_{41}^{(1)} = K_{42}^{(1)} = K_{43}^{(1)} = 0, K_{44}^{(1)} = 1, K_{45}^{(1)} = K_{46}^{(1)} = 0, \tag{B.38}$$

$$K_{11}^{(2)} = K_{21}^{(2)} = -\frac{1}{(t_1+t_2)}, K_{12}^{(2)} = K_{22}^{(2)} = \frac{1}{(t_1+t_2)}, \tag{B.39}$$

$$K_{15}^{(2)} = -K_{25}^{(2)} = -\frac{3}{4}(t_1+t_2), K_{16}^{(2)} = 0, \tag{B.40}$$

$$K_{33}^{(2)} = K_{43}^{(2)} = -\frac{1}{(t_3+t_4)}, K_{34}^{(2)} = K_{44}^{(2)} = \frac{1}{(t_3+t_4)}, \tag{B.41}$$

$$K_{36}^{(2)} = -K_{46}^{(2)} = -\frac{3}{4}(t_3+t_4), K_{26}^{(2)} = 0, \tag{B.42}$$

$$K_{13}^{(2)} = K_{31}^{(2)} = K_{14}^{(2)} = K_{41}^{(2)} = K_{23}^{(2)} = K_{32}^{(2)} = K_{24}^{(2)} = K_{42}^{(2)} = 0, \tag{B.43}$$

$$K_{11}^{(3)} = K_{12}^{(3)} = K_{13}^{(3)} = K_{14}^{(3)} = 0, K_{15}^{(3)} = 1, K_{16}^{(3)} = 0, \tag{B.44}$$

$$K_{21}^{(3)} = K_{22}^{(3)} = K_{23}^{(3)} = K_{24}^{(3)} = 0, K_{25}^{(3)} = 1, K_{26}^{(3)} = 0, \tag{B.45}$$

$$K_{31}^{(3)} = K_{32}^{(3)} = K_{33}^{(3)} = K_{34}^{(3)} = K_{35}^{(3)} = 0, K_{36}^{(3)} = 1, \tag{B.46}$$

$$K_{41}^{(3)} = K_{42}^{(3)} = K_{43}^{(3)} = K_{44}^{(3)} = K_{45}^{(3)} = 0, K_{46}^{(3)} = 1. \tag{B.47}$$

B.2 Second-order plate theory

In this Appendix the K_{ij} matrix elements for the second-order plate theory presented in Subsections 4.1.2 and 4.2.2 are listed.

B.2.1 Undelaminated region

$$K_{31}^{(0)} = \frac{3}{8}t_3 - z_R^{(2)} + \frac{1}{2}t_2, K_{32}^{(0)} = \frac{3}{8}t_3t_2 - (z_R^{(2)})^2 + \frac{1}{4}t_2^2, K_{33}^{(0)} = \frac{1}{8}t_3, K_{34}^{(0)} = -\frac{1}{8}t_3t_4, \tag{B.48}$$

$$K_{41}^{(0)} = \frac{1}{2}t_3 - z_R^{(2)} + \frac{1}{2}t_2, K_{42}^{(0)} = \frac{1}{2}t_3t_2 - (z_R^{(2)})^2 + \frac{1}{4}t_2^2, \tag{B.49}$$

$$K_{43}^{(0)} = \frac{1}{2}t_3 + \frac{1}{2}t_4, K_{44}^{(0)} = -\frac{1}{4}t_4(t_4+2t_3), \tag{B.50}$$

$$K_{11}^{(1)} = \frac{1}{2}, K_{12}^{(1)} = -\frac{1}{2}t_2, K_{13}^{(1)} = \frac{1}{2}, K_{14}^{(1)} = \frac{1}{4}t_4, K_{21}^{(1)} = 1, K_{22}^{(1)} = 0, K_{23}^{(1)} = 0, K_{24}^{(1)} = 0, \tag{B.51}$$

$$K_{31}^{(1)} = \frac{1}{2}, K_{32}^{(1)} = \frac{1}{2}t_2, K_{33}^{(1)} = \frac{1}{2}, K_{34}^{(1)} = -\frac{1}{4}t_4, K_{41}^{(1)} = 0, K_{42}^{(1)} = 0, K_{43}^{(1)} = 1, K_{44}^{(1)} = 0, \tag{B.52}$$

$$K_{11}^{(2)} = \frac{1}{2t_1}, K_{12}^{(2)} = -\frac{1}{2}\frac{t_2}{t_1}, K_{13}^{(2)} = -\frac{1}{2t_1}, K_{14}^{(2)} = -\frac{1}{2}\frac{t_4}{t_1}, K_{21}^{(2)} = 0, K_{22}^{(2)} = 1, \tag{B.53}$$

$$K_{23}^{(2)} = 0, K_{24}^{(2)} = 0, K_{31}^{(2)} = -\frac{1}{2t_3}, K_{32}^{(2)} = -\frac{1}{2}\frac{t_2}{t_3}, K_{33}^{(2)} = \frac{1}{2t_3}, K_{34}^{(2)} = -\frac{1}{2}\frac{t_4}{t_3}, \tag{B.54}$$

$$K_{41}^{(2)} = 0, K_{42}^{(2)} = 0, K_{43}^{(2)} = 0, K_{44}^{(2)} = 1. \tag{B.55}$$

B.2.2 Delaminated region

$$K_{11}^{(0)}=-\frac{1}{4}\frac{t_2(2t_1+t_2)}{t_1}, K_{32}^{(0)}=\frac{1}{4}\frac{t_2^2}{t_1}, K_{33}^{(0)}=\frac{1}{4}\frac{t_2^2t_4}{t_1}, K_{21}^{(0)}=\frac{1}{4}\frac{(3t_1^2-t_2^2+t_1t_2)}{t_1}, \tag{B.56}$$

$$K_{22}^{(0)}=-\frac{1}{4}\frac{(t_1^2-t_2^2+t_1t_2)}{t_1}, K_{23}^{(0)}=-\frac{1}{4}\frac{t_4(t_1^2-t_2^2+t_1t_2)}{t_1}, K_{31}^{(0)}=0, K_{32}^{(0)}=-\frac{1}{2}t_4, \tag{B.57}$$

$$K_{33}^{(0)}=\frac{1}{4}\frac{t_4^3}{t_3}, K_{41}^{(0)}=0, K_{42}^{(0)}=\frac{1}{2}t_3, K_{43}^{(0)}=-\frac{1}{4}\frac{t_4(t_3^2-t_4^2+t_3t_4)}{t_3}, \tag{B.58}$$

$$K_{11}^{(1)}=1, K_{12}^{(1)}=K_{13}^{(1)}=0, K_{21}^{(1)}=1, K_{22}^{(1)}=K_{23}^{(1)}=0, \tag{B.59}$$

$$K_{31}^{(1)}=0, K_{32}^{(1)}=1, K_{33}^{(1)}=0, K_{41}^{(1)}=0, K_{42}^{(1)}=1, K_{43}^{(1)}=0, \tag{B.60}$$

$$K_{11}^{(2)}=\frac{1}{t_1}, K_{12}^{(2)}=-\frac{1}{t_1}, K_{13}^{(2)}=-\frac{t_4}{t_1}, K_{21}^{(2)}=-\frac{1}{t_2}, K_{22}^{(2)}=\frac{1}{t_2}, K_{23}^{(2)}=\frac{t_4}{t_2}, \tag{B.61}$$

$$K_{31}^{(2)}=0, K_{32}^{(2)}=0, K_{33}^{(2)}=-\frac{t_4}{t_3}, K_{41}^{(2)}=0, K_{42}^{(2)}=0, K_{43}^{(2)}=1. \tag{B.62}$$

B.3 First-order plate theory

This Appendix collects the K_{ij} matrix elements of the FSDT solution detailed in Subsections 4.1.3 and 4.2.3.

B.3.1 Undelaminated region

$$K_{11}^{(0)}=-\frac{1}{2}t_1, K_{12}^{(0)}=-z_R^{(2)}-\frac{1}{2}t_2, K_{13}^{(0)}=K_{14}^{(0)}=K_{21}^{(0)}=0, K_{22}^{(0)}=-z_R^{(2)}, K_{23}^{(0)}=K_{24}^{(0)}=0, \tag{B.63}$$

$$K_{31}^{(0)}=0, K_{32}^{(0)}=-z_R^{(2)}+\frac{1}{2}t_2, K_{33}^{(0)}=\frac{1}{2}t_3, K_{34}^{(0)}=0, \tag{B.64}$$

$$K_{41}^{(0)}=0, K_{42}^{(0)}=-z_R^{(2)}+\frac{1}{2}t_2, K_{43}^{(0)}=t_3, K_{44}^{(0)}=\frac{1}{2}t_3, \tag{B.65}$$

$$K_{41}^{(0)}=0, K_{42}^{(0)}=-z_R^{(2)}+\frac{1}{2}t_2, K_{43}^{(0)}=t_3, K_{44}^{(0)}=\frac{1}{2}t_4, \tag{B.66}$$

$$K_{11}^{(1)}=1, K_{12}^{(1)}=K_{13}^{(1)}=K_{14}^{(1)}=0, K_{21}^{(1)}=0, K_{22}^{(1)}=1, K_{23}^{(1)}=K_{24}^{(1)}=0, \tag{B.67}$$

$$K_{31}^{(1)}=K_{32}^{(1)}=0, K_{33}^{(1)}=1, K_{34}^{(1)}=0, K_{41}^{(1)}=K_{42}^{(1)}=K_{43}^{(1)}=0, K_{44}^{(1)}=1. \tag{B.68}$$

B.3.2 Delaminated region

$$K_{11}^{(0)}=-\frac{1}{2}t_2, K_{12}^{(0)}=K_{13}^{(0)}=K_{14}^{(0)}=0, K_{21}^{(0)}=\frac{1}{2}(t_1-t_2), K_{22}^{(0)}=\frac{1}{2}t_2, K_{23}^{(0)}=K_{24}^{(0)}=0, \tag{B.69}$$

$$K_{31}^{(0)}=K_{32}^{(0)}=0, K_{33}^{(0)}=-\frac{1}{2}t_4, K_{34}^{(0)}=0, K_{41}^{(0)}=K_{42}^{(0)}=0, K_{43}^{(0)}=\frac{1}{2}(t_3-t_4), K_{44}^{(0)}=\frac{1}{2}t_4, \tag{B.70}$$

dc_1254_16

$$K_{11}^{(1)} = 1, K_{12}^{(1)} = K_{13}^{(1)} = K_{14}^{(1)} = 0, K_{21}^{(1)} = 0, K_{22}^{(1)} = 1, K_{23}^{(1)} = K_{24}^{(1)} = 0, \tag{B.71}$$

$$K_{31}^{(1)} = K_{32}^{(1)} = 0, K_{33}^{(1)} = 1, K_{34}^{(1)} = 0, K_{41}^{(1)} = K_{42}^{(1)} = K_{43}^{(1)} = 0, K_{44}^{(1)} = 1. \tag{B.72}$$

C

System matrices of the state space models

C.1 Method of 2ESLs

C.1.1 Reddy's third-order plate theory

In this Appendix the system matrix of the Reddy TSDT presented in Sections 5.2 is shown. The matrix elements are quite lengthy, and therefore these are not detailed an this thesis.

C.1.1.1 Undelaminated region

$$\mathbf{T}^{(ud)} = \begin{pmatrix}
0 & 1 & 0 & 0 & 0 & 0 & 0 & 0 & 0 & 0 & 0 & 0 & 0 & 0 & 0 & 0 & 0 & 0 & 0 & 0 \\
\tilde{S}_1 & 0 & 0 & \tilde{S}_2 & \tilde{S}_3 & 0 & 0 & \tilde{S}_4 & \tilde{S}_5 & 0 & 0 & \tilde{S}_6 & \tilde{S}_7 & 0 & 0 & \tilde{S}_8 & 0 & \tilde{S}_9 & 0 & \tilde{S}_{10} \\
0 & 0 & 0 & 1 & 0 & 0 & 0 & 0 & 0 & 0 & 0 & 0 & 0 & 0 & 0 & 0 & 0 & 0 & 0 & 0 \\
0 & \tilde{S}_{11} & \tilde{S}_{12} & 0 & 0 & \tilde{S}_{13} & \tilde{S}_{14} & 0 & 0 & \tilde{S}_{15} & \tilde{S}_{16} & 0 & 0 & \tilde{S}_{17} & \tilde{S}_{18} & 0 & \tilde{S}_{19} & 0 & \tilde{S}_{20} & 0 \\
0 & 0 & 0 & 0 & 0 & 1 & 0 & 0 & 0 & 0 & 0 & 0 & 0 & 0 & 0 & 0 & 0 & 0 & 0 & 0 \\
\tilde{S}_{21} & 0 & 0 & \tilde{S}_{22} & \tilde{S}_{23} & 0 & 0 & \tilde{S}_{24} & \tilde{S}_{25} & 0 & 0 & \tilde{S}_{26} & \tilde{S}_{27} & 0 & 0 & \tilde{S}_{28} & 0 & \tilde{S}_{29} & 0 & \tilde{S}_{30} \\
0 & 0 & 0 & 0 & 0 & 0 & 0 & 1 & 0 & 0 & 0 & 0 & 0 & 0 & 0 & 0 & 0 & 0 & 0 & 0 \\
0 & \tilde{S}_{31} & \tilde{S}_{32} & 0 & 0 & \tilde{S}_{33} & \tilde{S}_{34} & 0 & 0 & \tilde{S}_{35} & \tilde{S}_{36} & 0 & 0 & \tilde{S}_{37} & \tilde{S}_{38} & 0 & \tilde{S}_{39} & 0 & \tilde{S}_{40} & 0 \\
0 & 0 & 0 & 0 & 0 & 0 & 0 & 0 & 0 & 1 & 0 & 0 & 0 & 0 & 0 & 0 & 0 & 0 & 0 & 0 \\
\tilde{S}_{41} & 0 & 0 & \tilde{S}_{42} & \tilde{S}_{43} & 0 & 0 & \tilde{S}_{44} & \tilde{S}_{45} & 0 & 0 & \tilde{S}_{46} & \tilde{S}_{47} & 0 & 0 & \tilde{S}_{48} & 0 & \tilde{S}_{49} & 0 & \tilde{S}_{50} \\
0 & 0 & 0 & 0 & 0 & 0 & 0 & 0 & 0 & 0 & 0 & 1 & 0 & 0 & 0 & 0 & 0 & 0 & 0 & 0 \\
0 & \tilde{S}_{51} & \tilde{S}_{52} & 0 & 0 & \tilde{S}_{53} & \tilde{S}_{54} & 0 & 0 & \tilde{S}_{55} & \tilde{S}_{56} & 0 & 0 & \tilde{S}_{57} & \tilde{S}_{58} & 0 & \tilde{S}_{59} & 0 & \tilde{S}_{60} & 0 \\
0 & 0 & 0 & 0 & 0 & 0 & 0 & 0 & 0 & 0 & 0 & 0 & 0 & 1 & 0 & 0 & 0 & 0 & 0 & 0 \\
\tilde{S}_{61} & 0 & 0 & \tilde{S}_{62} & \tilde{S}_{63} & 0 & 0 & \tilde{S}_{64} & \tilde{S}_{65} & 0 & 0 & \tilde{S}_{66} & \tilde{S}_{67} & 0 & 0 & \tilde{S}_{68} & 0 & \tilde{S}_{69} & 0 & \tilde{S}_{70} \\
0 & 0 & 0 & 0 & 0 & 0 & 0 & 0 & 0 & 0 & 0 & 0 & 0 & 0 & 0 & 1 & 0 & 0 & 0 & 0 \\
0 & \tilde{S}_{71} & \tilde{S}_{72} & 0 & 0 & \tilde{S}_{73} & \tilde{S}_{74} & 0 & 0 & \tilde{S}_{75} & \tilde{S}_{76} & 0 & 0 & \tilde{S}_{77} & \tilde{S}_{78} & 0 & \tilde{S}_{79} & 0 & \tilde{S}_{80} & 0 \\
0 & 0 & 0 & 0 & 0 & 0 & 0 & 0 & 0 & 0 & 0 & 0 & 0 & 0 & 0 & 0 & 0 & 1 & 0 & 0 \\
0 & 0 & 0 & 0 & 0 & 0 & 0 & 0 & 0 & 0 & 0 & 0 & 0 & 0 & 0 & 0 & 0 & 0 & 1 & 0 \\
0 & 0 & 0 & 0 & 0 & 0 & 0 & 0 & 0 & 0 & 0 & 0 & 0 & 0 & 0 & 0 & 0 & 0 & 0 & 1 \\
0 & \tilde{S}_{81} & \tilde{S}_{82} & 0 & 0 & \tilde{S}_{83} & \tilde{S}_{84} & 0 & 0 & \tilde{S}_{85} & \tilde{S}_{86} & 0 & 0 & \tilde{S}_{87} & \tilde{S}_{88} & 0 & \tilde{S}_{89} & 0 & \tilde{S}_{90} & 0
\end{pmatrix}, \quad (C.1)$$

where the parameters denoted by $\tilde{S}$ are constants and can be found in *Szekrényes (2014c)*.

C.1.1.2 Delaminated region

$$\mathbf{T}^{(d)} = \begin{pmatrix}
0 & 1 & 0 & 0 & 0 & 0 & 0 & 0 & 0 & 0 & 0 & 0 & 0 & 0 & 0 & 0 & 0 & 0 & 0 & 0 \\
\bar{S}_1 & 0 & 0 & \bar{S}_2 & \bar{S}_3 & 0 & 0 & \bar{S}_4 & 0 & 0 & 0 & 0 & 0 & 0 & 0 & 0 & 0 & \bar{S}_5 & 0 & \bar{S}_6 \\
0 & 0 & 0 & 1 & 0 & 0 & 0 & 0 & 0 & 0 & 0 & 0 & 0 & 0 & 0 & 0 & 0 & 0 & 0 & 0 \\
0 & \bar{S}_7 & \bar{S}_8 & 0 & 0 & \bar{S}_9 & \bar{S}_{10} & 0 & 0 & 0 & 0 & 0 & 0 & 0 & 0 & 0 & \bar{S}_{11} & 0 & \bar{S}_{12} & 0 \\
0 & 0 & 0 & 0 & 0 & 1 & 0 & 0 & 0 & 0 & 0 & 0 & 0 & 0 & 0 & 0 & 0 & 0 & 0 & 0 \\
\bar{S}_{13} & 0 & 0 & \bar{S}_{14} & \bar{S}_{15} & 0 & 0 & \bar{S}_{16} & 0 & 0 & 0 & 0 & 0 & 0 & 0 & 0 & 0 & \bar{S}_{17} & 0 & \bar{S}_{18} \\
0 & 0 & 0 & 0 & 0 & 0 & 0 & 1 & 0 & 0 & 0 & 0 & 0 & 0 & 0 & 0 & 0 & 0 & 0 & 0 \\
0 & \bar{S}_{19} & \bar{S}_{20} & 0 & 0 & \bar{S}_{21} & \bar{S}_{22} & 0 & 0 & 0 & 0 & 0 & 0 & 0 & 0 & 0 & \bar{S}_{23} & 0 & \bar{S}_{24} & 0 \\
0 & 0 & 0 & 0 & 0 & 0 & 0 & 0 & 0 & 1 & 0 & 0 & 0 & 0 & 0 & 0 & 0 & 0 & 0 & 0 \\
0 & 0 & 0 & 0 & 0 & 0 & 0 & 0 & \bar{S}_{25} & 0 & 0 & \bar{S}_{26} & \bar{S}_{27} & 0 & 0 & \bar{S}_{28} & 0 & \bar{S}_{29} & 0 & \bar{S}_{30} \\
0 & 0 & 0 & 0 & 0 & 0 & 0 & 0 & 0 & 0 & 0 & 1 & 0 & 0 & 0 & 0 & 0 & 0 & 0 & 0 \\
0 & 0 & 0 & 0 & 0 & 0 & 0 & 0 & 0 & \bar{S}_{31} & \bar{S}_{32} & 0 & 0 & \bar{S}_{33} & \bar{S}_{34} & 0 & \bar{S}_{35} & 0 & \bar{S}_{36} & 0 \\
0 & 0 & 0 & 0 & 0 & 0 & 0 & 0 & 0 & 0 & 0 & 0 & 0 & 1 & 0 & 0 & 0 & 0 & 0 & 0 \\
0 & 0 & 0 & 0 & 0 & 0 & 0 & 0 & \bar{S}_{37} & 0 & 0 & \bar{S}_{38} & \bar{S}_{39} & 0 & 0 & \bar{S}_{40} & 0 & \bar{S}_{41} & 0 & \bar{S}_{42} \\
0 & 0 & 0 & 0 & 0 & 0 & 0 & 0 & 0 & 0 & 0 & 0 & 0 & 0 & 0 & 1 & 0 & 0 & 0 & 0 \\
0 & 0 & 0 & 0 & 0 & 0 & 0 & 0 & 0 & \bar{S}_{43} & \bar{S}_{44} & 0 & 0 & \bar{S}_{45} & \bar{S}_{46} & 0 & \bar{S}_{47} & 0 & \bar{S}_{48} & 0 \\
0 & 0 & 0 & 0 & 0 & 0 & 0 & 0 & 0 & 0 & 0 & 0 & 0 & 0 & 0 & 0 & 0 & 1 & 0 & 0 \\
0 & 0 & 0 & 0 & 0 & 0 & 0 & 0 & 0 & 0 & 0 & 0 & 0 & 0 & 0 & 0 & 0 & 0 & 1 & 0 \\
0 & 0 & 0 & 0 & 0 & 0 & 0 & 0 & 0 & 0 & 0 & 0 & 0 & 0 & 0 & 0 & 0 & 0 & 0 & 1 \\
0 & \bar{S}_{49} & \bar{S}_{50} & 0 & 0 & \bar{S}_{51} & \bar{S}_{52} & 0 & 0 & \bar{S}_{53} & \bar{S}_{54} & 0 & 0 & \bar{S}_{55} & \bar{S}_{56} & 0 & \bar{S}_{57} & 0 & \bar{S}_{58} & 0
\end{pmatrix}. \quad \text{(C.2)}$$

C.1.2 Second-order plate theory

In this Appendix the system matrices of the SSDT solution can be found. The state space models were developed in Section 5.3.

C.1.2.1 Undelaminated region

$$\mathbf{T}^{(ud)} = \begin{pmatrix}
0 & 1 & 0 & 0 & 0 & 0 & 0 & 0 & 0 & 0 & 0 & 0 & 0 & 0 & 0 & 0 & 0 & 0 & 0 & 0 & 0 & 0 \\
\tilde{R}_1 & 0 & 0 & \tilde{R}_2 & \tilde{R}_3 & 0 & 0 & \tilde{R}_4 & \tilde{R}_5 & 0 & 0 & \tilde{R}_6 & \tilde{R}_7 & 0 & 0 & \tilde{R}_8 & \tilde{R}_9 & 0 & 0 & \tilde{R}_{10} & 0 & \tilde{R}_{11} \\
0 & 0 & 0 & 1 & 0 & 0 & 0 & 0 & 0 & 0 & 0 & 0 & 0 & 0 & 0 & 0 & 0 & 0 & 0 & 0 & 0 & 0 \\
0 & \tilde{R}_{12} & \tilde{R}_{13} & 0 & 0 & \tilde{R}_{14} & \tilde{R}_{15} & 0 & 0 & \tilde{R}_{16} & \tilde{R}_{17} & 0 & 0 & \tilde{R}_{18} & \tilde{R}_{19} & 0 & 0 & \tilde{R}_{20} & \tilde{R}_{21} & 0 & \tilde{R}_{22} & 0 \\
0 & 0 & 0 & 0 & 0 & 1 & 0 & 0 & 0 & 0 & 0 & 0 & 0 & 0 & 0 & 0 & 0 & 0 & 0 & 0 & 0 & 0 \\
\tilde{R}_{23} & 0 & 0 & \tilde{R}_{24} & \tilde{R}_{25} & 0 & 0 & \tilde{R}_{26} & \tilde{R}_{27} & 0 & 0 & \tilde{R}_{28} & \tilde{R}_{29} & 0 & 0 & \tilde{R}_{30} & \tilde{R}_{31} & 0 & 0 & \tilde{R}_{32} & 0 & \tilde{R}_{33} \\
0 & 0 & 0 & 0 & 0 & 0 & 0 & 1 & 0 & 0 & 0 & 0 & 0 & 0 & 0 & 0 & 0 & 0 & 0 & 0 & 0 & 0 \\
0 & \tilde{R}_{34} & \tilde{R}_{35} & 0 & 0 & \tilde{R}_{36} & \tilde{R}_{37} & 0 & 0 & \tilde{R}_{38} & \tilde{R}_{39} & 0 & 0 & \tilde{R}_{40} & \tilde{R}_{41} & 0 & 0 & \tilde{R}_{42} & \tilde{R}_{43} & 0 & \tilde{R}_{44} & 0 \\
0 & 0 & 0 & 0 & 0 & 0 & 0 & 0 & 0 & 1 & 0 & 0 & 0 & 0 & 0 & 0 & 0 & 0 & 0 & 0 & 0 & 0 \\
\tilde{R}_{45} & 0 & 0 & \tilde{R}_{46} & \tilde{R}_{47} & 0 & 0 & \tilde{R}_{48} & \tilde{R}_{49} & 0 & 0 & \tilde{R}_{50} & \tilde{R}_{51} & 0 & 0 & \tilde{R}_{52} & \tilde{R}_{53} & 0 & 0 & \tilde{R}_{54} & 0 & \tilde{R}_{55} \\
0 & 0 & 0 & 0 & 0 & 0 & 0 & 0 & 0 & 0 & 0 & 1 & 0 & 0 & 0 & 0 & 0 & 0 & 0 & 0 & 0 & 0 \\
0 & \tilde{R}_{56} & \tilde{R}_{57} & 0 & 0 & \tilde{R}_{58} & \tilde{R}_{59} & 0 & 0 & \tilde{R}_{60} & \tilde{R}_{61} & 0 & 0 & \tilde{R}_{62} & \tilde{R}_{63} & 0 & 0 & \tilde{R}_{64} & \tilde{R}_{65} & 0 & \tilde{R}_{66} & 0 \\
0 & 0 & 0 & 0 & 0 & 0 & 0 & 0 & 0 & 0 & 0 & 0 & 0 & 1 & 0 & 0 & 0 & 0 & 0 & 0 & 0 & 0 \\
\tilde{R}_{67} & 0 & 0 & \tilde{R}_{68} & \tilde{R}_{69} & 0 & 0 & \tilde{R}_{70} & \tilde{R}_{71} & 0 & 0 & \tilde{R}_{72} & \tilde{R}_{73} & 0 & 0 & \tilde{R}_{74} & \tilde{R}_{75} & 0 & 0 & \tilde{R}_{76} & 0 & \tilde{R}_{77} \\
0 & 0 & 0 & 0 & 0 & 0 & 0 & 0 & 0 & 0 & 0 & 0 & 0 & 0 & 0 & 1 & 0 & 0 & 0 & 0 & 0 & 0 \\
0 & \tilde{R}_{78} & \tilde{R}_{79} & 0 & 0 & \tilde{R}_{80} & \tilde{R}_{81} & 0 & 0 & \tilde{R}_{82} & \tilde{R}_{83} & 0 & 0 & \tilde{R}_{84} & \tilde{R}_{85} & 0 & 0 & \tilde{R}_{86} & \tilde{R}_{87} & 0 & \tilde{R}_{88} & 0 \\
0 & 0 & 0 & 0 & 0 & 0 & 0 & 0 & 0 & 0 & 0 & 0 & 0 & 0 & 0 & 0 & 0 & 1 & 0 & 0 & 0 & 0 \\
\tilde{R}_{89} & 0 & 0 & \tilde{R}_{90} & \tilde{R}_{91} & 0 & 0 & \tilde{R}_{92} & \tilde{R}_{93} & 0 & 0 & \tilde{R}_{94} & \tilde{R}_{95} & 0 & 0 & \tilde{R}_{96} & \tilde{R}_{97} & 0 & 0 & \tilde{R}_{98} & 0 & \tilde{R}_{99} \\
0 & 0 & 0 & 0 & 0 & 0 & 0 & 0 & 0 & 0 & 0 & 0 & 0 & 0 & 0 & 0 & 0 & 0 & 0 & 1 & 0 & 0 \\
0 & \tilde{R}_{100} & \tilde{R}_{101} & 0 & 0 & \tilde{R}_{102} & \tilde{R}_{103} & 0 & 0 & \tilde{R}_{104} & \tilde{R}_{105} & 0 & 0 & \tilde{R}_{106} & \tilde{R}_{107} & 0 & 0 & \tilde{R}_{108} & \tilde{R}_{109} & 0 & \tilde{R}_{110} & 0 \\
0 & 0 & 0 & 0 & 0 & 0 & 0 & 0 & 0 & 0 & 0 & 0 & 0 & 0 & 0 & 0 & 0 & 0 & 0 & 0 & 0 & 1 \\
0 & \tilde{R}_{111} & \tilde{R}_{112} & 0 & 0 & \tilde{R}_{113} & \tilde{R}_{114} & 0 & 0 & \tilde{R}_{115} & \tilde{R}_{116} & 0 & 0 & \tilde{R}_{117} & \tilde{R}_{118} & 0 & 0 & \tilde{R}_{119} & \tilde{R}_{120} & 0 & \tilde{R}_{121} & 0
\end{pmatrix}. \quad \text{(C.3)}$$

C.1.2.2 Delaminated region

$$
\mathbf{T}^{(d)} = \begin{pmatrix}
0 & 1 & 0 & 0 & 0 & 0 & 0 & 0 & 0 & 0 & 0 & 0 & 0 & 0 & 0 & 0 & 0 & 0 & 0 & 0 & 0 & 0 & 0 & 0 & 0 & 0 \\
\bar{R}_{1} & 0 & 0 & \bar{R}_{2} & \bar{R}_{3} & 0 & 0 & \bar{R}_{4} & \bar{R}_{5} & 0 & 0 & \bar{R}_{6} & 0 & 0 & 0 & 0 & 0 & 0 & 0 & 0 & 0 & 0 & 0 & 0 & 0 & \bar{R}_{7} \\
0 & 0 & 0 & 1 & 0 & 0 & 0 & 0 & 0 & 0 & 0 & 0 & 0 & 0 & 0 & 0 & 0 & 0 & 0 & 0 & 0 & 0 & 0 & 0 & 0 & 0 \\
0 & \bar{R}_{8} & \bar{R}_{9} & 0 & 0 & \bar{R}_{10} & \bar{R}_{11} & 0 & 0 & \bar{R}_{12} & \bar{R}_{13} & 0 & 0 & 0 & 0 & 0 & 0 & 0 & 0 & 0 & 0 & 0 & 0 & 0 & \bar{R}_{14} & 0 \\
0 & 0 & 0 & 0 & 0 & 1 & 0 & 0 & 0 & 0 & 0 & 0 & 0 & 0 & 0 & 0 & 0 & 0 & 0 & 0 & 0 & 0 & 0 & 0 & 0 & 0 \\
\bar{R}_{15} & 0 & 0 & \bar{R}_{16} & \bar{R}_{17} & 0 & 0 & \bar{R}_{18} & \bar{R}_{19} & 0 & 0 & \bar{R}_{20} & 0 & 0 & 0 & 0 & 0 & 0 & 0 & 0 & 0 & 0 & 0 & 0 & 0 & \bar{R}_{21} \\
0 & 0 & 0 & 0 & 0 & 0 & 0 & 1 & 0 & 0 & 0 & 0 & 0 & 0 & 0 & 0 & 0 & 0 & 0 & 0 & 0 & 0 & 0 & 0 & 0 & 0 \\
0 & \bar{R}_{22} & \bar{R}_{23} & 0 & 0 & \bar{R}_{24} & \bar{R}_{25} & 0 & 0 & \bar{R}_{26} & \bar{R}_{27} & 0 & 0 & 0 & 0 & 0 & 0 & 0 & 0 & 0 & 0 & 0 & 0 & 0 & \bar{R}_{28} & 0 \\
0 & 0 & 0 & 0 & 0 & 0 & 0 & 0 & 0 & 1 & 0 & 0 & 0 & 0 & 0 & 0 & 0 & 0 & 0 & 0 & 0 & 0 & 0 & 0 & 0 & 0 \\
\bar{R}_{29} & 0 & 0 & \bar{R}_{30} & \bar{R}_{31} & 0 & 0 & \bar{R}_{32} & \bar{R}_{33} & 0 & 0 & \bar{R}_{34} & 0 & 0 & 0 & 0 & 0 & 0 & 0 & 0 & 0 & 0 & 0 & 0 & 0 & \bar{R}_{35} \\
0 & 0 & 0 & 0 & 0 & 0 & 0 & 0 & 0 & 0 & 0 & 1 & 0 & 0 & 0 & 0 & 0 & 0 & 0 & 0 & 0 & 0 & 0 & 0 & 0 & 0 \\
0 & \bar{R}_{36} & \bar{R}_{37} & 0 & 0 & \bar{R}_{38} & \bar{R}_{39} & 0 & 0 & \bar{R}_{40} & \bar{R}_{41} & 0 & 0 & 0 & 0 & 0 & 0 & 0 & 0 & 0 & 0 & 0 & 0 & 0 & \bar{R}_{42} & 0 \\
0 & 0 & 0 & 0 & 0 & 0 & 0 & 0 & 0 & 0 & 0 & 0 & 0 & 1 & 0 & 0 & 0 & 0 & 0 & 0 & 0 & 0 & 0 & 0 & 0 & 0 \\
0 & 0 & 0 & 0 & 0 & 0 & 0 & 0 & 0 & 0 & 0 & 0 & \bar{R}_{43} & 0 & 0 & \bar{R}_{44} & \bar{R}_{45} & 0 & 0 & \bar{R}_{46} & \bar{R}_{47} & 0 & 0 & \bar{R}_{48} & 0 & \bar{R}_{49} \\
0 & 0 & 0 & 0 & 0 & 0 & 0 & 0 & 0 & 0 & 0 & 0 & 0 & 0 & 0 & 1 & 0 & 0 & 0 & 0 & 0 & 0 & 0 & 0 & 0 & 0 \\
0 & 0 & 0 & 0 & 0 & 0 & 0 & 0 & 0 & 0 & 0 & 0 & 0 & \bar{R}_{50} & \bar{R}_{51} & 0 & 0 & \bar{R}_{52} & \bar{R}_{53} & 0 & 0 & \bar{R}_{54} & \bar{R}_{55} & 0 & \bar{R}_{56} & 0 \\
0 & 0 & 0 & 0 & 0 & 0 & 0 & 0 & 0 & 0 & 0 & 0 & 0 & 0 & 0 & 0 & 0 & 1 & 0 & 0 & 0 & 0 & 0 & 0 & 0 & 0 \\
0 & 0 & 0 & 0 & 0 & 0 & 0 & 0 & 0 & 0 & 0 & 0 & \bar{R}_{57} & 0 & 0 & \bar{R}_{58} & \bar{R}_{59} & 0 & 0 & \bar{R}_{60} & \bar{R}_{61} & 0 & 0 & \bar{R}_{62} & 0 & \bar{R}_{63} \\
0 & 0 & 0 & 0 & 0 & 0 & 0 & 0 & 0 & 0 & 0 & 0 & 0 & 0 & 0 & 0 & 0 & 0 & 0 & 1 & 0 & 0 & 0 & 0 & 0 & 0 \\
0 & 0 & 0 & 0 & 0 & 0 & 0 & 0 & 0 & 0 & 0 & 0 & 0 & \bar{R}_{64} & \bar{R}_{65} & 0 & 0 & \bar{R}_{66} & \bar{R}_{67} & 0 & 0 & \bar{R}_{68} & \bar{R}_{69} & 0 & \bar{R}_{70} & 0 \\
0 & 0 & 0 & 0 & 0 & 0 & 0 & 0 & 0 & 0 & 0 & 0 & 0 & 0 & 0 & 0 & 0 & 0 & 0 & 0 & 0 & 1 & 0 & 0 & 0 & 0 \\
0 & 0 & 0 & 0 & 0 & 0 & 0 & 0 & 0 & 0 & 0 & 0 & \bar{R}_{71} & 0 & 0 & \bar{R}_{72} & \bar{R}_{73} & 0 & 0 & \bar{R}_{74} & \bar{R}_{75} & 0 & 0 & \bar{R}_{76} & 0 & \bar{R}_{77} \\
0 & 0 & 0 & 0 & 0 & 0 & 0 & 0 & 0 & 0 & 0 & 0 & 0 & 0 & 0 & 0 & 0 & 0 & 0 & 0 & 0 & 0 & 0 & 1 & 0 & 0 \\
0 & 0 & 0 & 0 & 0 & 0 & 0 & 0 & 0 & 0 & 0 & 0 & 0 & \bar{R}_{78} & \bar{R}_{79} & 0 & 0 & \bar{R}_{80} & \bar{R}_{81} & 0 & 0 & \bar{R}_{82} & \bar{R}_{83} & 0 & \bar{R}_{84} & 0 \\
0 & 0 & 0 & 0 & 0 & 0 & 0 & 0 & 0 & 0 & 0 & 0 & 0 & 0 & 0 & 0 & 0 & 0 & 0 & 0 & 0 & 0 & 0 & 0 & 0 & 1 \\
0 & 0 & 0 & 0 & 0 & \bar{R}_{85} & \bar{R}_{86} & 0 & 0 & \bar{R}_{87} & \bar{R}_{88} & 0 & 0 & 0 & 0 & 0 & 0 & \bar{R}_{89} & \bar{R}_{90} & 0 & 0 & \bar{R}_{91} & \bar{R}_{92} & 0 & \bar{R}_{93} & 0
\end{pmatrix}. \tag{C.4}
$$

C.1.3 First-order plate theory

This Appendix contains the system matrices of the FSDT model detailed in Section 5.4.

C.1.3.1 Undelaminated region

$$
\mathbf{T}^{(ud)} = \begin{pmatrix}
0 & 1 & 0 & 0 & 0 & 0 & 0 & 0 & 0 & 0 & 0 & 0 & 0 & 0 \\
\tilde{Q}_{1} & 0 & 0 & \tilde{Q}_{2} & \tilde{Q}_{3} & 0 & 0 & \tilde{Q}_{4} & \tilde{Q}_{5} & 0 & 0 & \tilde{Q}_{6} & 0 & \tilde{Q}_{7} \\
0 & 0 & 0 & 1 & 0 & 0 & 0 & 0 & 0 & 0 & 0 & 0 & 0 & 0 \\
0 & \tilde{Q}_{8} & \tilde{Q}_{9} & 0 & 0 & \tilde{Q}_{10} & \tilde{Q}_{11} & 0 & 0 & \tilde{Q}_{12} & \tilde{Q}_{13} & 0 & \tilde{Q}_{14} & 0 \\
0 & 0 & 0 & 0 & 0 & 1 & 0 & 0 & 0 & 0 & 0 & 0 & 0 & 0 \\
\tilde{Q}_{15} & 0 & 0 & \tilde{Q}_{16} & \tilde{Q}_{17} & 0 & 0 & \tilde{Q}_{18} & \tilde{Q}_{19} & 0 & 0 & \tilde{Q}_{20} & 0 & \tilde{Q}_{21} \\
0 & 0 & 0 & 0 & 0 & 0 & 0 & 1 & 0 & 0 & 0 & 0 & 0 & 0 \\
0 & \tilde{Q}_{22} & \tilde{Q}_{23} & 0 & 0 & \tilde{Q}_{24} & \tilde{Q}_{25} & 0 & 0 & \tilde{Q}_{26} & \tilde{Q}_{27} & 0 & \tilde{Q}_{28} & 0 \\
0 & 0 & 0 & 0 & 0 & 0 & 0 & 0 & 0 & 1 & 0 & 0 & 0 & 0 \\
\tilde{Q}_{29} & 0 & 0 & \tilde{Q}_{30} & \tilde{Q}_{31} & 0 & 0 & \tilde{Q}_{32} & \tilde{Q}_{33} & 0 & 0 & \tilde{Q}_{34} & 0 & \tilde{Q}_{35} \\
0 & 0 & 0 & 0 & 0 & 0 & 0 & 0 & 0 & 0 & 0 & 1 & 0 & 0 \\
0 & \tilde{Q}_{36} & \tilde{Q}_{37} & 0 & 0 & \tilde{Q}_{38} & \tilde{Q}_{39} & 0 & 0 & \tilde{Q}_{40} & \tilde{Q}_{41} & 0 & \tilde{Q}_{42} & 0 \\
0 & 0 & 0 & 0 & 0 & 0 & 0 & 0 & 0 & 0 & 0 & 0 & 0 & 1 \\
0 & \tilde{Q}_{43} & \tilde{Q}_{44} & 0 & 0 & \tilde{Q}_{45} & \tilde{Q}_{46} & 0 & 0 & \tilde{Q}_{47} & \tilde{Q}_{48} & 0 & \tilde{Q}_{49} & 0
\end{pmatrix}. \tag{C.5}
$$

C.1.3.2 Delaminated region

$$
\mathbf{T}^{(d)} = \begin{pmatrix}
0 & 1 & 0 & 0 & 0 & 0 & 0 & 0 & 0 & 0 & 0 & 0 & 0 & 0 & 0 & 0 & 0 & 0 \\
\bar{Q}_1 & 0 & 0 & \bar{Q}_2 & \bar{Q}_3 & 0 & 0 & \bar{Q}_4 & 0 & 0 & 0 & 0 & 0 & 0 & 0 & 0 & 0 & \bar{Q}_5 \\
0 & 0 & 0 & 1 & 0 & 0 & 0 & 0 & 0 & 0 & 0 & 0 & 0 & 0 & 0 & 0 & 0 & 0 \\
0 & \bar{Q}_6 & \bar{Q}_7 & 0 & 0 & \bar{Q}_8 & \bar{Q}_9 & 0 & 0 & 0 & 0 & 0 & 0 & 0 & 0 & 0 & \bar{Q}_{10} & 0 \\
0 & 0 & 0 & 0 & 0 & 1 & 0 & 0 & 0 & 0 & 0 & 0 & 0 & 0 & 0 & 0 & 0 & 0 \\
\bar{Q}_{11} & 0 & 0 & \bar{Q}_{12} & \bar{Q}_{13} & 0 & 0 & \bar{Q}_{14} & 0 & 0 & 0 & 0 & 0 & 0 & 0 & 0 & 0 & \bar{Q}_{15} \\
0 & 0 & 0 & 0 & 0 & 0 & 0 & 1 & 0 & 0 & 0 & 0 & 0 & 0 & 0 & 0 & 0 & 0 \\
0 & \bar{Q}_{16} & \bar{Q}_{17} & 0 & 0 & \bar{Q}_{18} & \bar{Q}_{19} & 0 & 0 & 0 & 0 & 0 & 0 & 0 & 0 & 0 & \bar{Q}_{20} & 0 \\
0 & 0 & 0 & 0 & 0 & 0 & 0 & 0 & 0 & 1 & 0 & 0 & 0 & 0 & 0 & 0 & 0 & 0 \\
0 & 0 & 0 & 0 & 0 & 0 & 0 & 0 & \bar{Q}_{21} & 0 & 0 & \bar{Q}_{22} & \bar{Q}_{23} & 0 & 0 & \bar{Q}_{24} & 0 & \bar{Q}_{25} \\
0 & 0 & 0 & 0 & 0 & 0 & 0 & 0 & 0 & 0 & 0 & 1 & 0 & 0 & 0 & 0 & 0 & 0 \\
0 & 0 & 0 & 0 & 0 & 0 & 0 & 0 & 0 & \bar{Q}_{26} & \bar{Q}_{27} & 0 & 0 & \bar{Q}_{28} & \bar{Q}_{29} & 0 & \bar{Q}_{30} & 0 \\
0 & 0 & 0 & 0 & 0 & 0 & 0 & 0 & 0 & 0 & 0 & 0 & 0 & 1 & 0 & 0 & 0 & 0 \\
0 & 0 & 0 & 0 & 0 & 0 & 0 & 0 & \bar{Q}_{31} & 0 & 0 & \bar{Q}_{32} & \bar{Q}_{33} & 0 & 0 & \bar{Q}_{34} & 0 & \bar{Q}_{35} \\
0 & 0 & 0 & 0 & 0 & 0 & 0 & 0 & 0 & 0 & 0 & 1 & 0 & 0 & 0 & 0 & 0 & 0 \\
0 & 0 & 0 & 0 & 0 & 0 & 0 & 0 & 0 & \bar{Q}_{36} & \bar{Q}_{37} & 0 & 0 & \bar{Q}_{38} & \bar{Q}_{39} & 0 & \bar{Q}_{40} & 0 \\
0 & 0 & 0 & 0 & 0 & 0 & 0 & 0 & 0 & 0 & 0 & 0 & 0 & 1 & 0 & 0 & 0 & 0 \\
0 & 0 & 0 & 0 & 0 & \bar{Q}_{41} & \bar{Q}_{42} & 0 & 0 & 0 & 0 & 0 & 0 & \bar{Q}_{43} & \bar{Q}_{44} & 0 & \bar{Q}_{45} & 0
\end{pmatrix}. \tag{C.6}
$$

C.2 Method of 4ESLs

C.2.1 Third-order plate theory

This Appendix presents the system matrices of the TSDT model detailed in Section 5.5.

C.2.1.1 Undelaminated region

$$
\mathbf{T}^{(ud)} = \begin{pmatrix}
0 & 1 & 0 & 0 & 0 & 0 & 0 & 0 & 0 & 0 & 0 & 0 & 0 & 0 & 0 & 0 & 0 & 0 & 0 & 0 & 0 & 0 & 0 & 0 & 0 & 0 \\
\tilde{S}_1 & 0 & 0 & \tilde{S}_2 & \tilde{S}_3 & 0 & 0 & \tilde{S}_4 & \tilde{S}_5 & 0 & 0 & \tilde{S}_6 & \tilde{S}_7 & 0 & 0 & \tilde{S}_8 & \tilde{S}_9 & 0 & 0 & \tilde{S}_{10} & \tilde{S}_{11} & 0 & 0 & \tilde{S}_{12} & 0 & \tilde{S}_{13} \\
0 & 0 & 0 & 1 & 0 & 0 & 0 & 0 & 0 & 0 & 0 & 0 & 0 & 0 & 0 & 0 & 0 & 0 & 0 & 0 & 0 & 0 & 0 & 0 & 0 & 0 \\
0 & \tilde{\mathcal{T}}_1 & \tilde{\mathcal{T}}_2 & 0 & 0 & \tilde{\mathcal{T}}_3 & \tilde{\mathcal{T}}_4 & 0 & 0 & \tilde{\mathcal{T}}_5 & \tilde{\mathcal{T}}_6 & 0 & 0 & \tilde{\mathcal{T}}_7 & \tilde{\mathcal{T}}_8 & 0 & 0 & \tilde{\mathcal{T}}_9 & \tilde{\mathcal{T}}_{10} & 0 & 0 & \tilde{\mathcal{T}}_{11} & \tilde{\mathcal{T}}_{12} & 0 & \tilde{\mathcal{T}}_{13} & 0 \\
0 & 0 & 0 & 0 & 0 & 1 & 0 & 0 & 0 & 0 & 0 & 0 & 0 & 0 & 0 & 0 & 0 & 0 & 0 & 0 & 0 & 0 & 0 & 0 & 0 & 0 \\
\tilde{S}_{14} & 0 & 0 & \tilde{S}_{15} & \tilde{S}_{16} & 0 & 0 & \tilde{S}_{17} & \tilde{S}_{18} & 0 & 0 & \tilde{S}_{19} & \tilde{S}_{20} & 0 & 0 & \tilde{S}_{21} & \tilde{S}_{22} & 0 & 0 & \tilde{S}_{23} & \tilde{S}_{24} & 0 & 0 & \tilde{S}_{25} & 0 & \tilde{S}_{26} \\
0 & 0 & 0 & 0 & 0 & 0 & 0 & 1 & 0 & 0 & 0 & 0 & 0 & 0 & 0 & 0 & 0 & 0 & 0 & 0 & 0 & 0 & 0 & 0 & 0 & 0 \\
0 & \tilde{\mathcal{T}}_{14} & \tilde{\mathcal{T}}_{15} & 0 & 0 & \tilde{\mathcal{T}}_{16} & \tilde{\mathcal{T}}_{17} & 0 & 0 & \tilde{\mathcal{T}}_{18} & \tilde{\mathcal{T}}_{19} & 0 & 0 & \tilde{\mathcal{T}}_{20} & \tilde{\mathcal{T}}_{21} & 0 & 0 & \tilde{\mathcal{T}}_{22} & \tilde{\mathcal{T}}_{23} & 0 & 0 & \tilde{\mathcal{T}}_{24} & \tilde{\mathcal{T}}_{25} & 0 & \tilde{\mathcal{T}}_{26} & 0 \\
0 & 0 & 0 & 0 & 0 & 0 & 0 & 0 & 0 & 1 & 0 & 0 & 0 & 0 & 0 & 0 & 0 & 0 & 0 & 0 & 0 & 0 & 0 & 0 & 0 & 0 \\
\tilde{S}_{27} & 0 & 0 & \tilde{S}_{28} & \tilde{S}_{29} & 0 & 0 & \tilde{S}_{30} & \tilde{S}_{31} & 0 & 0 & \tilde{S}_{32} & \tilde{S}_{33} & 0 & 0 & \tilde{S}_{34} & \tilde{S}_{35} & 0 & 0 & \tilde{S}_{36} & \tilde{S}_{37} & 0 & 0 & \tilde{S}_{38} & 0 & \tilde{S}_{39} \\
0 & 0 & 0 & 0 & 0 & 0 & 0 & 0 & 0 & 0 & 0 & 1 & 0 & 0 & 0 & 0 & 0 & 0 & 0 & 0 & 0 & 0 & 0 & 0 & 0 & 0 \\
0 & \tilde{\mathcal{T}}_{27} & \tilde{\mathcal{T}}_{28} & 0 & 0 & \tilde{\mathcal{T}}_{29} & \tilde{\mathcal{T}}_{30} & 0 & 0 & \tilde{\mathcal{T}}_{31} & \tilde{\mathcal{T}}_{32} & 0 & 0 & \tilde{\mathcal{T}}_{33} & \tilde{\mathcal{T}}_{34} & 0 & 0 & \tilde{\mathcal{T}}_{35} & \tilde{\mathcal{T}}_{36} & 0 & 0 & \tilde{\mathcal{T}}_{37} & \tilde{\mathcal{T}}_{38} & 0 & \tilde{\mathcal{T}}_{39} & 0 \\
0 & 0 & 0 & 0 & 0 & 0 & 0 & 0 & 0 & 0 & 0 & 0 & 0 & 1 & 0 & 0 & 0 & 0 & 0 & 0 & 0 & 0 & 0 & 0 & 0 & 0 \\
\tilde{S}_{40} & 0 & 0 & \tilde{S}_{41} & \tilde{S}_{42} & 0 & 0 & \tilde{S}_{43} & \tilde{S}_{44} & 0 & 0 & \tilde{S}_{45} & \tilde{S}_{46} & 0 & 0 & \tilde{S}_{47} & \tilde{S}_{48} & 0 & 0 & \tilde{S}_{49} & \tilde{S}_{50} & 0 & 0 & \tilde{S}_{51} & 0 & \tilde{S}_{52} \\
0 & 0 & 0 & 0 & 0 & 0 & 0 & 0 & 0 & 0 & 0 & 0 & 0 & 0 & 0 & 1 & 0 & 0 & 0 & 0 & 0 & 0 & 0 & 0 & 0 & 0 \\
0 & \tilde{\mathcal{T}}_{40} & \tilde{\mathcal{T}}_{41} & 0 & 0 & \tilde{\mathcal{T}}_{42} & \tilde{\mathcal{T}}_{43} & 0 & 0 & \tilde{\mathcal{T}}_{44} & \tilde{\mathcal{T}}_{45} & 0 & 0 & \tilde{\mathcal{T}}_{46} & \tilde{\mathcal{T}}_{47} & 0 & 0 & \tilde{\mathcal{T}}_{48} & \tilde{\mathcal{T}}_{49} & 0 & 0 & \tilde{\mathcal{T}}_{50} & \tilde{\mathcal{T}}_{51} & 0 & \tilde{\mathcal{T}}_{52} & 0 \\
0 & 0 & 0 & 0 & 0 & 0 & 0 & 0 & 0 & 0 & 0 & 0 & 0 & 0 & 0 & 0 & 0 & 1 & 0 & 0 & 0 & 0 & 0 & 0 & 0 & 0 \\
\tilde{S}_{53} & 0 & 0 & \tilde{S}_{54} & \tilde{S}_{55} & 0 & 0 & \tilde{S}_{56} & \tilde{S}_{57} & 0 & 0 & \tilde{S}_{58} & \tilde{S}_{59} & 0 & 0 & \tilde{S}_{60} & \tilde{S}_{61} & 0 & 0 & \tilde{S}_{62} & \tilde{S}_{63} & 0 & 0 & \tilde{S}_{64} & 0 & \tilde{S}_{65} \\
0 & 0 & 0 & 0 & 0 & 0 & 0 & 0 & 0 & 0 & 0 & 0 & 0 & 0 & 0 & 0 & 0 & 0 & 0 & 1 & 0 & 0 & 0 & 0 & 0 & 0 \\
0 & \tilde{\mathcal{T}}_{53} & \tilde{\mathcal{T}}_{54} & 0 & 0 & \tilde{\mathcal{T}}_{55} & \tilde{\mathcal{T}}_{56} & 0 & 0 & \tilde{\mathcal{T}}_{57} & \tilde{\mathcal{T}}_{58} & 0 & 0 & \tilde{\mathcal{T}}_{59} & \tilde{\mathcal{T}}_{60} & 0 & 0 & \tilde{\mathcal{T}}_{61} & \tilde{\mathcal{T}}_{62} & 0 & 0 & \tilde{\mathcal{T}}_{63} & \tilde{\mathcal{T}}_{64} & 0 & \tilde{\mathcal{T}}_{65} & 0 \\
0 & 0 & 0 & 0 & 0 & 0 & 0 & 0 & 0 & 0 & 0 & 0 & 0 & 0 & 0 & 0 & 0 & 0 & 0 & 0 & 0 & 1 & 0 & 0 & 0 & 0 \\
\tilde{S}_{66} & 0 & 0 & \tilde{S}_{67} & \tilde{S}_{68} & 0 & 0 & \tilde{S}_{69} & \tilde{S}_{70} & 0 & 0 & \tilde{S}_{71} & \tilde{S}_{72} & 0 & 0 & \tilde{S}_{73} & \tilde{S}_{74} & 0 & 0 & \tilde{S}_{75} & \tilde{S}_{76} & 0 & 0 & \tilde{S}_{77} & 0 & \tilde{S}_{78} \\
0 & 0 & 0 & 0 & 0 & 0 & 0 & 0 & 0 & 0 & 0 & 0 & 0 & 0 & 0 & 0 & 0 & 0 & 0 & 0 & 0 & 0 & 0 & 1 & 0 & 0 \\
0 & \tilde{\mathcal{T}}_{66} & \tilde{\mathcal{T}}_{67} & 0 & 0 & \tilde{\mathcal{T}}_{68} & \tilde{\mathcal{T}}_{69} & 0 & 0 & \tilde{\mathcal{T}}_{70} & \tilde{\mathcal{T}}_{71} & 0 & 0 & \tilde{\mathcal{T}}_{72} & \tilde{\mathcal{T}}_{73} & 0 & 0 & \tilde{\mathcal{T}}_{74} & \tilde{\mathcal{T}}_{75} & 0 & 0 & \tilde{\mathcal{T}}_{76} & \tilde{\mathcal{T}}_{77} & 0 & \tilde{\mathcal{T}}_{78} & 0 \\
0 & 0 & 0 & 0 & 0 & 0 & 0 & 0 & 0 & 0 & 0 & 0 & 0 & 0 & 0 & 0 & 0 & 0 & 0 & 0 & 0 & 0 & 0 & 0 & 0 & 1 \\
0 & 0 & 0 & 0 & 0 & \tilde{S}_{79} & \tilde{S}_{80} & 0 & 0 & \tilde{S}_{81} & \tilde{S}_{82} & 0 & 0 & \tilde{S}_{83} & \tilde{S}_{84} & 0 & 0 & \tilde{S}_{85} & \tilde{S}_{86} & 0 & 0 & \tilde{S}_{87} & \tilde{S}_{88} & 0 & \tilde{S}_{89} & 0
\end{pmatrix}. \tag{C.7}
$$

C.2.1.2 Delaminated region

$$
\mathbf{T}^{(d)} = \left(\begin{array}{cccccccccccccccccccccccccccccccccc}
0 & 1 & 0 & 0 & 0 & 0 & 0 & 0 & 0 & 0 & 0 & 0 & 0 & 0 & 0 & 0 & 0 & 0 & 0 & 0 & 0 & 0 & 0 & 0 & 0 & 0 & 0 & 0 & 0 & 0 & 0 & 0 & 0 & 0 \\
\bar{S}_1 & 0 & 0 & \bar{S}_2 & \bar{S}_3 & 0 & 0 & \bar{S}_4 & \bar{S}_5 & 0 & 0 & \bar{S}_6 & \bar{S}_7 & 0 & 0 & \bar{S}_8 & 0 & 0 & 0 & 0 & 0 & 0 & 0 & 0 & 0 & 0 & 0 & 0 & 0 & 0 & 0 & 0 & 0 & \bar{S}_9 \\
0 & 0 & 0 & 1 & 0 & 0 & 0 & 0 & 0 & 0 & 0 & 0 & 0 & 0 & 0 & 0 & 0 & 0 & 0 & 0 & 0 & 0 & 0 & 0 & 0 & 0 & 0 & 0 & 0 & 0 & 0 & 0 & 0 & 0 \\
0 & \bar{\mathcal{T}}_1 & \bar{\mathcal{T}}_2 & 0 & 0 & \bar{\mathcal{T}}_3 & \bar{\mathcal{T}}_4 & 0 & 0 & \bar{\mathcal{T}}_5 & \bar{\mathcal{T}}_6 & 0 & 0 & \bar{\mathcal{T}}_7 & \bar{\mathcal{T}}_8 & 0 & 0 & 0 & 0 & 0 & 0 & 0 & 0 & 0 & 0 & 0 & 0 & 0 & 0 & 0 & 0 & 0 & \bar{\mathcal{T}}_9 & 0 \\
0 & 0 & 0 & 0 & 0 & 1 & 0 & 0 & 0 & 0 & 0 & 0 & 0 & 0 & 0 & 0 & 0 & 0 & 0 & 0 & 0 & 0 & 0 & 0 & 0 & 0 & 0 & 0 & 0 & 0 & 0 & 0 & 0 & 0 \\
\bar{S}_{10} & 0 & 0 & \bar{S}_{11} & \bar{S}_{12} & 0 & 0 & \bar{S}_{13} & \bar{S}_{14} & 0 & 0 & \bar{S}_{15} & \bar{S}_{16} & 0 & 0 & \bar{S}_{17} & 0 & 0 & 0 & 0 & 0 & 0 & 0 & 0 & 0 & 0 & 0 & 0 & 0 & 0 & 0 & 0 & 0 & \bar{S}_{18} \\
0 & 0 & 0 & 0 & 0 & 0 & 0 & 1 & 0 & 0 & 0 & 0 & 0 & 0 & 0 & 0 & 0 & 0 & 0 & 0 & 0 & 0 & 0 & 0 & 0 & 0 & 0 & 0 & 0 & 0 & 0 & 0 & 0 & 0 \\
0 & \bar{\mathcal{T}}_{10} & \bar{\mathcal{T}}_{11} & 0 & 0 & \bar{\mathcal{T}}_{12} & \bar{\mathcal{T}}_{13} & 0 & 0 & \bar{\mathcal{T}}_{14} & \bar{\mathcal{T}}_{15} & 0 & 0 & \bar{\mathcal{T}}_{16} & \bar{\mathcal{T}}_{17} & 0 & 0 & 0 & 0 & 0 & 0 & 0 & 0 & 0 & 0 & 0 & 0 & 0 & 0 & 0 & 0 & 0 & \bar{\mathcal{T}}_{18} & 0 \\
0 & 0 & 0 & 0 & 0 & 0 & 0 & 0 & 0 & 1 & 0 & 0 & 0 & 0 & 0 & 0 & 0 & 0 & 0 & 0 & 0 & 0 & 0 & 0 & 0 & 0 & 0 & 0 & 0 & 0 & 0 & 0 & 0 & 0 \\
\bar{S}_{19} & 0 & 0 & \bar{S}_{20} & \bar{S}_{21} & 0 & 0 & \bar{S}_{22} & \bar{S}_{23} & 0 & 0 & \bar{S}_{24} & \bar{S}_{25} & 0 & 0 & \bar{S}_{26} & 0 & 0 & 0 & 0 & 0 & 0 & 0 & 0 & 0 & 0 & 0 & 0 & 0 & 0 & 0 & 0 & 0 & \bar{S}_{27} \\
0 & 0 & 0 & 0 & 0 & 0 & 0 & 0 & 0 & 0 & 0 & 1 & 0 & 0 & 0 & 0 & 0 & 0 & 0 & 0 & 0 & 0 & 0 & 0 & 0 & 0 & 0 & 0 & 0 & 0 & 0 & 0 & 0 & 0 \\
0 & \bar{\mathcal{T}}_{19} & \bar{\mathcal{T}}_{20} & 0 & 0 & \bar{\mathcal{T}}_{21} & \bar{\mathcal{T}}_{22} & 0 & 0 & \bar{\mathcal{T}}_{23} & \bar{\mathcal{T}}_{24} & 0 & 0 & \bar{\mathcal{T}}_{25} & \bar{\mathcal{T}}_{26} & 0 & 0 & 0 & 0 & 0 & 0 & 0 & 0 & 0 & 0 & 0 & 0 & 0 & 0 & 0 & 0 & 0 & \bar{\mathcal{T}}_{27} & 0 \\
0 & 0 & 0 & 0 & 0 & 0 & 0 & 0 & 0 & 0 & 0 & 0 & 0 & 1 & 0 & 0 & 0 & 0 & 0 & 0 & 0 & 0 & 0 & 0 & 0 & 0 & 0 & 0 & 0 & 0 & 0 & 0 & 0 & 0 \\
\bar{S}_{28} & 0 & 0 & \bar{S}_{29} & \bar{S}_{30} & 0 & 0 & \bar{S}_{31} & \bar{S}_{32} & 0 & 0 & \bar{S}_{33} & \bar{S}_{34} & 0 & 0 & \bar{S}_{35} & 0 & 0 & 0 & 0 & 0 & 0 & 0 & 0 & 0 & 0 & 0 & 0 & 0 & 0 & 0 & 0 & 0 & \bar{S}_{36} \\
0 & 0 & 0 & 0 & 0 & 0 & 0 & 0 & 0 & 0 & 0 & 0 & 0 & 0 & 0 & 1 & 0 & 0 & 0 & 0 & 0 & 0 & 0 & 0 & 0 & 0 & 0 & 0 & 0 & 0 & 0 & 0 & 0 & 0 \\
0 & \bar{\mathcal{T}}_{28} & \bar{\mathcal{T}}_{29} & 0 & 0 & \bar{\mathcal{T}}_{30} & \bar{\mathcal{T}}_{31} & 0 & 0 & \bar{\mathcal{T}}_{32} & \bar{\mathcal{T}}_{33} & 0 & 0 & \bar{\mathcal{T}}_{34} & \bar{\mathcal{T}}_{35} & 0 & 0 & 0 & 0 & 0 & 0 & 0 & 0 & 0 & 0 & 0 & 0 & 0 & 0 & 0 & 0 & 0 & \bar{\mathcal{T}}_{36} & 0 \\
0 & 0 & 0 & 0 & 0 & 0 & 0 & 0 & 0 & 0 & 0 & 0 & 0 & 0 & 0 & 0 & 0 & 1 & 0 & 0 & 0 & 0 & 0 & 0 & 0 & 0 & 0 & 0 & 0 & 0 & 0 & 0 & 0 & 0 \\
0 & 0 & 0 & 0 & 0 & 0 & 0 & 0 & 0 & 0 & 0 & 0 & 0 & 0 & 0 & 0 & \bar{S}_{37} & 0 & 0 & \bar{S}_{38} & \bar{S}_{39} & 0 & 0 & \bar{S}_{40} & \bar{S}_{41} & 0 & 0 & \bar{S}_{42} & \bar{S}_{43} & 0 & 0 & \bar{S}_{44} & 0 & \bar{S}_{45} \\
0 & 0 & 0 & 0 & 0 & 0 & 0 & 0 & 0 & 0 & 0 & 0 & 0 & 0 & 0 & 0 & 0 & 0 & 0 & 1 & 0 & 0 & 0 & 0 & 0 & 0 & 0 & 0 & 0 & 0 & 0 & 0 & 0 & 0 \\
0 & 0 & 0 & 0 & 0 & 0 & 0 & 0 & 0 & 0 & 0 & 0 & 0 & 0 & 0 & 0 & 0 & \bar{\mathcal{T}}_{37} & \bar{\mathcal{T}}_{38} & 0 & 0 & \bar{\mathcal{T}}_{39} & \bar{\mathcal{T}}_{40} & 0 & 0 & \bar{\mathcal{T}}_{41} & \bar{\mathcal{T}}_{42} & 0 & 0 & \bar{\mathcal{T}}_{43} & \bar{\mathcal{T}}_{44} & 0 & \bar{\mathcal{T}}_{45} & 0 \\
0 & 0 & 0 & 0 & 0 & 0 & 0 & 0 & 0 & 0 & 0 & 0 & 0 & 0 & 0 & 0 & 0 & 0 & 0 & 0 & 0 & 1 & 0 & 0 & 0 & 0 & 0 & 0 & 0 & 0 & 0 & 0 & 0 & 0 \\
0 & 0 & 0 & 0 & 0 & 0 & 0 & 0 & 0 & 0 & 0 & 0 & 0 & 0 & 0 & 0 & \bar{S}_{46} & 0 & 0 & \bar{S}_{47} & \bar{S}_{48} & 0 & 0 & \bar{S}_{49} & \bar{S}_{50} & 0 & 0 & \bar{S}_{51} & \bar{S}_{52} & 0 & 0 & \bar{S}_{53} & 0 & \bar{S}_{54} \\
0 & 0 & 0 & 0 & 0 & 0 & 0 & 0 & 0 & 0 & 0 & 0 & 0 & 0 & 0 & 0 & 0 & 0 & 0 & 0 & 0 & 0 & 0 & 1 & 0 & 0 & 0 & 0 & 0 & 0 & 0 & 0 & 0 & 0 \\
0 & 0 & 0 & 0 & 0 & 0 & 0 & 0 & 0 & 0 & 0 & 0 & 0 & 0 & 0 & 0 & 0 & \bar{\mathcal{T}}_{46} & \bar{\mathcal{T}}_{47} & 0 & 0 & \bar{\mathcal{T}}_{48} & \bar{\mathcal{T}}_{49} & 0 & 0 & \bar{\mathcal{T}}_{50} & \bar{\mathcal{T}}_{51} & 0 & 0 & \bar{\mathcal{T}}_{52} & \bar{\mathcal{T}}_{53} & 0 & \bar{\mathcal{T}}_{54} & 0 \\
0 & 0 & 0 & 0 & 0 & 0 & 0 & 0 & 0 & 0 & 0 & 0 & 0 & 0 & 0 & 0 & 0 & 0 & 0 & 0 & 0 & 0 & 0 & 0 & 0 & 1 & 0 & 0 & 0 & 0 & 0 & 0 & 0 & 0 \\
0 & 0 & 0 & 0 & 0 & 0 & 0 & 0 & 0 & 0 & 0 & 0 & 0 & 0 & 0 & 0 & \bar{S}_{55} & 0 & 0 & \bar{S}_{56} & \bar{S}_{57} & 0 & 0 & \bar{S}_{58} & \bar{S}_{59} & 0 & 0 & \bar{S}_{60} & \bar{S}_{61} & 0 & 0 & \bar{S}_{62} & 0 & \bar{S}_{63} \\
0 & 0 & 0 & 0 & 0 & 0 & 0 & 0 & 0 & 0 & 0 & 0 & 0 & 0 & 0 & 0 & 0 & 0 & 0 & 0 & 0 & 0 & 0 & 0 & 0 & 0 & 0 & 1 & 0 & 0 & 0 & 0 & 0 & 0 \\
0 & 0 & 0 & 0 & 0 & 0 & 0 & 0 & 0 & 0 & 0 & 0 & 0 & 0 & 0 & 0 & 0 & \bar{\mathcal{T}}_{55} & \bar{\mathcal{T}}_{56} & 0 & 0 & \bar{\mathcal{T}}_{57} & \bar{\mathcal{T}}_{58} & 0 & 0 & \bar{\mathcal{T}}_{59} & \bar{\mathcal{T}}_{60} & 0 & 0 & \bar{\mathcal{T}}_{61} & \bar{\mathcal{T}}_{62} & 0 & \bar{\mathcal{T}}_{63} & 0 \\
0 & 0 & 0 & 0 & 0 & 0 & 0 & 0 & 0 & 0 & 0 & 0 & 0 & 0 & 0 & 0 & 0 & 0 & 0 & 0 & 0 & 0 & 0 & 0 & 0 & 0 & 0 & 0 & 0 & 1 & 0 & 0 & 0 & 0 \\
0 & 0 & 0 & 0 & 0 & 0 & 0 & 0 & 0 & 0 & 0 & 0 & 0 & 0 & 0 & 0 & \bar{S}_{64} & 0 & 0 & \bar{S}_{65} & \bar{S}_{66} & 0 & 0 & \bar{S}_{67} & \bar{S}_{68} & 0 & 0 & \bar{S}_{69} & \bar{S}_{70} & 0 & 0 & \bar{S}_{71} & 0 & \bar{S}_{72} \\
0 & 0 & 0 & 0 & 0 & 0 & 0 & 0 & 0 & 0 & 0 & 0 & 0 & 0 & 0 & 0 & 0 & 0 & 0 & 0 & 0 & 0 & 0 & 0 & 0 & 0 & 0 & 0 & 0 & 0 & 0 & 1 & 0 & 0 \\
0 & 0 & 0 & 0 & 0 & 0 & 0 & 0 & 0 & 0 & 0 & 0 & 0 & 0 & 0 & 0 & 0 & \bar{\mathcal{T}}_{64} & \bar{\mathcal{T}}_{65} & 0 & 0 & \bar{\mathcal{T}}_{66} & \bar{\mathcal{T}}_{67} & 0 & 0 & \bar{\mathcal{T}}_{68} & \bar{\mathcal{T}}_{69} & 0 & 0 & \bar{\mathcal{T}}_{70} & \bar{\mathcal{T}}_{71} & 0 & \bar{\mathcal{T}}_{72} & 0 \\
0 & 0 & 0 & 0 & 0 & 0 & 0 & 0 & 0 & 0 & 0 & 0 & 0 & 0 & 0 & 0 & 0 & 0 & 0 & 0 & 0 & 0 & 0 & 0 & 0 & 0 & 0 & 0 & 0 & 0 & 0 & 0 & 0 & 1 \\
0 & 0 & 0 & 0 & 0 & \bar{S}_{73} & \bar{S}_{74} & 0 & 0 & \bar{S}_{75} & \bar{S}_{76} & 0 & 0 & \bar{S}_{77} & \bar{S}_{78} & 0 & 0 & 0 & 0 & 0 & 0 & \bar{S}_{79} & \bar{S}_{80} & 0 & 0 & \bar{S}_{81} & \bar{S}_{82} & 0 & 0 & \bar{S}_{83} & \bar{S}_{84} & 0 & \bar{S}_{85} & 0
\end{array}\right). \qquad \text{(C.8)}
$$

D
The virtual crack closure technique

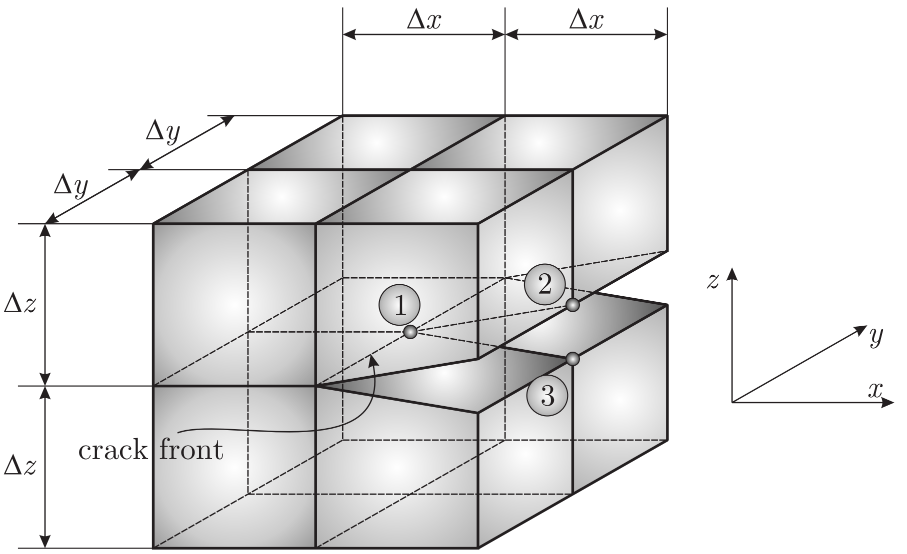

Figure D.1: Reference system and parameters of the virtual crack closure technique (VCCT).

In accordance with the VCCT the ERRs in a 3D FE model can be calculated as:

$$G_I = \frac{1}{2\Delta x \Delta y} F_{z1}(w_2 - w_3),\ G_{II} = \frac{1}{2\Delta x \Delta y} F_{y1}(v_2 - v_3),\ G_{III} = \frac{1}{2\Delta x \Delta y} F_{x1}(u_2 - u_3), \quad \text{(D.1)}$$

where F_{x1}, F_{y1} and F_{z1} are the sum of positive nodal forces coming from those corner of the neighboring elements, that coincide with node ①, u_2, u_3, v_2, v_3, w_2 and w_3 are the nodal displacements at nodes ② and ③ in Figure D.1.

E
3D distributions of shear strains and interlaminar stresses

dc_1254_16

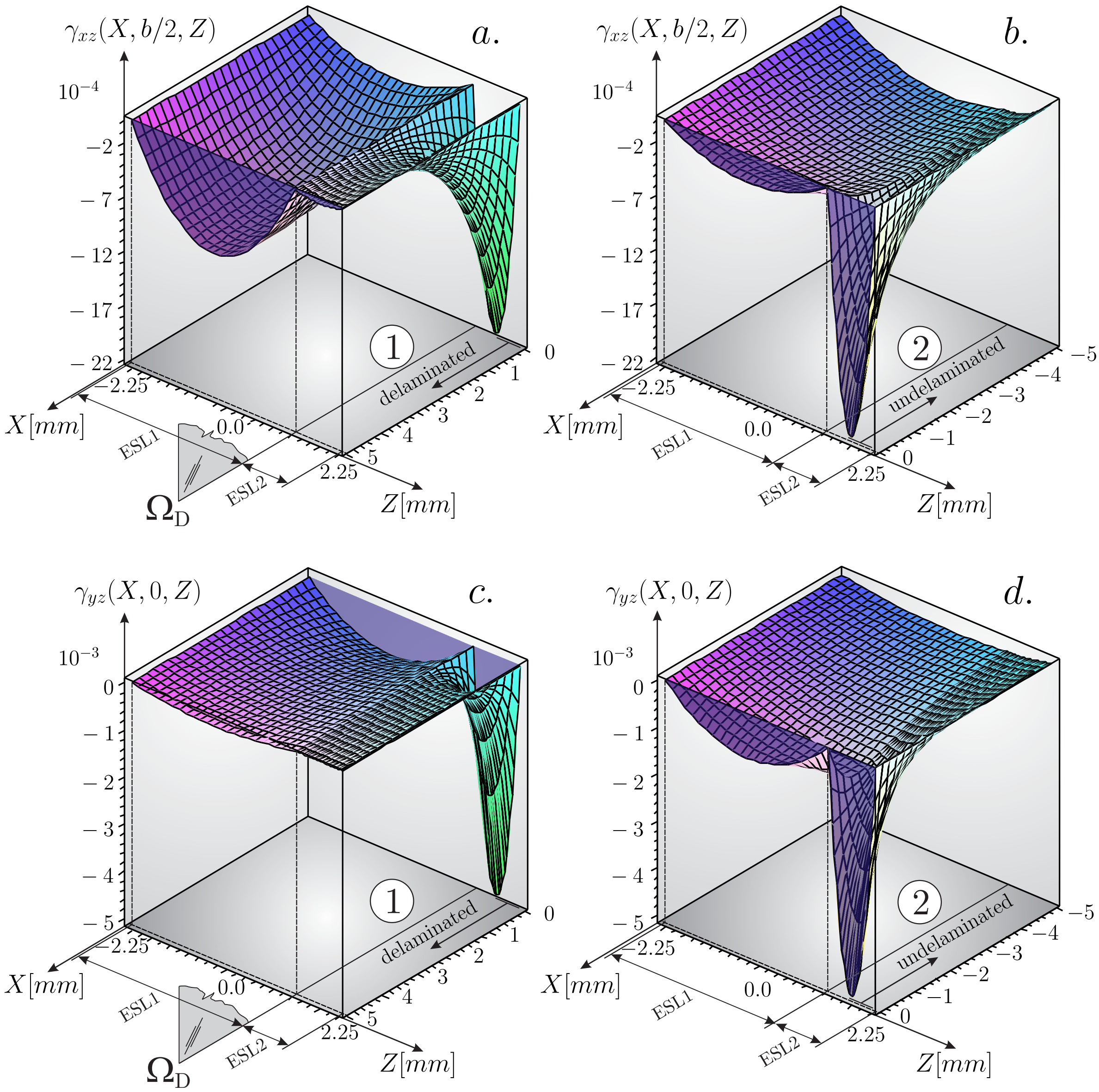

Figure E.1: Distribution of the shear strains γ_{xz} ((a) and (b)) and γ_{yz} ((c) and (d)) by Reddy TSDT at the transition between the delaminated and undelaminated regions at Y=$b/2$ and Y=0 (case III, b=100 mm), Ω_D is the delamination plane (method of 2ESLs).

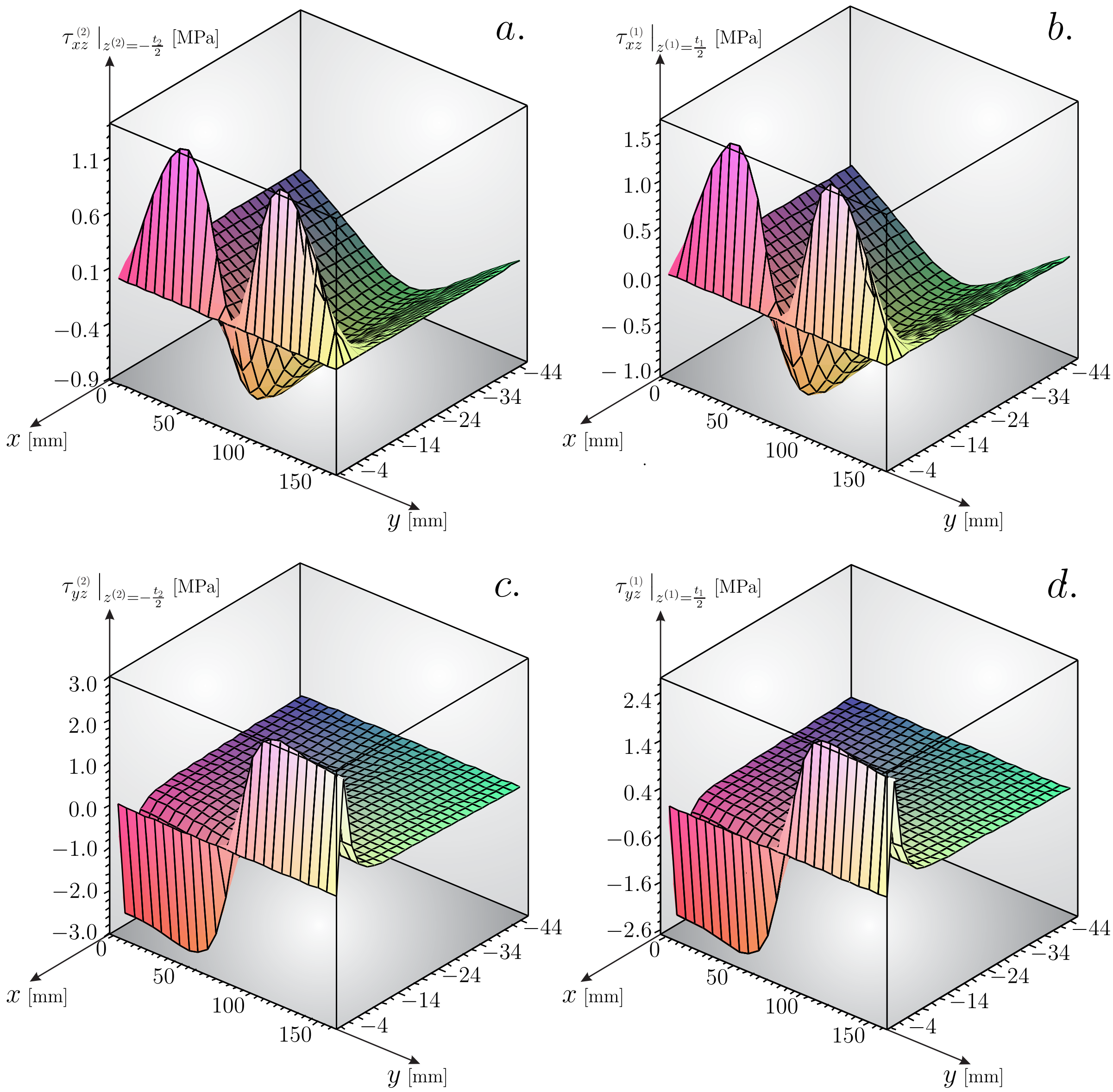

Figure E.2: Distribution of the interlaminar shear stress by Reddy TSDT for case III, b=160 mm, $\tau_{xz}^{(2)}$ (a), $\tau_{xz}^{(1)}$ (b), $\tau_{yz}^{(2)}$ (c) and $\tau_{yz}^{(1)}$ (d) (method of 2ESLs).

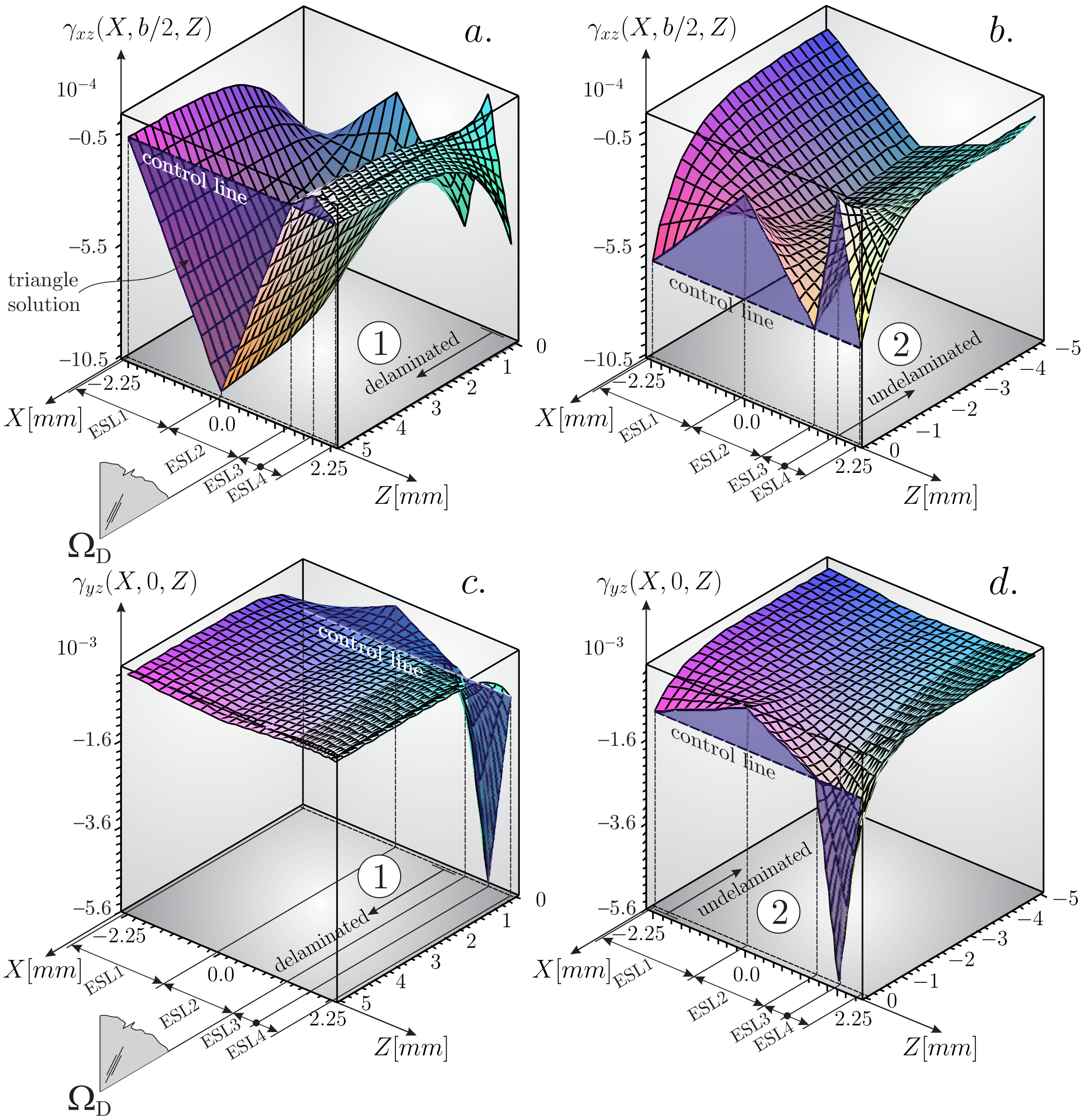

Figure E.3: Distribution of the shear strains γ_{xz} ((a) and (b)) and γ_{yz} ((c) and (d)) by SSDT at the transition between the delaminated and undelaminated regions at $Y=b/2$ and $Y=0$ (case III, b=100 mm), Ω_D is the delamination plane (method of 4ESLs).

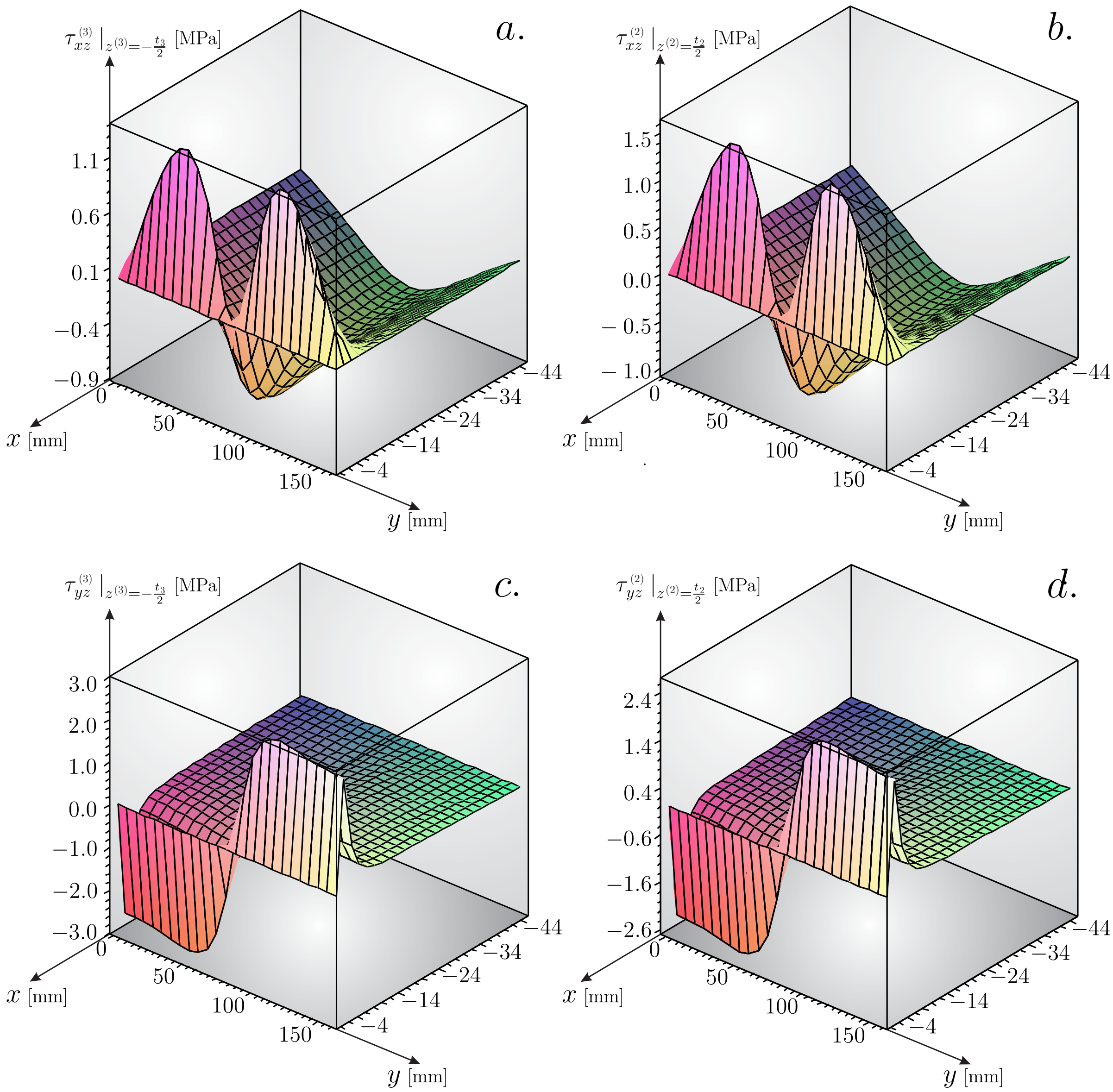

Figure E.4: Distribution of the interlaminar shear stress by SSDT for case III, b=160 mm, $\tau_{xz}^{(3)}$ (a), $\tau_{xz}^{(2)}$ (b), $\tau_{yz}^{(3)}$ (c) and $\tau_{yz}^{(2)}$ (d) (method of 4ESLs).